SANDIA REPORT

Thermal Measurements from a Series of Tests with a Large Cylindrical Calorimeter on the Leeward Edge of a JP-8 Pool Fire in Cross-Flow

Jill M. Suo-Anttila and Louis A. Gritzo

Inside of Cover Page

Thermal Measurements from a Series of Tests with a Large Cylindrical Calorimeter on the Leeward Edge of a JP-8 Pool Fire in Cross-Flow

Jill M. Suo-Anttila and Louis A. Gritzo
Fire Science and Technology
Sandia National Laboratories
P.O. Box 5800
Albuquerque, New Mexico 87185-0836

Abstract

As part of the full scale fuel fire experimental program, a series of JP-8 pool fire experiments with a large cylindrical calorimeter (3.66 m diameter), representing a C-141 aircraft fuselage, at the lee end of the fuel pool were performed at Naval Air Warfare Center, Weapons Division (NAWCWPNS). The series was designed to support Weapon System Safety Assessment (WSSA) needs by addressing the case of a transport aircraft subjected to a large fuel fire. The data collected from this mock series will allow for characterization of the fire environment via a survivable test fixture. This characterization will provide important background information for a future test series utilizing the same fuel pool with an actual C-141 aircraft in place of the cylindrical calorimeter.

Acknowledgments

Table of Contents

List of Figures

List of Tables

1. Introduction

1.1 Background

Exposure to a large hydrocarbon pool fire is one of the many scenarios to be considered when assessing the fire survivability of engineered systems. Such fires can occur as a result of transportation accidents. The spectrum of technologies required to accurately predict the fire environment for such scenarios is presently under development at Sandia National Laboratories (SNL). Due to the complex interaction of nonlinear phenomena present in fires, an integrated approach including full scale experiments, the development of advanced diagnostic techniques and the development of a suite of numerical models is required for significant, applicable technical progress to be realized.

In support of this integrated effort, an extensive full scale fuel fire experimental program was initiated at the Naval Air Warfare Center, Weapons Division (NAWCWPNS). The objectives of this program are to: 1) gain a better understanding of fire phenomenology, 2) provide empirical input parameter estimates for simplified, deterministic Risk Assessment Compatible Fire Models (RACFMs) [1], 3) assist in continuing fire field model validation and development [2], and 4) enhance the data base of fire temperature and heat flux distributions on objects. These experiments are supported by the Defense Threat Reduction Agency (DTRA) (Defense Special Weapons Agency (DSWA) at the time of these tests) as part of a Fuel Fire Technology Base Program. The goal of the Fuel Fire Technology Base Program is to develop validated numerical tools capable of predicting the thermal environment in a fuel fire resulting from an aircraft or ground transportation accident. These numerical simulation capabilities are required to improve the fidelity of Weapons System Safety Assessments (WSSAs).

As part of the full scale fuel fire experimental program, a series of JP-8 pool fire experiments with a large cylindrical calorimeter (3.66 m diameter), representing a C-141 fuselage, at the lee end of the fuel pool were performed at NAWCWPNS. The series was designed to support WSSA needs by addressing the case of a transport aircraft subjected to a large fuel fire. The data collected from this series will allow for characterization of the fire environment via a survivable test fixture. This characterization will provide important background information for a future test series utilizing the same fuel pool with an actual C-141 aircraft in place of the cylindrical calorimeter (commonly referred to as the mock fuselage in this report). Experience and knowledge gained in conducting the Mock Fuselage Test Series will be used for planning the C-141 tests since the heat fluxes to the actual system are difficult to measure and changes in the geometry due to the exposure of the actual system pose additional challenges in the ability to characterize the fire.

In addition to supplying data of direct relevance to WSSAs, another objective of this series is to obtain the data required to validate and further the development of fire field models which can be used to address other fire scenarios. In general, the ability to numerically model the fire environment is required to improve the design and assessment of fire-survivable engineered systems. Fire modeling, including the influence of objects on the fire environment and the thermal response of objects, requires that many coupled, nonlinear, physical phenomena be represented. Currently, a fire field model is under development at SNL to predict the fire environment from a "first principles" approach whereby the governing transport and phenomenological equations are solved for all primary relevant variables. The comparison of model predictions and high fidelity experimental data is an essential component of the model development process. Depending on the results of such comparisons, it may be possible to obtain increased confidence in the ability of the model to predict certain variable fields within the uncertainty inherent in the experimental measurements. In this sense limited "validation" of one or more aspects of the model can be achieved.

When discrepancies between model predictions and experimental results are observed, an understanding of the fire phenomenology is required to reconcile the differences. This understanding must frequently be developed by investigating the characteristics of the measurements and the details of the model predictions. Based on the results of these investigations, the model and experimental technology development processes are supported in the most efficient manner possible by directing research efforts towards the appropriate areas.

Large computational times are required to perform fire field model simulations. They are therefore not well-suited for the initial series of numerous calculations required by Probabilistic Safety Assessments (PSAs). A suite of simplified, deterministic, Risk Assessment Compatible Fire Models (RACFMs) have been developed at SNL for this purpose. These models apply first principles to the dominant physical phenomena (radiative and advective transport) and rely on empirically-determined parameters to represent the remaining physics [1]. Using this approach, run times are reduced to a level acceptable for PSAs. Presently, predicting the heat release due to combustion, which is largely controlled by mixing and hence requires the numerical simulation of the flow field, is beyond the scope of these models [3]. It is therefore necessary to represent the temperature and radiative property fields which result from combustion of the fuel using empirical parameters. Data generated from large scale experiments, complemented by fire field model simulations, are used to develop the necessary empirical relationships and constants. In many cases, significant differences are observed between these data and commonly accepted estimates which appear in fire protection engineering handbooks [4]. These deviations can largely be attributed to the lack of a precise knowledge of the relevant physics, and the existence of large scale fire data. It is

therefore necessary to supplement the existing knowledge base with data from carefully designed experiments.

For all of the fire scenarios which include an engulfed object, experimental results and model predictions must be compared for cases when the object size and shape is such that the geometry of the flame zone is altered due to the presence of the object. These scenarios are difficult to address because the alteration of the flow field due to the presence of the object, and the influence of the altered flow field on the fire physics, must be known. The presence of the mock fuselage adjacent to the fuel pool may cause global changes in the continuous flame zone and heat fluxes measured within the fire depending on the wind conditions. Despite the foundational importance of these type of scenarios, this case has not been addressed prior to this study.

1.2 Objectives

The objectives of the Mock Fuselage Test Series were to obtain:

1. spatial and temporal distributions of temperature, heat flux, and pressure on the surface of the mock fuselage,
2. spatial and temporal distributions of temperature and heat flux in the vicinity of the mock fuselage,
3. spatial and temporal distribution of heat flux to the fuel pool surface, and
4. spatial and temporal distribution of emissive power from the continuous flame zone.

The objectives of this report are to:

1. document the instrumentation employed in the series of experiments,
2. document the conditions under which each experiment in the series was performed,
3. present the data collected during the series in a manner suitable for comparison with numerical model predictions, and
4. investigate and document trends observed in the data.

Each of these objectives will be addressed in the chapters which follow.

2. Instrumentation

2.1 Overview of Experimental Setup

The experiments were performed at the NAWCWPNS CT-4 test site. The experimental setup consisted of a large, culvert pipe cylindrical calorimeter, which served as a mock fuselage, located at the lee side of a pool fire test pit (Figure 2.1, and chapter 11 for photographs). The site was at the bottom of a gradually-sloping valley which was approximately 800 m wide. The test pit was approximately 25 cm deep and was initially filled with approximately 15 cm of water. Prior to each experiment, a fuel pool was formed in the pit by floating military-grade JP-8 fuel on top of the water. The fuel was ignited at three locations by triggering a 110V signal across a book of matches. Experiments were concluded when all of the fuel was consumed.

The calorimeter was placed such that the calorimeter's longitudinal axis was normal to prevailing valley wind direction (which is approximately 210° clockwise from south). Fire environment instrumentation included an array of thermocouple poles and heat flux gauges positioned within the fuel pool on the windward and the leeward sides of the calorimeter as well as dense instrumentation in close proximity to the mock fuselage for two different pool sizes (nominally 10 m and 20 m diameter).

Temperature measurements were obtained using type-K thermocouples. The maximum type-K thermocouple error using the manufacturer's calibration is $\pm 9.4^{\circ}$C at 1250°C. The location of the thermocouples within the flame zone has an uncertainty of approximately 0.1 m (4"). The locations of the thermocouples mounted inside the mock fuselage are known to approximately the same accuracy. It is acknowledged that, due to several mechanisms including radiative transport, thermal shunting, and thermal inertia, the temperature measured by a thermocouple is not, in general, equal to the local media temperature [13]. Cost and robustness limitations, however, continue to dictate the use of thermocouples for spatial characterization of large fires. Correction to the local gas temperature from the thermocouple temperature requires extensive information about the fire environment which was not obtained in these experiments.

Heat fluxes were measured using Sandia heat flux gauges (HFGs). Previous experimental analyses determined that applying a simple thermal response model to SNL HFG data yields calculated incident heat fluxes within about 5% of measured values, provided the input flux is steady [20]. However, the dynamic time results may be in considerable error. A detailed discussion of the effect of unsteady heat flux conditions on the gauge is given by Blanchat [5].

Figure 2.1 - Placement of the mock fuselage and pool size

Extensions

Object Instrumentation
Assembly

10 m

Steel Fuselage Section

20 m

Prevailing Wind
Direction
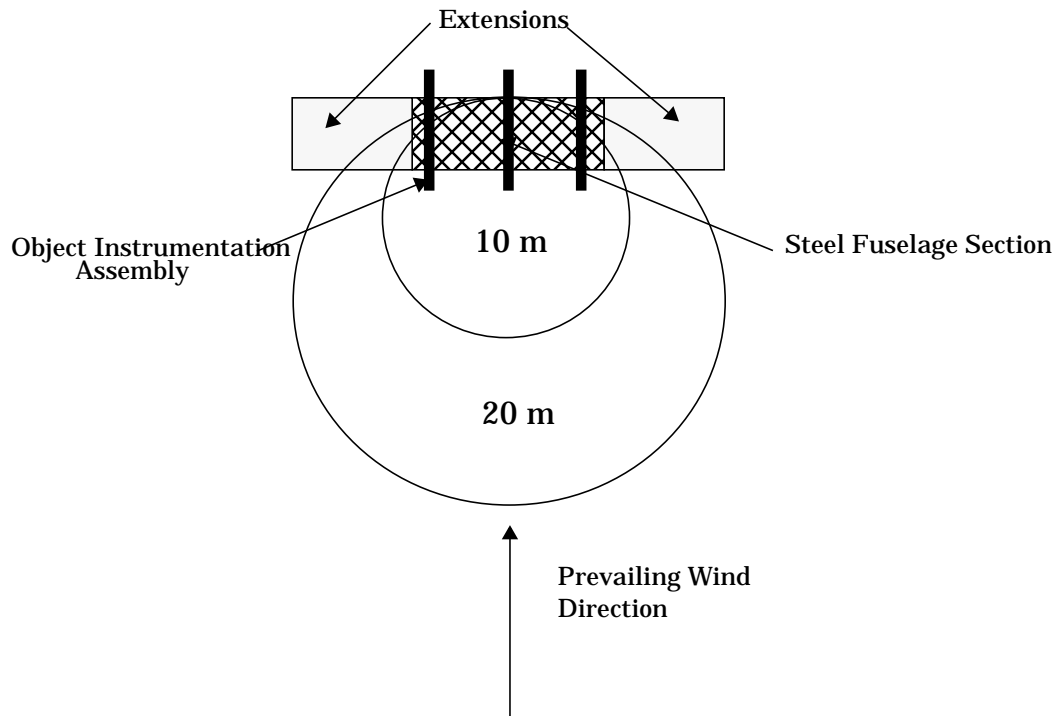
2.2 Test and Environmental Conditions

The series of eight tests, each containing a large cylindrical calorimeter, targeted several different configurations and environmental conditions. For six of the tests, the cylindrical calorimeter was located at the leeward edge of the 18.9 m pool of fuel as shown in Figure 2.1. The remaining two tests utilized a 9.45 m diameter pool with the calorimeter at the leeward edge of the pool. The actual diameters of the pool are 18.9 m and 9.45 m but they will be referred to as 20 m and 10 m, respectively. The tests were performed for a range of different wind conditions to support analysis of wind effects on the fire environment. The wind conditions are defined in terms of the direction and the speed of the prevailing winds at the test facility. Each test must contain two minutes of stable wind conditions for it to be considered a success.

2.3 Test Hardware and Instrumentation

2.3.1 Construction of the Mock Fuselage

As illustrated in Figure 2.2, the mock fuselage was constructed by joining three sections of 16 gauge (0.16 cm thick) mild steel culvert pipe with a nominal diameter of 3.66 m. The middle section of the pipe was approximately 9.14 m in length, and the outer two sections were approximately 4.57 m in length. To support the assembly above the pool surface a lattice of spokes was constructed from angle iron attached to a 15.24 cm-wide circular band of mild steel and a W14 x 61 I-Beam spine. Steel studs were used to connect the band to the interior of the culvert pipe.   The bands were spaced approximately 0.91 m apart throughout the interior. An A-frame constructed from steel tubing was attached to the spine at each end of the center section. To prevent ingression of flame to the interior of the mock fuselage, a large, circular, 16 gauge mild steel plate with an access door was attached to the outer ends of the assembly.

After the mock fuselage was instrumented, the interior was insulated with two layers of 2.54 cm thick ceramic fiber blanket insulation. The insulation was located between the inside surface of the mock fuselage and the mild steel bands. In addition, the first six inches of the spokes, from the band inward, were insulated with one layer of 2.54 cm thick ceramic fiber blanket insulation. The interiors of the end-plates were also insulated with two layers of insulation.

Figure 2.2 - Mock Fuselage constructed from three sections of culvert pipe
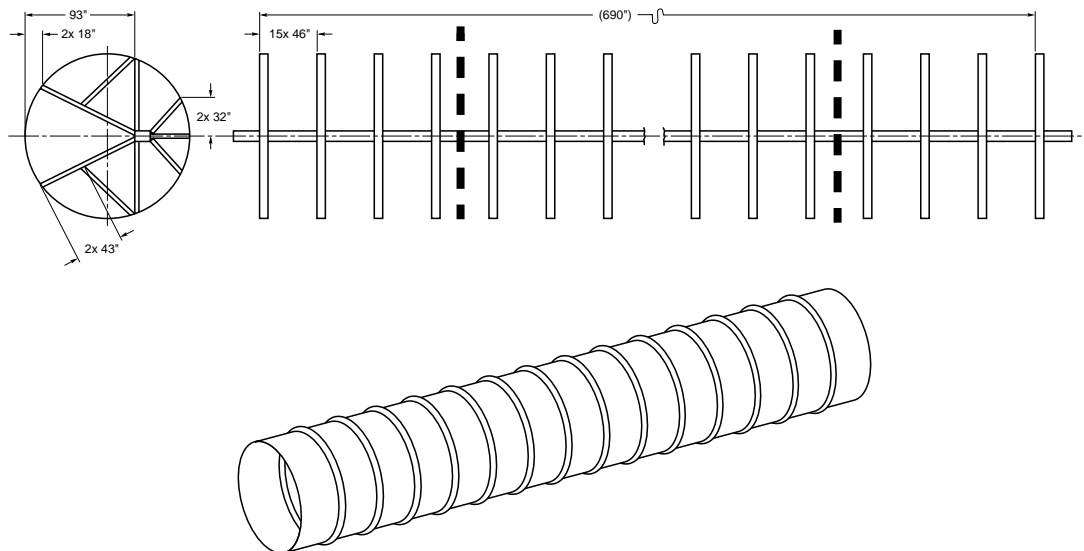
2.3.2 Mock Fuselage Surface Measurements

To obtain data needed to develop RACFMs for a large cylinder in cross-flow, temperature and heat flux measurements were performed on the surface and in the vicinity of the mock fuselage (Figure 2.3 and 2.6). In addition, these measurements were used to deduce the coupled influence of a large, cylindrical object and wind on the local combustion process in the vicinity of the object. Type K, 1.6 mm diameter, inconel sheathed, ungrounded junction thermocouples were used to monitor the inner surface temperature of the mock fuselage.

Hemispherical heat flux gauges (HFGs), designed by SNL and constructed as prescribed by SNL Drawing R45066 were used to provide estimates of the incident heat flux on the surface of the mock fuselage. The HFGs used a large (6 cm) diameter, thin (0.02 mm) flat sensor surface with a thermocouple attached to the interior side. The sensor surface was thermally isolated from the remainder of the gauge and hence rapidly (limited by the time constant of the thermocouple) came to equilibrium with the fire environment. A Pyromark™ black coating was applied to yield a diffuse and gray sensor surface. When convection is negligible, (as is typical for many locations in large fires) the emissive power of the diffuse, gray sensor surface, in equilibrium with the surroundings, provides a measurement of the incident heat flux. For steady-state operation in favorable (low convection) areas uncertainty of +5% / -20%, depending on conditions, is estimated for these gauges. A number of exploratory heat flux gauges, designed by NAWCWPNS, were also used.

2.3.3 Temperature

The mock fuselage served as a calorimeter by attaching thermocouples to the inner surface at eight stations along the longitudinal axis of the mock fuselage. As illustrated in Figure 2.3, six of the eight longitudinal stations straddled the assembly (HFG/TC Array) which was used to measure the temperature and heat flux in the vicinity of the mock fuselage. At the stations which straddled the HFG/TC Arrays, eight thermocouples were spaced evenly around the circumference of the mock fuselage. At the axial stations located 3.05 m from each end of the mock fuselage, four thermocouples were spaced evenly around the circumference of the mock fuselage.

The notation for locating the thermocouples was such that bottom-center of the mock fuselage was zero degrees, and the longitudinal stations were numbered consecutively from left to right when facing the windward side of the mock fuselage. A counterclockwise notation was used to denote the angular location of the thermocouple when viewing the mock fuselage from the left end.

Figure 2.3 - Location of thermocouples on the mock fuselage
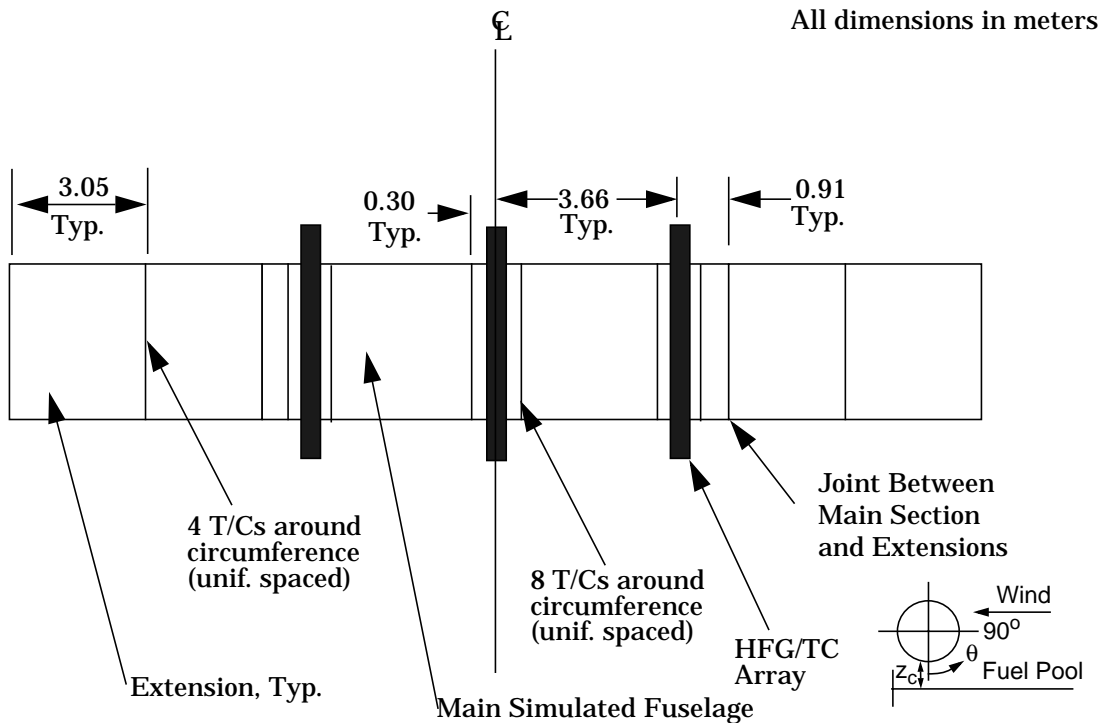
To track the fire survivability of the test fixture, eight thermocouples were used to monitor the temperature of the critical structural components of the mock fuselage. Two thermocouples were placed at the center of each end-plate, and three thermocouples were evenly distributed along the length of the spine. In addition, a thermocouple was placed as close as possible to the mock fuselage inner skin on the three vertical spokes. The location of the three vertical spokes corresponds to the same axial location used to monitor the temperature of the spine.

Thermocouples used to monitor surface temperatures on the mock fuselage were attached by bending the end to form a "J-hook" and nichrome strips were used to tack-weld the thermocouple to the surface. The thermocouple leads from each axial station were bundled and neatly routed out of the test fixture. To reduce the potential for shorting, ceramic fiber insulation was wrapped around the bundle up to the point where the thermocouple leads were submerged into the pool. Once the thermocouple leads emerged from the pool, they were thermally protected and routed to the junction box.

2.3.4 Heat Flux

HFG's were located on the surface of the mock fuselage at five axial stations. As illustrated in Figure 2.3, one station was located at the centerline of the mock fuselage. Two additional stations straddled the centerline and were separated by 7.32 m. The remaining two stations were located 3.05 m from the two ends of the mock fuselage (See Figure 2.3). Twenty-six of the SNL HFG's (shown in Figure 2.4), and twelve of the NAWCWPNS heat flux gauges, were located around the circumference of the mock fuselage. The angular location of the gauges is given in Figure 2.4. The HFG's were mounted on the surface of the mock fuselage by attaching the gauges to the weldment illustrated in Figure 2.5. The weldment was bolted to the exterior skin of the mock fuselage using over-sized holes (to allow for thermal expansion) and washers. The weldment was constructed to minimize the disturbance of the flow field in the vicinity of the gauge sensing surface. The upper and lower sections of the weldment, therefore, were rolled to conform to the curvature of the mock fuselage. In addition, the lead edge of the lower plate was

Figure 2.4 - Weldment used to mount the HFG's to the outer surface of the fuselage
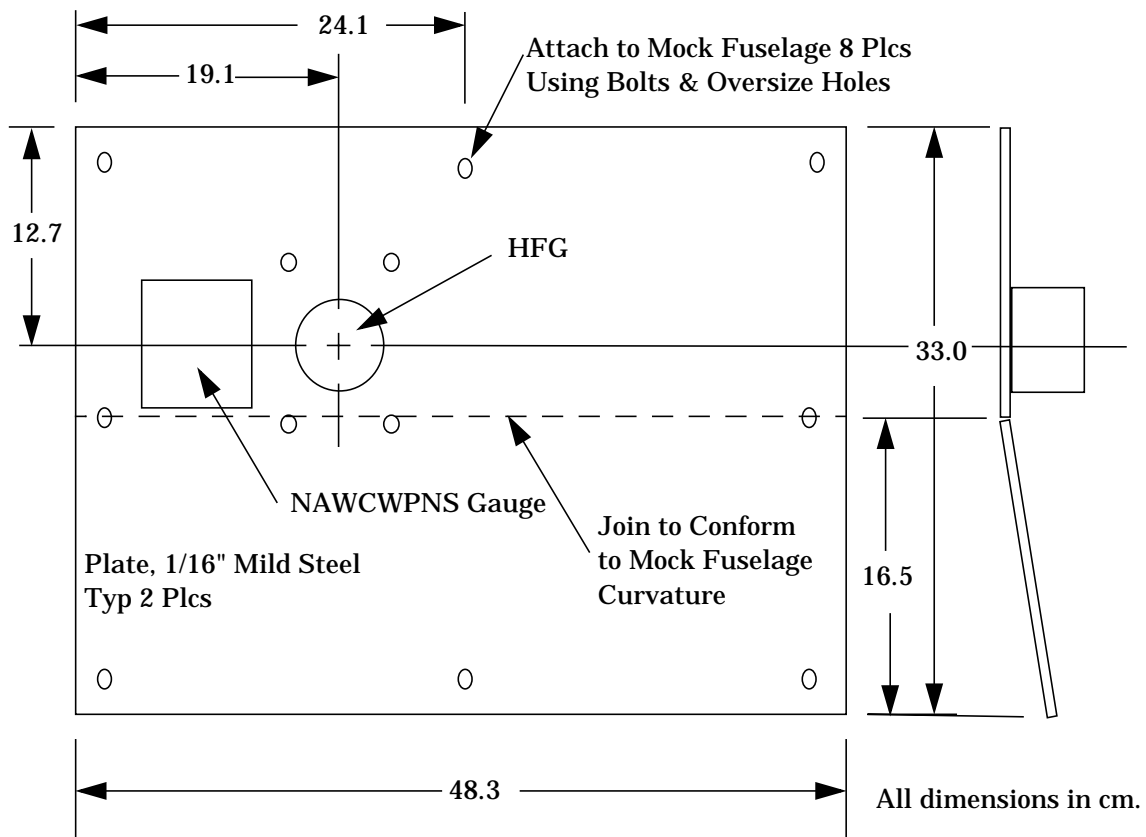
Figure 2.5 - Location of heat flux gauges on the surface of the fuselage

2.7m
Typ.

B

A

3.7m
Typ.

C

B

A

C

Gauge Locations

Wind

C̶L̶

90

45

0

B-B
Typ. 2 plcs.

90

45

0

A-A

90

0

C-C
Typ. 2 plcs.
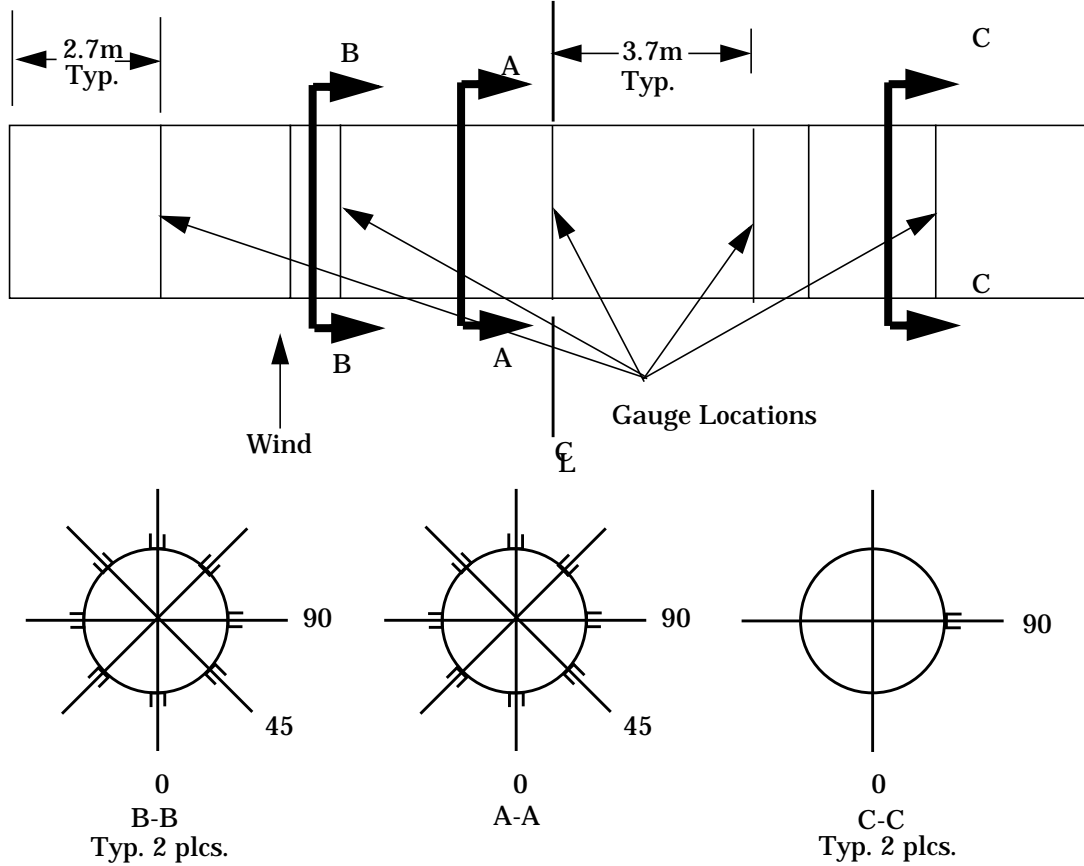
Location of SNL Hemispherical Heat Flux Gauges

90

0

B-B
Typ. 2 plcs.

90

0

A-A

90

0

C-C
Typ. 2 plcs.
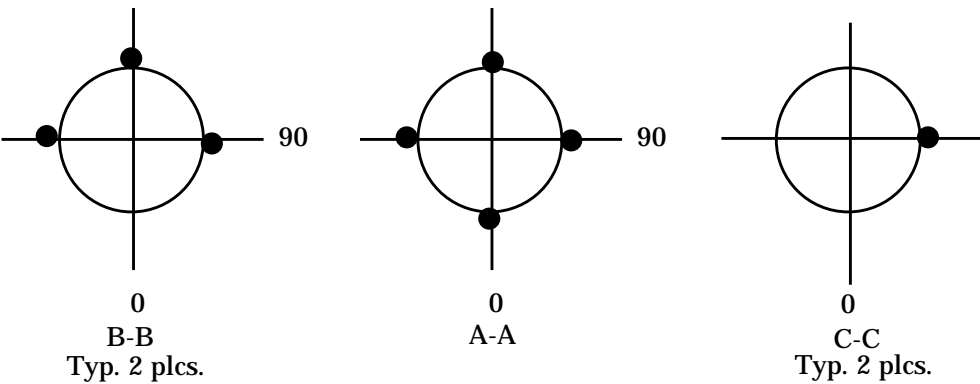
Location of NAWCWPNS Heat Flux Gauges

10

approximately 20.3 cm from the center of the gauge sensing surface.   At locations where both types of gauges were installed, the gauges were positioned side by side, and the SNL HFG's were aligned with the thermocouples located on the HFG/TC Array. The thermocouple leads from the gauges at each axial station were bundled and routed along the mock fuselage support structure and out of the mock fuselage. Insulation was wrapped around the bundle up to the point where the thermocouple leads were submerged into the pool. Once the thermocouple leads emerged from the pool, they were thermally protected and routed to the junction box. The same notation used to locate the thermocouples on the surface of the mock fuselage was used to locate the HFG's.

2.3.5 Pressure

The difference in pressure between the windward and leeward side of the mock fuselage is valuable for comparison with results predicted by fire field models. These measurements also yield an improved understanding of the flow field in the vicinity of the test section, and hence smoke transport for commercial aircraft safety concerns. Pressure taps were therefore located at 90 and 270 degrees at three axial locations coincident with the HFG/TC arrays. Pressure taps were also located in the fuel pool and outside the fuel pool to provide a fourth differential pressure. A differential pressure transducer was connected to the pressure taps at each location. The transducers were located outside of the continuous flame zone and protected from thermal insult. Lines between the pressure taps and the transducers were routed such that all joints were submerged in the pool and hence protected from leaks caused by thermal expansion.

2.3.6 Temperature and Heat Flux Measurements in the Vicinity of the Mock Fuselage

The array assembly used to measure temperature and heat flux distribution near the mock fuselage is depicted in Figure 2.6. The largest assembly supported 12 two-sided HFG's and 37 thermocouples. The two-sided HFG's were equally spaced around the mock fuselage at seven angular positions and two radial locations, starting with 45 degrees from the bottom of the mock fuselage. Three thermocouples were equally spaced (~25 cm apart) between the two-sided HFG's, and, with the exception of the 315 degree location, three thermocouples were equally spaced (~25 cm apart) between the innermost gauge and the outer surface of the mock fuselage. Four thermocouples were equally-spaced at the 315 degree location. A smaller assembly at the base of the mock fuselage (0 degree) supported a single-sided HFG at the fuel surface and three equally-spaced (~15 cm apart) thermocouples. The first two tests did not have thermocouple arrays on the lower

Figure 2.6 - Location of HFG's and thermocouples in the vicinity of the fuselage

- Thermocouple
- HFG Flux gauge, 2-Sided, Stringer Mount
- HFG Flux gauge, 1-Sided, Surface Mount

25.4 cm Typ.

Fuselage Model

~ 2.1m

~ 7.3 m

15.2 cm Typ.

~ 0.6 m

4 Thermocouples at 315 degree location only

Stringer Tube

Attaching Tab

Hangar Bracket

Thermocouple Wire Guides (Unistrut)

Attaching Tab

20.3cm

Tower

HFG Body ~ 10.2cm Dia. 12.7cm Long.

Stringer Tube 3.8 cm Dia.

Hangar Bracket
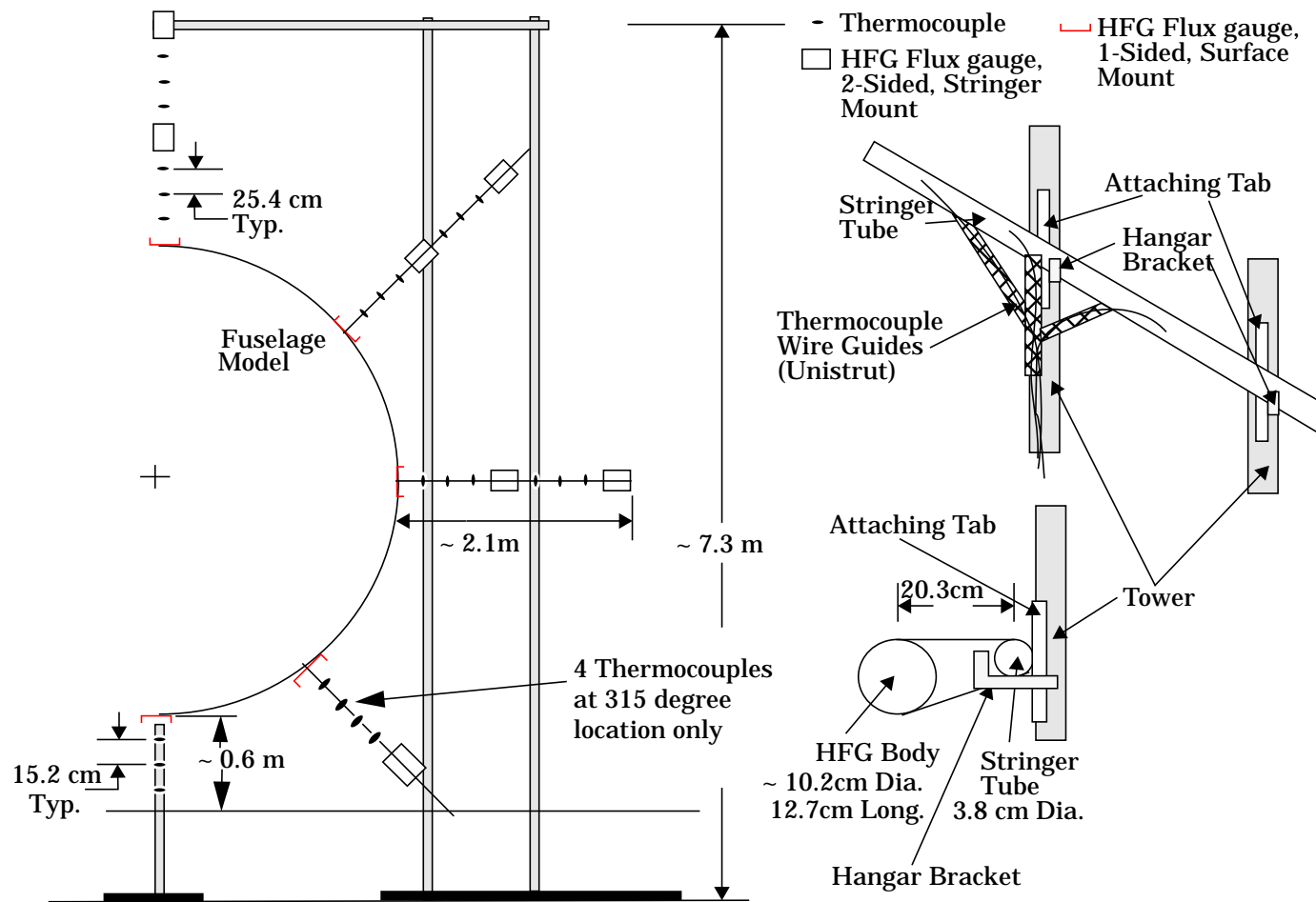
side of the mock fuselage (0, 45, 315 degree locations). To ensure fire survivability, both assemblies were entirely wrapped with nominally 1 inch (2.5 cm) thick ceramic fiber blanket insulation. Care was taken to ensure no gaps to prevent flames from impinging on the structure) existed between the insulation and the structure.   Prior to insulating the structure, all thermocouples were routed along the assembly down to the pool surface. Thermocouple leads were then bundled and carefully routed to the junction box.

2.3.7 Measurement of Heat Flux to the Fuel Surface and Terrain

Twenty single-sided, upward-facing, HFG's were used to measure the spatial distribution of incident heat flux to the fuel pool surface from the continuous flame zone. Six HFG's were placed in the prevailing wind direction along the centerline of the pool, and the remaining fourteen HFG's were symmetrically positioned on either side of the pool centerline as shown in Figure 2.7 for the 20 m pool. The first two tests did not contain the two HFG's nearest to the leading edge of the fuel pool. These gauges were added later based on trends observed in the data.

In an attempt to measure the incident flux from the large standing vortices that were expected to form on the lee side of the mock fuselage assembly, several upward-facing HFG's were located outside the pool. The HFG's located outside the pool were positioned such that the sensing surface of the gauge was level with the ground. With the mock fuselage at the leeward edge of the fuel pool, five single-sided, upward-facing HFG's were located outside the pool as shown in Figure 2.7.

For the 10 m diameter pool test conditions, Figure 2.8 gives the location of the single-sided HFG's within and on the leeward side of the pool. Twelve single-sided HFG's were located within the pool and eight were located outside the pool on the leeward side of the mock fuselage.

The single-sided HFG's were constructed according to SNL drawing R45065. In constructing the gauges, the thermocouple leads were sufficiently long to traverse from the farthest gauge position to the junction box. HFGs located within the fuel pool were mounted to a square baseplate. Screws located at the corners of the baseplate were used to level the gauges and to position the gauge sensor surface approximately 6.45 cm above the surface of the fuel. A closed, end-cap was used in place of the base plate for the HFGs located within the terrain. A watertight junction between the gauge body and the end-cap or baseplate, and the pass-through in the body of the gauge for the thermocouple leads, was included. All thermocouple leads from the gauge were bundled and routed along the bottom of the pool to the junction box. For those gauges located outside the pool, the thermocouple leads were insulated up to the point where they entered the pool.

Figure 2.7 - Location of single-sided, upward facing HFG's and TC towers - 20 m pool

HFG/TC Array

TC Pole facing right, i.e.

Upward-Facing HFG

2.7 m

2.7 m

3.6m Typ.

2.7 m

4.1 m Typ.

1.8 m

0.6 m

1.8 m

3.2 m Typ.

Prevailing Wind

6.1 m Typ.

14
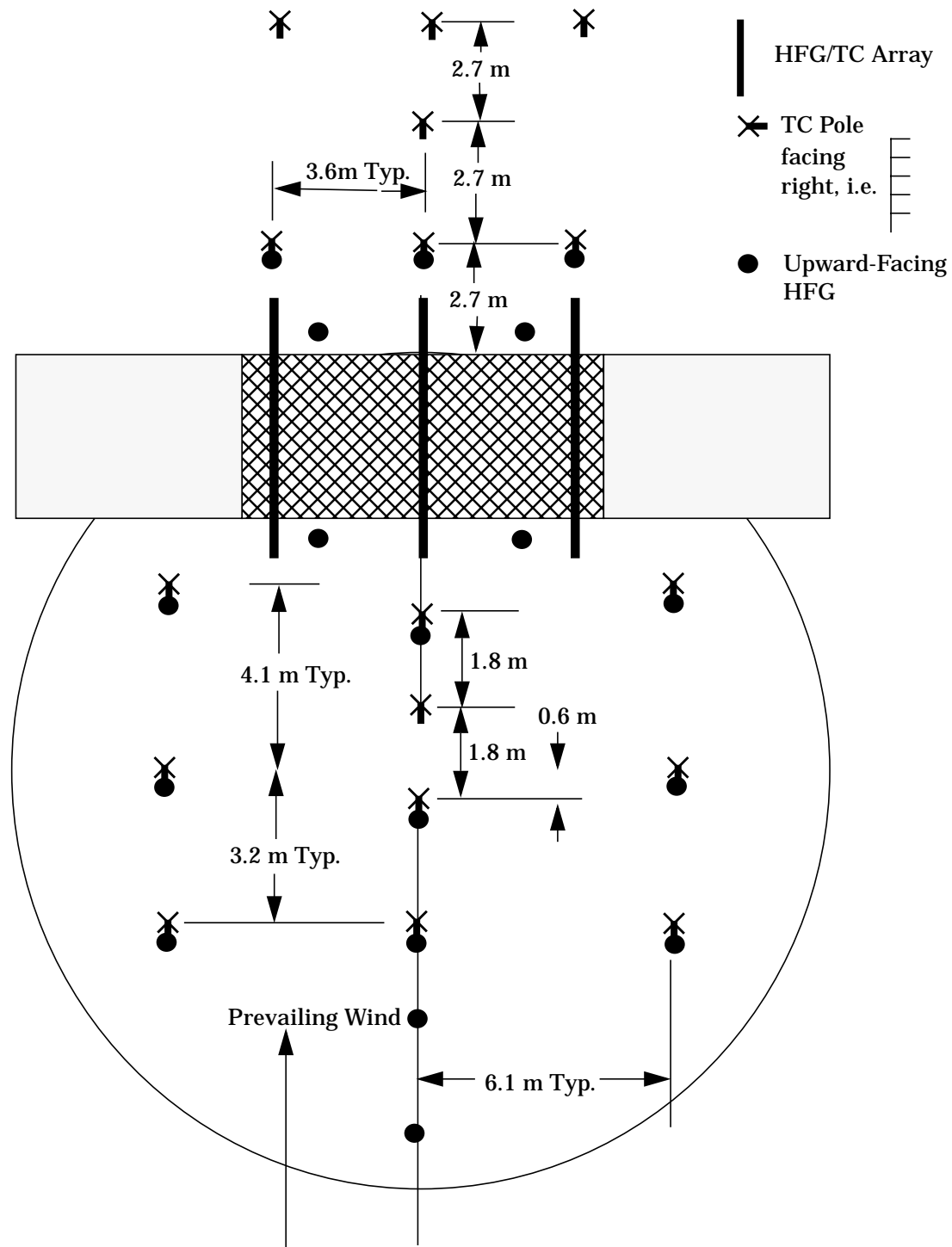
Figure 2.8 - Location of single-sided, upward facing HFG's and TC towers - 10 m pool

HFG/TC Array

TC Pole facing right, i.e.

Upward-Facing HFG

3.6 Typ.

1.5

1.8 Typ.

2.0

0.6 Typ.

1.2 Typ.

0.5

1.8 Typ.

0.6

2.0

1.4 Typ.

3.4

0.1 Typ.

0.1 Typ.

3.0 Typ.

30° Typ.
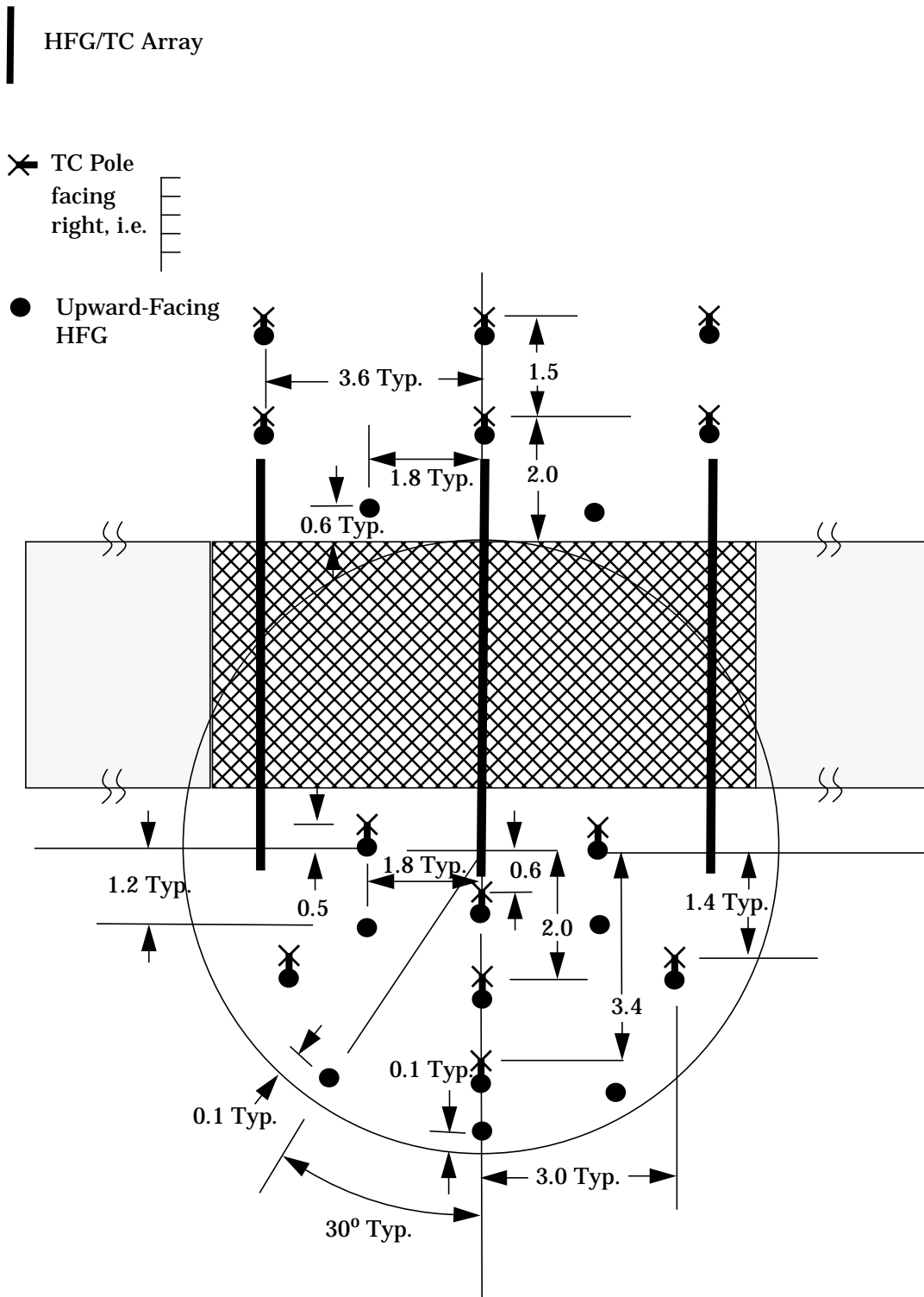
2.3.8 Temperature Measurements within the Fuel Layer

Two arrays of thermocouples were used to monitor the local fuel temperature and to deduce the fuel recession rate. The local fuel recession rate, deduced from the thermocouple measurements, in conjunction with the heat flux measurements to the pool surface, was used to estimate the thermal energy transmitted from the fire to the fuel surface and dissipated within the fuel. This information served to enhance the understanding of the fire-induced thermal response of the fuel, and was essential in developing an improved fuel recession submodel for fire models. Figure 2.9 depicts the vertical spacing between the six thermocouples which were mounted on a 2.54 cm OD stainless steel pipe. Large thermal gradients through the thickness of the fuel layer were expected. Therefore, as illustrated in Figure 2.9, the vertical spacing was weighted towards the free surface of the fuel. To ensure fire survivability of the array and thermocouples, the interior of the pipe was water-cooled. To allow correlation of the fuel temperature with the local heat flux, the arrays of fuel thermocouples were located adjacent to an upward-looking HFG. Immediately prior to a given test, the exact elevations of the thermocouples with respect to the water level were measured.

2.3.9 Heat Flux Measurements from the Fire Exterior

Spatial and temporal heat flux measurements from the exterior of the fire were useful for comparison with RACFMs which predicts the heat flux to an object located a finite distance from the continuous flame zone. To characterize the heat flux to an object near the flame zone, four water-cooled, 2.03 cm foil-type Gardon gauge calorimeters with signal conditioning amplifiers were placed 30 m from pool center; 1 windward, 1 leeward, and 1 on each side. A minimum of 1/8 GPM of cooling water at a temperature above the local dew point was supplied to each gauge. To quantify the heat flux to an object a significant distance from the flame zone (a region where existing correlations are expected to be inaccurate), 1 heat sink gauge was placed on the lee side of the pool at a distance of ~ 80 m from the pool center. All gauges were mounted in the insulated, adjustable angle fixture shown in Figure 2.10. A thermocouple mounted to the back side of the fixture provided a second technique for estimating the heat flux. In an attempt to resolve the primary transient changes in emission due to fire "puffing", the Gardon Gauge measurements were acquired every 0.1 seconds.

2.3.10 Temperature Measurements within the Continuous Flame Zone

Portable thermocouple (TC) towers, each containing five Type-K, 3.2 mm. sheathed thermocouples, were used to characterize the temperature within the lower portion of the continuous flame zone. It is acknowledged that, due to several mechanisms including radiative transport and thermal inertia, the temperature measured by a thermocouple is not, in general, equal to the local media temperature [13]. Cost and robustness limitations, however, continue to dictate the use of thermocouples for spatial characterization of large fires. These portable TC towers,

Figure 2.9 - Thermocouple array to measure the local fuel temperature
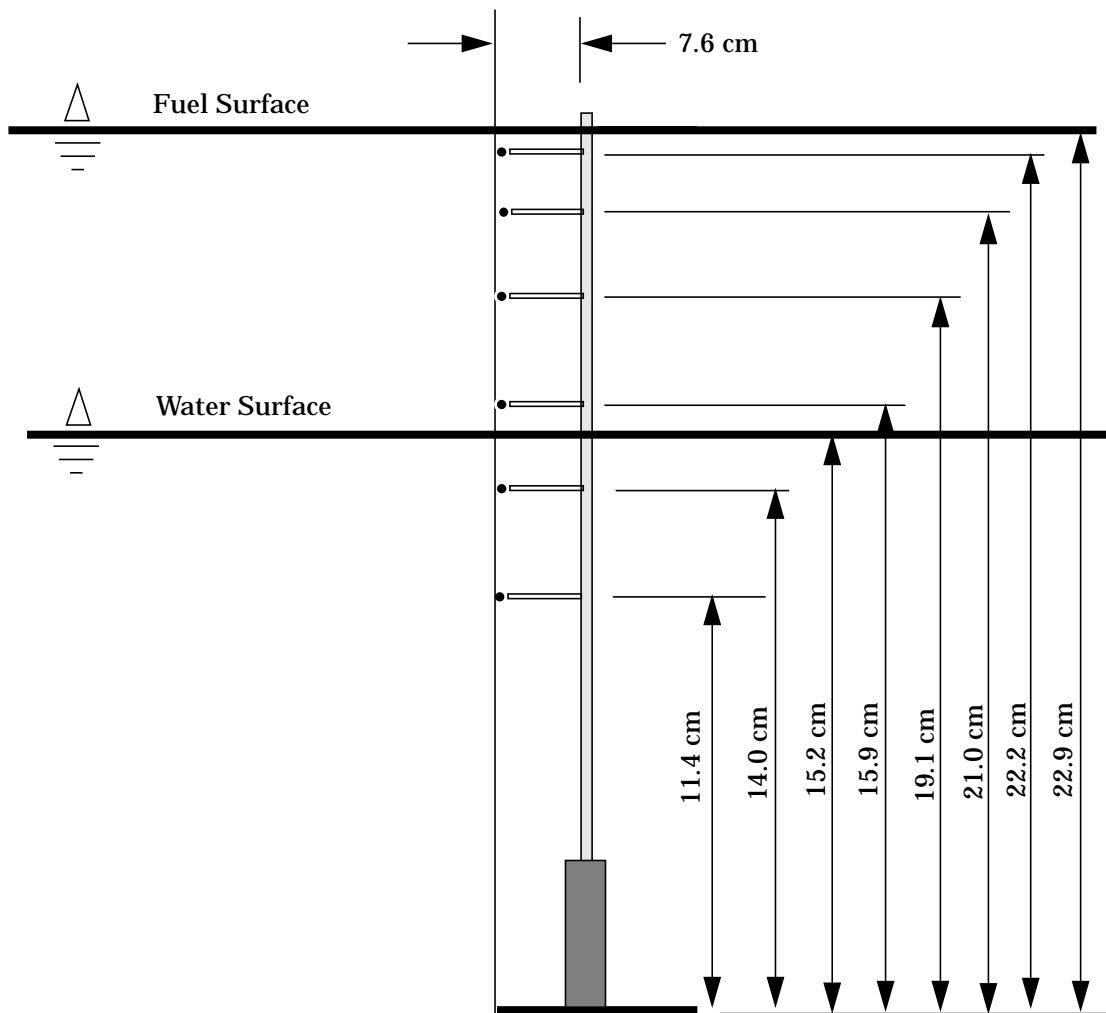
Figure 2.10 - Stand-Off Radiative Flux Gauge Mounting Assembly

A

2.54 cm Ceramic Fiber Insulation
Wire in Place

Foil Calorimeter

Support Link
Typ. 2 plcs

Plate, 0.3 cm
Mild Steel
Typ. 2 plcs

$45^{o}<\phi<90^{o}$

ϕ

Counterweight
to Prevent
Toppling

A

20.3 cm

Thermocouple
Mounted with
Nichrome Strips

20.3 cm

12.7 cm

7.6 cm

10.2 cm

30.5 cm

Front Facing View From A-A

18
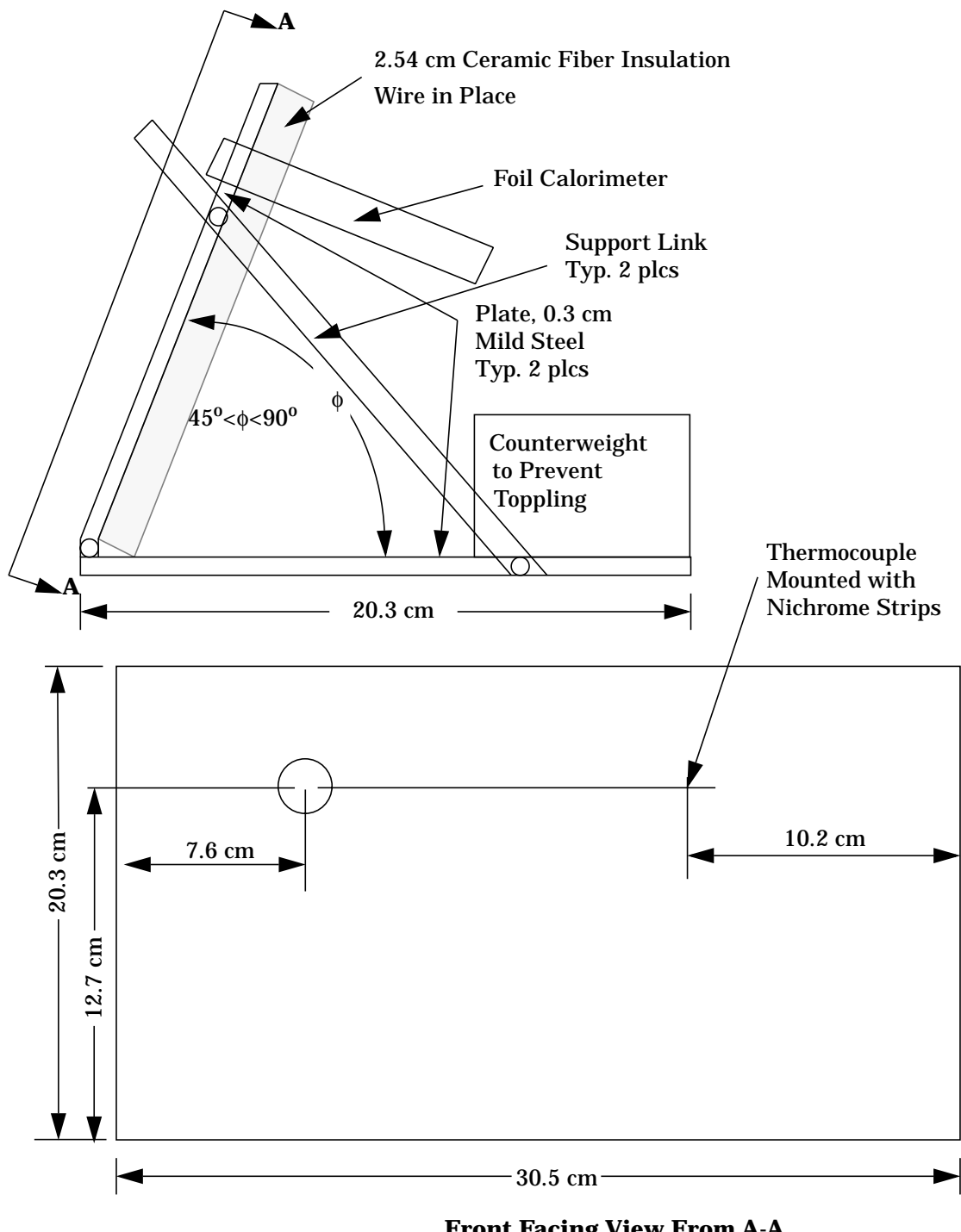
Figure 2.11 - Thermocouple (TC) tower

0.46

0.91

0.91

0.91

0.91

~ 0.30

Fuel Surface

All dimensions are in meters.
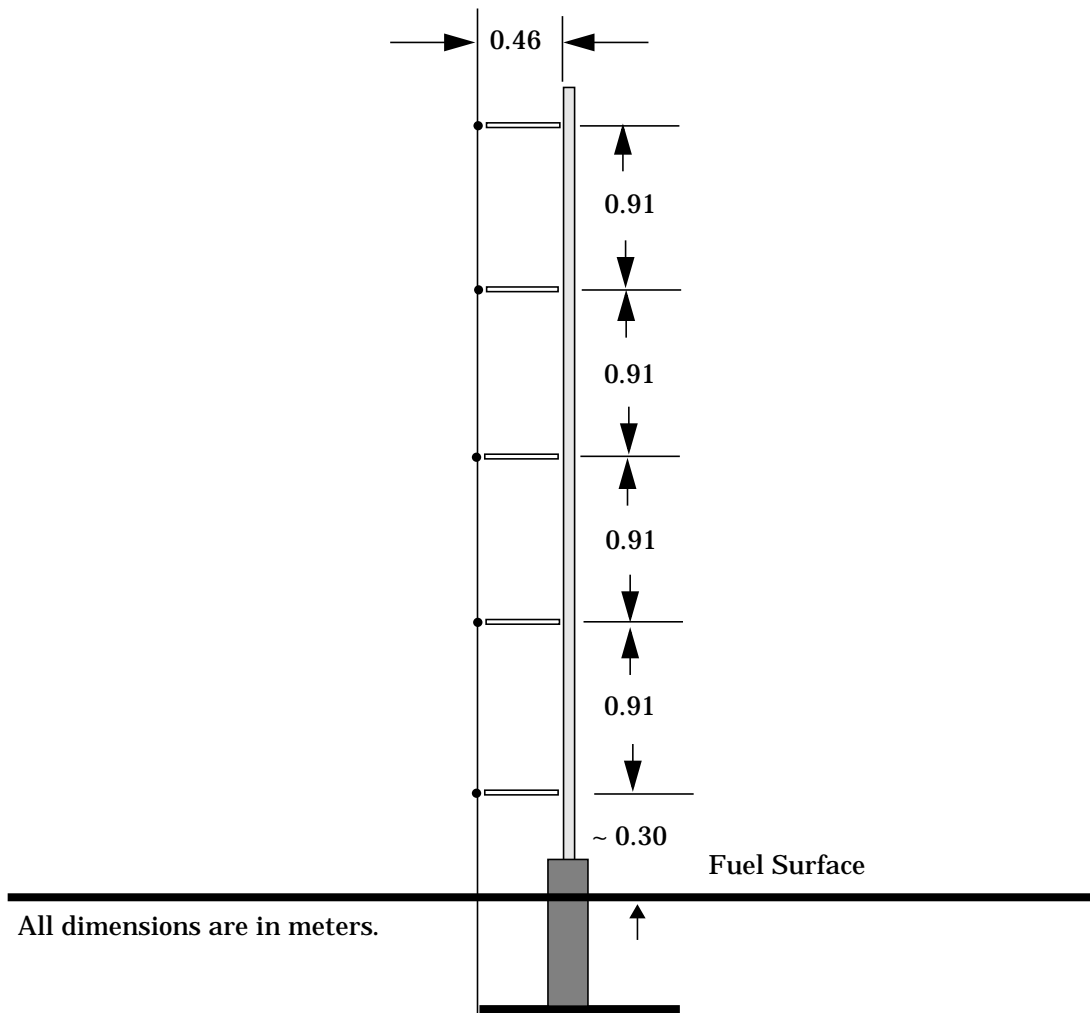
supported by mobile slip-fit stands, are depicted in Figure 2.11. The thermocouples were fastened to the towers to make measurements at 0.3-, 1.2-, 2.1-, 3.0-, and 4.0- m above the fuel surface. The minimum horizontal distance between the towers and the thermocouple junction was 0.46 m. To ensure fire survivability of the towers and thermocouples, the interior of the towers was water-cooled, and the exterior was insulated with a 2.54 cm thick ceramic fiber blanket insulation.

Figure 2.7 illustrates the position of the TC towers for the 20 m diameter pool configuration. For this condition, seven towers were positioned along the centerline of the pool. Of the seven towers, four were located on the windward side of the mock fuselage, and three were located outside the pool on the leeward side of the mock fuselage.

Ten additional towers were symmetrically positioned on both sides of the pool centerline. Of the five towers on each side of the centerline, three were located within the pool, and two were located outside the pool on the leeward side of the mock fuselage. Twelve were positioned such that the thermocouple beads were directly above the single-sided, upward-facing HFG's. At these locations, the towers were located 0.46 m downwind from the corresponding HFG, and the towers were aligned such that the thermocouples were parallel to the prevailing wind direction. The vertical distribution of flame temperature directly above the surface HFG was expected to provide valuable insight into the nature of the fuel vapor dome.

All thermocouple leads from the TC towers were bundled and routed along the bottom of the pool to the junction box. For those towers located outside the pool, the thermocouple leads were insulated up to the point where they entered the pool.

For the 10 m diameter pool test conditions, Figure 2.8 gives the location of the thermocouple poles. Seven thermocouple towers were located within the pool on the windward side of the mock fuselage, and six towers were located outside the pool on the leeward side of the mock fuselage.

2.3.11 Wind Condition Instrumentation

Wind speed and direction was measured sufficiently far from the boundary of the pool to reduce the influence of air entrained by the fire from the surrounding environment and the potential effects of radiant heat from the fire. As shown in Figure 2.12, measurements were performed approximately 30 m upwind of the leading edge of the pool at two locations 30° on either side of the prevailing wind direction. To determine the vertical velocity distribution, the measurements were made at elevations of 1.8 m, 5.5 m, and 9.1 m above the ground surface for both locations.

Wind measurements were performed using vane-type gauges. The gauges were calibrated within the stated accuracy of the instruments and a consistency check was performed to ensure that gauges provided the same indication of speed and direction when placed in the same location.

2.4 Photometric Coverage of the Fire Plume and Interior of the Mock Fuselage

Video camera coverage of the fire was acquired at four locations. The vertical field of view for all four cameras initially extended from the pool surface to a height of approximately 54.9 m above the pool surface. As appropriate during the test, the vertical field of view of all of the cameras was adjusted to encompass the entire

height of the continuous flame zone. Camera 1 was located 270° clockwise from the prevailing wind direction, as shown in Figure 2.13. The horizontal field of view of Camera 1 extends from about 90 cm downwind of the pool leading-edge to about one pool diameter downwind of the pool. Camera 2 was located 180° clockwise from the prevailing wind direction, and Camera 3 was aligned with the prevailing wind direction. The horizontal field of view of Cameras 2 and 3 extended to about 3 m on either side of the pool. The fourth camera was a permanent camera which was located on a tower approximately 12.2 m above the pool surface.

Digital, color infrared video data was obtained for the duration of the test. Positions of the digital infrared cameras coincided with Cameras 1 and 2. In addition, a video camera with a light was located within the interior of the mock fuselage to allow flame egression to be assessed. The field of view of the camera included the entire length of the mock fuselage.

Figure 2.12 - Position of wind measurements
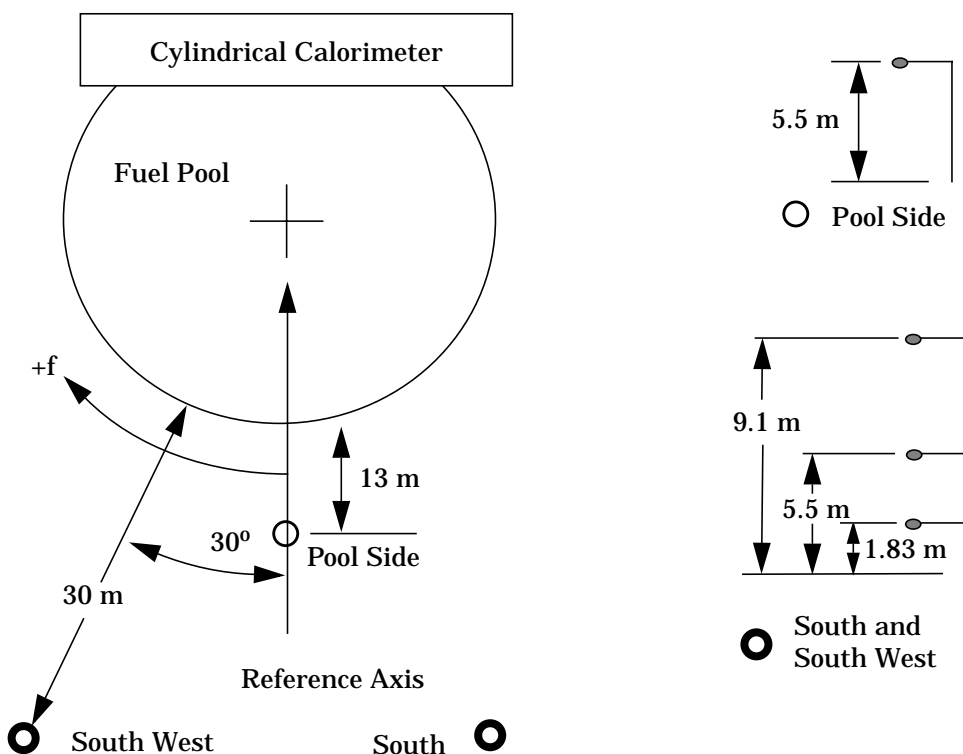
Figure 2.13 - Position of the video cameras around the pool

Camera 2
& Color IR

Field of
View

Initially Set to **D** - Adjust to
End of the Continuous Flame Zone

Camera 1
& Color IR

Field of
View

Pool of Diameter **D**

~ 3.0 m
Typ.

~ 0.91 m

Prevailing Wind Direction

Field of
View

Camera 4
Tower Camera
(Fixed)

Note: The Field of View for ALL
      Cameras Should Include the
      Entire Continuous Flame Zone

Camera 3
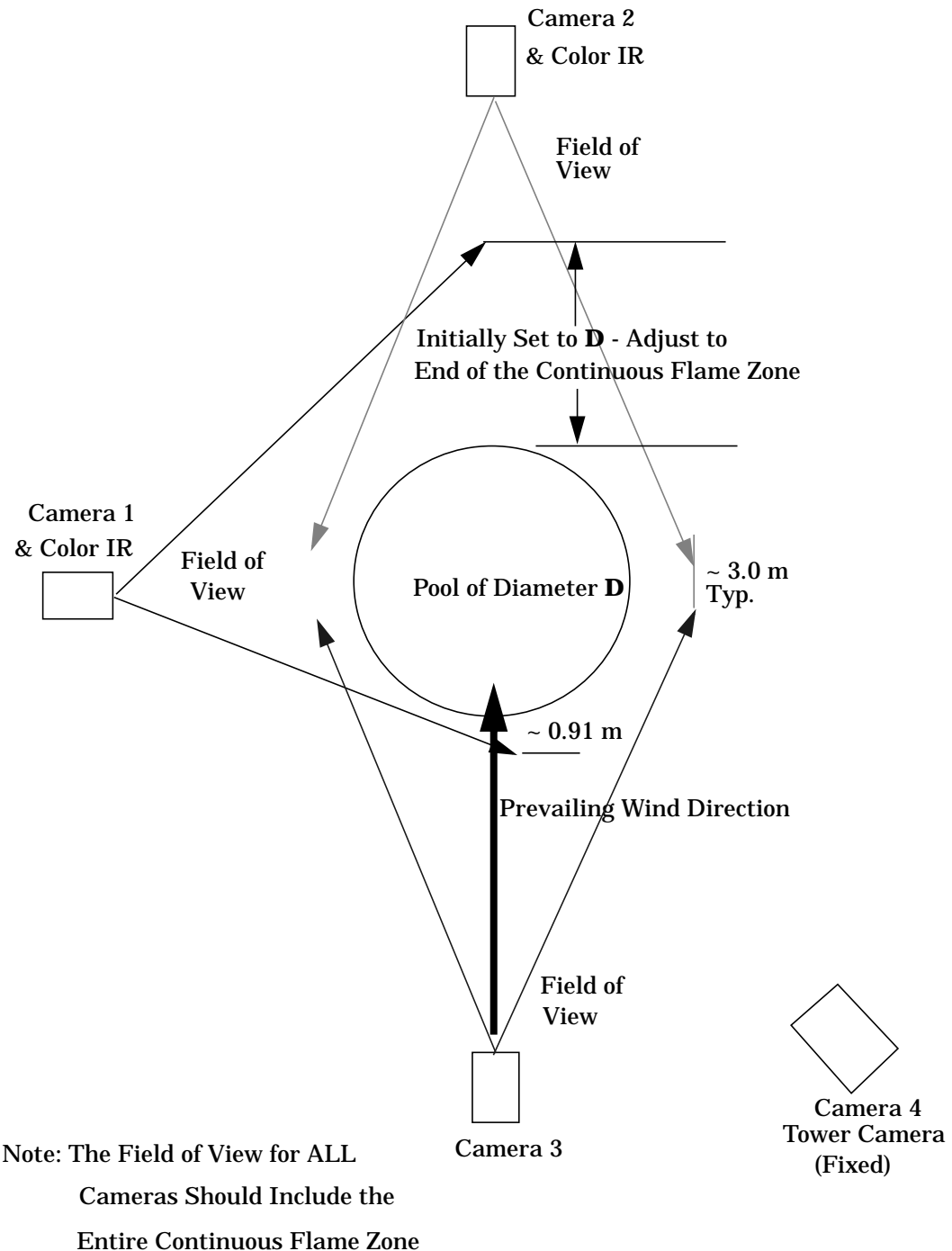
2.5 Sampling of Fuel

Samples of the hydrocarbon fuel (JP-8) were taken at the time the fuel was poured into the pool, prior to igniting the fuel. The samples were used to characterize the combustion properties of the fuel. The samples were archived by NAWCWPNS for a period of time not to exceed one year following the test.

2.6 Data Acquisition and Summary

A summary of the Type-K thermocouple data acquired is given in Table 2.1. The integrity of all channels was evaluated prior to each test. Data were sampled simultaneously for all channels, at a rate of one sample per second (with the exception of the gardon gauges). Sampling started approximately two minutes (+/-1min) prior to ignition of the fuel, and continued until two minutes (+/- 1min) after all of the fuel was consumed. Temperature and wind data are provided in magnetic disk files, and the files give temperature values in Fahrenheit, wind speed values in m.p.h., and wind direction in degrees referenced to the prevailing wind direction. Following the test, all data (temperature, wind, and video) was normalized to include a common timing reference (e.g., time of fuel ignition).

Table 2.1: Summary of the Type-K Thermocouple Instrumentation

Instrumentation	No. of Gauges	TC/Gauge	No. of TC
Upward facing HFG's	20	1	20
Fuel Temperature	2	6	12
Subtotal			**32**
	No. of Poles	TC/Pole	No. of TC
TC Poles	17	5	85
Subtotal			**85**
Mock Fuselage - Heat Flux Gauges	No. of Gauges	TC/Gauge	No. of TC
SNL Single Sided HFG Section B-B	18	1	18
SNL Single Sided HFG Section A-A	9	1	9
SNL Single Sided HFG Section C-C	2	1	2
Subtotal			**29**
SNL Double Sided HFG Section B-B	24	2	48

Table 2.1: Summary of the Type-K Thermocouple Instrumentation

Instrumentation	No. of Gauges	TC/Gauge	No. of TC
SNL Double Sided HFG Section A-A	12	2	24
Subtotal			**72**
NAWC Heat Flux Gauges Section A-B	6	1	6
NAWC Heat Flux Gauges Section A-A	4	1	4
NAWC Heat Flux Gauges Section C-C	2	1	2
Subtotal			**12**
Mock Fuselage -- Thermocouples	**No. of Stations**	**TC/Station**	**No. TC**
Axial Stations -- Near HFG	6	8	48
Axial Stations -- Away from HFG	2	4	8
End Plates	2	1	2
Spine	3	1	3
Spokes	3	1	3
Subtotal			**64**
Thermocouples - HFG/TC Array	**No. of Stations**	**TC/Stations**	**No. TC**
At 0 Degrees	3	3	9
At 45 and 315 Degrees	3	7	21
At 90, 135, 180, 225, and 270 Degrees	3	30	90
Subtotal			**120**
GRAND TOTAL			**414**

3. Experimental Results - Wind Conditions

3.1 Overview

Results presented here include a general description of the wind measurements obtained during the experiments and the identification of periods of quasi-steady behavior to be used for temporal averaging of the results.

3.2 Wind Conditions

The wind conditions are defined by the direction and speed of the winds at the test facility as measured at the locations presented in the previous chapter. Changes in the wind conditions are primarily responsible for the changes in the continuous flame zone and the measured temperatures and heat fluxes. Wind directions are specified in terms of the direction of the wind vector, where the reference axis corresponds to zero degrees and angles clockwise from the reference axis are positive (see Figure 3.1). A wind direction of 180° is hence in the opposite direction of the reference axis.

Wind measurements from all locations (South, Southwest, and Poolside poles) are provided to allow improved boundary condition specification for fire field model simulations performed to compare model predictions and experimental data. As expected, the wind data generally show an increase in wind speed with increasing elevation due to boundary layer effects at the ground surface. These data will be displayed in graphs following a description of the individual tests. Some deviation in wind direction, most likely due to variations in site topography and the presence of nearby structures, is also evident in the wind data. Data from the Poolside location is included for relative information only since these measurements will be affected by air entrainment by the fire and fire-induced heating of the gauge. Since the measurements acquired at the maximum elevation are least subject to ground and topography effects, an average of the measurements from the South and Southwest locations at an elevation of 9.1 m is taken as the representative wind condition for each interval.

In the first two tests, the wind data were acquired using only two poles, denoted S1 and SW1 in Figures 3.1-3.2. Wind measurements were acquired at one elevation (5.5 m) above the ground. These poles were located approximately 30 m from the windward edge of the fuel pool, at an angle of 30° on either side of the reference axis (the same location as South and Southwest poles in all other tests). The average of both poles was taken as the representative wind condition for the interval for tests 1 and 2.

3.2.1 Wind Measurements for Test 1

Wind data for Test 1 were recorded at two measurement locations. This test, along with Test 2, used wind instrumentation that differed from the other tests conducted in the same test series. Figure 3.1 shows the wind variation throughout the testing period. Test 1 was classified as a medium wind speed test. The wind speed remained relatively constant throughout the test except for a peak of approximately 7.0 m/s at 750 seconds following ignition. The average wind speed during the test was 4.0 m/s. The wind direction was also stable at approximately 25° for the majority of the test, with the exception of a brief period of winds at 60° around 150 seconds and a brief period of -35° winds 400 seconds after ignition.

3.2.2 Wind Measurements for Test 2

The wind data for Test 2 were also recorded by two weather stations located approximately 30 m from the windward edge of the pool. Figure 3.2 displays the variation in wind direction and speed during the fire. Test 2 was classified as a low wind speed test. The wind speed was stable throughout the entire test. The maximum deviation from the average wind speed of 2 m/s was approximately 0.5 m/s. The wind direction varied considerably from the average direction of -40°

Figure 3.1 - Wind Speed and Direction - Test 1

27
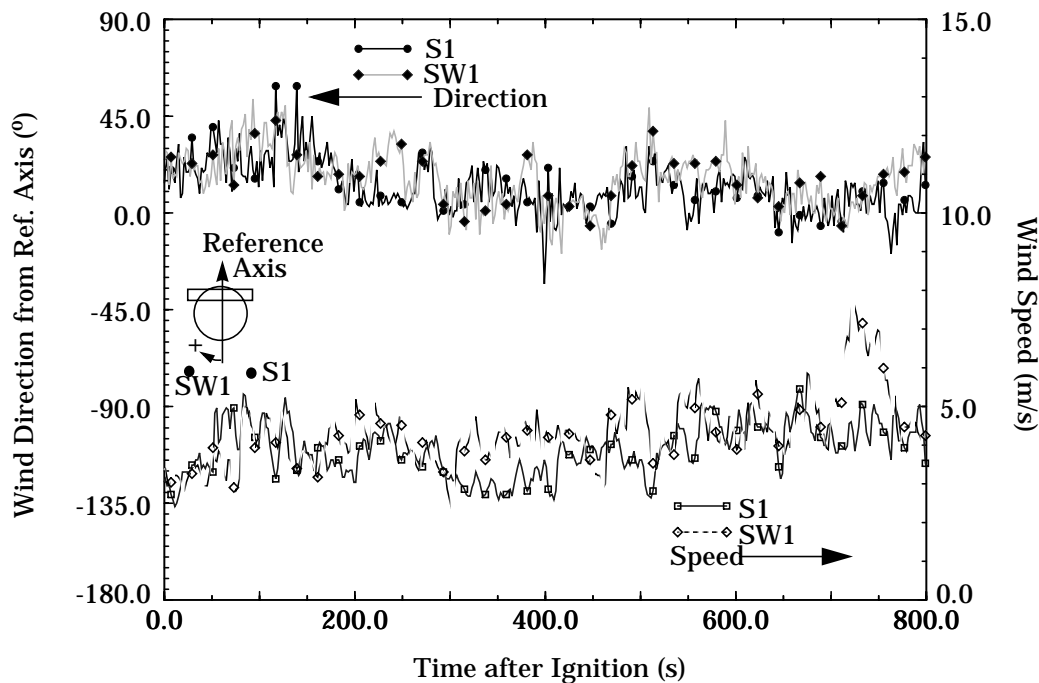
Figure 3.2 - Wind Speed and Direction - Test 2
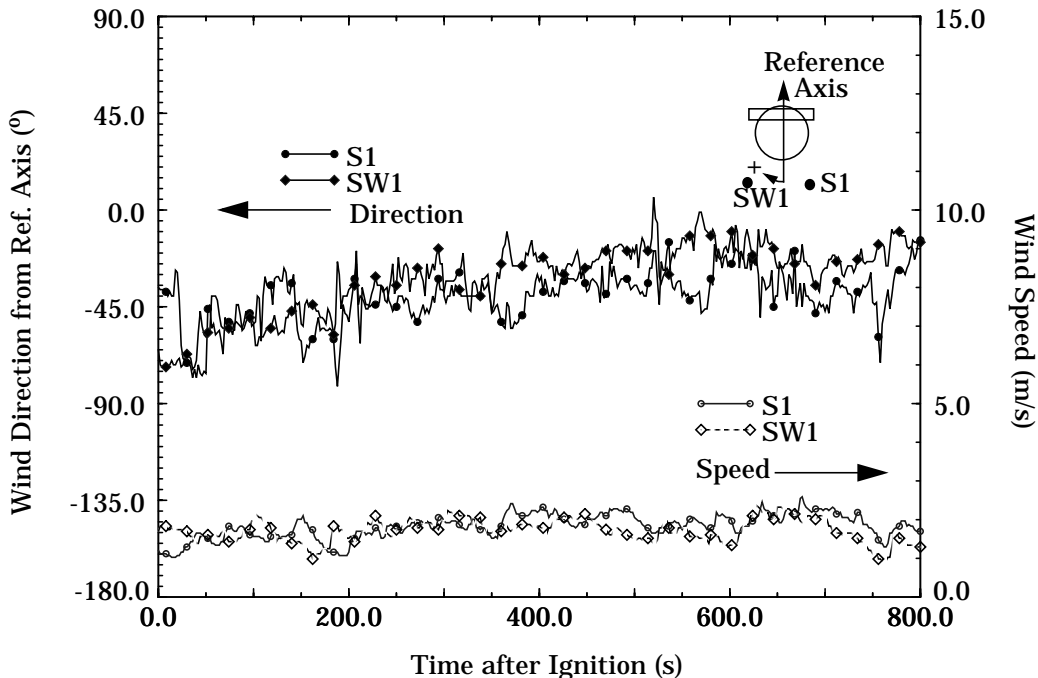
especially in the beginning and the end of the test. The wind direction appears to be moving slowly clockwise over the course of the test. A variation of approximately 25° from the average wind direction of 40° was observed in the results. The most stable time period, for both wind speed and direction, occurred in the middle of the test from 225 to 500 seconds after ignition.

3.2.3 Wind Measurements for Test 3

The wind data from Test 3, a high wind speed test, are shown Figures 3.3-3.5 for wind data collection poles labeled Poolside, South, and Southwest, respectively. The data recorded by all three poles display a steady oscillation of wind speed and direction throughout the test. The wind direction fluctuated from -40° to 35°, with the average of -20°. Wind speeds range from 5 m/s to 15 m/s, with an average wind speed of 10 m/s. The Poolside pole measurements display the most significant fluctuations most likely due to the close proximity of this gauge to the fire. The data recorded by the gauge on the pole near the fuel pool will be affected by the air entrained by the fire and the heating of the gauge. These Poolside gauge measurements were not used in calculating the representative wind speed and direction.

28

Figure 3.3 - Poolside Wind Speed and Direction - Test 3

Wind Direction from Ref. Axis (º) / Wind Speed (m/s)

Reference Axis

5.5 m Direction

5.5 m Speed

PS

Time after Ignition (s)
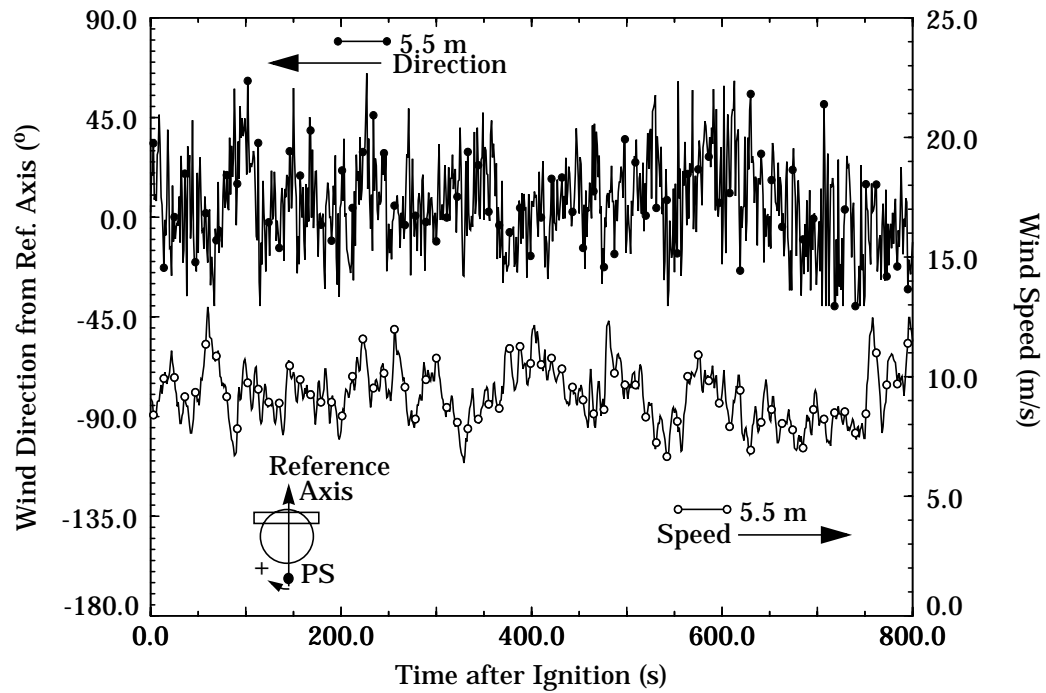
Figure 3.4 - South Wind Speed and Direction - Test 3

Wind Direction from Ref. Axis (º) / Wind Speed (m/s)

Reference Axis

S

1.83 m
5.5 m
9.15 m
Direction

1.83 m
5.5 m
9.15 m
Speed

Time after Ignition (s)

29
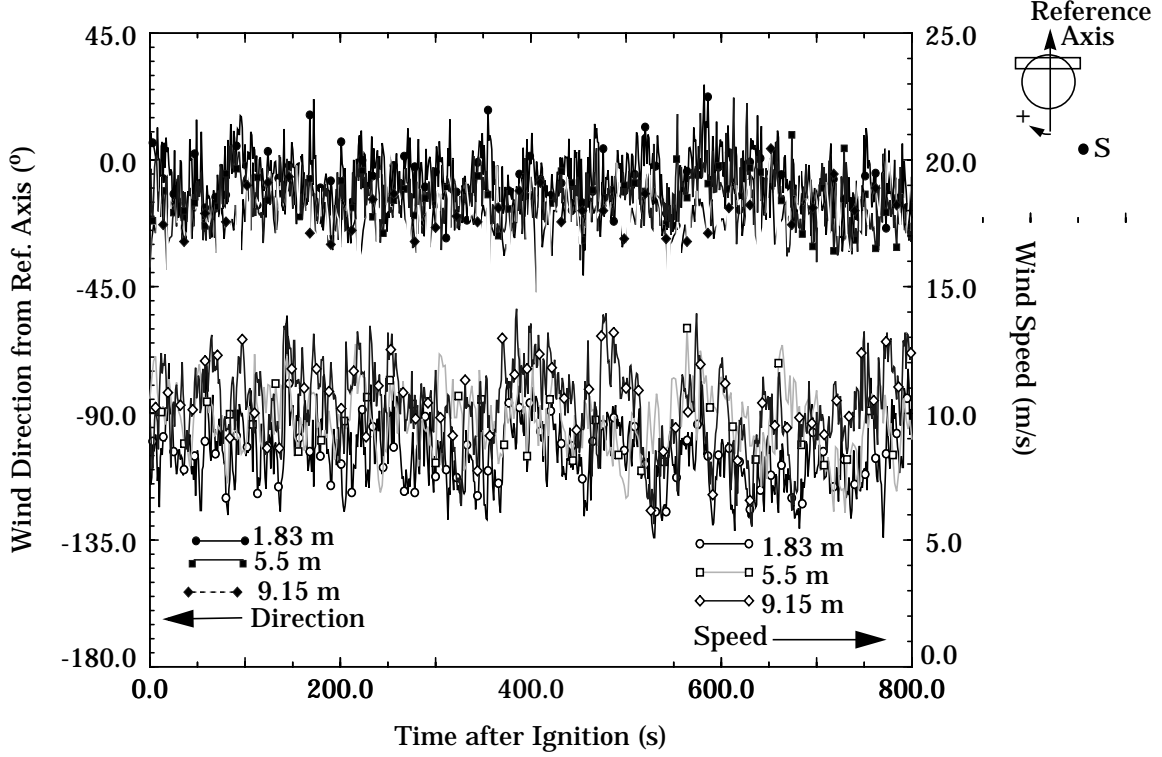
Figure 3.5 - Southwest Wind Speed and Direction - Test 3
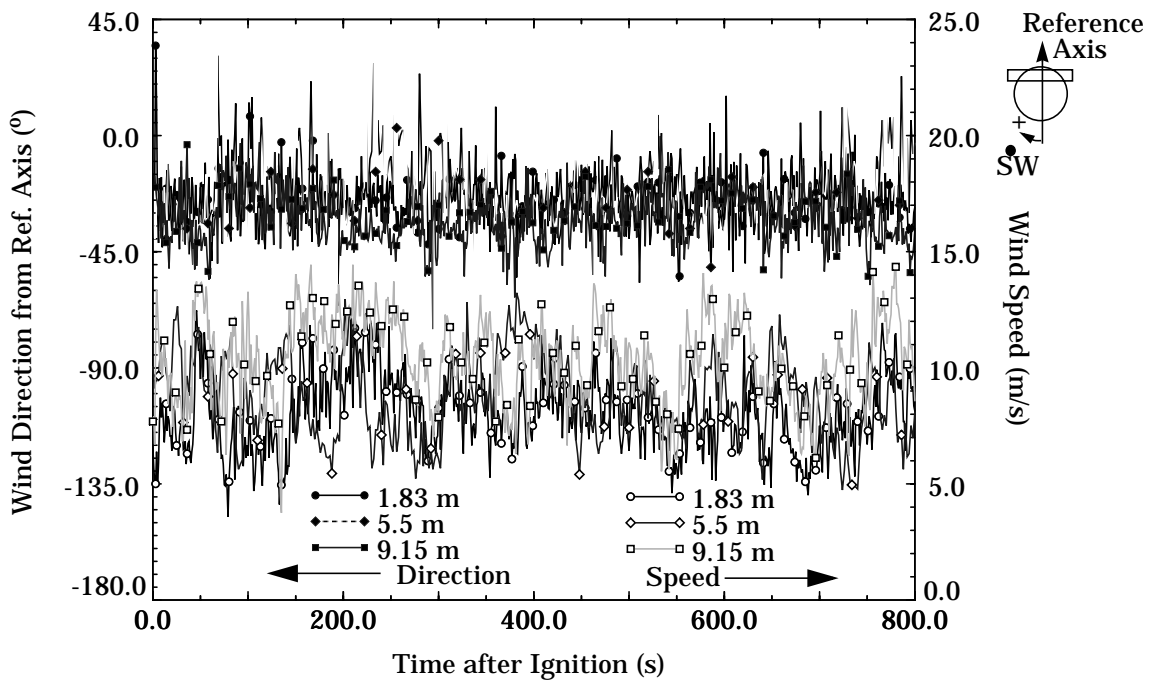
3.2.4 Wind Measurements for Test 4

The wind data from Test 4, a medium wind speed test, are shown in Figures 3.6-3.8 for Poolside, South, and Southwest wind data collection poles, respectively. The wind speed fluctuated between 3 m/s and 7 m/s with an average speed of approximately 5 m/s. The test began with a wind speed of 5 m/s. The speed dropped to 3 m/s at 50 seconds after ignition before increasing to 7 m/s around 150 seconds after ignition. Winds were reasonably steady at a speed of 4 m/s between 350 and 500 seconds before increasing to 6 m/s by the end of the test.

The wind direction data were less stable than the wind speed data. Major fluctuations between -55⁰ and 45⁰ occurred throughout the testing period. Malfunctioning of the Poolside pole in Figure 3.6 is shown as a distinct minimum value of -40⁰ being repeatedly recorded by the gauge. This "fall out" is believed to be due to heating of the gauge. This trend was not seen in the South and Southwest poles which were further away from the fire.

Figure 3.6 - Poolside Wind Speed and Direction - Test 4
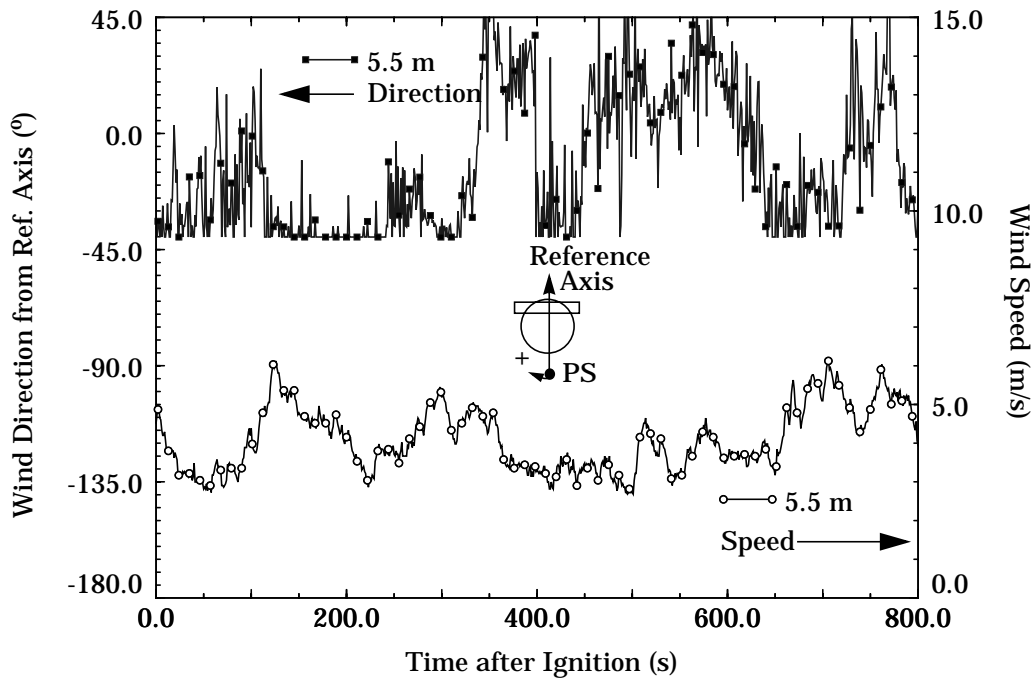
Figure 3.7 - South Wind Speed and Direction - Test 4

31
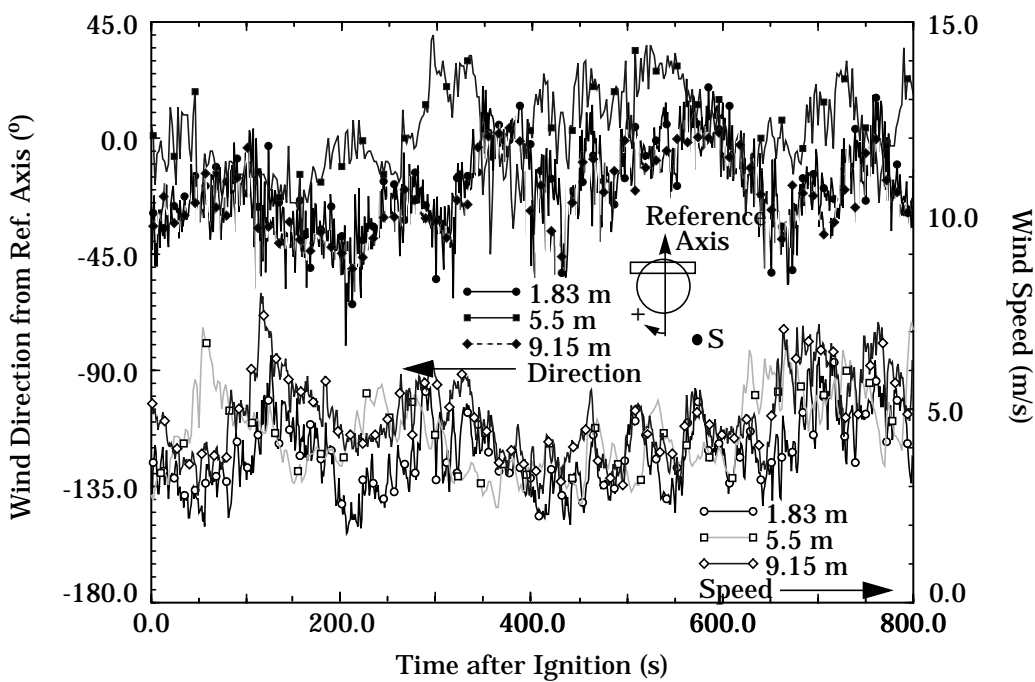
Figure 3.8 - Southwest Wind Speed and Direction - Test 4
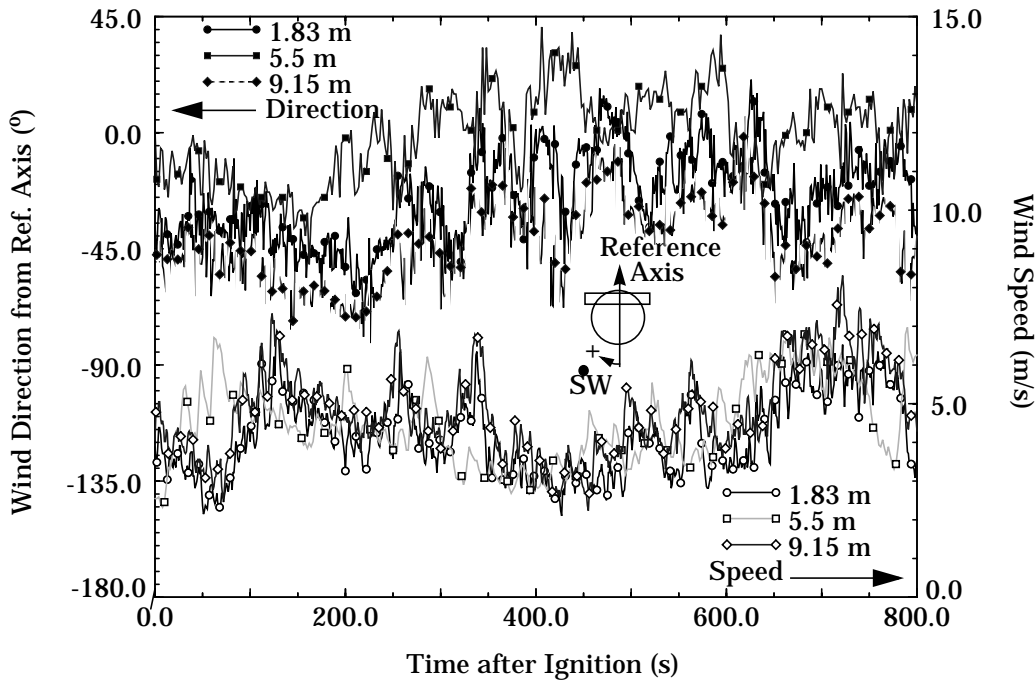
3.2.5 Wind Measurements for Test 5

The wind data from Test 5, a medium wind speed test, are shown in Figures 3.9-3.11 for Poolside, South, and Southwest wind data collection poles, respectively. The wind speed during Test 5 was highly variable. The wind fluctuated between 4 m/s and 14 m/s, with one stable period of approximately 5 m/s winds from 375-500 seconds. The maximum speed of 14 m/s occurred between 200-350 seconds after ignition. Following this time period, the winds decreased and remained stable at 5 m/s for about 150 seconds and then steadily increased for the remainder of the test.

The wind direction typically oscillated between -20⁰ and 20⁰ throughout the test with brief periods of winds over 30⁰ from the reference axis. Approximately 600 seconds after ignition, a brief period of winds with extreme variation between -45⁰ and 75⁰ was measured by all gauges. Measurements then returned to the normal range stated above.

Figure 3.9 - Poolside Wind Speed and Direction - Test 5
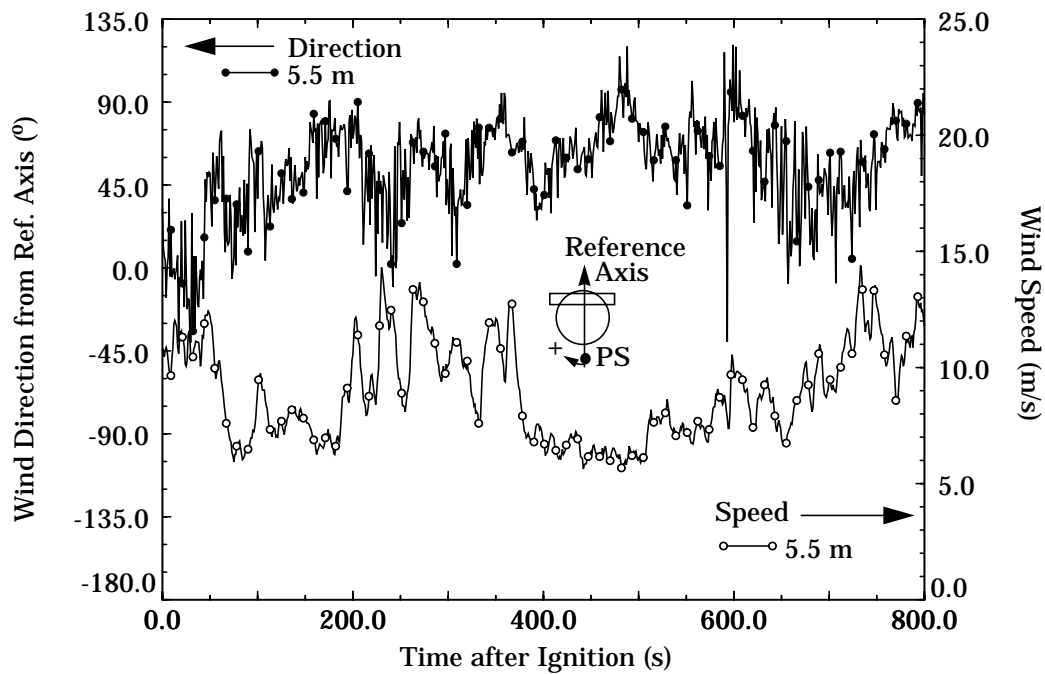
Figure 3.10 - South Wind Speed and Direction - Test 5

33
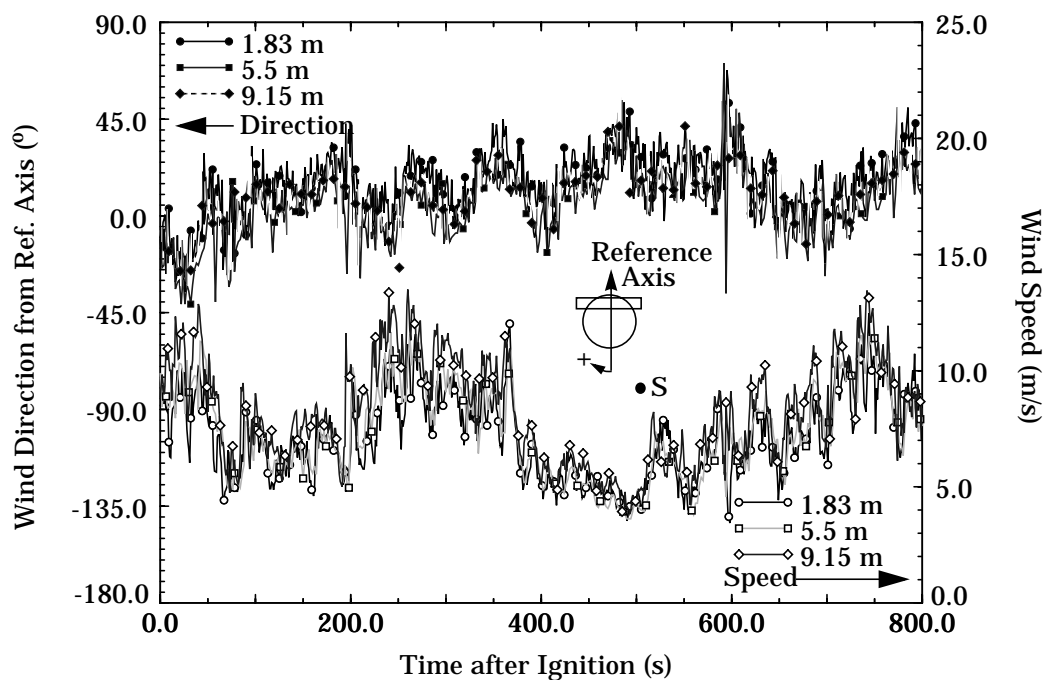
Figure 3.11 - Southwest Wind Speed and Direction - Test 5
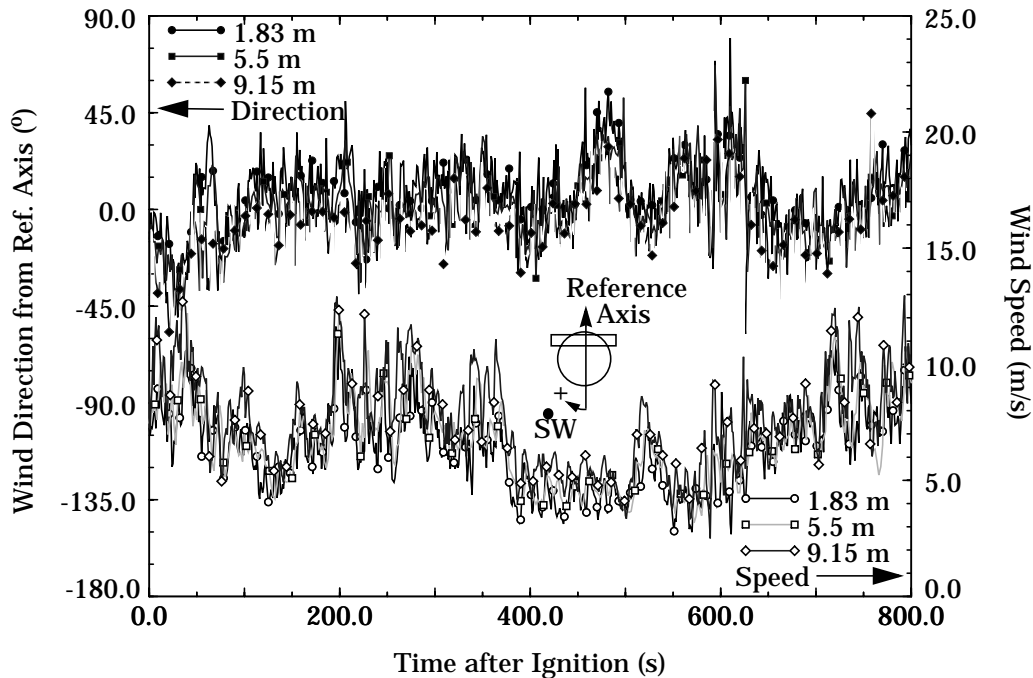
3.2.6 Wind Measurements for Test 6

The wind data from Test 6, a high wind speed test, are shown Figures 3.12-3.14 for Poolside, South, and Southwest wind data collection poles, respectively. The wind speed was stable after the fire had been burning for 250 seconds. Prior to this time, there was a slight decrease in wind speed, a short steady period, and then an increase in both the wind speed and direction. After 250 seconds, the wind became stable with speeds between 7 m/s and 11 m/s and an average speed near 10 m/s. In general, the wind direction remained between -10° and 30° for the duration of the test.

Figure 3.12 - Poolside Wind Speed and Direction - Test 6
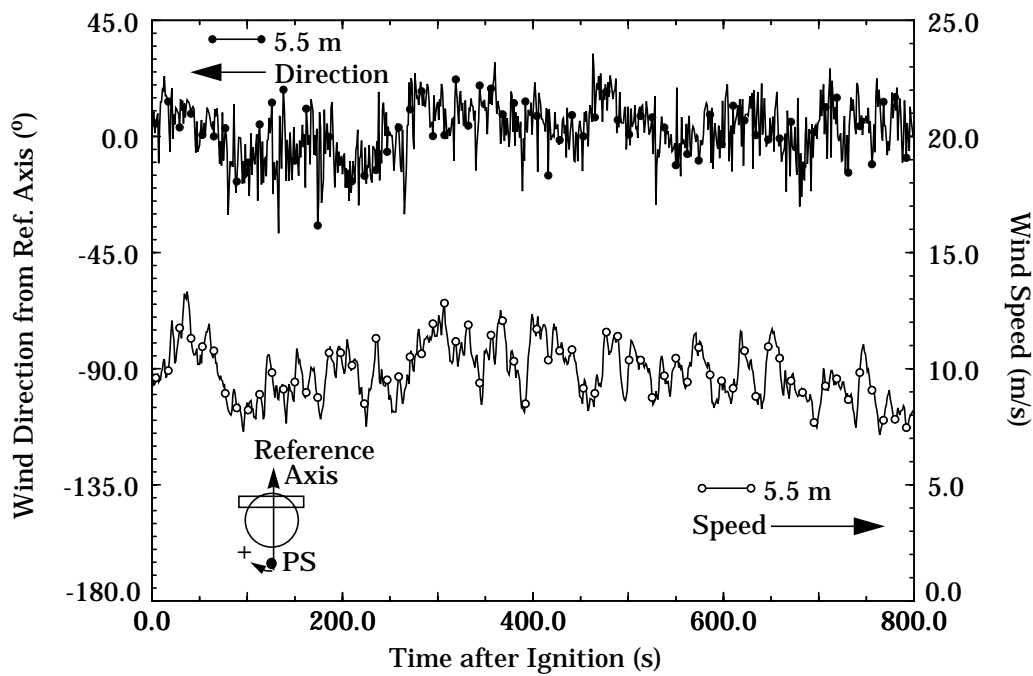
Figure 3.13 - South Wind Speed and Direction - Test 6

35
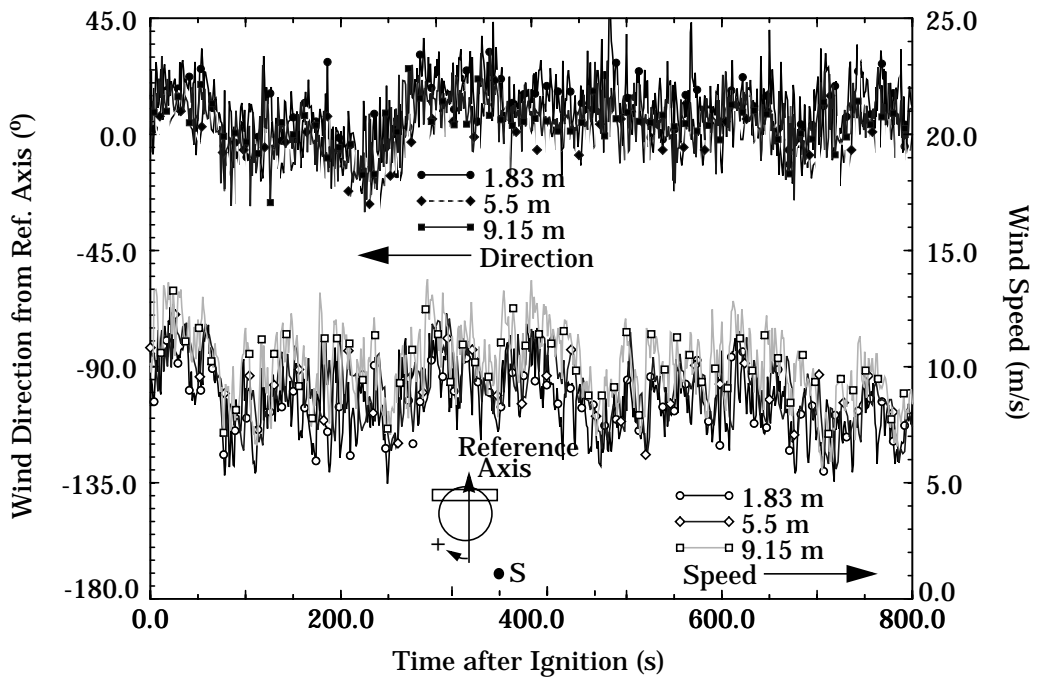
Figure 3.14 - Southwest Wind Speed and Direction - Test 6
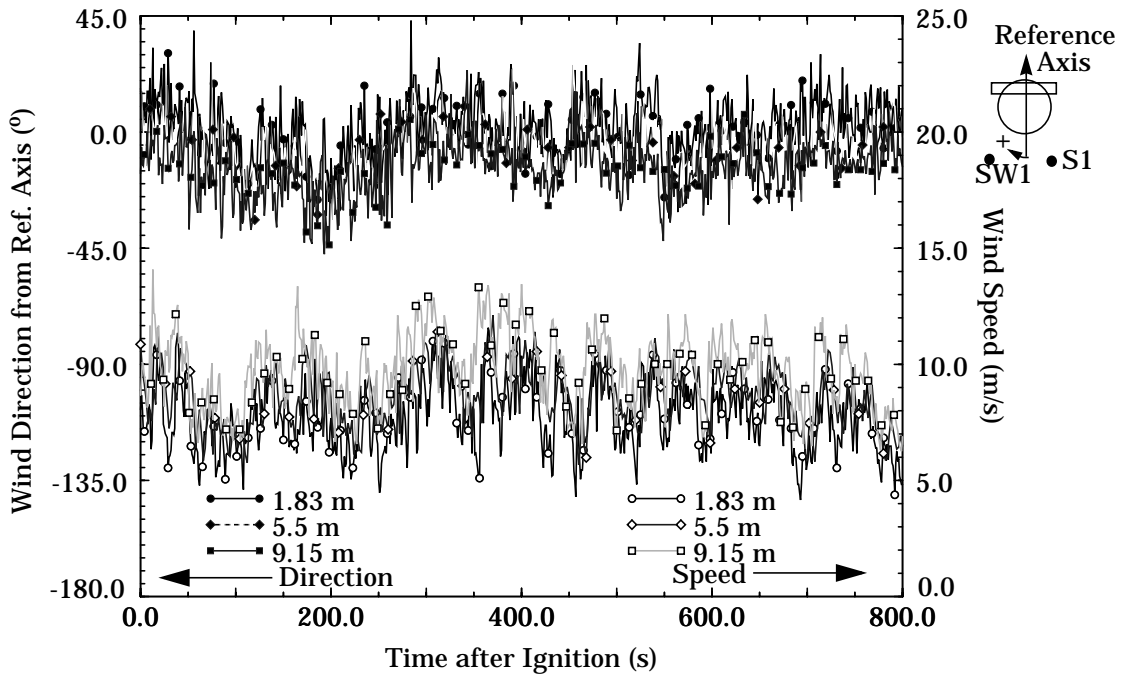
3.2.7 Wind Measurements for Test 7

The wind data from Test 7, a low wind speed test, are shown Figures 3.15-3.17 for Poolside, South, and Southwest wind data collection poles, respectively. Wind direction in Test 7 was not as stable as the wind speed. Winds were essentially calm for the test, never exceeding 3 m/s. The average wind speed was approximately 2 m/s, with occasional drops to almost 0 m/s. As expected, decrease in wind speed (<1 m/s) corresponded to erratic measurements (-160° to 60° in Figure 3.17) of the wind direction during the same time period since the wind direction measurement

Figure 3.15 - Poolside Wind Speed and Direction - Test 7
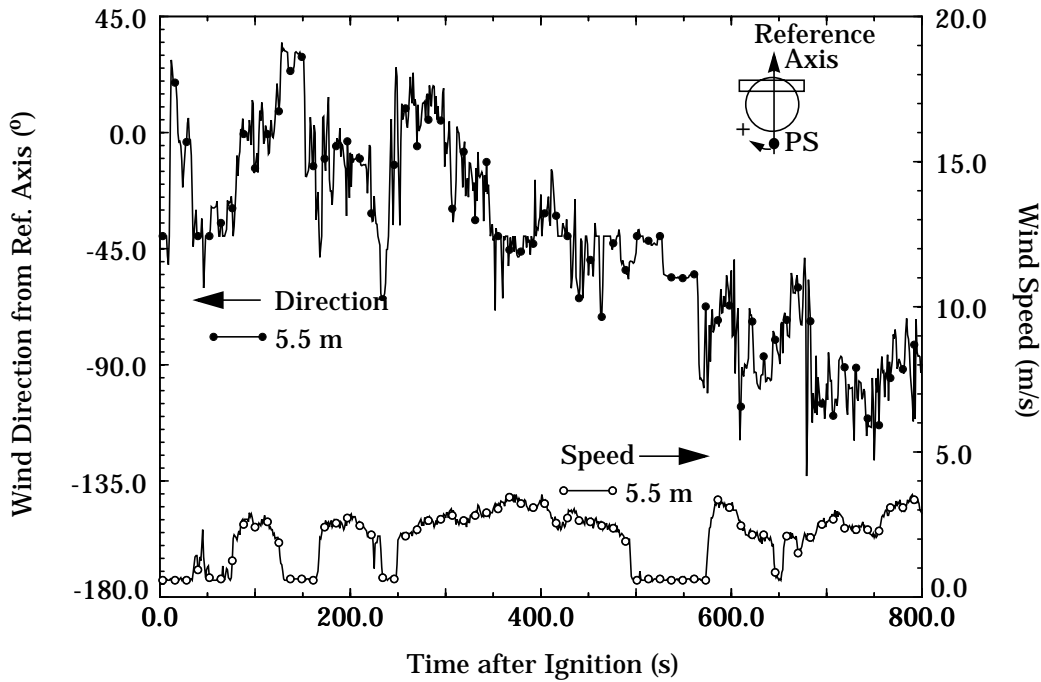
Figure 3.16 - South Wind Speed and Direction - Test 7

37
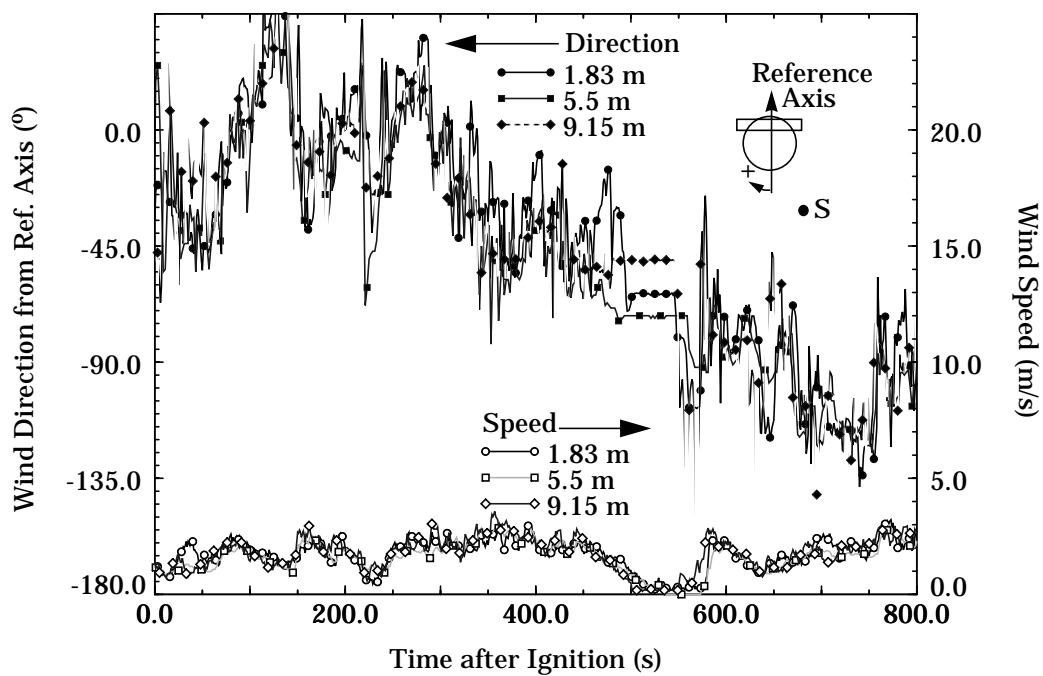
has less meaning under virtually calm conditions. At the beginning of the test, from 0 to 300 seconds, the wind direction fluctuated between -45° and 45° until it decreased steadily to wind directions of approximately -135°.

3.2.8 Wind Measurements for Test 8

The wind data from Test 8, a high wind speed test, are shown Figures 3.18-3.20 for wind data collection poles labeled Poolside, South, and Southwest, respectively. The line plots for wind speed and direction during Test 8 show generally steady winds with uniform oscillations about an overall steady average value. The wind speed fluctuated between 6 m/s and 14 m/s with a consistent average value of approximately 10 m/s. The direction ranged from 5° to -40°, with an average value of -20°.

3.3 Summary of Test Conditions

The mock fuselage test series included fires performed for a range of conditions to obtain a suite of experimental data for the previously stated purposes, including comparisons with fire models. The tests were classified as low (0-3 m/s), medium (4-7 m/s), and high (>8 m/s) wind conditions. The test series included a variety of wind

Figure 3.17 - Southwest Wind Speed and Direction - Test 7
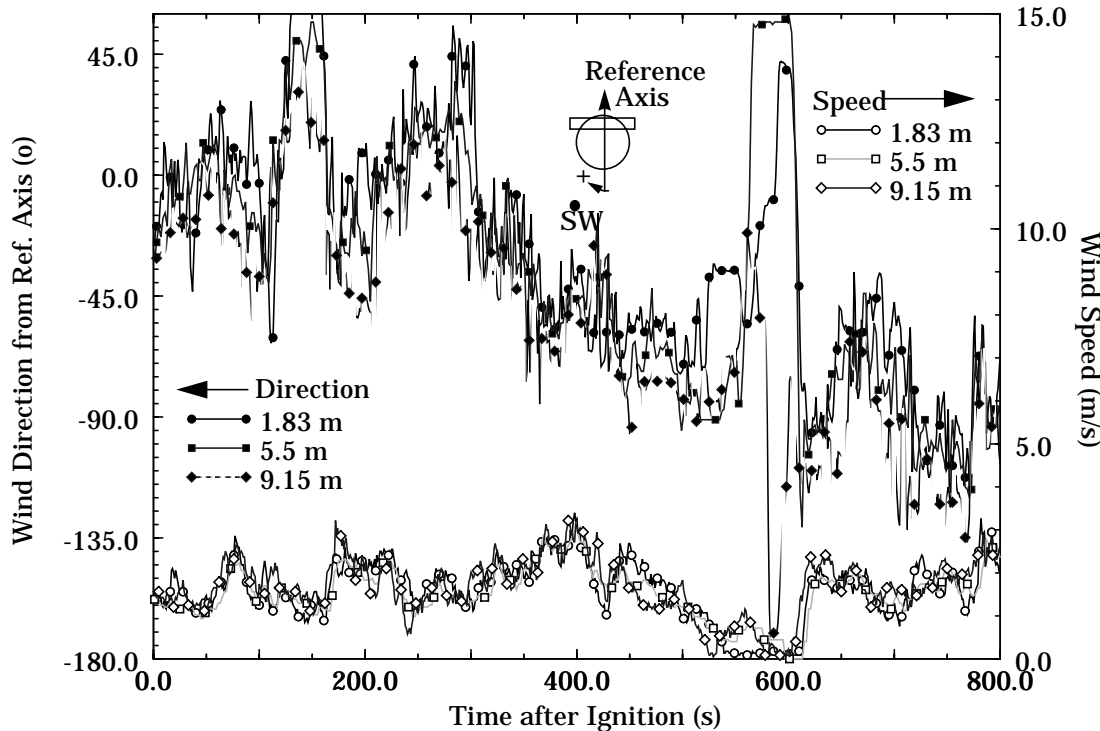
Figure 3.18 - Poolside Wind Speed and Direction - Test 8
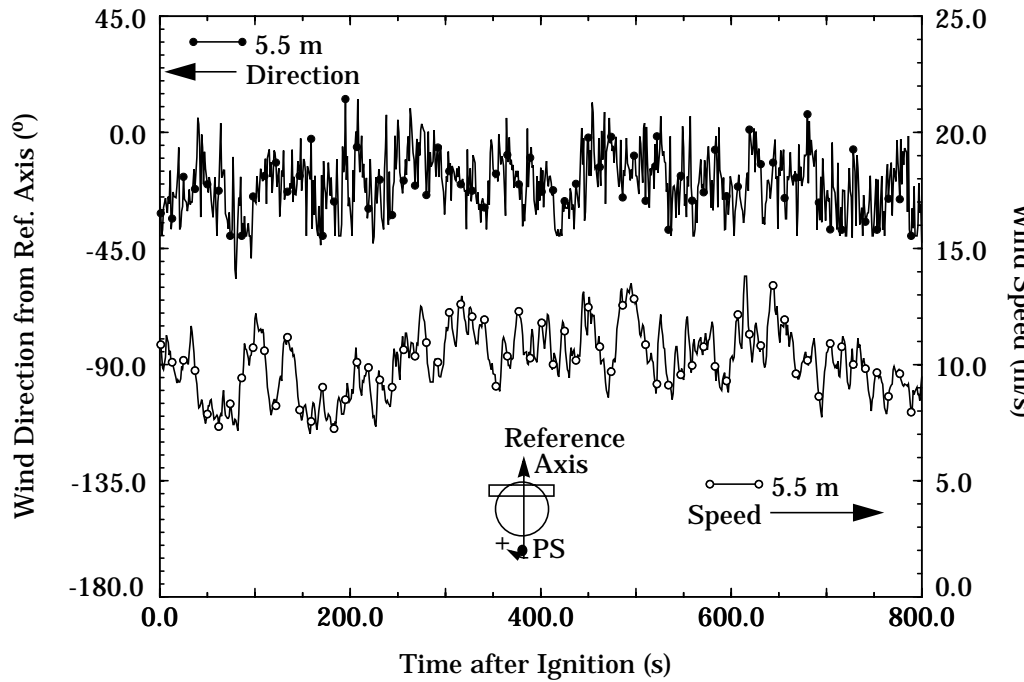
Figure 3.19 - South Wind Speed and Direction - Test 8

39
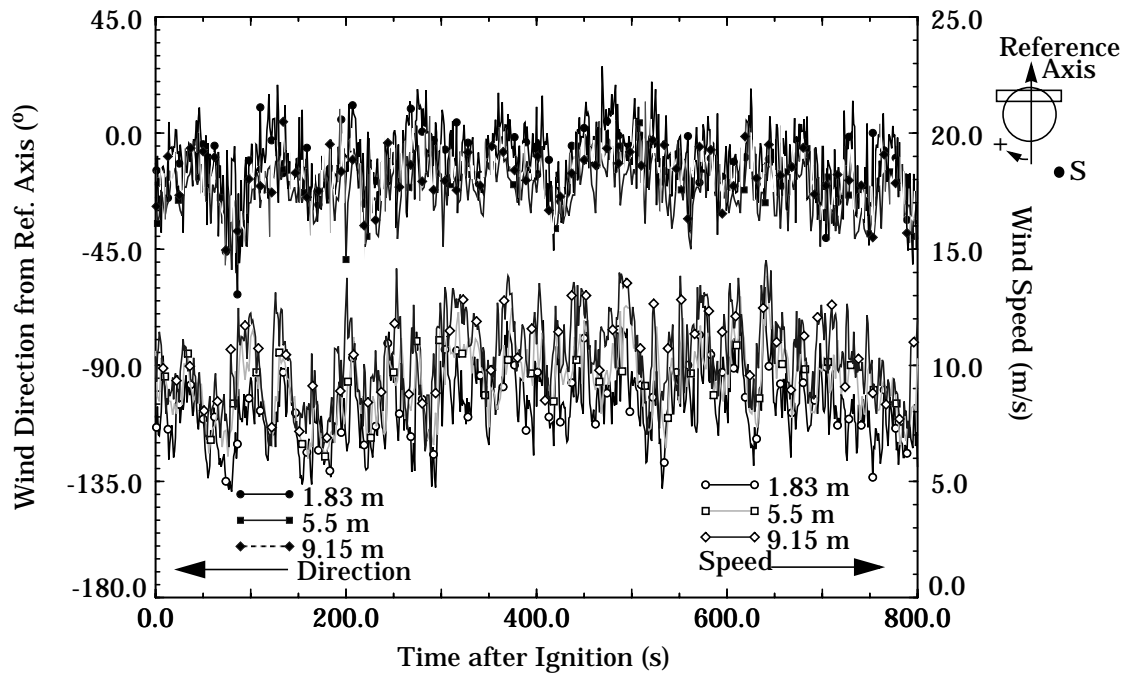
Figure 3.20 - Southwest Wind Speed and Direction - Test 8
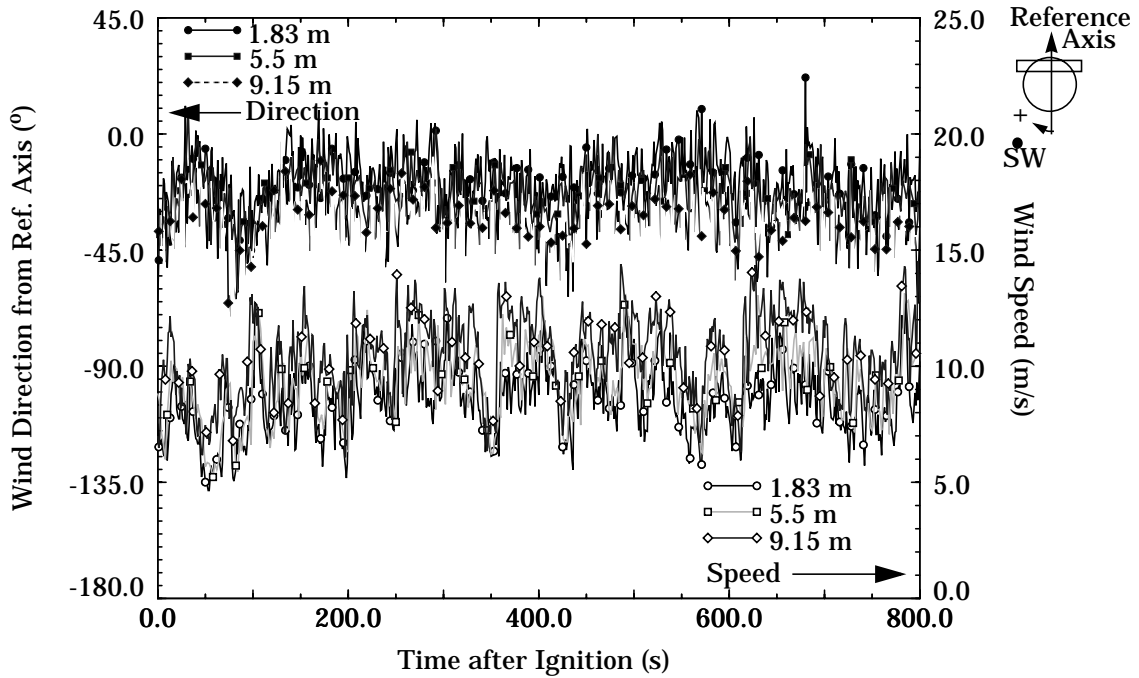
conditions for both the 10 m and the 20 m fuel pool fires. Low and high speed tests were conducted in the 10 m pool. One low, three medium, and two high speed tests were performed in the 20 m pool to allow for comparison and repeatability analysis of the results.

3.4 Periods of Quasi-Steady Behavior

Fire data are characterized by rapid changes in temperature and heat flux due to the interaction of instrumentation such as thermocouples and heat flux gauges with turbulent flame sheets. In order to spatially characterize the fire environment, data are averaged over a period of quasi-steady behavior. For each experiment, time periods of quasi-steady behavior were identified that follow ignition by a sufficient time for all initial fire transients to stabilize. The quasi-steady time periods, identified from the most stable periods of wind speed and direction, along with the wind conditions during the time period, are shown in Table 3.1. During these periods, no major changes in the flame geometry were observed in the video record of the experiment, and wind, temperature, and heat flux data oscillated uniformly about a constant mean value. The sections which follow focus on results obtained by averaging data over these time periods.

40

Table 3.1: Quasi-Steady Time Periods

Test Number	Time After Ignition (s)	Wind Speed (m/s) Avg. and Std. Dev.	Wind Direction from Reference Axis Avg. and Std. Dev.
1	300-480	3.8 $\pm$ 0.9 (MED)	26.2 $\pm$ 6.2
2	225-350	1.9 $\pm$ 0.2 (LOW)	-36.9 $\pm$ 5.7
3	300-600 680-715	10.2 $\pm$ 1.7 (HIGH) 8.6 $\pm$ 0.9 (HIGH)	-22.7 $\pm$ 8.3 -22.9 $\pm$ 9.8
4	120-240 360-480	5.1 $\pm$ 0.8 (MED) 3.6 $\pm$ 0.5 (MED)	-52.8 $\pm$ 5.3 -26.7 $\pm$ 16.2
5	400-575 250-670	5.4 $\pm$ 1.2 (MED) 6.7 $\pm$ 1.9 (MED)	11.4 $\pm$ 12.5 5.6 $\pm$ 13.7
6	270-390	9.5 $\pm$ 1.9 (HIGH)	2.0 $\pm$ 9.1
7	250-500	2.0 $\pm$ 0.6 (LOW)	-36.1 $\pm$ 25.4
8	475-598	9.9 $\pm$ 1.8 (HIGH)	-19.5 $\pm$ 8.0

4. Experimental Results - Flame Zone Contours

4.1 Overview of Experiments

Data from thermocouple arrays and thermocouple poles were reduced and assembled into contour plots of thermocouple temperatures at selected planes. The thermocouple measurement locations are shown in Figure 4.1. The contour plots show the flame zone of the fire during each quasi-steady time period. It is acknowledged that, due to several mechanisms including radiative transport and thermal inertia, the temperature measured by a thermocouple is not, in general, equal to the local media temperature [13]. Cost and robustness considerations, however, continue to dictate the use of thermocouples for spatial characterization of large fires. Contour plots along three measurement planes were produced for each time period. These plots present the data in a suitable format for time-averaged fire model comparisons. In the contour plots, a uniform temperature distribution of 510 K was applied at the fuel surface based on measured fuel temperatures. The range of temperatures shown is 300-1600 K. A temperature greater than 800 K is indicative of an actively burning region. Smoothing of the contour plots was not performed; therefore, some coarseness in the contours occurs as a result of the linear interpolation of values between experimental data points.

4.2 Large Pool Flame Shapes

The first six tests were conducted in a 18.9 m pool of JP-8 jet fuel. The measurement planes are at the centerline and approximately 6 m on either side of the centerline. The fire environment is instrumented as specified previously in Chapter 2. Differences in the actual test instrumentation and the specifications in Chapter 2, and the locations of malfunctioning thermocouples, will be stated as the results are presented in each section. Figure 4.1 shows the locations of the measurement planes, the thermocouples included in each measurement plane, and the variation in instrumentation in the different tests conducted. Note that the thermocouple arrays and thermocouple poles are not exactly aligned (0.5 m offset) in the side measurement planes but are still considered to be in the same measurement plane for these flame zone contours.

4.2.1 Flame Contours for Test 1

A quasi-steady time period was observed between 300 and 480 seconds following ignition for Test 1 (medium wind test). The time-averaged wind speed and direction from the reference axis were 3.8 m/s and 26.2⁰, respectively. A small diagram depicting the wind conditions during the time period is included in the contour plots.

Figure 4.1 - Location of Measurement Planes for Contour Plots- 20 m pool

TC Array

TC Pole facing right, i.e.

Note: A total of three planes are shown in the diagram. The view for the contours is from the right side of the pool. Tests 1 and 2 do not contain TC arrays A3-A7.

T12 T7 T17

T6

T1 T5 T16

A

A

T10 T15

T4

T3

T9 T14

T2

T8 T1 T13

Prevailing Wind

Section A-A

A1

A8 A2

Fuselage Model

A7 A3

A5

A6 A4

Fuselage

Thermocouple Measurement Locations (side view)

43
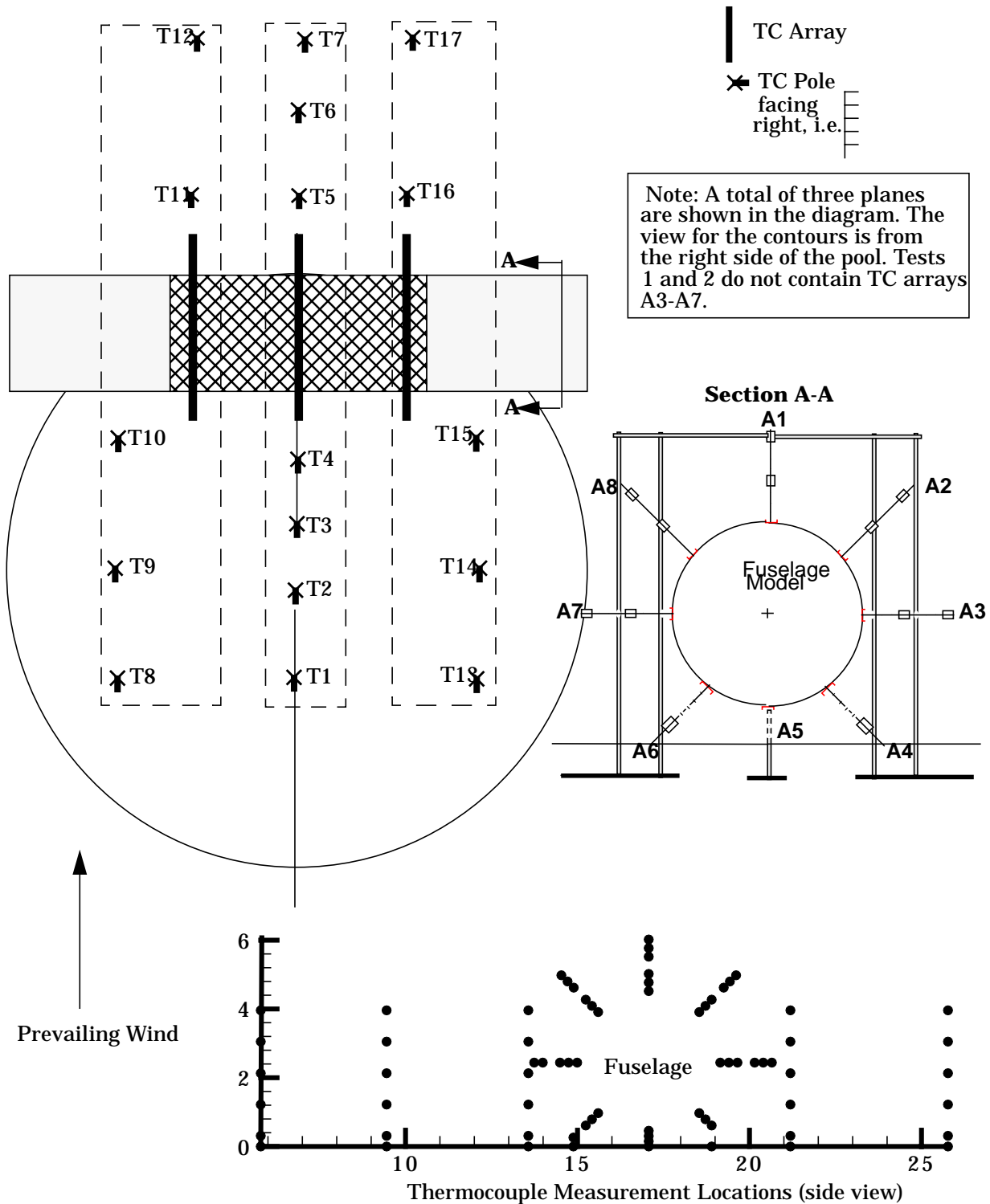
Figure 4.2 - Test 1 Thermocouple Temperature Contour, Windward of Center, 300-480s
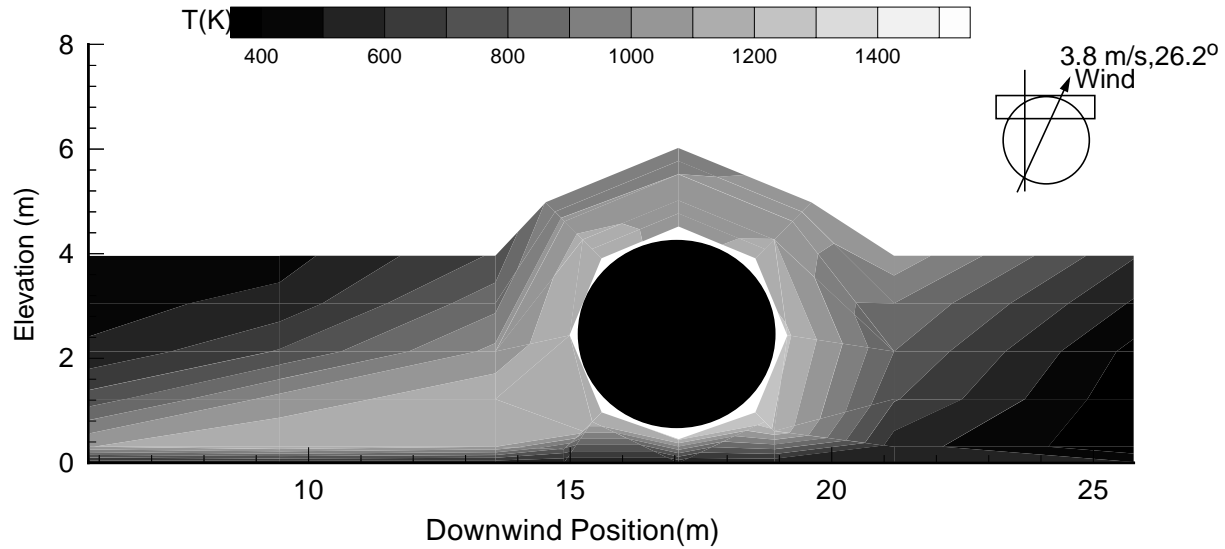
The thermocouple arrays on the bottom half of the mock fuselage were not included in this test (Arrays A3-A7 in Figure 4.1). Temperatures at these nodes are interpolated in the contour plot. The first thermocouple tower was located approximately 6 m from the leading edge of the fuel pool, therefore the flame coverage near the leading edge is not shown in these contour plots. A uniform temperature distribution of 510 K was specified at the fuel surface based on measurements of fuel temperature during the experiments. The thermocouple near the fuel surface of thermocouple tower T4 (shown in Figure 4.1) malfunctioned. The temperature of this thermocouple was therefore interpolated from surrounding time-averaged thermocouple temperatures in the contour plot.

The contour plots of the thermocouple temperatures at each of the three measurement planes are shown in Figures 4.2-4.4. The general shape of the flame zone and the mean thermocouple trends in the fire are illustrated in the plots. Figure 4.2 shows the plane of thermocouple temperatures to the windward side of the centerline. The highest temperatures (1200 K) are located near the fuel surface, extending horizontally from the windward side of the fuel pool to slightly past the leeward side of the mock fuselage. A small (45°) section at the top of the mock fuselage is characterized by slightly reduced temperatures (1000 K). Significantly lower temperatures are observed in this measurement plane than in the other two measurement planes since the component of the wind along the mock fuselage axis directs the main portion of the flame zone away from this measurement plane.

The thermocouple temperature contour plot of the data acquired along the centerline is shown in Figure 4.3. Much higher temperatures are observed in the centerline measurement plane. The combined influence of the wind and the entrained air results in a 45⁰ angle between the main flame zone and the horizontal. An oxygen-starved region, characterized by lower temperatures (1000 K), can be observed between the main continuous flame zone and the fuel pool on the windward side of the mock fuselage. The highest (1500 K) temperatures are located near the top of the windward side of the mock fuselage. The position of the high temperature region is consistent with the wind speed and direction which tend to place the majority of the continuous flame zone adjacent to, and on top of the mock fuselage. Increased temperatures may also result from the enhanced turbulent mixing caused by the presence of the mock fuselage subjected to a wind composed of components perpendicular to, and along the axis of, the mock fuselage. The component perpendicular to the mock fuselage axis deflects the buoyant flow within the flame zone such that it appears to impinge on the side near the top of the windward side of the mock fuselage. Additional mixing of the fuel and air is therefore expected as the flow is directed over the top and into the wake region. The component of the wind parallel to the axis will also enhance the mixing of air in the region where a large portion of the flame zone extends over the top of the mock fuselage. Increased fuel/air mixing can also be caused by counter-rotating vortices produced by wind interactions with the fire plume. The vortices serve to entrain air which will result in high temperature regions.

Figure 4.3 - Test 1 Thermocouple Temperature Contour, Centerline, 300-480s
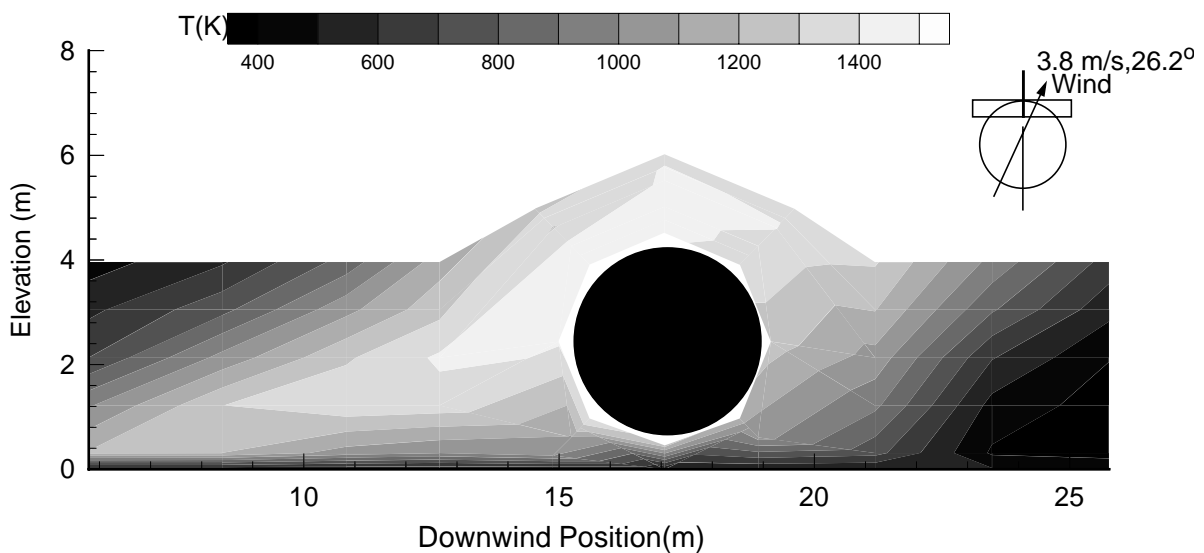
Figure 4.4 - Test 1 Thermocouple Temperature Contour, Leeward of Center, 300-480s
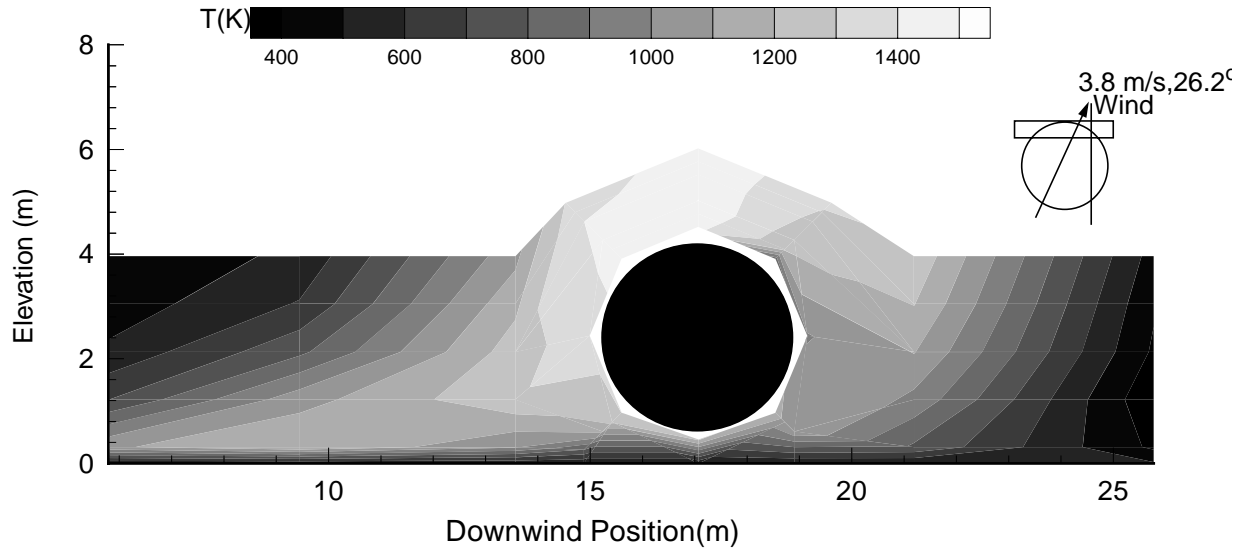
Figure 4.4 shows the thermocouple temperature data for the measurement plane on the leeward side of the centerline. The temperatures are nearly the same as the temperatures for the centerline, but the maximum temperature (1450 K) region is smaller and located almost directly on top of the mock fuselage. The region of 1200 K temperatures extends over the top instead of around the mock fuselage as seen in Figure 4.3.

The data indicate that the thermocouple temperatures are highly dependent on the wind conditions during the quasi-steady time period. The wind causes a change in the flame cover due to redirection of the flame zone, and enhanced mixing due to wind/object and vorticity/object interaction.

4.2.2 Flame Contours for Test 2

A quasi-steady time period during Test 2 (a low wind test) between 225 and 350 seconds following ignition was defined. As shown by the diagram included in these contour plots, the time-averaged wind speed and direction were 1.9 m/s and -36.9°, respectively. The thermocouple arrays on the bottom half of the mock fuselage were not included in the test (Arrays A3-A7 in Figure 4.1). Temperatures at these nodes were interpolated in the contour plot. A uniform temperature distribution of 510 K was specified at the fuel surface. The thermocouple on pole T5 (see Figure 4.1), near

Figure 4.5 - Test 2 Thermocouple Temperature Contour, Leeward of Center, 225-350s
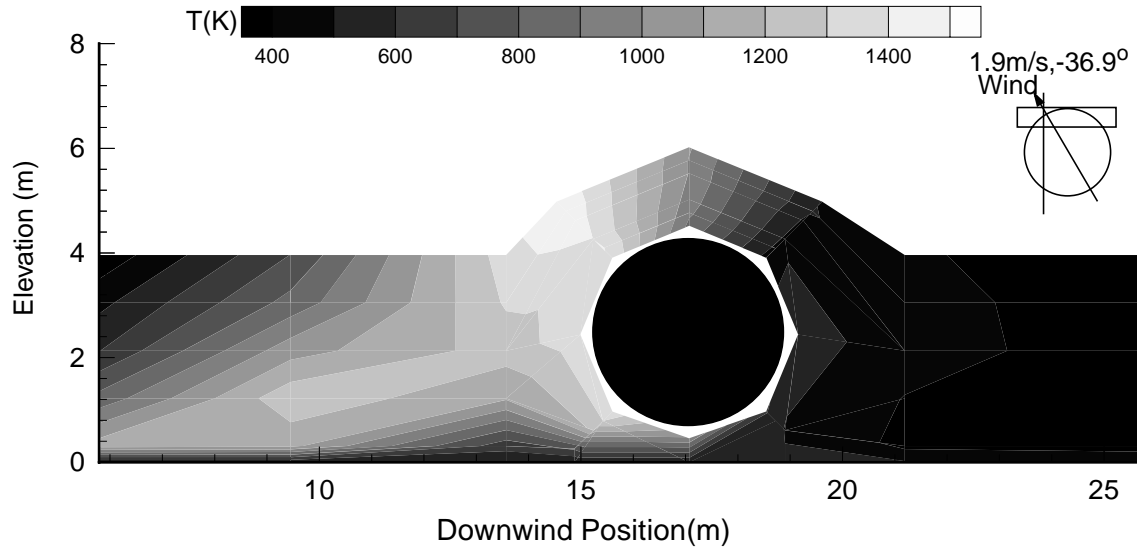
the top of the pole malfunctioned and therefore temperatures at this location were interpolated from adjacent measurements.

The contour plots of thermocouple temperatures measured in the three measurement planes during Test 2 are shown in Figures 4.5-4.7. Figure 4.5 displays the temperature distribution above the fuel pool for a plane of thermocouples on the leeward side of the centerline. The flame cover was directed towards this measurement plane by the component of the wind direction parallel to the axis of the mock fuselage, as evident upon examination of the high temperature (>1400 K) region shown in the contour plot. This high temperature region is located primarily on the windward side of the mock fuselage, with the maximum temperature (1450 K) occurring approximately 45⁰ from the top of the mock fuselage. The lower wind speed, as compared to Test 1, produced a high temperature region on the windward side of the calorimeter from the wind-directed impingement of the buoyant plume on the windward surface of the mock fuselage. The main flame zone extends from the edge of the pool at a 40⁰ angle towards the top of the mock fuselage. Underneath the main flame zone there is an oxygen-starved region near the fuel pool surface approximately 2 m from the windward side of the mock fuselage characterized by low temperatures (<800 K). Another low temperature region (<700 K) exists on the leeward side of the mock fuselage where there is intermittent or nonexistent flame cover.

Figure 4.6 - Test 2 Thermocouple Temperature, Centerline, 225-350s
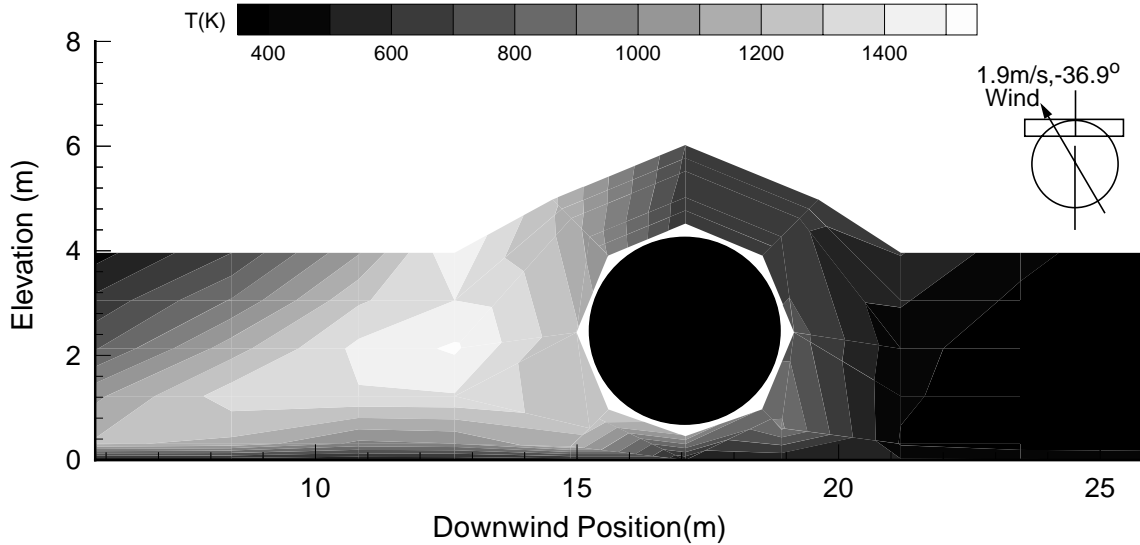
Figure 4.6 displays the temperature distribution above the fuel pool for a plane of thermocouples at the centerline (see Figure 4.1 for the location of each measurement plane and the associated thermocouple arrays). Figure 4.6 shows a small high temperature region (1500 K) of increased flame cover is located several meters from the windward edge of the mock fuselage. The flame zone is located almost completely in front of the calorimeter and directly above the fuel pool. The location of the flame zone is a direct consequence of the nearly quiescent conditions which result in a flame zone dominated by buoyancy.

Figure 4.7 shows the temperature distribution in the measurement plane on the windward side of the centerline. The low, uniform temperature on the lee side indicates a lack of flame cover. The component of the wind vector parallel to the axis of the mock fuselage is directing the continuous flame zone away from this measurement plane. The region near (less than 2 m above the pool surface) the fuel surface, from the leading edge of the fuel pool to slightly beyond the leeward side of the mock fuselage, is the only area with temperatures (800-1200 K) representative of flame cover.

All contour plots from Test 2 show a low temperature region behind the calorimeter. The wind speeds appear to be insufficient to direct the flames to the lee side of the mock fuselage. Flames are directed away from the windward measurement plane by the component of the wind vector parallel to the axis of the mock fuselage (Figure 4.7). There is evidence of an oxygen-starved region between the main flame zone and the fuel surface in Figures 4.5 and 4.6. The main flame zone is located primarily above the fuel surface, which is typical of fires under quiescent conditions [19].

4.2.3 Flame Contours for Test 3

Two quasi-steady time periods were identified for Test 3 (high wind) from 300-600 seconds and 680-715 seconds following ignition. The temperature contour plots for the first quasi-steady time period are presented in Figures 4.8-4.10. This test shows the pronounced effect of high wind speed (10.2 m/s) on the temperature distribution near an object. The momentum of the wind is sufficient to overcome buoyancy and the high temperature region is deflected to the leeward side of the mock fuselage during the test.

Figure 4.8 is a contour plot of the temperature distribution in the measurement plane on the leeward side of the centerline. A thermocouple on array A1 (see Figure 4.1), near the top of the array malfunctioned and hence temperatures at this location were interpolated to create continuity in the plots of the flame shapes. The large high temperature region extends mainly from the windward edge of the mock fuselage to the end of the measurement plane. The thermocouple pole at the leading edge of the fuel pool recorded a temperature of 1200 K for all elevations. The video record confirms that a malfunction must have occurred; therefore, the data from this malfunctioning pole were excluded from the contour plot.

There is a high temperature (1400 K) region near the windward side of the mock fuselage caused by the flames impinging on the mock fuselage and also by the presence of counter-rotating vortices which increase the entrained air and hence increase the temperatures recorded by the thermocouples in the area. The wind

Figure 4.7 - Test 2 Thermocouple Temperature, Windward of Center, 225-350s
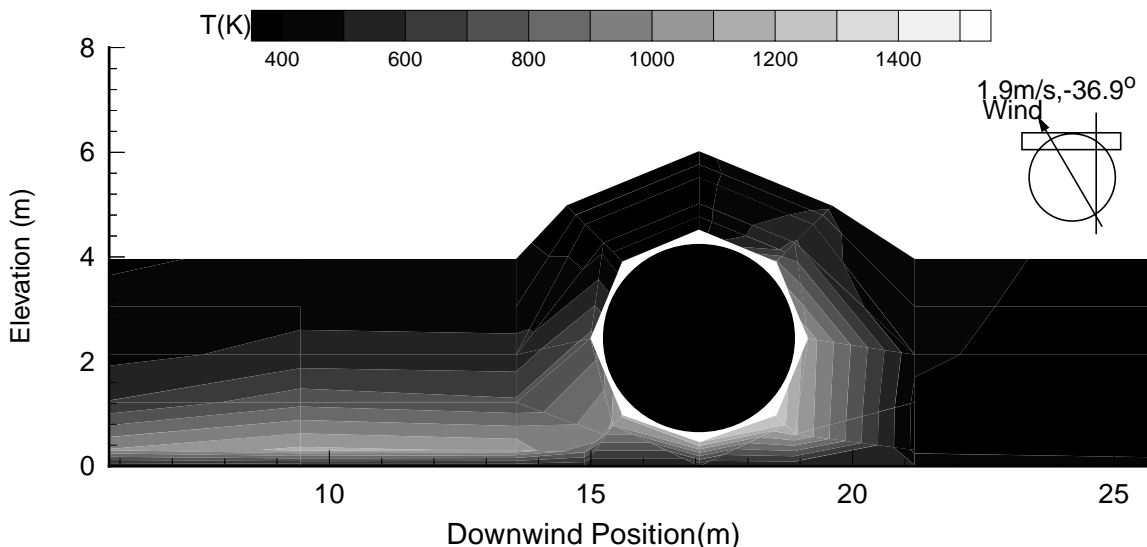
Figure 4.8 - Test 3 Thermocouple Temperature, Leeward of Center, 300-600s
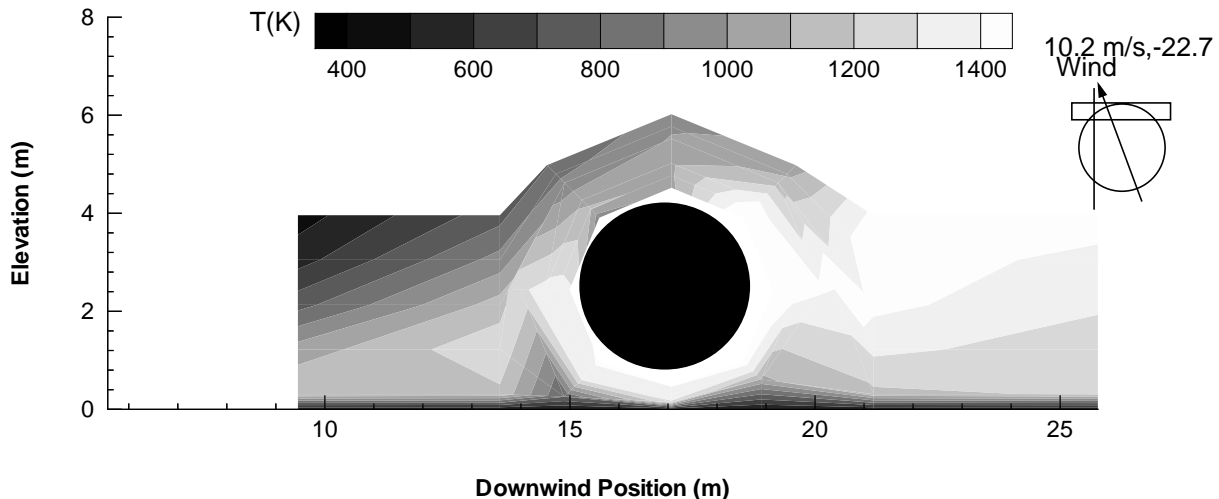
forces the flames over the mock fuselage and accelerates the flow between the mock fuselage and the fuel surface to create a low pressure region on the leeward side. The flow also mixes the air from over the top of the mock fuselage and the fuel rich air accelerated under the mock fuselage to produce the high temperature (1500-1600 K) region in the wake.

Figure 4.9 shows the temperature distribution along the centerline plane. The thermocouple on array A2 (see Figure 4.1), near the top of the array malfunctioned hence temperatures at this location were interpolated to create continuity in the plots. Trends similar to those described for Figure 4.8 are observed along the centerline measurement plane. The continuous flame zone extends from the leading edge of the fuel pool, at an angle of approximately 45°, to the leeward edge of the measurement plane. A high temperature (~1650 K) region occurs on the leeward side of the mock fuselage due to wind interactions with the flame zone and the mock fuselage creating a wake area with enhanced fuel/air mixing.

Figure 4.10 shows the temperature distribution along the measurement plane to the windward side of the centerline. A thermocouple on pole T15 and array A6 (see Figure 4.1) malfunctioned therefore temperatures at this location were interpolated from surrounding measurements. The windward measurement plane for the quasi-steady time period displays the same trends as already described. The mixing of fuel and air in the wake due to flow over the top of the mock fuselage and the forced flow under the mock fuselage causes the high temperature (~1600 K) region on the leeward side. There is also a high temperature (1500 K) region on the windward side near the mock fuselage. A considerable oxygen-starved region, characterized by

50

Figure 4.9 - Test 3 Thermocouple Temperature, Centerline, 300-600s
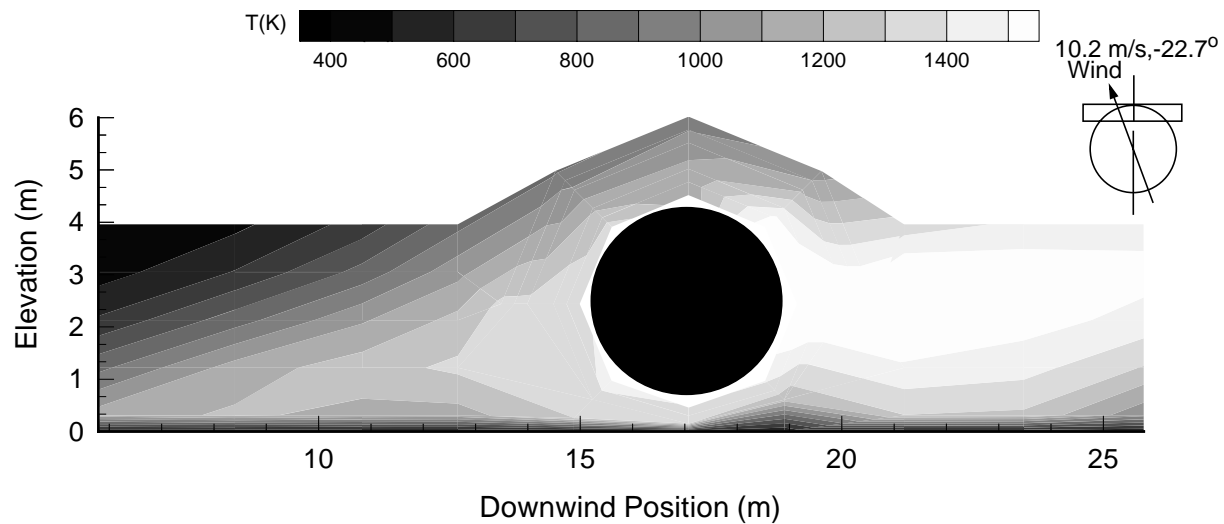
Figure 4.10 - Test 3 Thermocouple Temperature, Windward of Center, 300-600s
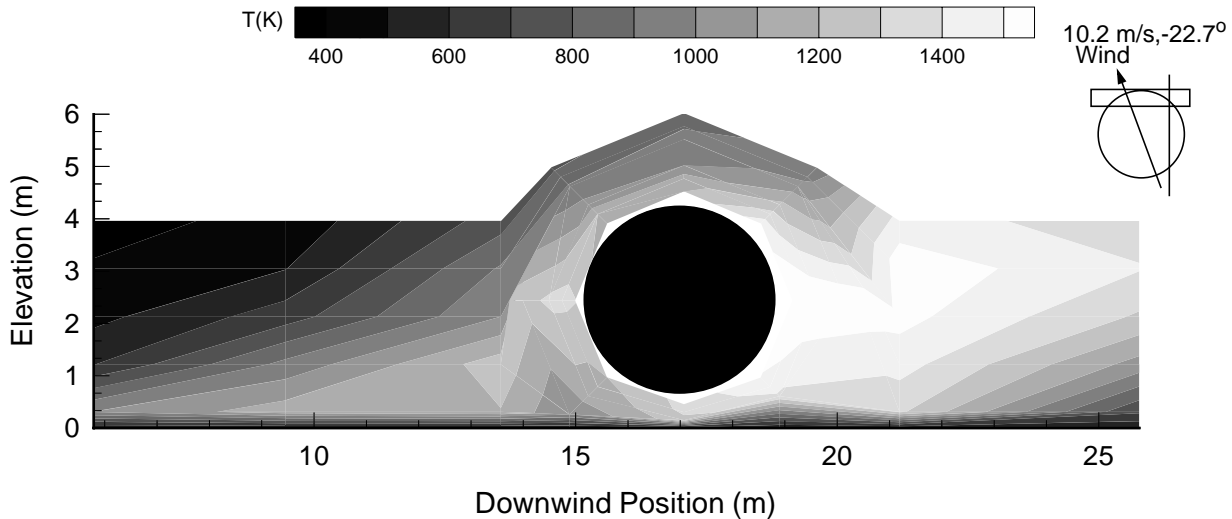
reduced temperatures (700 K), is present on the windward side of the mock fuselage, near the fuel surface 15 m from the leading edge of the fuel pool.

The same trends seen in the first quasi-steady period occur in the second quasi-steady time period (Figure 4.11, 4.12, 4.13) for a wind speed of 8.6 m/s.

Figure 4.11 - Test 3 Thermocouple Temperatures, Leeward of Center, 680-715s
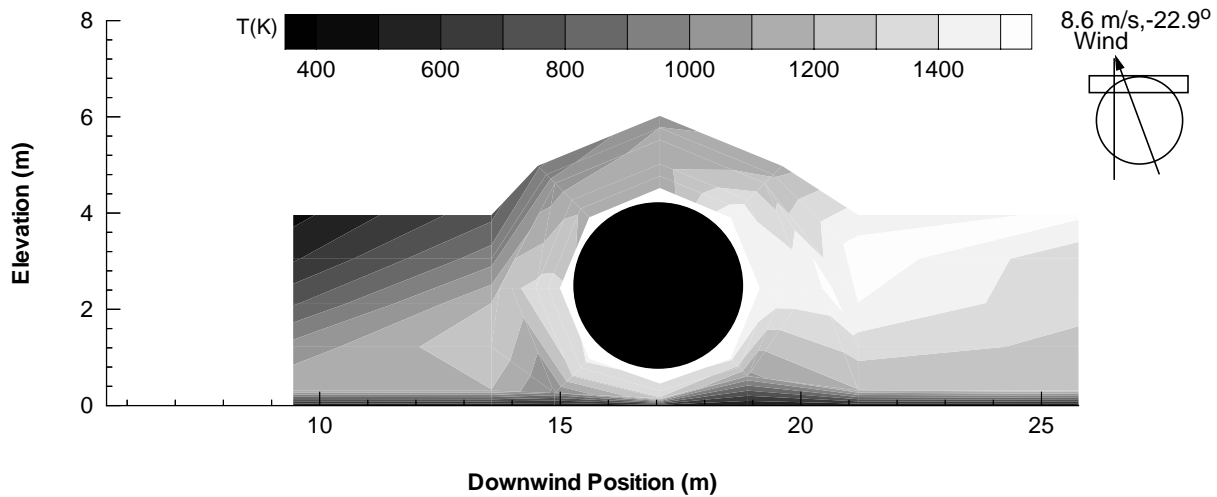
Overall, the contour plots are very similar which shows repeatability of the trends observed. The test produced much higher temperatures than would normally be expected due to increased air entrainment and fuel/air mixing caused by the wind/

Figure 4.12 - Test 3 Thermocouple Temperature, Centerline, 680-715s
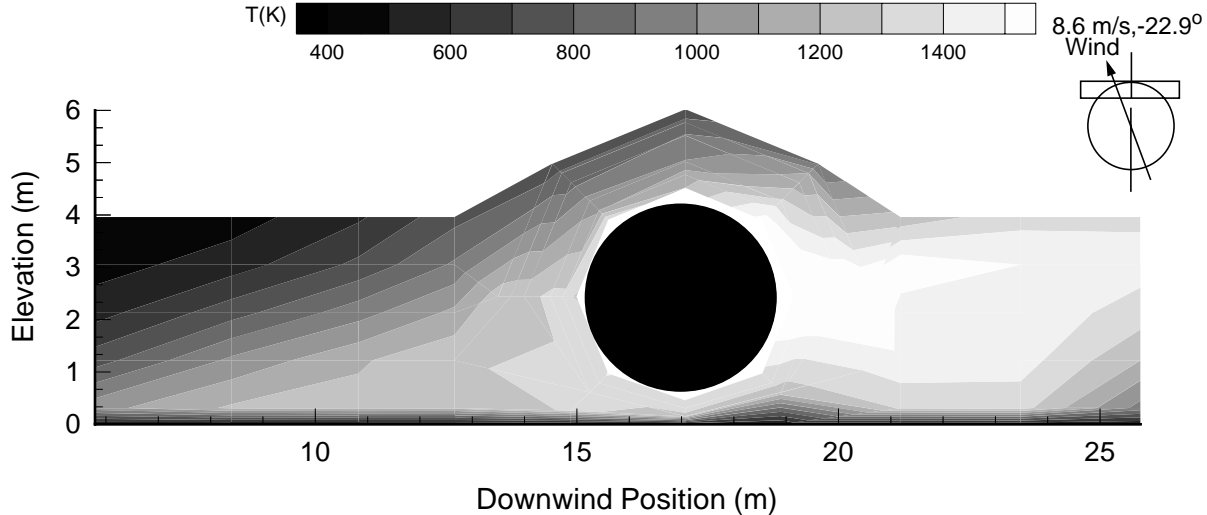
Figure 4.13 - Test 3 Thermocouple Temperature, Windward of Center, 680-715s
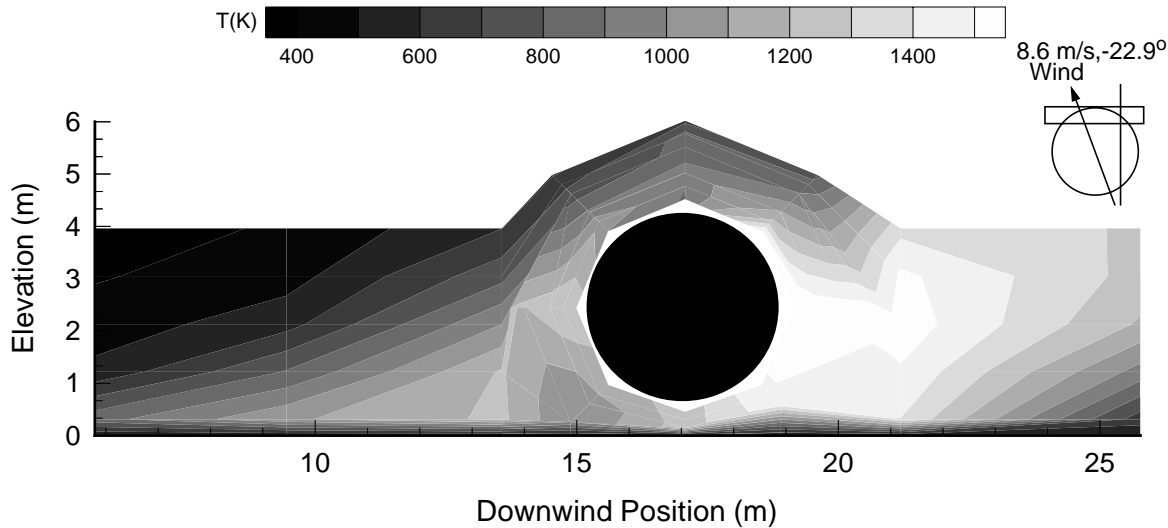
object interactions. All of the measurement planes show the trends already
mentioned: 1) high temperature (~1600 K) in the wake, 2) high temperature (1500 K)
region just on the windward side of the mock fuselage, 3) high temperature regions
caused by increased fuel/air mixing due to wind interactions with the plume and the
object, and 4) a small oxygen-starved region on the windward side of the mock
fuselage near the fuel surface where flame cover is thick and air entrainment is
minimal.

4.2.4 Flame Contours for Test 4

Two quasi-steady time periods were located for Test 4 (medium winds). The periods
were 120-240 seconds following ignition with an average wind speed of 5.1 m/s and
360-480 seconds following ignition with an average wind speed of 3.6 m/s. The wind
speeds and directions are depicted in a small diagram in the figures.

Figure 4.14 shows the temperature distribution of the measurement plane to the
leeward side of the centerline. A thermocouple on pole T11 (see Figure 4.1), near the
bottom of the pole, malfunctioned, hence temperatures at this location were
interpolated. The highest temperatures (~1500 K) are observed near the windward
side of the mock fuselage. The main flame zone rises at a 45⁰ angle from the leading
edge of the fuel pool and continues over the mock fuselage. The high temperature
region on the windward side of the mock fuselage is expected to be a result of the
enhanced mixing resulting from flames impinging on the test fixture. As air and fuel

Figure 4.14 - Test 4 Thermocouple Temperature, Leeward of Center, 120-240s
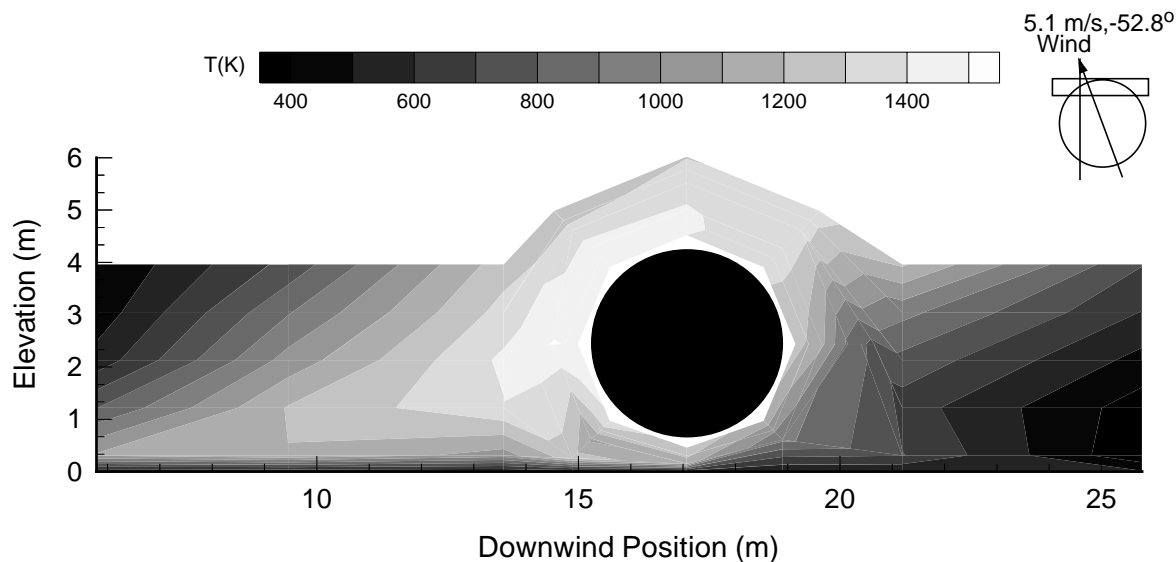
flow over the top and the bottom of the mock fuselage, and meet air from the leeward side of the fuselage to produce a region of intermittent, thin flame cover (1000-1200 K). Lastly, a small oxygen starved region exists in the contour plot characterized by lower temperatures (~900 K) underneath the high temperature region on the windward side of the calorimeter.

The measurement plane along the centerline is shown in Figure 4.15. A fairly small high temperature region (1500 K) is located on the windward side approximately 1 m from the mock fuselage. In this case the wind has insufficient momentum to advect the burning region over the top of the mock fuselage. The flame zone extends horizontally from the leading edge of the fuel pool at an angle of approximately 45°. An area of reduced temperature exists underneath the highest temperature region. A second high temperature region (1300 K) is evident on the lower leeward side of the mock fuselage where fuel rich flow from underneath the fuselage meets the cold air flow from the leeward side of the measurement plane.

Thermocouple results are shown in Figure 4.16 for the measurement plane to the windward side of the centerline. A thermocouple on pole T14 (see Figure 4.1), near the bottom of the pole, malfunctioned and the temperatures at this location were interpolated in the plots of the flame shapes. This measurement plane is outside the main continuous flame zone because the wind component parallel to the axis of the mock fuselage is directing the zone away from the measurement plane. The only area recording temperatures representative of flame cover (900-1100 K) occurs from

54

Figure 4.15 - Test 4 Thermocouple Temperature, Centerline, 120-240s
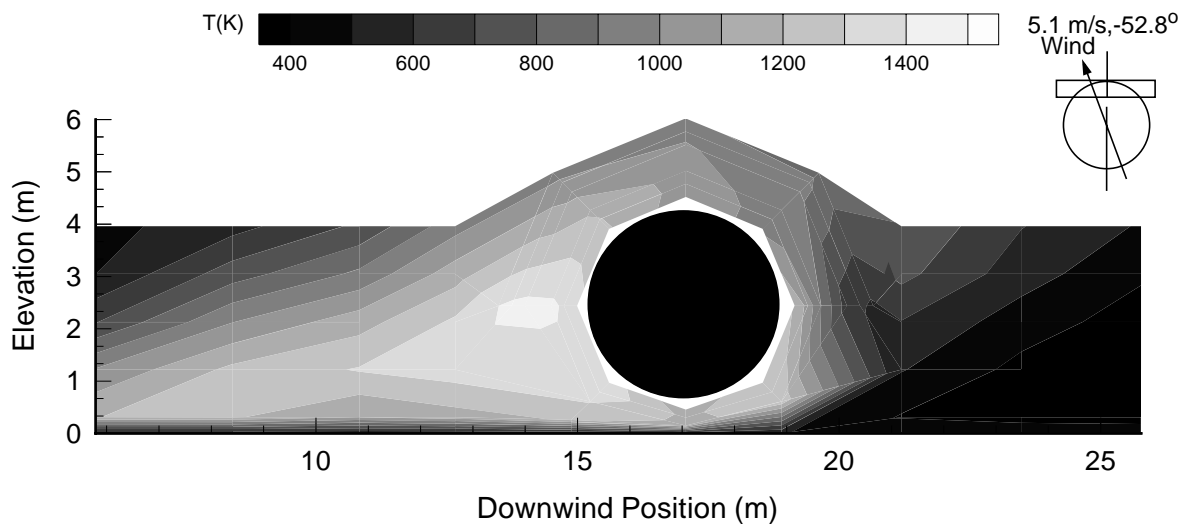
Figure 4.16 - Test 4 Thermocouple Temperature, Windward of Center, 120-240s
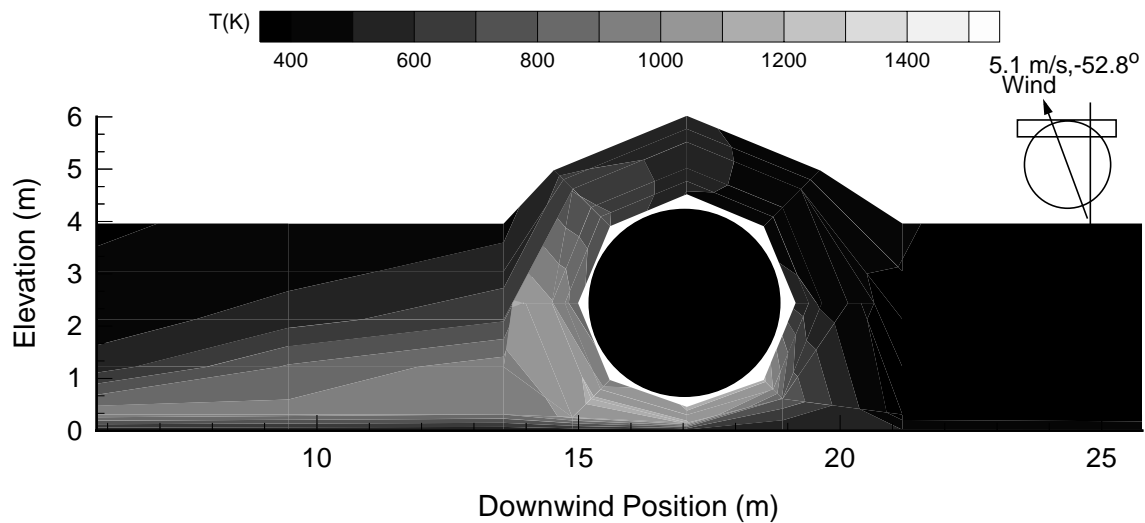
the leading edge of the fuel pool, below 2 m in elevation, to the windward side of the mock fuselage.

In the second quasi-steady time period the wind speed decreases from 5.1 m/s to 3.6 m/s and the temperature distribution shown in the contour plot changes. The wind

Figure 4.17 - Test 4 Thermocouple Temperature, Leeward of Center, 360-480s
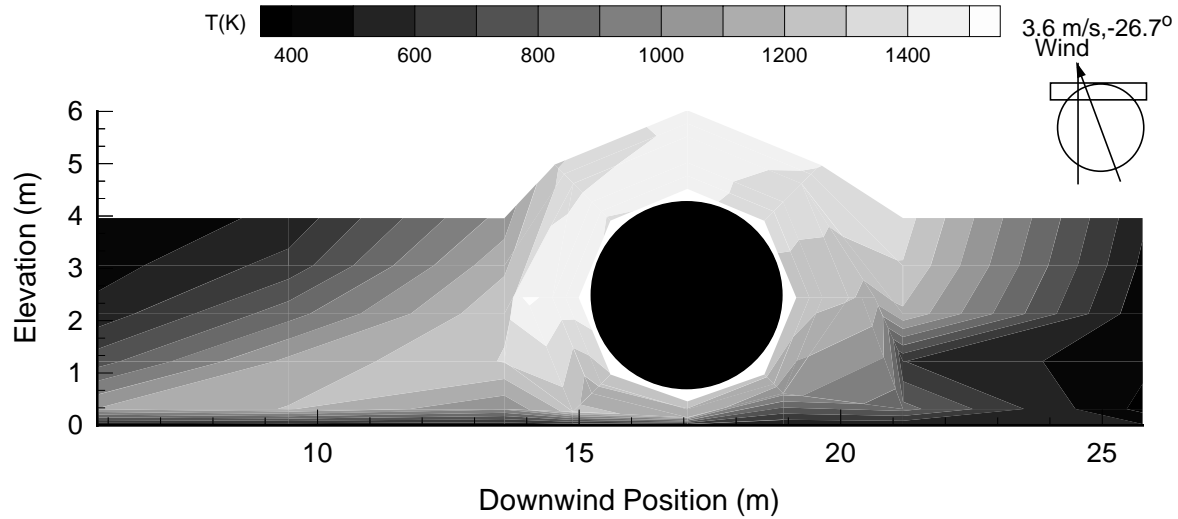
direction also changes from -52.8⁰ to -26.7⁰. This change allows for analysis of the effects of different wind conditions within a single test. The second period displays higher temperatures but the trends are very similar to the first quasi-steady time period.

The temperature contour plot for the lee measurement plane is in Figures 4.17. A thermocouple on pole T11 (see Figure 4.1 for location of the pole), near the bottom of the pole, malfunctioned during the test and the temperature at its location in the contour plot was interpolated from surrounding temperatures. As in the previous time period, the high temperature (~1500 K) region is observed on the windward side of the mock fuselage where mixing is enhanced by the interaction of flames and impingement on the surface of the mock fuselage due to the perpendicular wind component. The high temperature region continues over the mock fuselage. The entrainment of cold air on the lee side is evident in the existence of cold temperatures approaching the mock fuselage at an elevation of 1 m on the leeward side of the fuselage.

Figure 4.18 displays the temperature contour at the center measurement plane. The same trends are observed in this region as in the left measurement plane. The entrainment of cold air on the lee side is not as obvious. The high temperature (1500-1600 K) region extends approximately 2 m further towards the windward edge of the

Figure 4.18 - Test 4 Thermocouple Temperature, Centerline, 360-480s
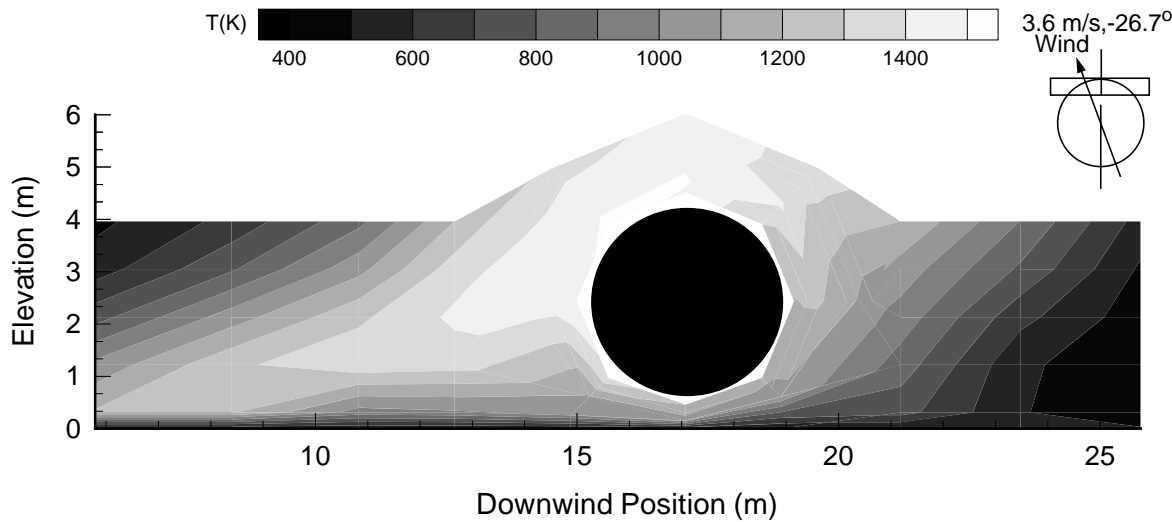
fuel pool. The highest temperatures (1600 K) are seen 45° from the top of the mock fuselage. The region is caused by enhanced mixing in the area.

The most different temperature contour for Test 4 is seen in Figure 4.19, which shows the measurement plane to the windward side of the centerline. The measured temperatures for this second time period are much higher than the temperatures of the previous time period. The wind direction has changed from -52.8^o to -26.7^o. The wind component parallel to the axis of the mock fuselage had decreased and is therefore not directing the continuous flame zone away from the thermocouples in the windward measurement plane as severely. The high temperature region (~1450 K) occurs on the lower windward side of the mock fuselage. A similar effect is seen in Figure 4.18 but this high temperature region is larger than was seen in the earlier time period.

4.2.5 Flame Contours for Test 5

As in the previous tests, two quasi-steady time periods were identified for Test 5 (medium winds). The time periods were 400-575 and 250-670 seconds following ignition with wind speeds of 5.4 m/s and 6.7 m/s, respectively.

Figure 4.19 - Test 4 Thermocouple Temperature, Windward of Center, 360-480s
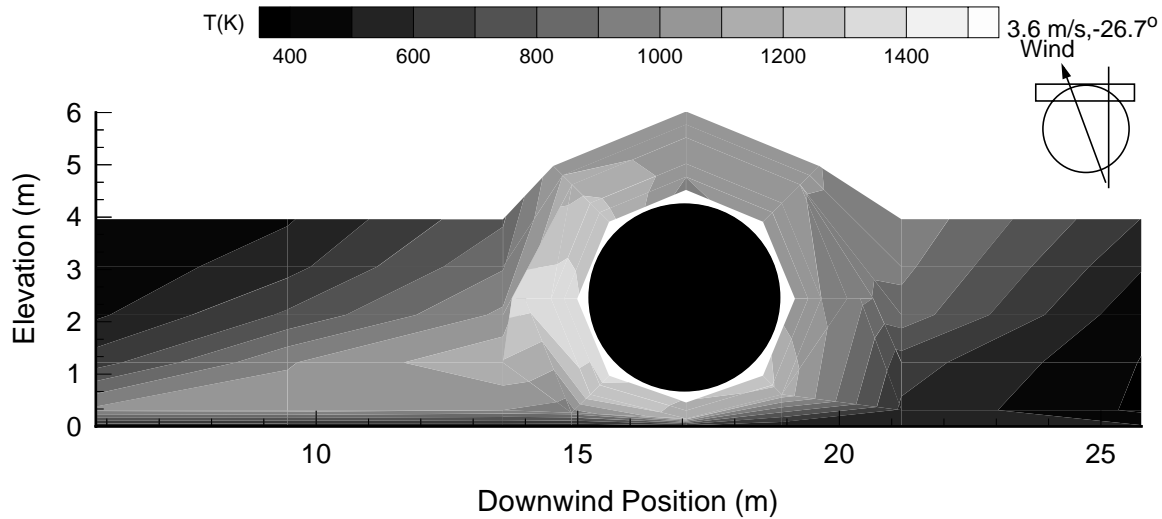
The temperature contours for the measurement plane on the windward side of the centerline for the first quasi-steady time period are displayed in Figure 4.20. The main flame zone extends horizontally from the windward edge of the fuel pool to slightly beyond the lower leeward surface of the mock fuselage. The highest temperatures (1000-1300 K) occur on the windward side as the wind causes the flames to impinge on the surface of the mock fuselage. High temperatures are also observed on the lower leeward side as the fuel rich air mixes with cold air from the lee side of the measurement plane. Temperatures of 800-1000 K were measured in the region on top of the mock fuselage indicating thin or intermittent flame cover. Approximately 15 m from the leading edge of the pool, just above the fuel surface, there is a low temperature (<800 K), oxygen-starved region.

Figure 4.21 displays the temperature distribution in the centerline measurement plane. Several thermocouples on arrays A1, A2, A7 (Figure 4.1) malfunctioned during the test and their temperatures were interpolated from surrounding temperatures. The highest temperatures (1500 K) occur in two regions approximately 1 m to the windward side of the mock fuselage and 45° from the top of the mock fuselage to the leeward side. The high temperature region on the windward side is due to enhanced air entrainment and mixing from wind/object interactions. The high temperature zone on the upper leeward side of the mock fuselage has not been observed in any of the temperature contours of previous tests. This region could

58

Figure 4.20 - Test 5 Thermocouple Temperature, Windward of Center, 400-575s
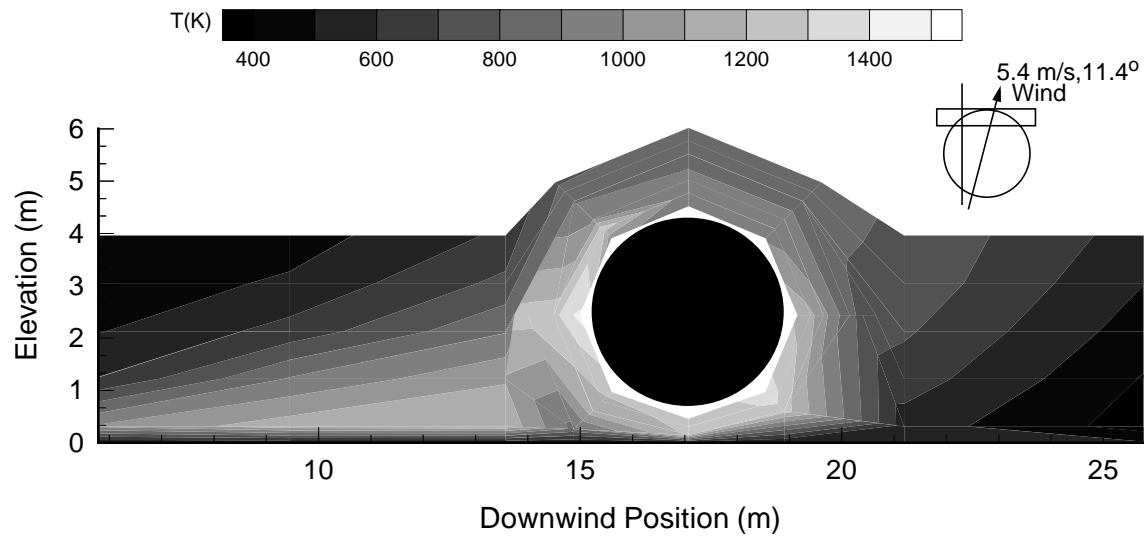
Figure 4.21 - Test 5 Thermocouple Temperature, Centerline, 400-575s
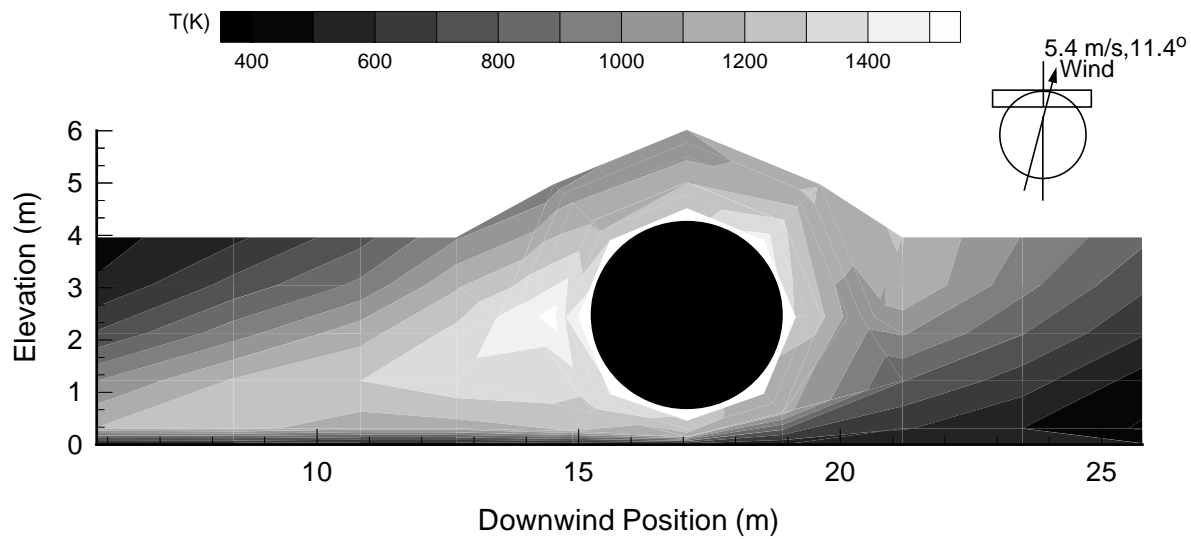
be formed by complex wind/vorticity interactions. The upper portion of the mock fuselage has a thin flame cover. Hot gases are being moved over the top of the mock fuselage creating steamwise vortices and fuel rich air is forced under the mock fuselage as well. There also appears to be a movement of cold air up from the far lee side of the measurement plane. These flows of air and fuel, combined with the wind component parallel to the axis of the fuselage may create a well-mixed region with flames attached to the upper lee side of the mock fuselage.

The temperature distribution in the leeward measurement plane for the first steady state time period is shown in Figure 4.22. The flame zone extends from the leading edge of the fuel pool at an angle of 40° to flow over the mock fuselage and slightly covering the leeward side of the mock fuselage. The impingement of the flames on the surface causes a high temperature (1500 K) region to appear attached to the windward surface of the mock fuselage. Directly underneath the high temperature region there is a small, cold, potentially oxygen-starved area just above the fuel surface. There is evidence of cold air being entrained into the fire by the low temperature region on the lower leeward side.

The second period, from 250-670 seconds after ignition, is shown in Figures 4.23, 4.24, and 4.25 for the three measurement planes. For this time period, one thermocouple on array A1 malfunctioned and its temperature is interpolated from surrounding thermocouple temperatures in the contour plot. The trends displayed in these plots are almost identical to the trends in the first time period. They show a

Figure 4.22 - Test 5 Thermocouple Temperature, Leeward of Center, 400-575s
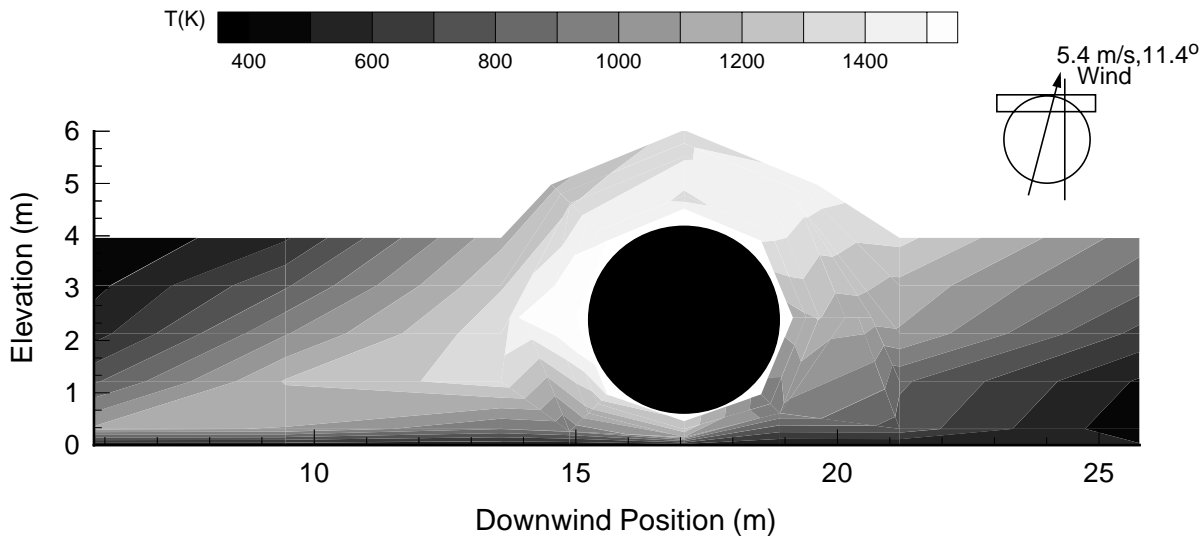
Figure 4.23 - Test 5 Thermocouple Temperature, Windward of Center, 250-670s
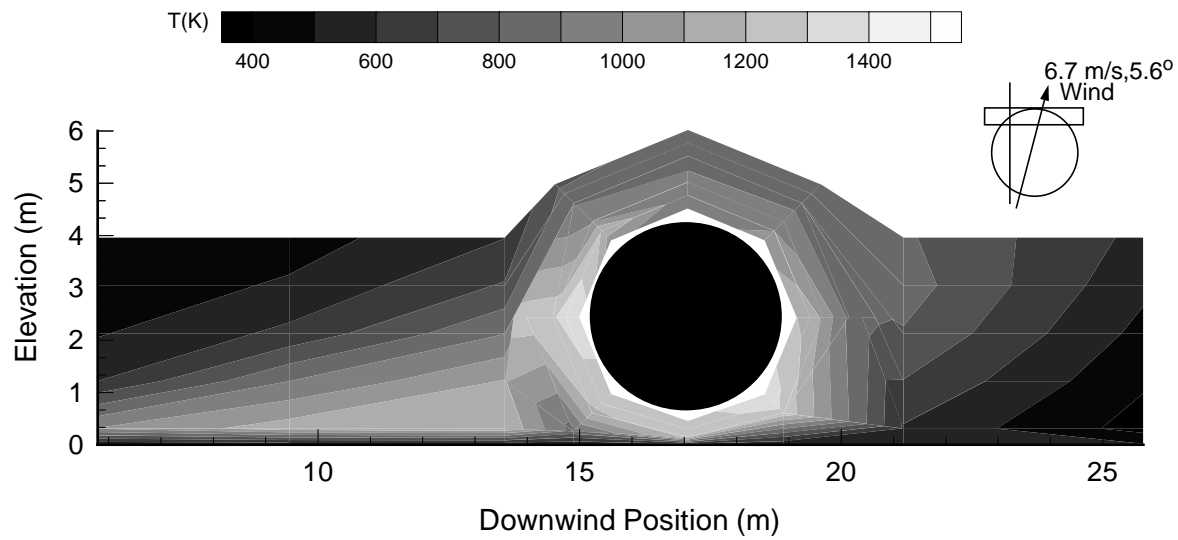
Figure 4.24 - Test 5 Thermocouple Temperature, Centerline, 250-670s
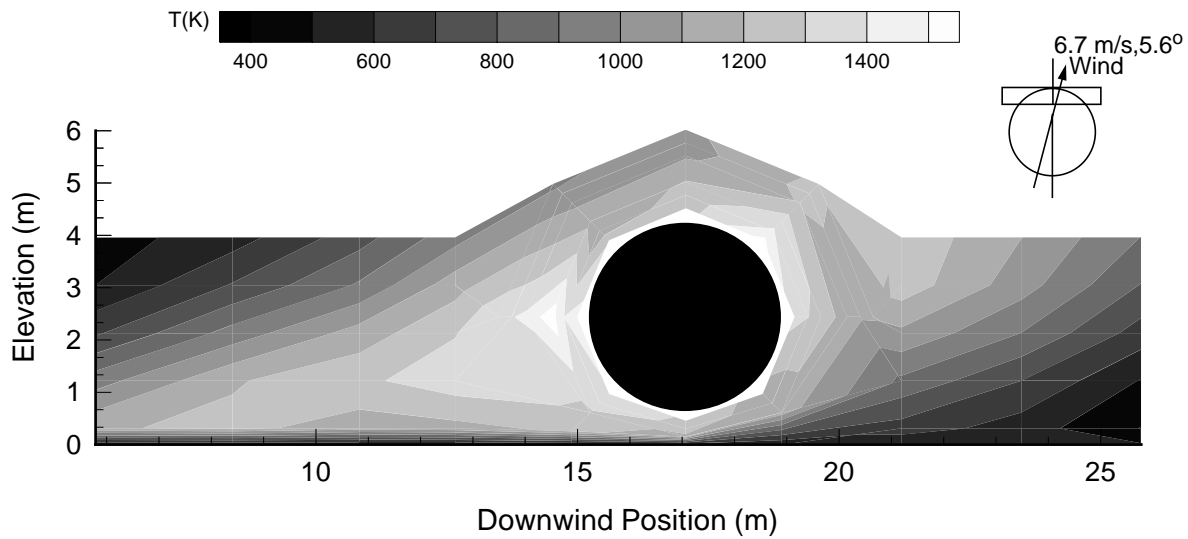
Figure 4.25 - Test 5 Thermocouple Temperature, Leeward of Center, 250-670s
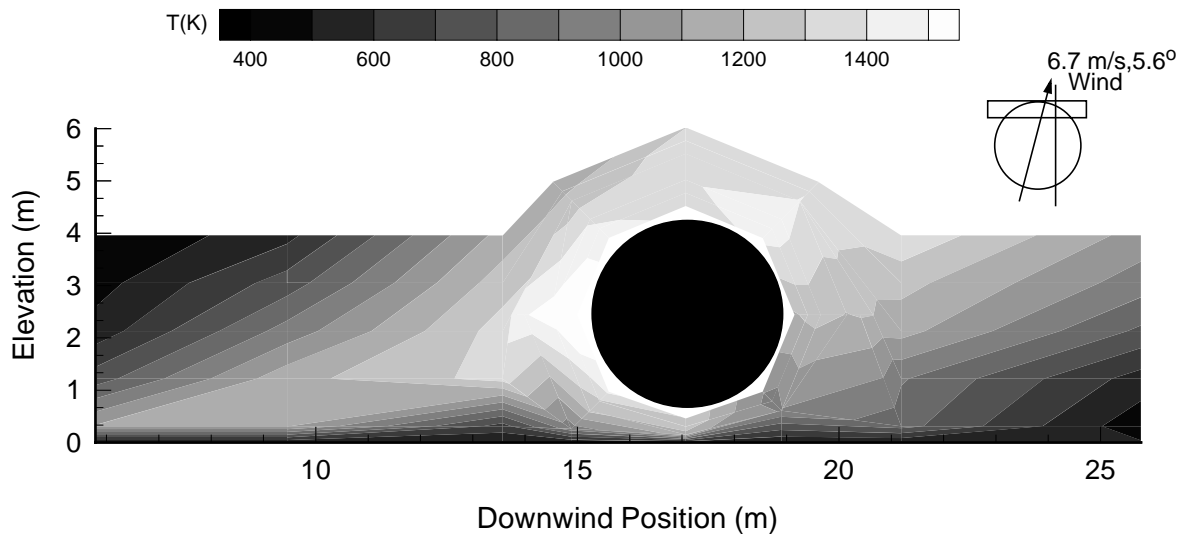
high temperature region (~1450K) on the windward edge of the calorimeter in the leeward and center measurement planes. The windward measurement plane remains fairly cool outside the continuous flame zone due to the direction of the wind away from these regions.

4.2.6 Flame Contours for Test 8

Test 8 was performed under high speed wind conditions with the intention of trying to reproduce the high temperatures achieved during Test 3. The wind during the quasi-steady time period 475-598 seconds after ignition was 9.9 m/s in the same direction as in Test 3. The data trends observed during Test 3 were successfully reproduced in Test 8.

Figures 4.26 displays the temperature distribution for a line of thermocouple towers and arrays leeward of the pool centerline. All six thermocouples on array A3 in the wake of the mock fuselage malfunctioned during the tests; therefore their temperatures were interpolated in the contour plots. Coarseness in the plots near the wake of the mock fuselage might have been caused by the interpolation. The mixing of cold air coming over the top of the fuselage and the fuel rich air being forced under the fuselage causes the high temperature (~1600 K) region in the wake. There is also a high temperature (1600 K) region on the windward side near the

Figure 4.26 - Test 8 Thermocouple Temperature, Leeward of Center, 475-598s
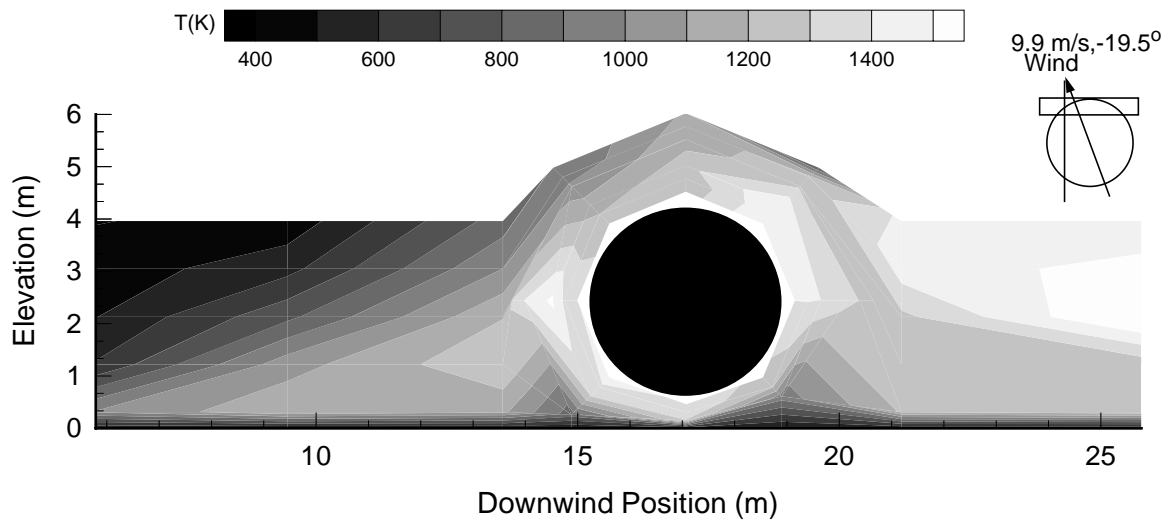
mock fuselage due to impingement. Two oxygen-starved regions are present on the windward and leeward sides of the mock fuselage.

The centerline measurement plane contour is shown in Figure 4.27. Thermocouples located in the middle of poles T6 and T7, on the leeward side of the mock fuselage, malfunctioned during the test and their temperatures were interpolated in the contour plots. The highest temperatures (>1600 K) occur on the leeward side of the mock fuselage due to increased mixing and air entrainment from wind/object interaction. There is evidence of a flow of cold air from underneath the mock fuselage characterized by low temperatures (1000-1200 K) extending from the fuel surface up the leeward side of the mock fuselage. This fuel-rich flow appears to meet another flow of cold air coming over the top of the mock fuselage to create a high temperature (1600 K) region on the upper leeward side of the mock fuselage. Another high temperature region (1500 K) occurs on the windward side of the mock fuselage due to increased fuel/air mixing when the component of the wind perpendicular to the mock fuselage directs the flame zone to impinge on the surface of the mock fuselage.

Figure 4.28 shows the temperature distribution and flame shape for the measurement plane on the windward side of the centerline during the quasi-steady time period. All six thermocouples on array A3 in the wake of the mock fuselage malfunctioned during the tests; therefore their temperatures were interpolated in the contour plots. Coarseness in the plots near the wake of the mock fuselage may be

Figure 4.27 - Test 8 Thermocouple Temperature, Centerline, 475-598s
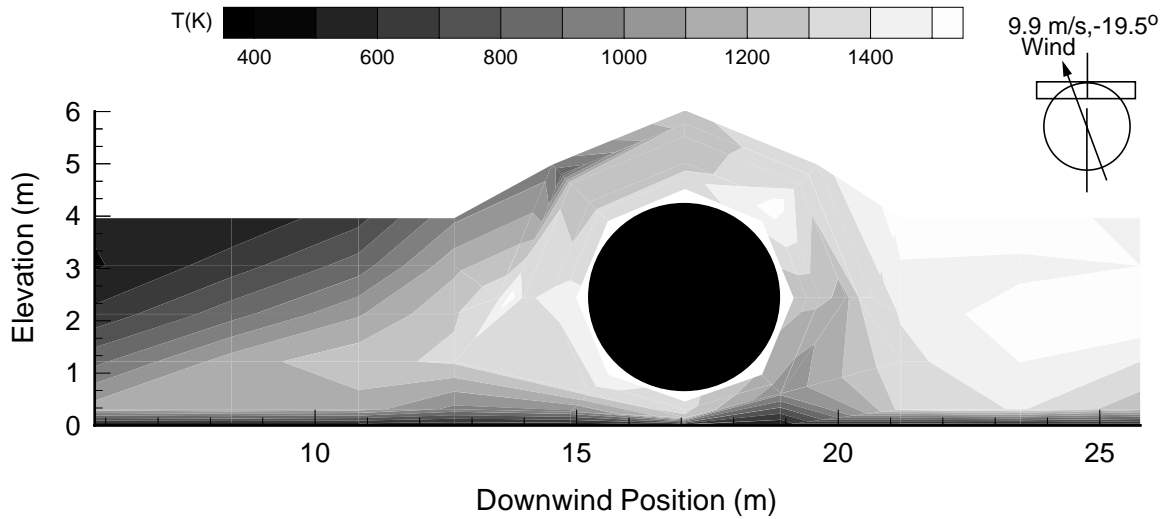
Figure 4.28 - Test 8 Thermocouple Temperature, Windward of Center, 475-598s
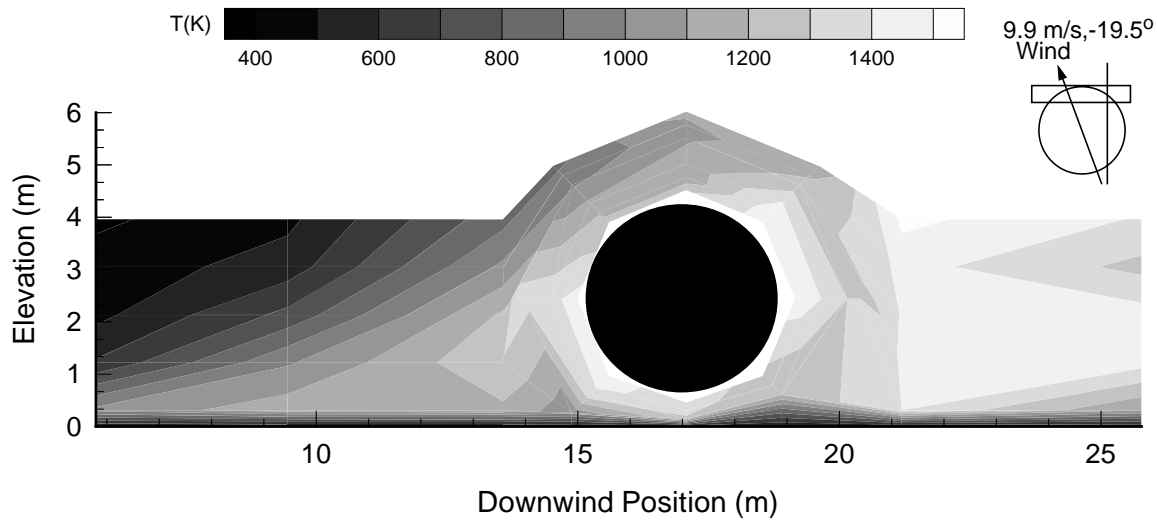
a result of linear interpolation between data points. The trends observed in this contour plot are nearly identical to the trends seen in Figure 4.26 on the leeward measurement plane.

All measurement planes recorded temperatures up to 1600K. The highest temperature region is located on the leeward side (i.e. in the wake region) of the fuselage due to increased mixing by the presence of the large cylindrical object and potentially streamwise vortices in the wake.

4.3   Small Pool Flame Shapes

Tests 6 and 7 were performed in a 10 m fuel pool instrumented according to the plan stated in Chapter 2. Three contour plots for each test were produced from experimental thermocouple data acquired from arrays throughout the pool and around the calorimeter. The coarseness that sometimes occurs in the contour plots is likely a result of temperature interpolation between nodes of the measurement plane. The locations of the measurement planes are at the centerline and approximately 3 m to either side of the centerline. Figure 4.29 shows the locations of the measurement planes and the thermocouples included in each measurement plane.

4.3.1   Flame Contours for Test 6

Test 6 was conducted in the small pool under high wind conditions of 9.5 m/s. During the quasi-steady time period from 270-390 seconds after ignition, the direction of wind was nearly normal (2.0⁰) to the longitudinal axis of the fuselage.

Figure 4.30 shows the temperature distribution in the windward measurement plane. A total of four thermocouples located in arrays T6, A3, A6, and A8 (see Figure 4.29 for thermocouple locations) malfunctioned during the test and their temperatures were interpolated from surrounding thermocouple temperatures in the contour plot. The temperature distribution given in Figure 4.30 shows overall lower temperatures when compared with the other measurement planes due to the redirection of the flame zone away from the measurement plane by the component of the wind vector parallel to the longitudinal axis of the mock fuselage. The only region with temperature indicative of flame cover seems to sweep under the fuselage to the leeward surface. The high temperature (800-1100 K) region on the windward side is consistent with the influence of buoyancy. The high temperatures (1000-1300 K) on the leeward side of the mock fuselage are expected to be due to increased fuel/ air mixing in the wake from the interaction of the wind with the object.

Figure 4.31 gives the temperature distribution in the centerline. The temperatures in this region are greater than the temperatures recorded on the left side. A total of

Figure 4.29 - Location of Measurement Planes- 10 m pool

TC Array

TC Pole
facing
right, i.e.

T9

T8

T5

T4

T13

T12

T7

T11

T3

T6

T2

T10

T1

Note: A total of three planes
are shown in the diagram. The
view for the contours is from
the right side of the pool.

Prevailing Wind

A1

A8

A2

Fuselage
Model

A7

A3

A5

A6

A4
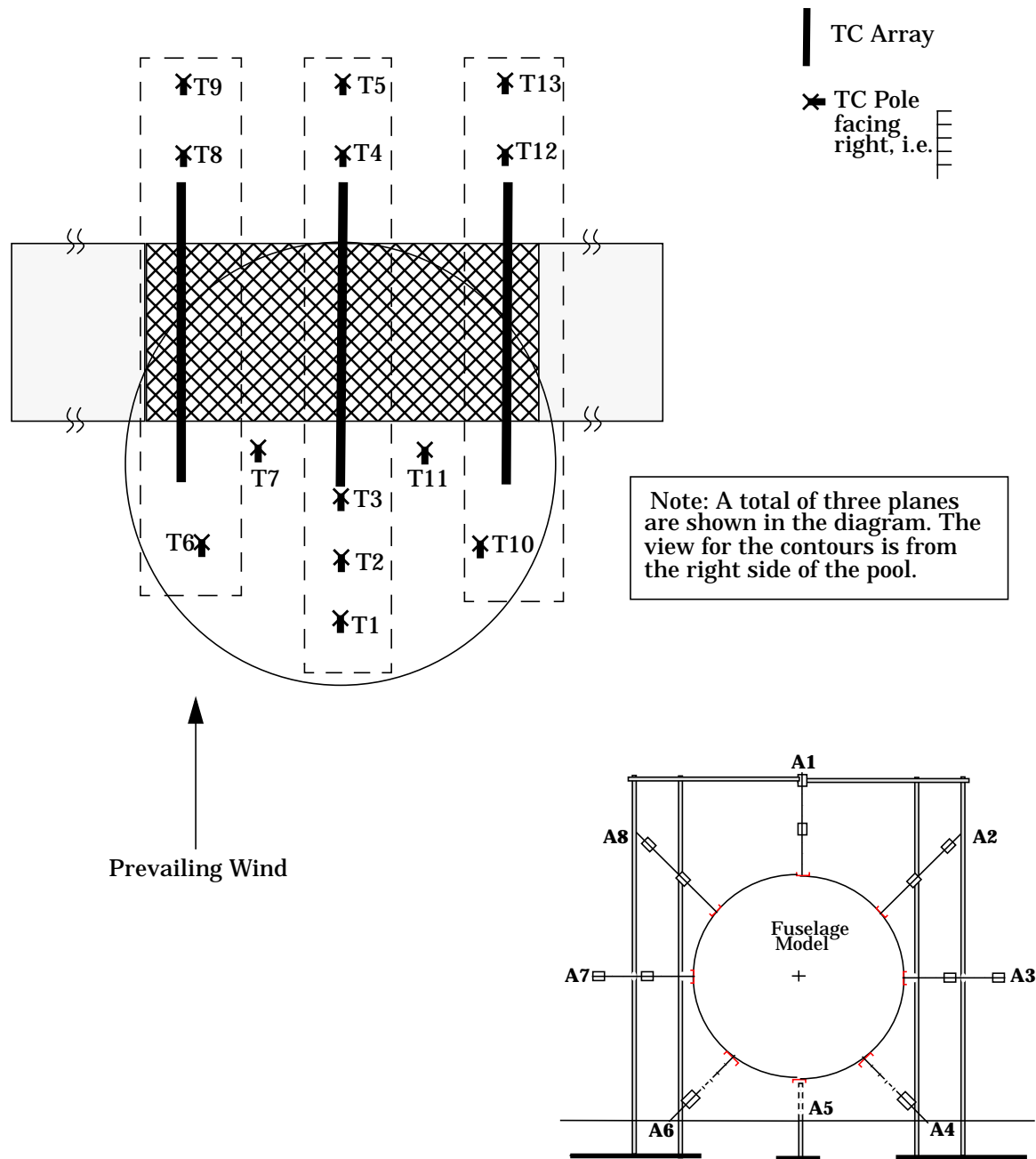
Figure 4.30 - Test 6 Thermocouple Temperature, Windward of Center, 270-390s
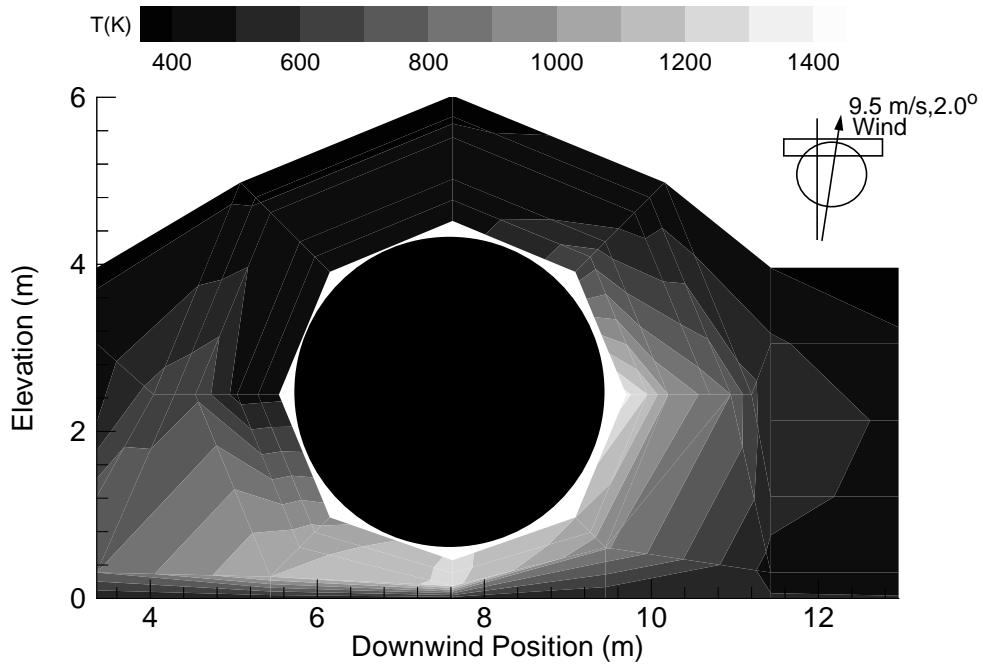
five thermocouples located in arrays T4, A3, A6, and A7 malfunctioned during the test and their temperatures were interpolated from surrounding thermocouple temperatures in the contour plot. This measurement plane shows trends similar to the left measurement plane but there is a much larger high temperature (~1500 K) region in the wake of the mock fuselage, likely caused by the mixing of cold air from over the top of the mock fuselage and fuel-rich air accelerated underneath the mock fuselage. The high temperature region on the leeward side resembles the flame zone in Test 3 and 8 under similar high speed wind conditions, but the region appears much smaller. A burning region (1100 K) is observed at approximately 4 m from the leading edge of the fuel pool, and the high temperature region (1200 K) on the lower windward side of the mock fuselage is due to the impingement of the buoyant plume on the surface of the mock fuselage.

In Figure 4.32, all of the thermocouples on array A3 and one thermocouple on pole T11 failed during the test. The temperatures were therefore interpolated in the contour plot (see Figure 4.29 for the location of the thermocouples). The highest temperatures (~1450 K) are observed in the wake of the mock fuselage in Figure 4.32 for the measurement plane to the leeward side of the centerline. This high

Figure 4.31 - Test 6 Thermocouple Temperature, Centerline, 270-390s
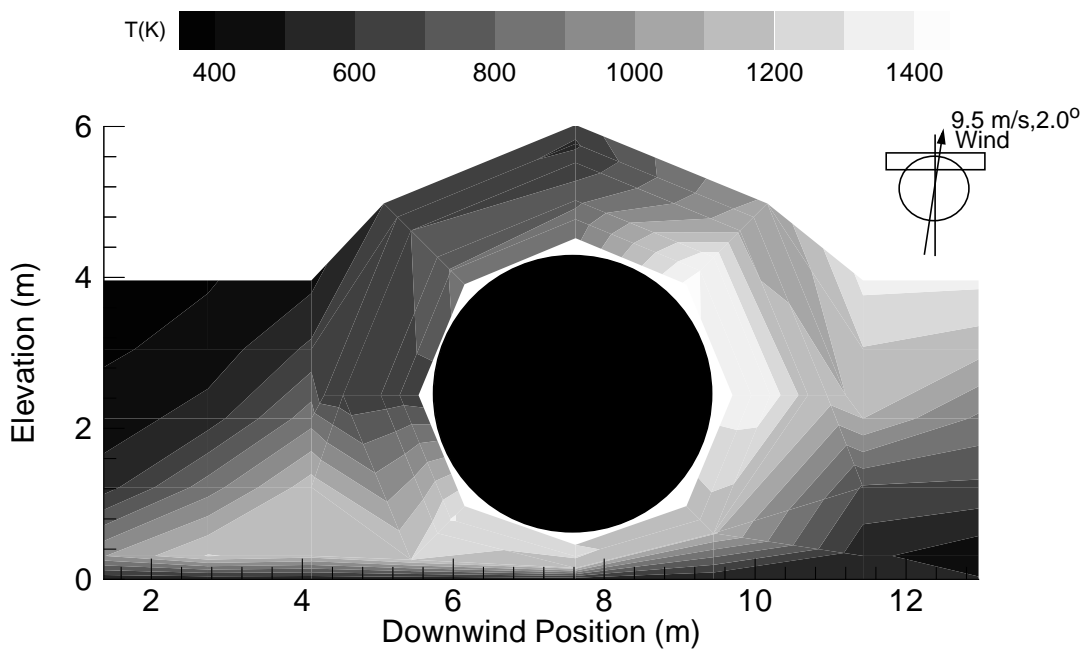
Figure 4.32 - Test 6 Thermocouple Temperature, Leeward of Center, 270-390s

68
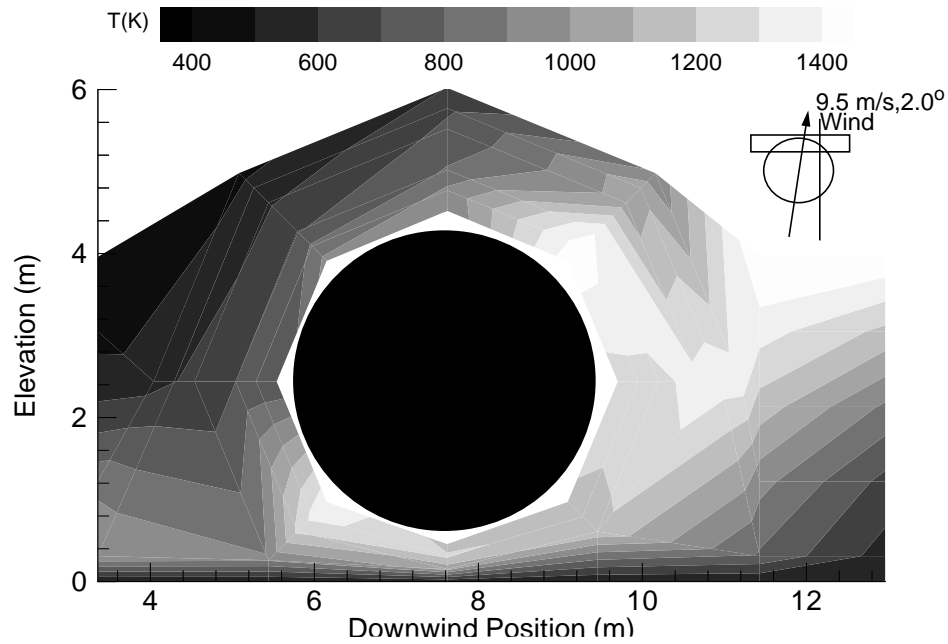
temperature region on the leeward side of the fuselage is similar to trends shown in data from temperature profiles for Tests 3 and 8 except that it is smaller and cooler for the small 10 m pool fire. There is a flow of cold air from over the top of the mock fuselage which extends into the high temperature region on the leeward side. The typical high temperature region on the windward side occurs as a result of impingement and mixing on the lower windward surface of the mock fuselage.

Although many similarities exist in the contour plots of Tests 3, 6, and 8 which were all conducted under high speed wind conditions, some differences also occur. In all three tests the highest temperatures always occur on the leeward side of the mock fuselage. A small high temperature region is observed on the lower windward side of the mock fuselage. As expected, the high temperature region in the wake of the mock fuselage is smaller in the 10 m pool fire than the 20 m pool fire. The location of the flame zone between the leading edge of the fuel pool and the mock fuselage is not as clear in the larger pool fires (Tests 3 and 8). Lastly, the overall temperatures recorded in the smaller pool (Test 6) are not quite as high as those observed in the larger fires.

4.3.2 Flame Contours for Test 7

Test 7 (low winds) was conducted in a small fuel pool with wind conditions of 2 m/s, -36.1⁰ during the quasi-steady time period from 250-500 seconds following ignition.

Figure 4.33 shows the temperature distribution and flame shape on the leeward side of the pool centerline. The highest temperatures (1100K) occur underneath the fuselage. A region of thin flame cover (900 K) extends to the leeward side of the mock fuselage.

The data obtained in a measurement plane located at the centerline are depicted in Figure 4.34. The main flame zone extends from the leading edge at a 50⁰ angle from the horizontal to the leeward side of the mock fuselage. There is a much larger high temperature (1400 K) region on the windward side of the mock fuselage than the other two measurement planes which occurs on the windward side of the mock fuselage. The high temperatures are most likely a result of enhanced mixing which occurs as a consequence of impinging flow in this area. A small oxygen-starved region, located between the high temperature region and the fuel surface, is characterized by reduced temperatures (~800 K). The highest temperatures are approximately 200 K less than the temperatures seen in large pool tests under similar wind conditions.

Figure 4.33 - Test 7 Thermocouple Temperature, Leeward of Center, 250-500s
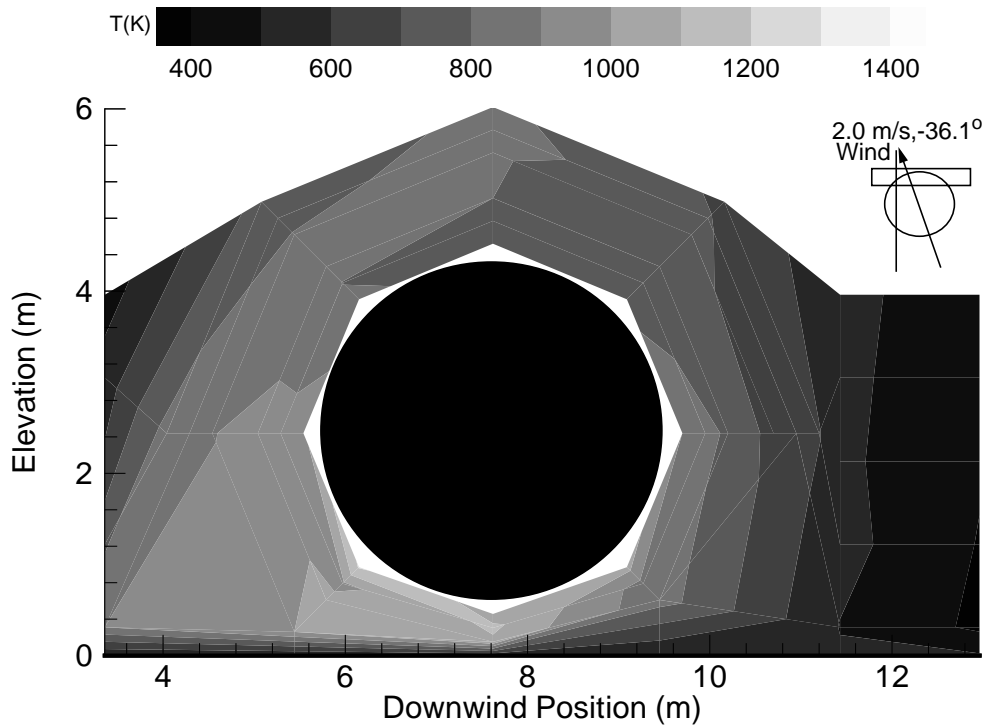
Figure 4.35 displays the temperature distribution in the windward measurement plane. Results in this region show a very limited area of flame cover. There is a very small high temperature (1100 K) region on the lower windward side of the mock fuselage. Temperatures in the remainder of the measurement plane are indicative of intermittent flame cover at most.

Figure 4.34 - Test 7 Thermocouple Temperature, Centerline, 250-500s
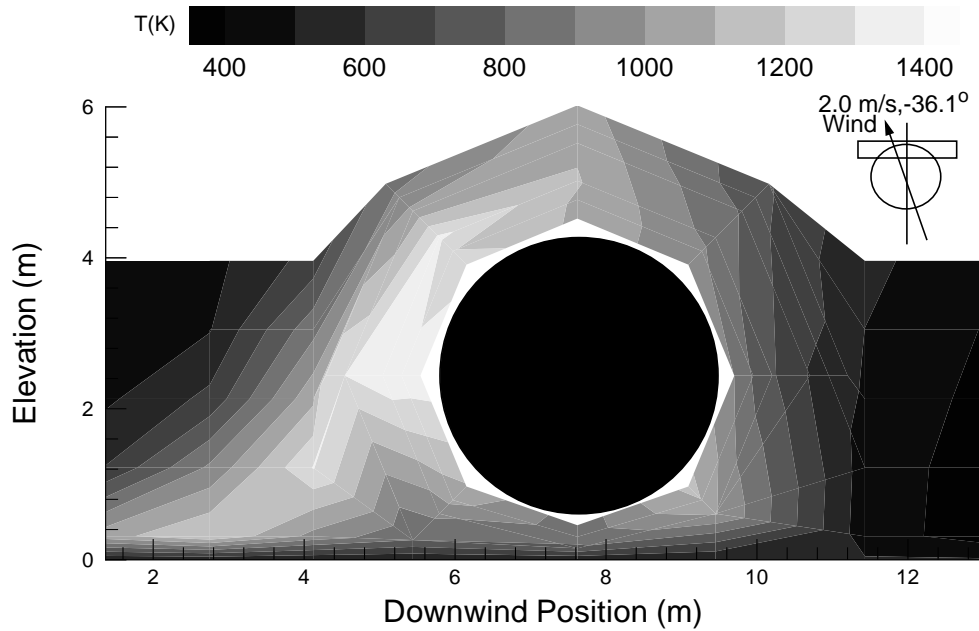
Figure 4.35 - Test 7 Thermocouple Temperature, Windward of Center, 250-500s
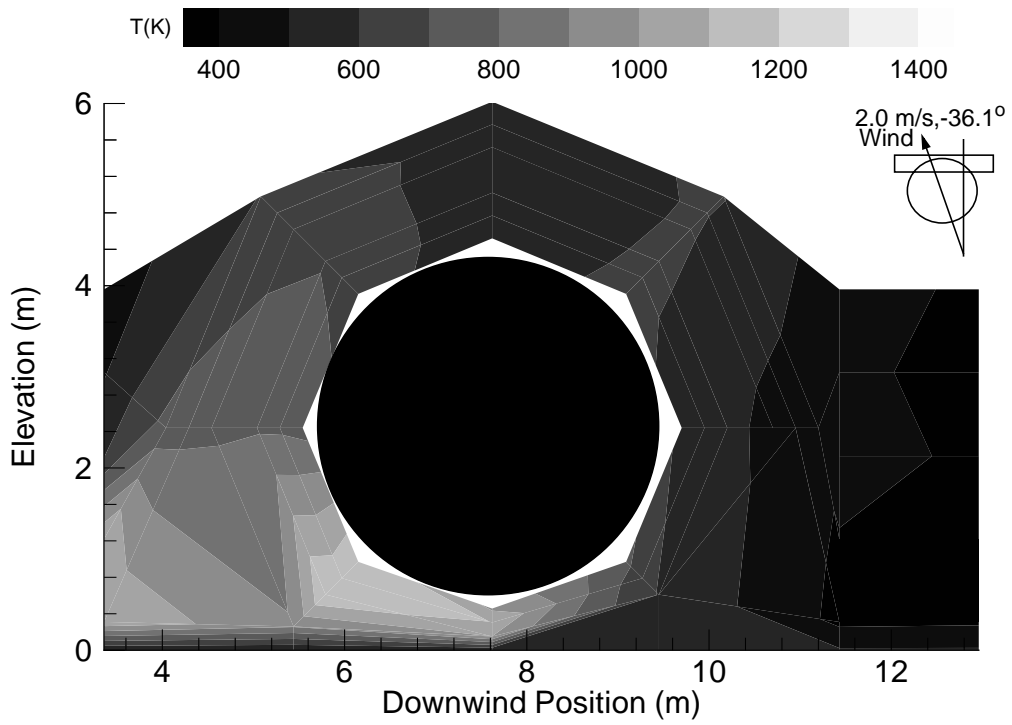
5. Experimental Results - Skin Temperatures

5.1 Overview of Experiments

Thermocouple data were transformed into contour plots to show the temperature distribution on the skin of the mock fuselage during each quasi-steady time period. Contour plots of the front and back of the mock fuselage were produced for each specified time period. The temperature distributions given in this chapter, along with the heat flux distributions in the following chapter, and the material properties of a specific system, are helpful in determining which components will have melted or remained intact at the specified time. These plots present the data in a suitable format for fire model comparisons provided the thermal response of the test fixture is simulated. Some coarseness in the plots occurs as a result of the interpolation of values between experimental data points.

5.2 Large Pool Skin Temperature Distributions

The first six tests were conducted in a 20 m pool of JP-8 jet fuel. The calorimeter was instrumented with thermocouples as stated in Chapter 2. Any differences in test instrumentation will be specified as the results are described, presented, and analyzed in each section.

5.2.1 Skin Temperatures for Test 1

A quasi-steady time period was identified between 300 and 480 seconds after ignition for Test 1. The time-averaged wind speed and direction were 3.8 m/s and 26.2^0, respectively. A thermocouple at x=6 m and an angle of 0^0 malfunctioned during the test and its temperature was interpolated from surrounding thermocouple temperatures.

Contour plots of the front and back of the calorimeter are shown in Figures 5.1 and Figure 5.2, respectively. The temperature distribution implies that the mock fuselage was covered by flames (>800 K) on both sides, in agreement with the contour plots of the flame shapes in Figures 4.2-4.4. Temperatures range from 650-1350 K with moderate (75 K/m) temperature gradients except near the bottom centerline of the mock fuselage. The lowest temperatures (650 K) and highest gradients (350 K/m) are observed near x=-6 m in Figures 5.1 and 5.2. This location corresponds to the oxygen-starved region in the measurement plane shown in Figure 4.2. The lowest temperatures of the three measurement planes were observed in this region. As expected, the highest temperatures (1350 K) occur on the windward side from 90^0-180^0 where the high temperature region of the flame zone impinges on the surface of the mock fuselage as shown in the flame shape contour in Figure 4.3.

Figure 5.1 - Test 1 Windward Side Skin Temperatures, 300-480 sec.
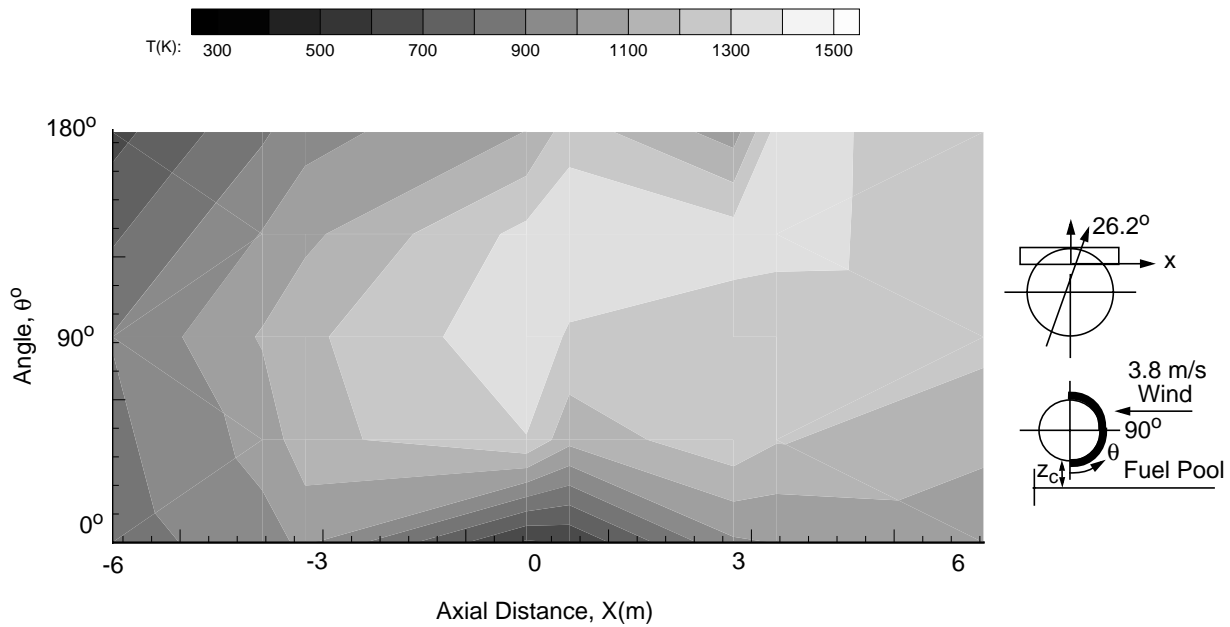
Figure 5.2 - Test 1 Leeward Side Skin Temperatures, 300-480 sec.

73
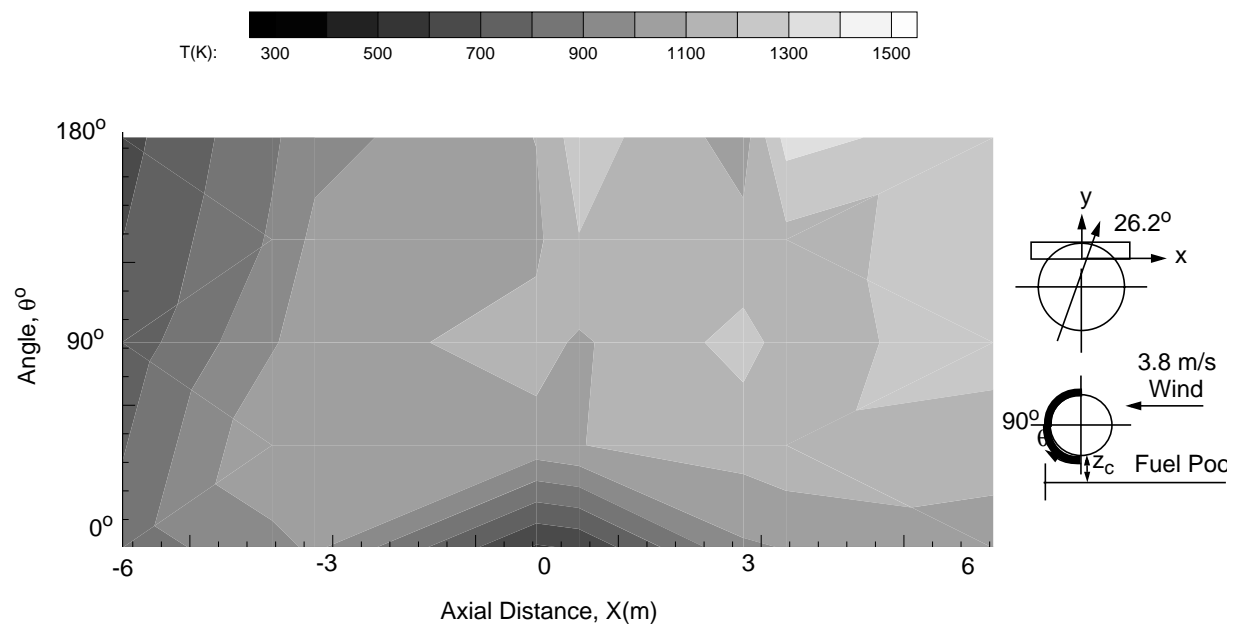
5.2.2 Skin Temperatures for Test 2

Data were averaged over a quasi-steady time period from 225 to 350 seconds following ignition for Test 2. The time-averaged wind speed and direction were 1.9 m/s and -36.9°, respectively. Mock fuselage skin temperature plots are shown in Figures 5.3 and 5.4. High temperature gradients (260 K/m) are observed near local high temperature regions. Temperatures range from 350-1400 K on the windward side and 350-1150 K on the leeward side.

Figure 5.3 shows the temperature distribution on the windward side of the mock fuselage with a high temperature region approaching 1500 K at an axial distance of x=-3 m and an angle of 90°. This high temperature (1400 K) area is expected to be a consequence of the redirection of the flame zone by low (1.9 m/s) winds directed 36.9° counter clockwise from normal to the longitudinal axis of the mock fuselage. These winds are expected to cause direct impingement of the actively combusting region (i.e. the burning region between the oxygen-starved interior and the exterior) on the mock fuselage. A high temperature region (1150 K) also exists on the leeward side of the mock fuselage (Figure 5.4) at x=3 m and an angle of 45°. The increased temperatures are likely caused by the flow being forced under the calorimeter and then attaching to the leeward surface of the calorimeter. The lowest temperatures

Figure 5.3 - Test 2 Windward Side Skin Temperatures, 225-350 sec.
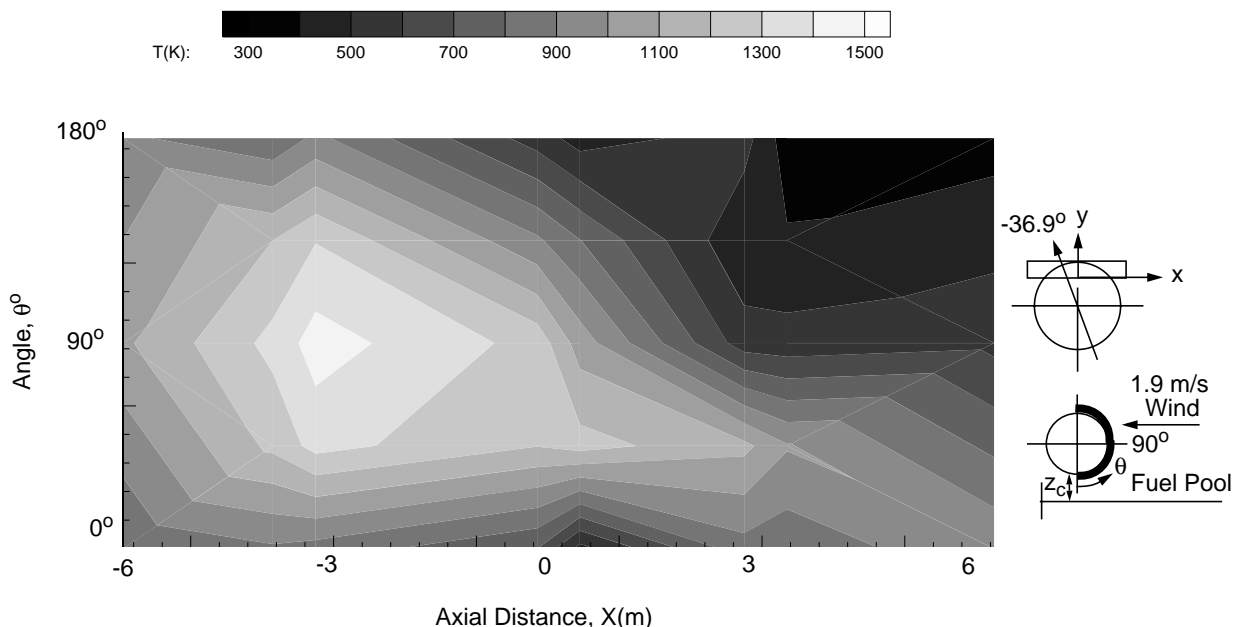
Figure 5.4 - Test 2 Leeward Side Skin Temperatures, 225-350 sec.
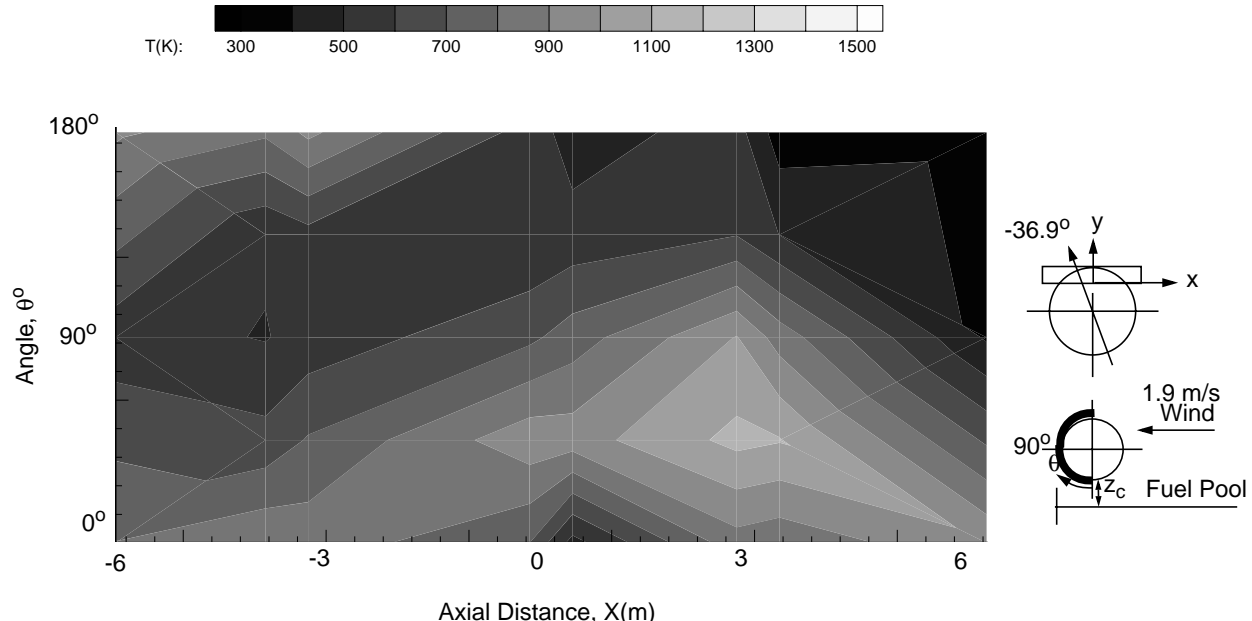
(350 K) occur on the upper part of the mock fuselage at x=6 m where there is no flame cover. These temperature trends are confirmed in the flame shape contours (Figures 4.5-4.7) presented in the previous chapter.

5.2.3 Skin Temperatures for Test 3

Two quasi-steady time periods, 300-600 seconds and 680-715 seconds following ignition, were identified for Test 3.

Temperature contour plots for the first quasi-steady time period are shown in Figures 5.5 and 5.6. The results show that high wind speeds (10.2 m/s, -22.7°) produce high temperatures (1000-1500 K) over the entire surface of the mock fuselage. A very high temperature region (1500 K) was recorded on the leeward side of the mock fuselage due to increased fuel/air mixing from interaction of the wind with the mock fuselage as described earlier during discussion of the flame shape contours in Figures 4.8-4.10. Figure 5.5 of the windward side shows a high temperature (1450 K) region low on the windward surface of the mock fuselage as a result of flame impingement and subsequently enhanced fuel/air mixing in the wake of the object.

75

Figure 5.5 - Test 3 Windward Side Skin Temperatures, 300-600 sec.
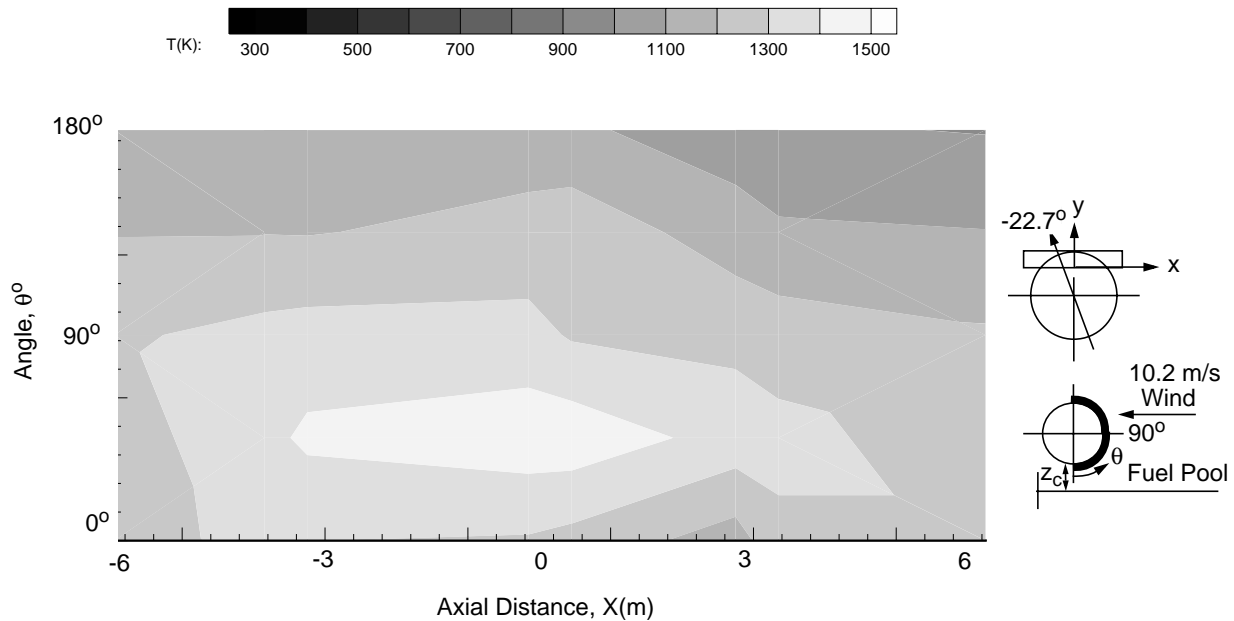
Figure 5.6 - Test 3 Leeward Side Skin Temperatures, 300-600 sec.
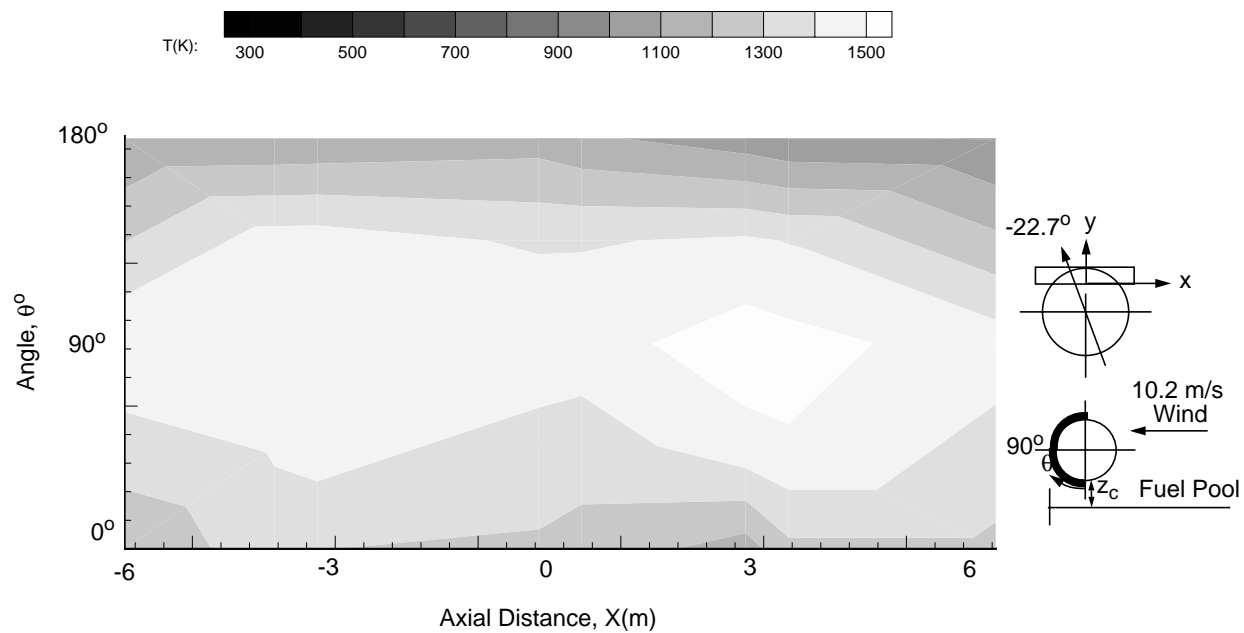
Figure 5.7 - Test 3 Windward Side Skin Temperatures, 680-715 sec.
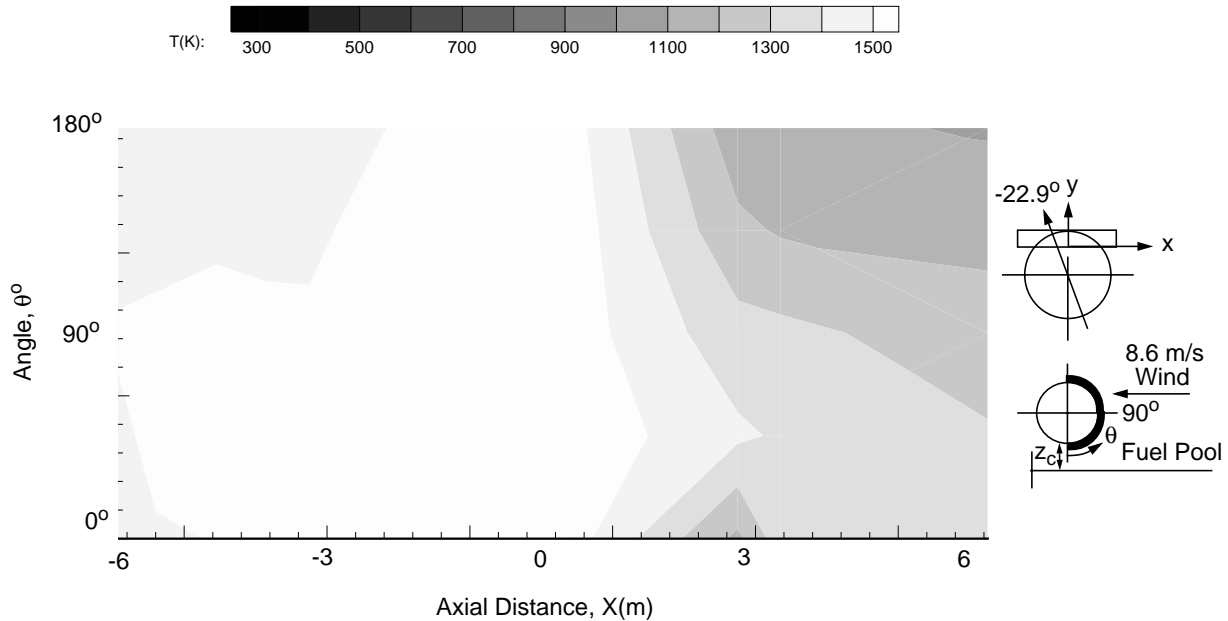
Plots of the temperature distributions for the second quasi-steady time period are shown in Figures 5.7 and 5.8. Although lower wind speeds (8.6 m/s, -22.9°) were measured during this time period, the same extreme temperature (1000-1600 K) regions with small (20-50 K/m) temperature gradients were observed in the results. The high temperature regions covered a much greater area in the second time period due to additional heating from the time of ignition. The lowest temperature regions were located on the top and bottom from x=3m to x=6 m, due to redirection of the flame zone by the wind component parallel to the longitudinal axis (as shown in the flame shape contours). The temperature trends are consistent with the contour plots of the flame shapes in Figures 4.11-4.13.

Temperatures greater than 1500 K are not shown in the plots due to the decreased reliability of the thermocouple reading close to the melting point of the instrument.

Figure 5.8 - Test 3 Leeward Side Skin Temperatures, 680-715 sec.
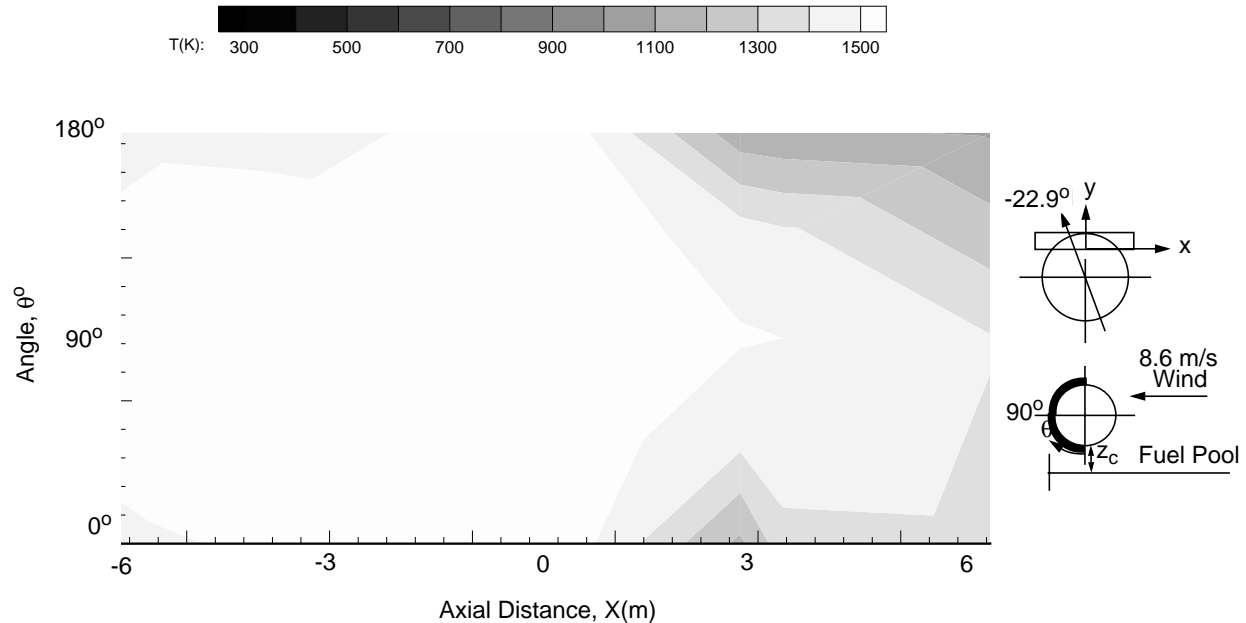
5.2.4 Skin Temperatures for Test 4

Two quasi-steady time periods were identified for Test 4. The periods occurred between 120-240 seconds following ignition, with an average wind speed of 5.1 m/s (at -52.8⁰) and 360-480 seconds following ignition, with an average wind speed of 3.6 m/s (at -26.7⁰). The wind speeds and directions are depicted in a small diagram in Figures 5.9-5.12.

Temperatures between 400 and 1350 K, with moderately high temperature gradients (70-100 K/m), were measured during the first quasi-steady time period. Figure 5.9 shows a high temperature (1200-1350 K) region near x=-6 m at angles between 45⁰ and 180⁰ on the windward side of the mock fuselage. Temperatures indicative of significant flame cover (1100 K) are also evident over the top of the mock fuselage to the leeward side of the mock fuselage near x=-6 m. High temperature regions were also observed in the thermocouple temperature plots in Figure 4.14 where the flame zone appears to be attached to the upper part of the windward side of the mock fuselage. The flame zone in Figure 4.15 appears to cover the mock fuselage at the axial centerline on both the leeward and windward sides which is confirmed by the 1000 K temperatures recorded on the skin at this plane. The temperatures are slightly higher on the lower windward and the lower leeward

Figure 5.9 - Test 4 Windward Side Skin Temperatures, 120-240 sec.
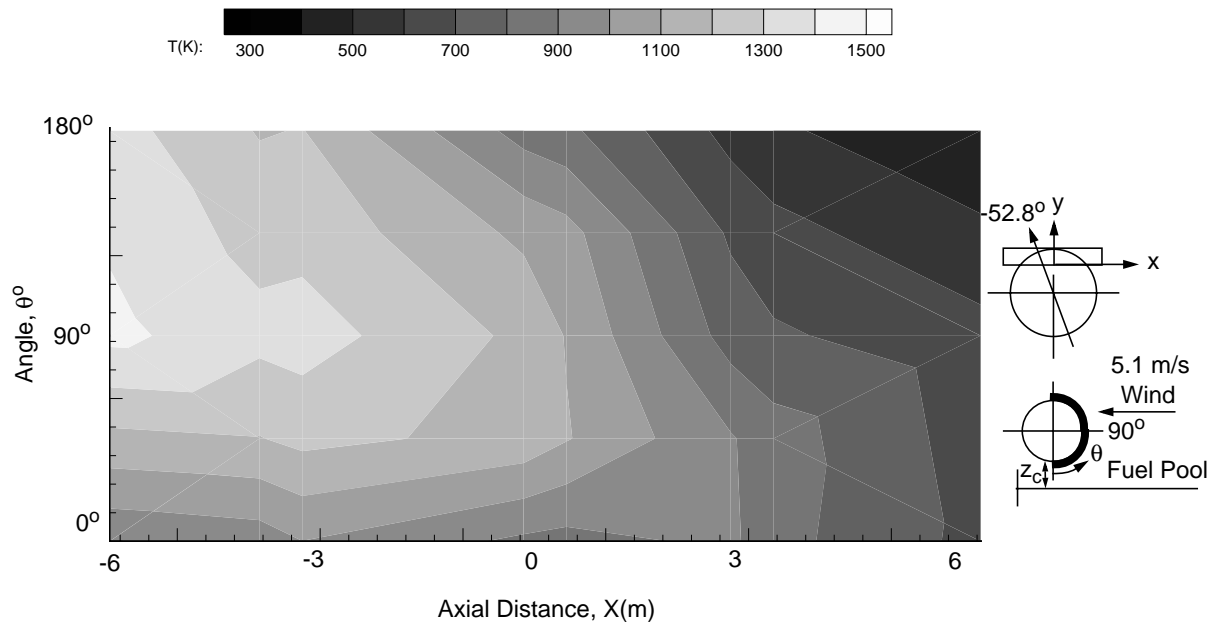
Figure 5.10 - Test 4 Leeward Side Skin Temperatures, 120-240 sec.
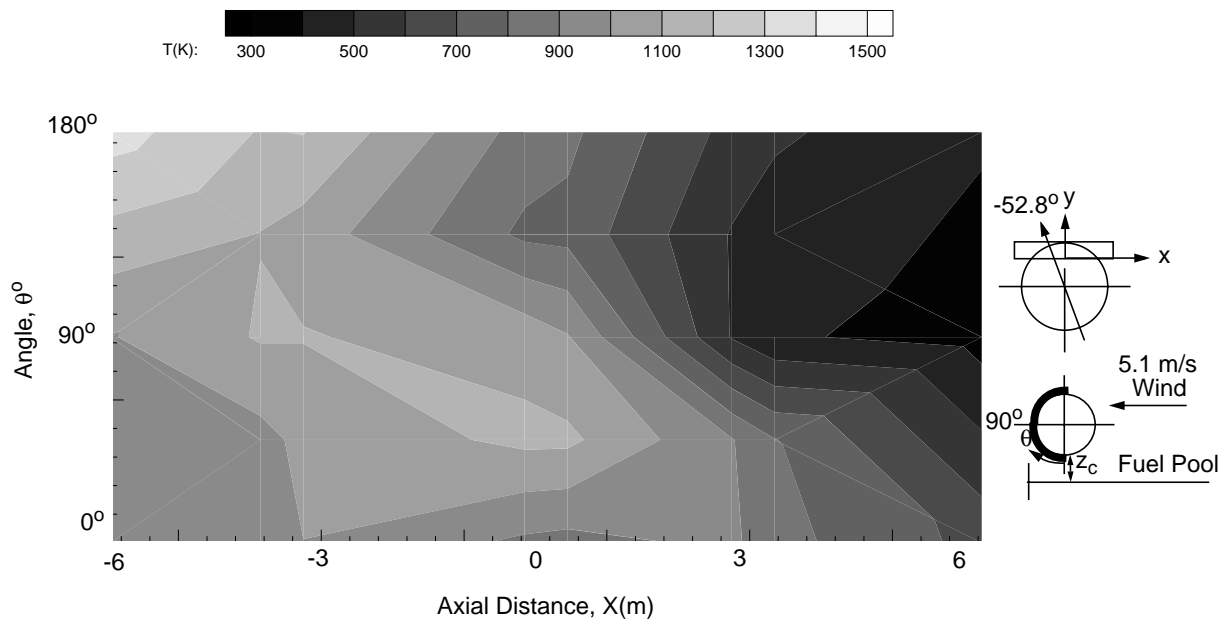
Figure 5.11 - Test 4 Windward Side Skin Temperatures, 360-480 sec.
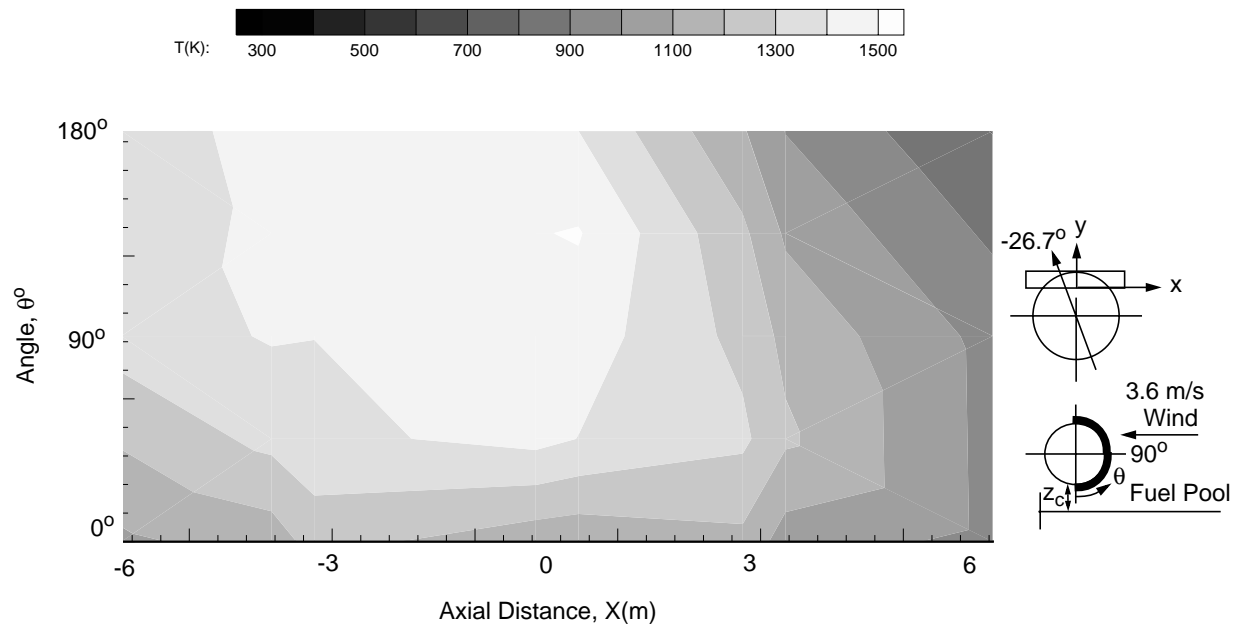
Figure 5.12 - Test 4 Leeward Side Skin Temperatures, 360-480 sec.
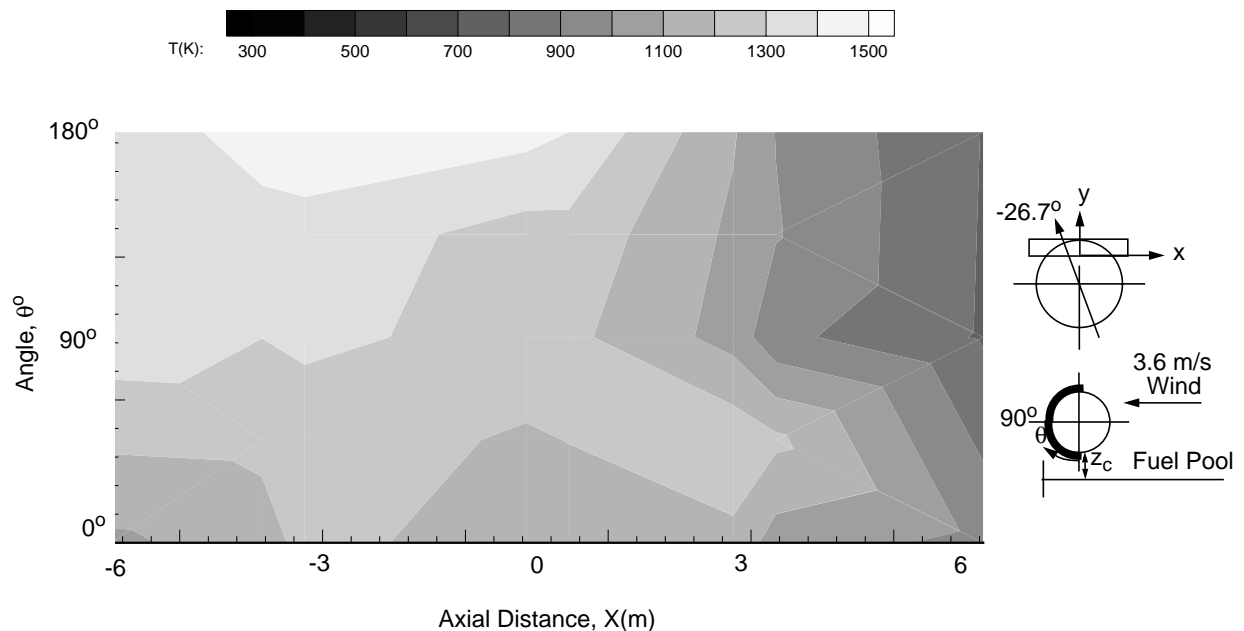
surfaces due to flame impingement and attachment, respectively, as was previously described in Figures 4.14-4.16.

As expected due to heating of the test fixture, the mock fuselage temperature data for the second time period are, in general, higher (700-1500 K) with smaller (30-90 K/m) temperature gradients. The flame shape contours for the centerline and the leeward measurement planes (Figures 4.17-4.18) showed a high temperature (1500 K) flame zone engulfing the upper half of the mock fuselage. The high temperature regions in Figures 5.11-5.12 occur in the same location on the mock fuselage as the flame coverage. The high temperature (1200 K) regions for the x=6 m plane occur between 0° and 90° on both the windward and the leeward surfaces due to the impingement and attachment of the flame zone described in the previous chapter.

5.2.5 Skin Temperatures for Test 5

As in the previous tests, two quasi-steady time periods were identified for Test 5. Measurements were averaged over periods between 400-575 and 250-670 seconds following ignition with wind speeds of 5.4 m/s (11.4^o) and 6.7 m/s (5.6^o), respectively. Figures 5.13-5.16 show almost identical temperature distributions for both time periods.

Figure 5.13 - Test 5 Windward Side Skin Temperatures, 400-575 sec.
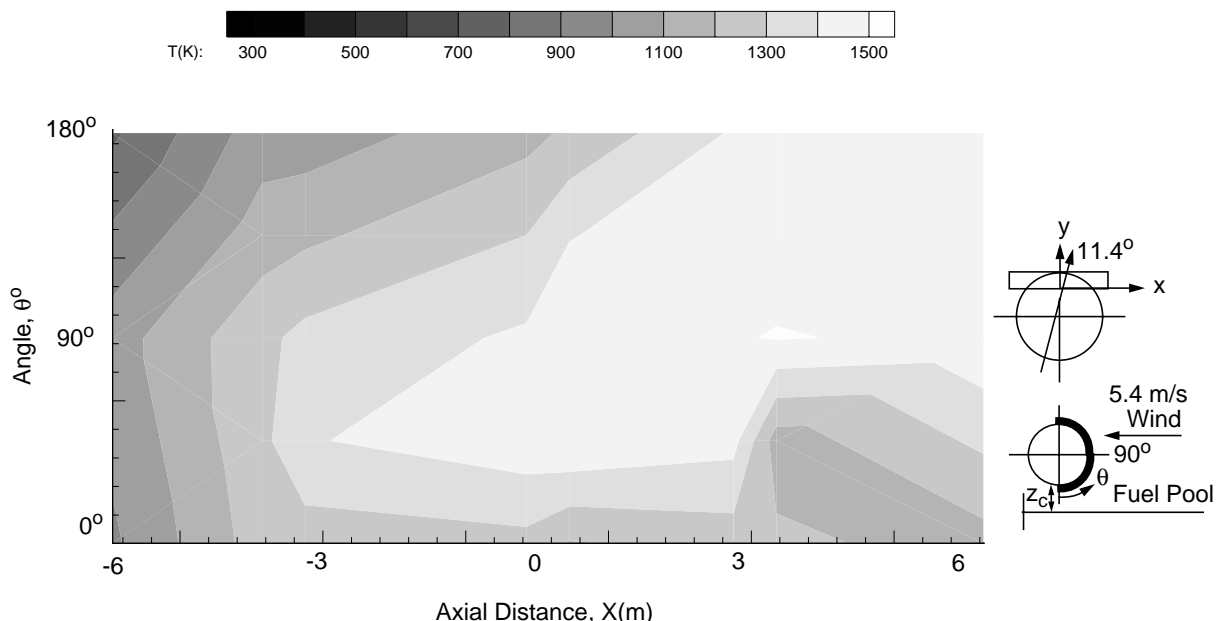
Figure 5.14 - Test 5 Leeward Side Skin Temperatures, 400-575 sec.
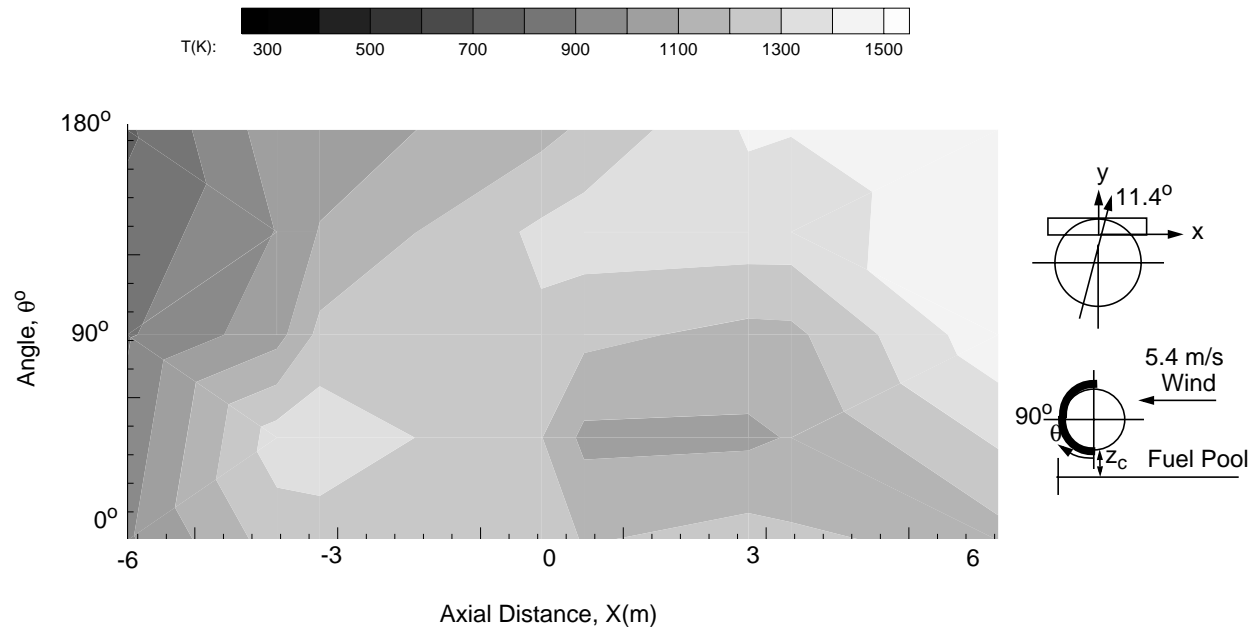
Figure 5.15 - Test 5 Windward Side Skin Temperatures, 250-670 sec.
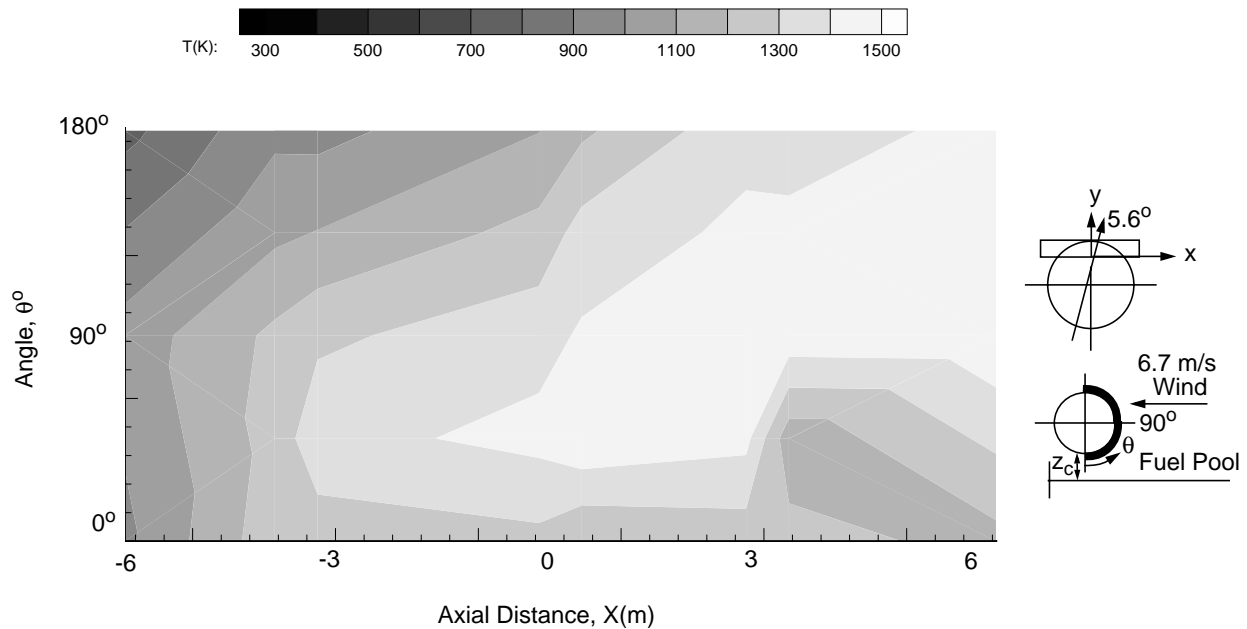
Figure 5.16 - Test 5 Leeward Side Skin Temperatures, 250-670 sec.
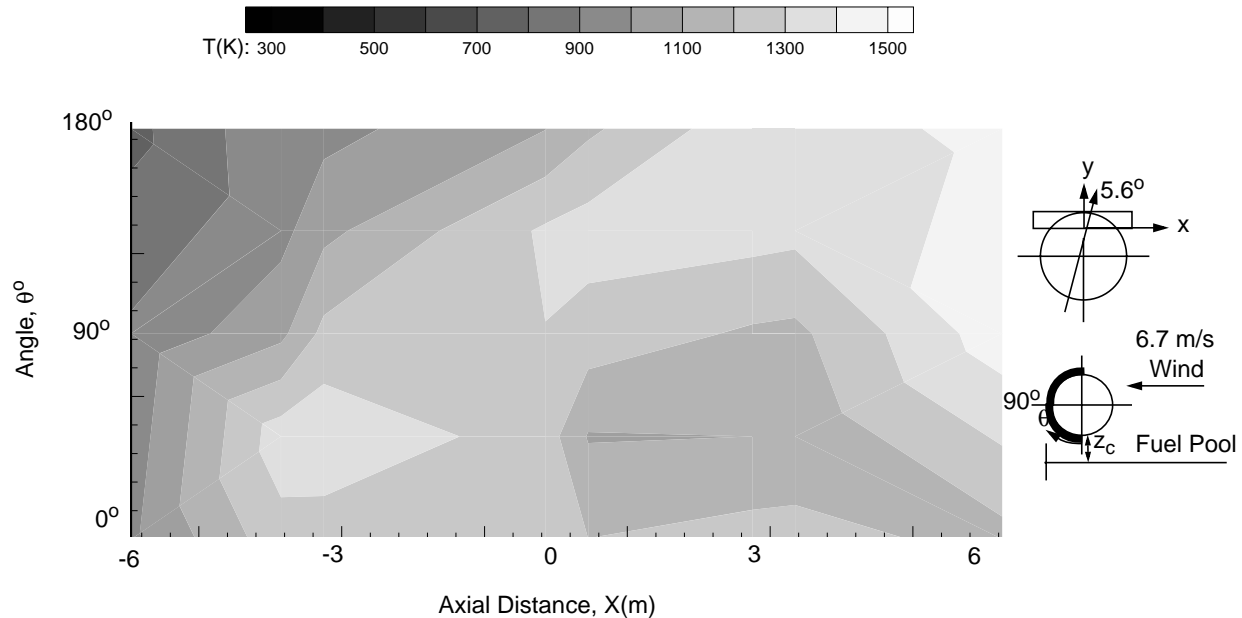
The temperatures range from 800-1500 K with fairly small (25-100 K/m) temperature gradients. The temperature distribution trends are consistent with the flame shape contours in Figures 4.20-4.22 and 4.23-4.25. Increased temperatures are observed on the lower windward and leeward surfaces near x=-6 m where impingement and flame attachment occur. Figures 4.20 and 4.23 also show high temperature flame cover in these regions. The centerline measurement plane skin temperatures agree with the trends shown in the flame shape contours. High temperature regions occur on the windward side (1500 K) from 45^0-135^0 and on the leeward side (1350 K) centered around 135^0. The low temperature (900-1000 K) region near the centerline of the mock fuselage from 0^0-90^0 is consistent with the reduced temperatures in the flame shape contours in Figures 4.21 and 4.24. High temperatures were measured on the upper windward and leeward surfaces of the mock fuselage skin at x=6 m due to the presence of extensive flame cover and hence, the main high temperature zone in the flame shape contours (Figure 4.22 and 4.25) extending from the windward side (45^0) and over the top to the leeward side (90^0).

5.2.6 Skin Temperatures for Test 8

Test 8 was performed with the intention of reproducing the high temperatures observed during Test 3 under high speed wind conditions. The wind during the quasi-steady time period 475-598 seconds after ignition was 9.9 m/s in the same

83

Figure 5.17 - Test 8 Windward Side Skin Temperatures, 475-598 sec.
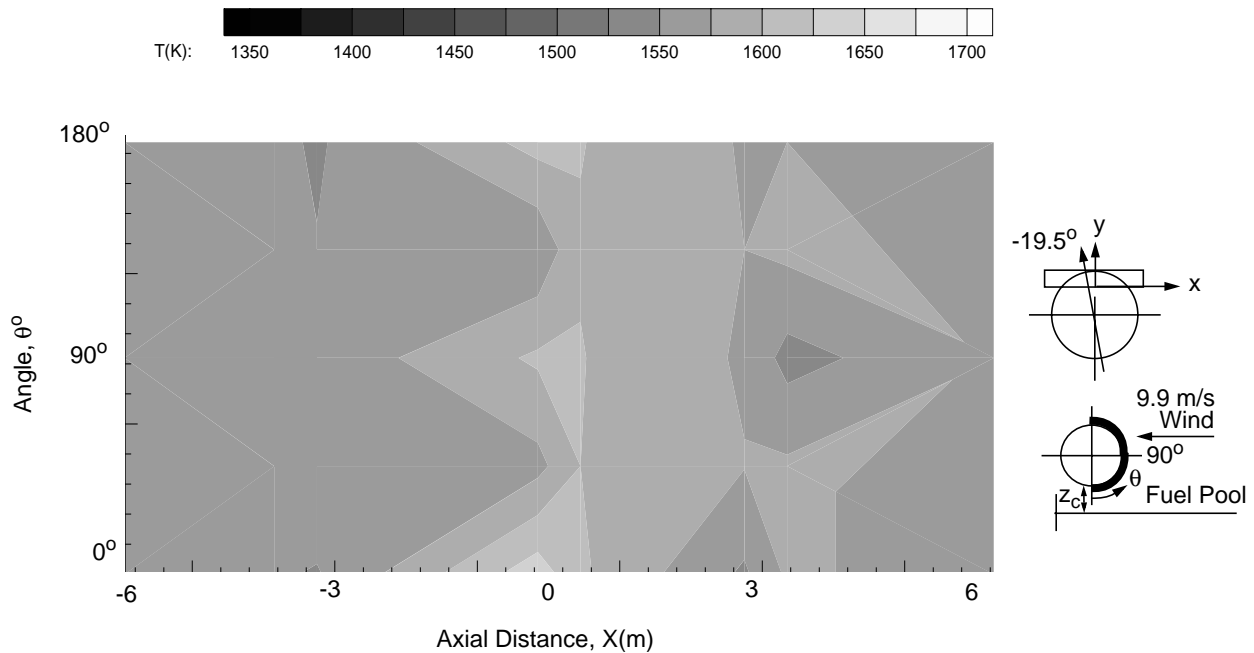
direction (-19.5°) as in Test 3. The temperature distribution contours shown in Figures 5.17 and 5.18 display very low (5-10 K/m) temperature gradients. When comparing the contour plots of Tests 3 and 8, note that the temperature scales are very different. The scale for Test 3 was 300-1500 K to allow comparison with data from other tests. The temperatures observed during Test 8 were greater than the temperatures of the scale used for the other tests; therefore, the scale used in Test 8 was 1350-1700 K. The actual range of temperatures recorded only covered a small portion of the scale from 1550-1675 K. The temperatures ranged from 1000-1500 K in Test 3 and ranged from 1550-1625 K in Test 8. Test 8 therefore successfully reproduced and even exceeded the extremely high temperatures seen in Test 3. Shortly after this quasi-steady time period, the temperatures exceeded the melting temperature of the Inconel thermocouples (1675 K) and therefore subsequent data are not presented. Temperatures above 1500 K are included in the scale since all temperatures recorded exceeded 1500 K. Before thermal failure of the thermocouples, it is evident that the mock fuselage was covered by flames on both sides as also shown in the flame shape contours in Figures 4.26-4.28.

84

Figure 5.18 - Test 8 Leeward Side Skin Temperatures, 475-598 sec.
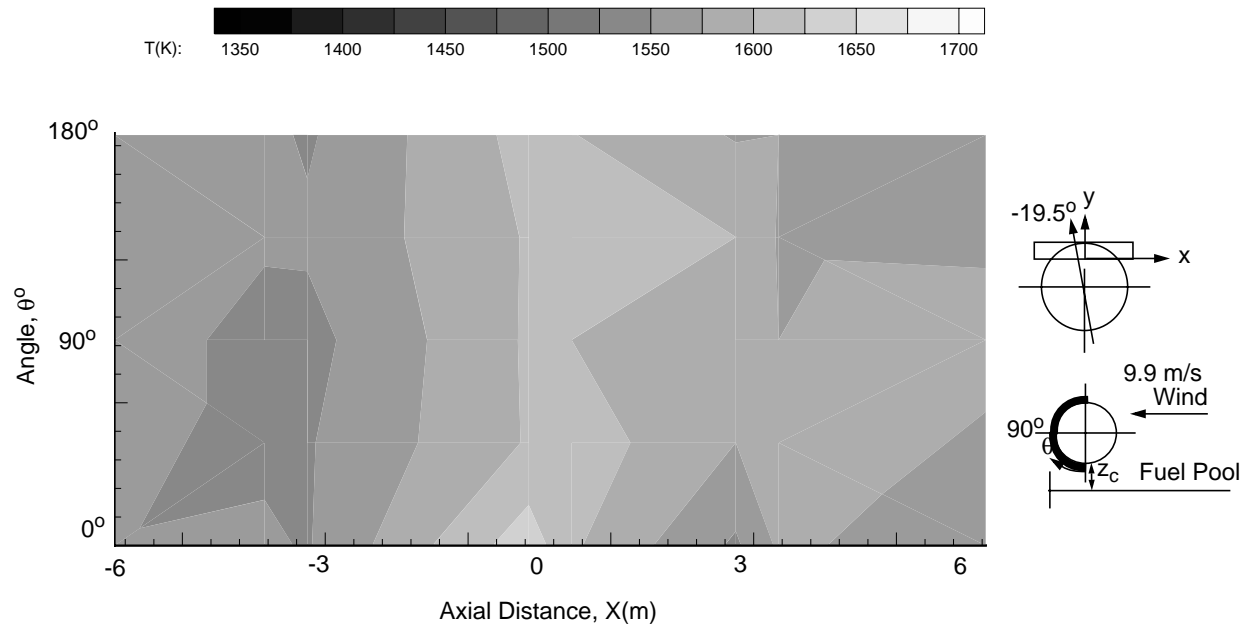
5.3 Small Pool Skin Temperature Distributions

Two tests, numbers six and seven, were performed in a 10 m fuel pool instrumented as stated in Chapter 2. Contour plots of the front and back skin temperatures were created for each test using thermocouple data. The coarse contours that sometimes occur in these plots are the result of interpolation between data points.

5.3.1 Skin Temperatures for Test 6

Test 6 was conducted in the 10 m diameter pool. High wind conditions of 9.5 m/s prevailed during the defined quasi-steady time period from 270 to 390 seconds after ignition. The direction of wind was nearly normal (2.0^0) to the longitudinal axis of the mock fuselage. The temperature distribution contours, with temperatures ranging from 500-1400 K, are shown in Figure 5.19 and Figure 5.20. From the wind conditions, the high temperature (1400 K) region that exists on the leeward side is expected given the previous analysis of the flame shape contours (Figures 4.30-4.32). The lower windward side also shows temperatures of approximately 1400 K, but overall greater temperatures are observed on the leeward side. The high temperature region on the windward side is a result of flame impingement on the surface of the mock fuselage while the high temperature region on the leeward side

85

Figure 5.19 - Test 6 Windward Side Skin Temperatures, 270-390 sec.
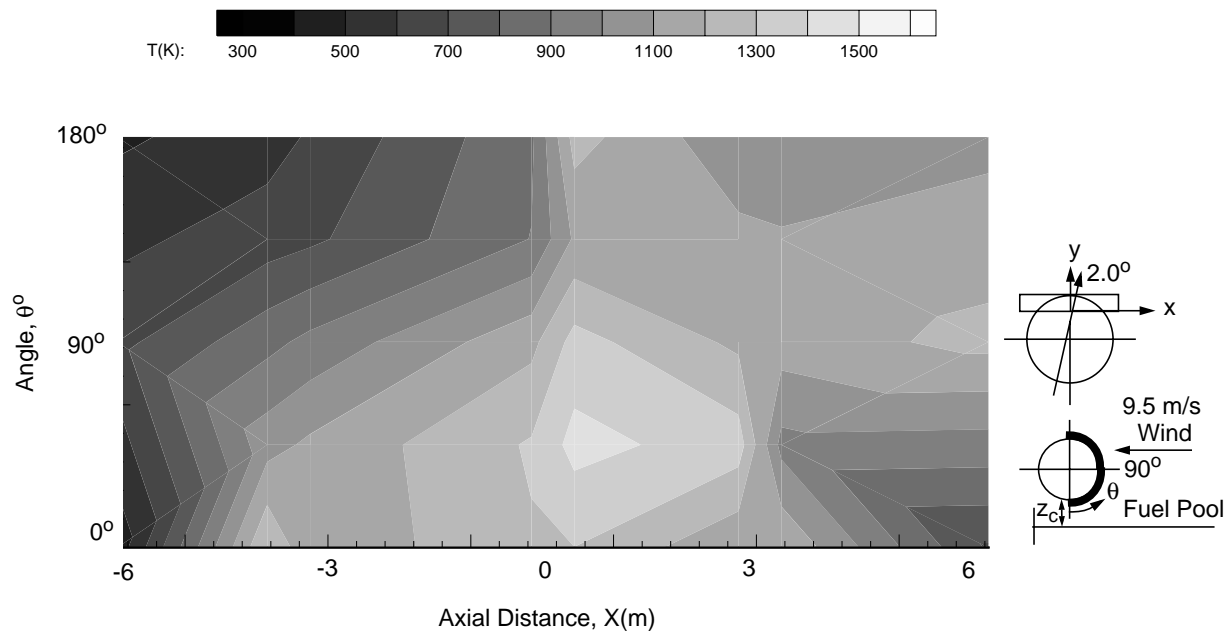
Figure 5.20 - Test 6 Leeward Side Skin Temperatures, 270-390 sec.
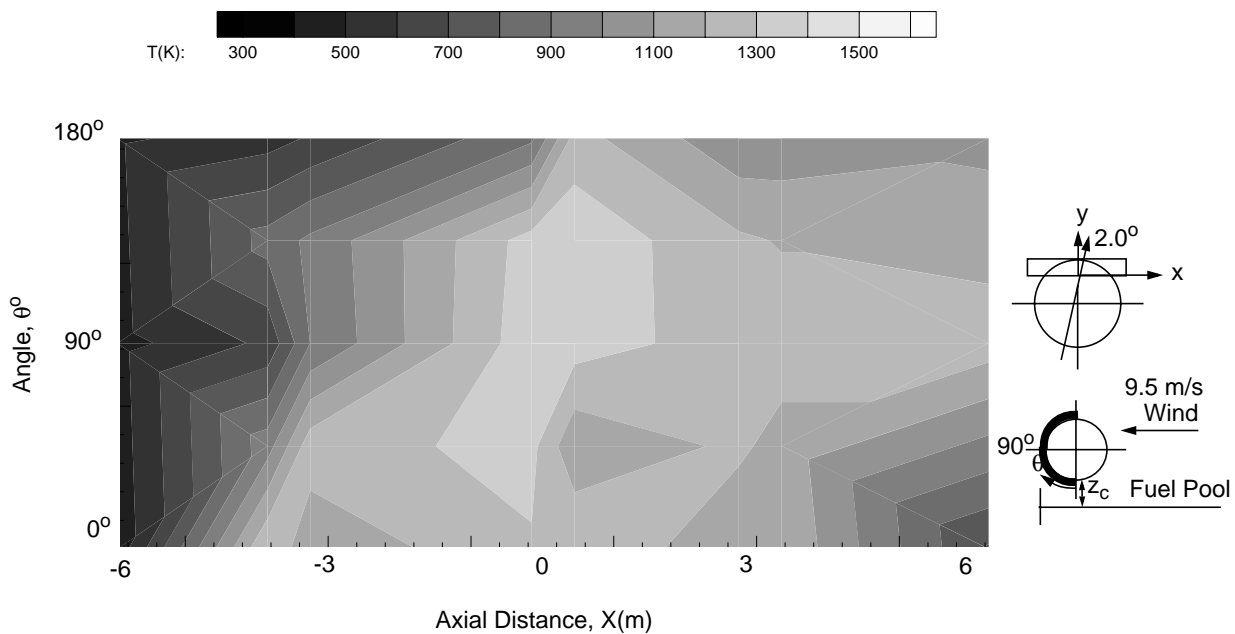
is a result of flame attachment to the surface of the mock fuselage. The locations of the high and low temperature regions are consistent with the contour plots of the flame shapes in Figures 4.30-4.32.

5.3.2 Skin Temperatures for Test 7

Test 7 was also conducted using a 10 m diameter fuel pool. Average wind conditions of 2.0 m/s at -36.1^o prevailed during the quasi-steady time period from 250-500 seconds following ignition. The temperature distributions contain temperature gradients (~125 K/m) at large axial distances from the centerline as shown in Figures 5.21 and 5.22. This test was conducted with a very low wind speed. The primary vertical rise of the flame zone produced a high temperature region (1400 K) on the windward side of the mock fuselage. This very high temperature region was also observed in Figure 4.34 which contained the thermocouple temperatures obtained at the centerline measurement plane from 90°-180°.

Figure 5.21 - Test 7 Windward Side Skin Temperatures, 250-500 sec.
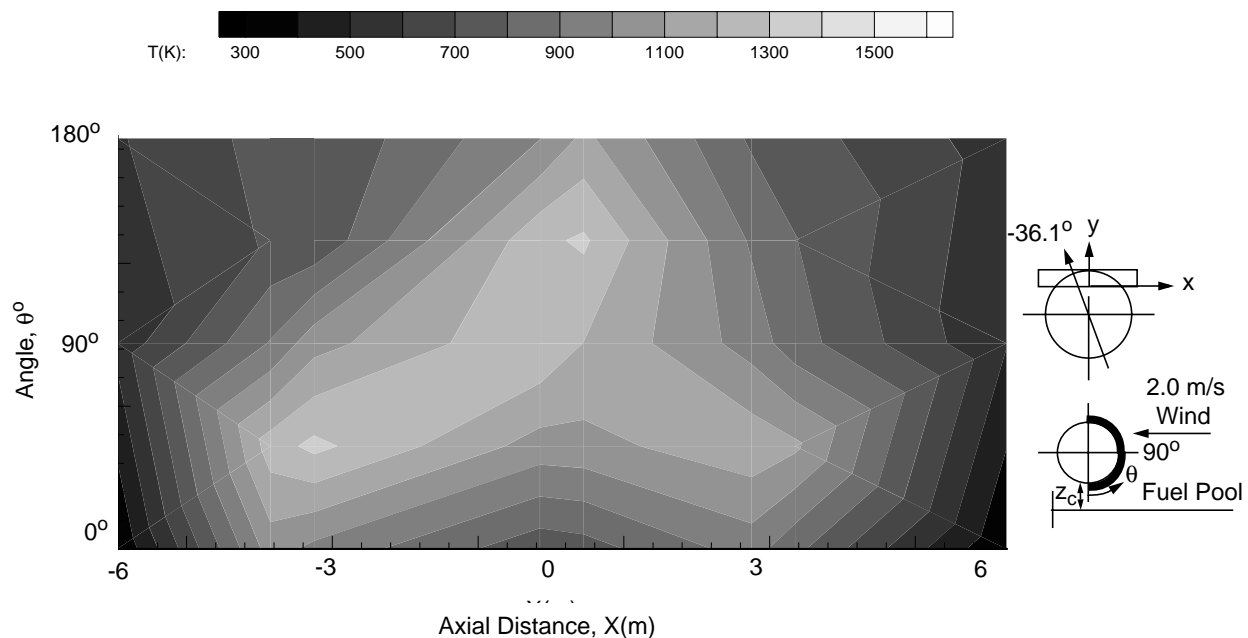
Figure 5.22 - Test 7 Leeward Side Skin Temperatures, 250-500 sec.
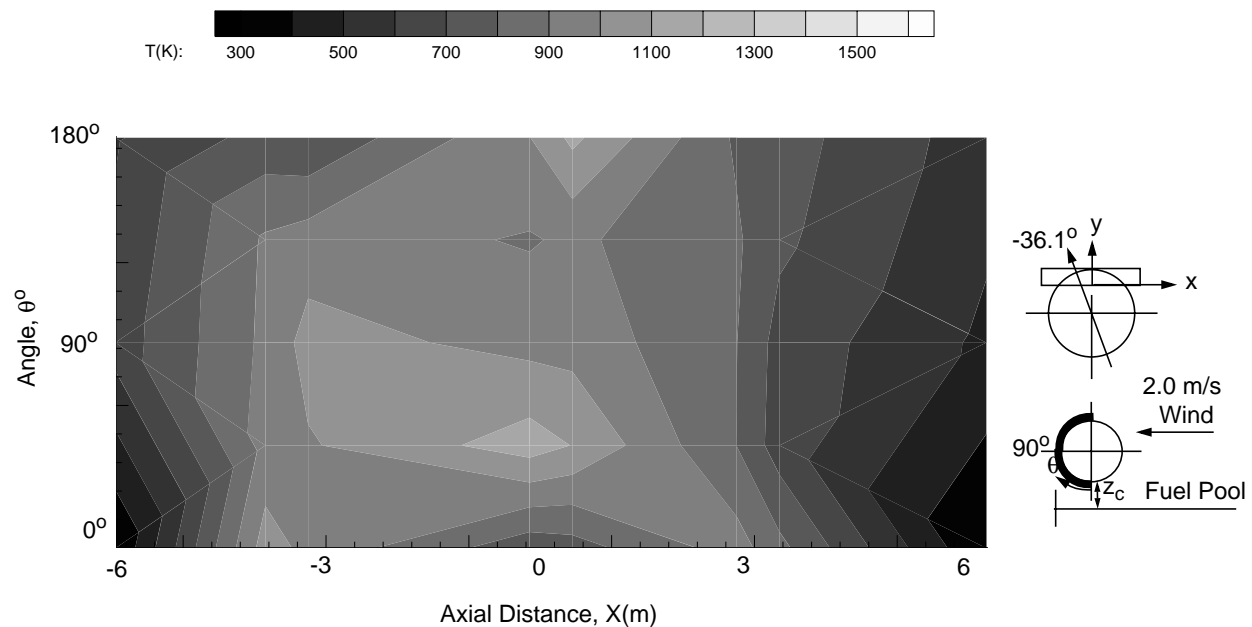
6. Experimental Results - Skin Heat Flux Distributions

6.1 Overview of Experiments

The heat flux data obtained from the thermocouple measurements were transformed into contour plots to show the heat flux distribution on the skin of the mock fuselage during the quasi-steady time periods for each test. The absorbed heat flux was calculated using the transient temperature change and the material properties. Contour plots of the windward and leeward sides of the mock fuselage were produced by averaging the heat flux over a quasi-steady time period. These plots present the data in a suitable format for fire model comparisons. Some coarseness in the plots occurs as a result of the interpolation of values between experimental data points.

6.2 Skin Heat Flux Distributions for Large Pool

The first six tests were conducted in a 20 m pool of JP-8 jet fuel. The calorimeter was instrumented according to the plan stated in Chapter 2 (Figure 2.4). Any differences in test instrumentation will be specified as the results are discussed in each section.

6.2.1 Skin Fluxes for Test 1

A quasi-steady time period was identified between 300 and 480 seconds after ignition for Test 1. The time-averaged wind speed and direction were 3.8 m/s and -26.2^o, respectively. The contour plots on the windward and leeward sides of the mock fuselage (Figures 6.1 and 6.2) contain a small diagram depicting the wind conditions during the time period.

The range of heat fluxes (30-220 kW/m^2) and moderately high heat flux gradients (25-40 kW/m^2/m) observed on the windward side of the mock fuselage are shown in Figure 6.1. As a result of flame impingement, a high heat flux (220 kW/m^2) region was observed on the windward side of the mock fuselage. The low heat flux (30 kW/m^2) region that exists on the lower windward and leeward sides is consistent with the presence of an oxygen starved region. The heat flux trends are a consequence of the flame cover, shown in Figure 4.3, which also produce the high skin temperatures seen in Figure 5.1.

The measurements on the leeward side include considerably lower heat fluxes and gradients in the range of 60-140 kW/m^2 and 10-25 kW/m^2/m, respectively. The highest heat flux on the leeward side was approximately 140 kW/m^2. The lowest heat fluxes (60 kW/m^2) were observed at the center of the lower windward and leeward sides of the mock fuselage due to the potential existence of an oxygen starved region

Figure 6.1 - Test 1 Windward Side Skin Heat Flux Distribution, 300-480 sec.
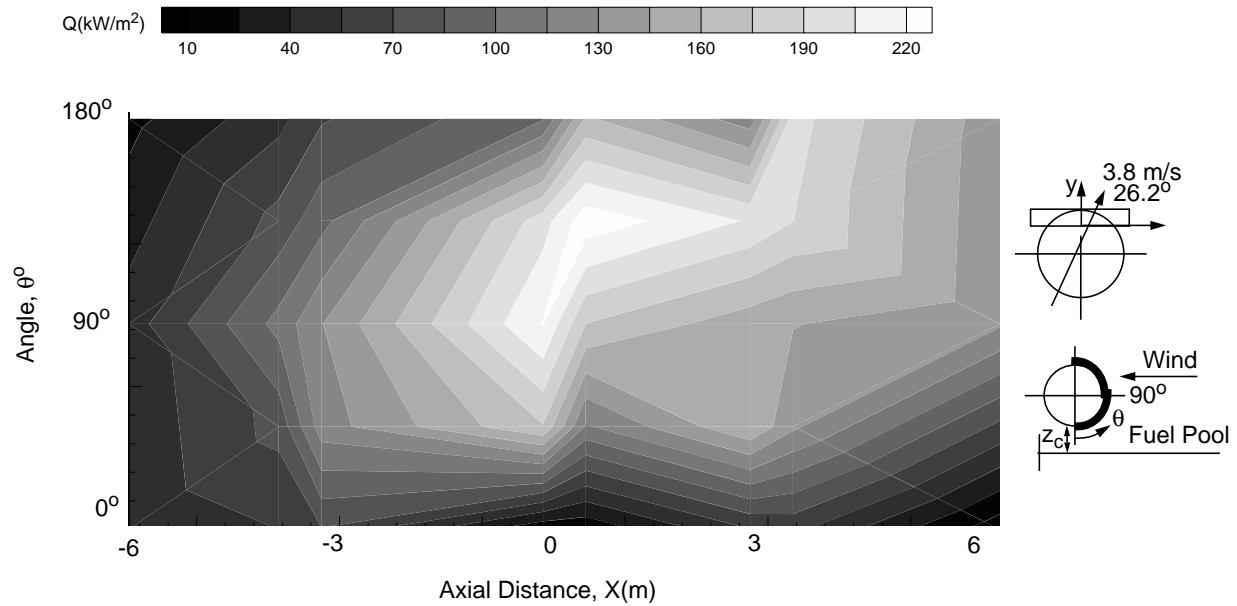
Figure 6.2 - Test 1 Leeward Side Skin Heat Flux Distribution, 300-480 sec.
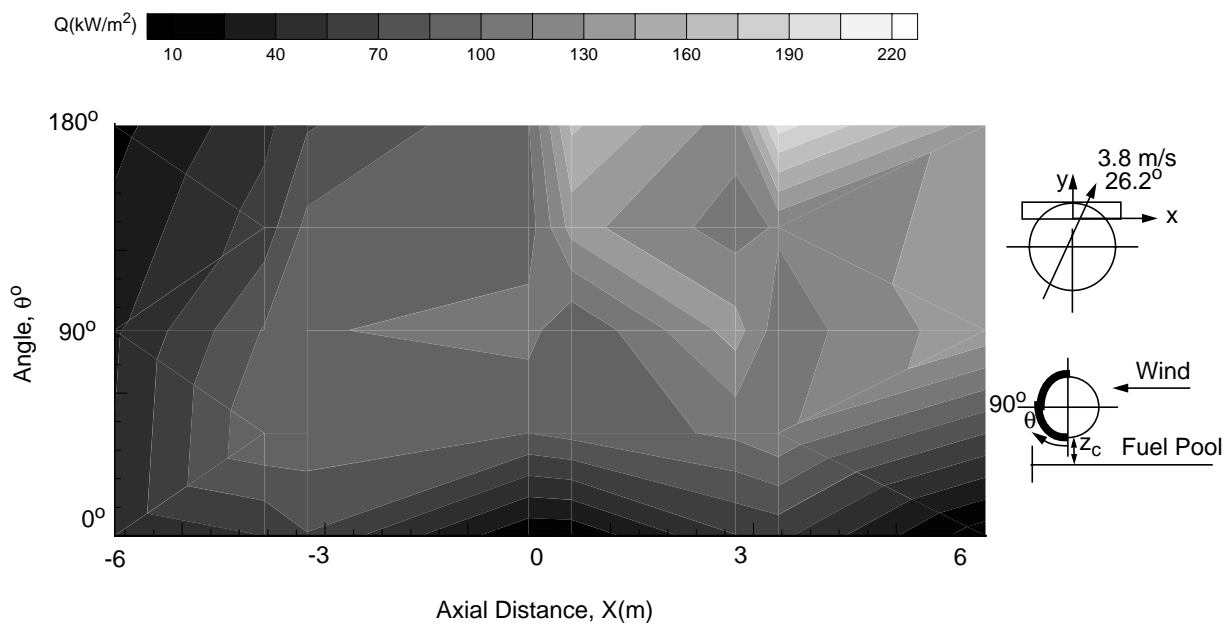
at the same location. The trends observed in these skin heat flux contours for Test 1 are very similar to the trends observed in the temperature contours (Figures 5.1 and 5.2) which were determined to be a direct consequence of the flame shape contours in Figures (4.2-4.4).

6.2.2 Skin Fluxes for Test 2

A quasi-steady time period was identified between 225 and 350 seconds following ignition for Test 2. The time-averaged wind speed and direction were 1.9 m/s and -36.9^0, respectively. The plots are shown in Figures 6.3 and 6.4 for the windward and leeward surfaces of the mock fuselage. The heat fluxes range between 10 and 220 kW/m^2 with maximum heat flux gradients (50 kW/m^2/m) near the high flux region on the windward side at 3 m to the left of the calorimeter centerline. This high heat flux region and the high temperature region, shown in Figure 5.3, are in the same location on the mock fuselage surface. The region is caused by impingement of the actively combusting region on the mock fuselage as previously stated in Chapters 4 and 5.

Lower heat fluxes (20-140 kW/m^2) with smaller gradients (30 kW/m^2/m) were observed on the leeward side of the mock fuselage. The maximum flux (140 kW/m^2) occurred on the leeward side of the calorimeter, 3 m to the right of the centerline at

Figure 6.3 - Test 2 Windward Side Skin Heat Flux Distribution, 225-350 sec.
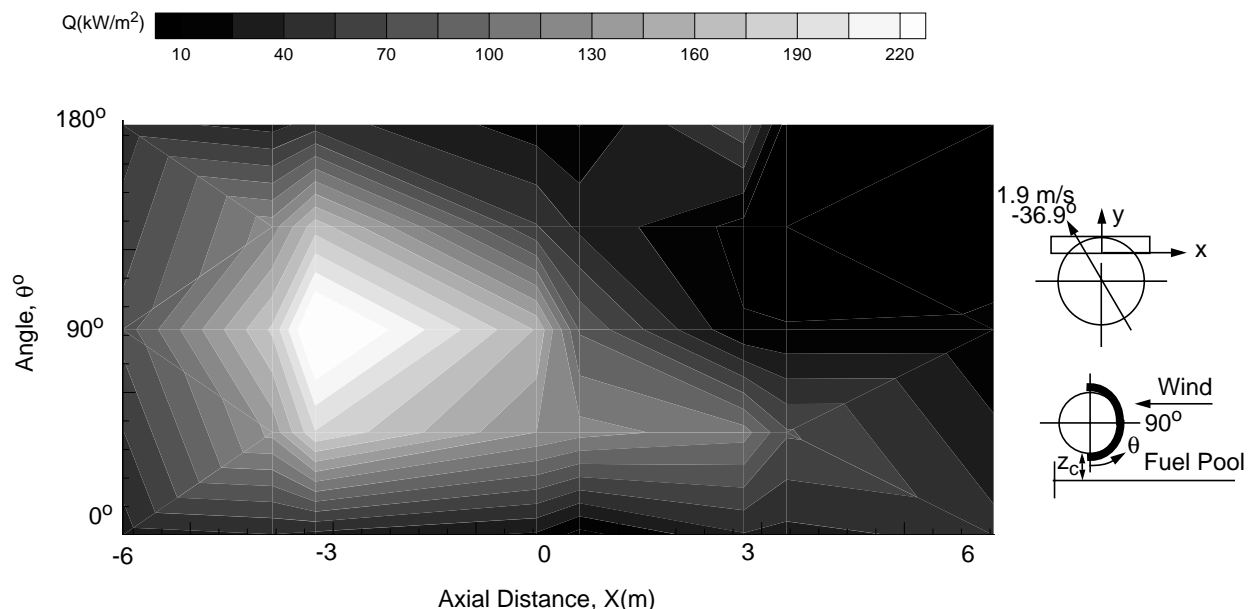
Figure 6.4 - Test 2 Leeward Side Skin Heat Flux Distribution, 225-350 sec.
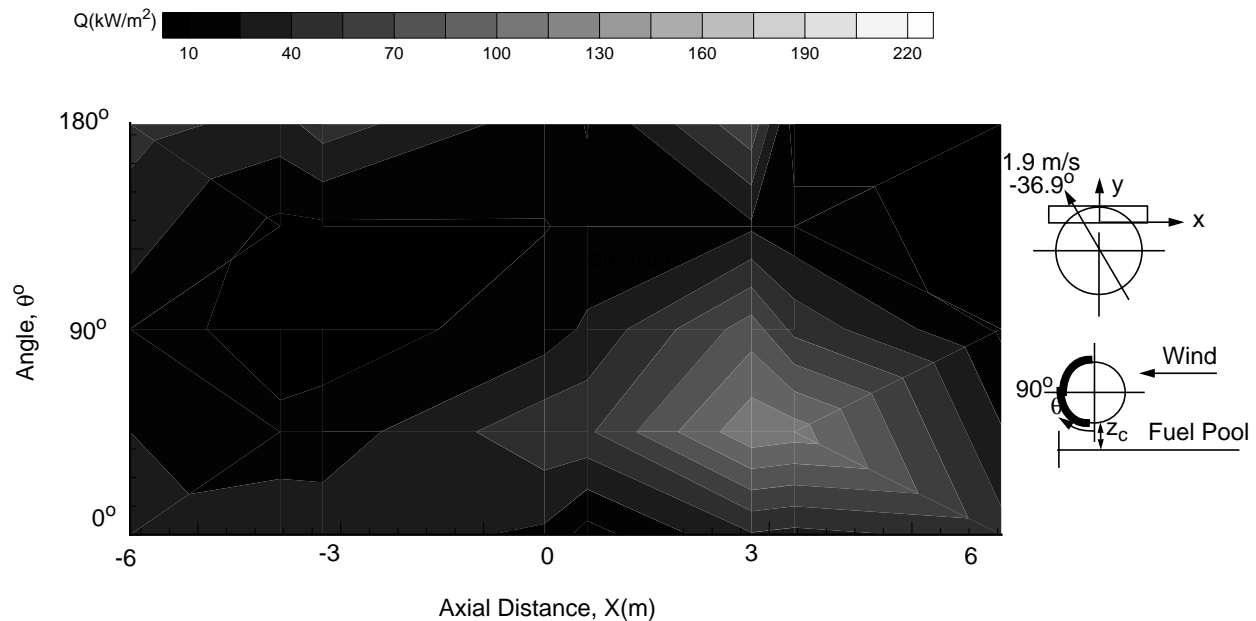
an angle of 45°. The presence of this maximum was also observed in the skin temperature contours (Figure 5.4) as a result of flame attachment to the surface of the mock fuselage as also seen in Figure 4.7 of the windward of centerline temperature contour plot.

6.2.3 Skin Fluxes for Test 3

The two quasi-steady time periods identified for Test 3 were 300-600 seconds following ignition and 680-715 seconds following ignition. The heat flux contour plots for the first quasi-steady time period are shown in Figures 6.5 and 6.6. Results from this test displayed the effects of high wind speed (10.2 m/s and 8.6 m/s) on the flux distribution. The heat fluxes are much higher than what is generally predicted, especially on the leeward side of the cylinder.

The highest heat fluxes are on the windward side of the mock fuselage are observed at about 45^0 and on the leeward side at approximately 90^0 in the first quasi-steady time period. On the windward side the maximum heat flux is 250 kW/m^2 with typical heat flux gradients of 10-30 kW/m^2/m. There are considerably higher (340 kW/m^2) heat fluxes and gradients (40 kW/m^2/m) on the leeward side of the calorimeter due to the presence of the object and the mixing induced by the high winds. The high wind speed throughout Test 3 increases the entrained air which directly affects the flame zone and the heat fluxes. The location of the lowest heat fluxes in the time period from 300-550s following ignition is on the top of the mock fuselage with a magnitude of approximately 80 kW/m^2. For the first quasi-steady period, the measured heat fluxes range from 80 kW/m^2 on the top of the mock

Figure 6.5 - Test 3 Windward Side Skin Heat Flux Distribution, 300-600 sec.
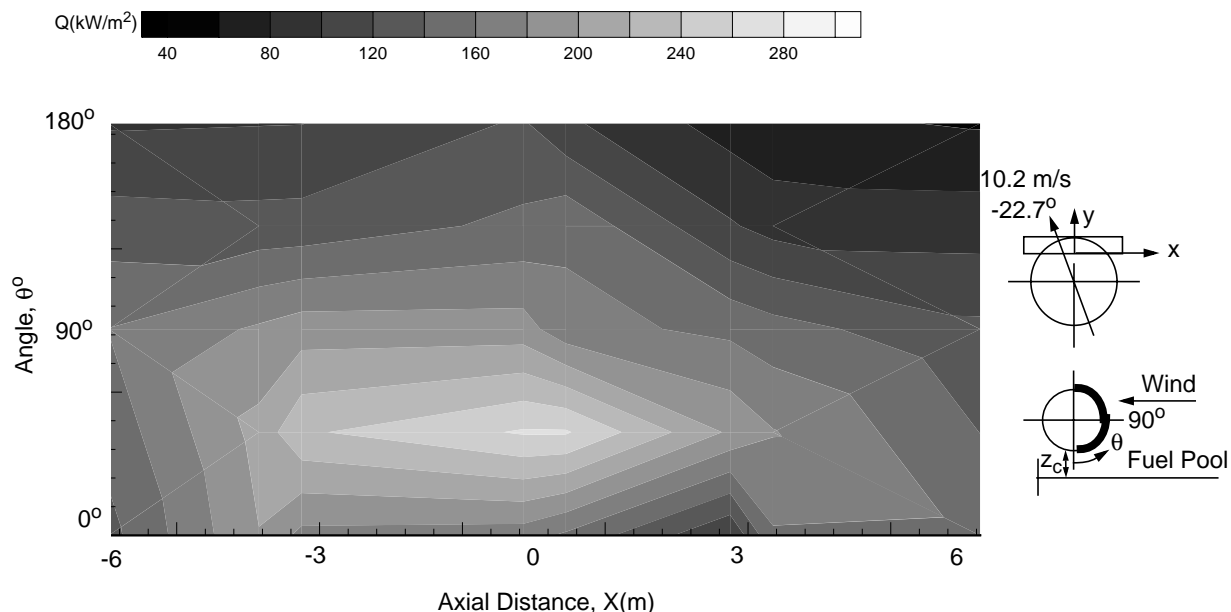
Figure 6.6 - Test 3 Leeward Side Skin Heat Flux Distribution, 300-600 sec.
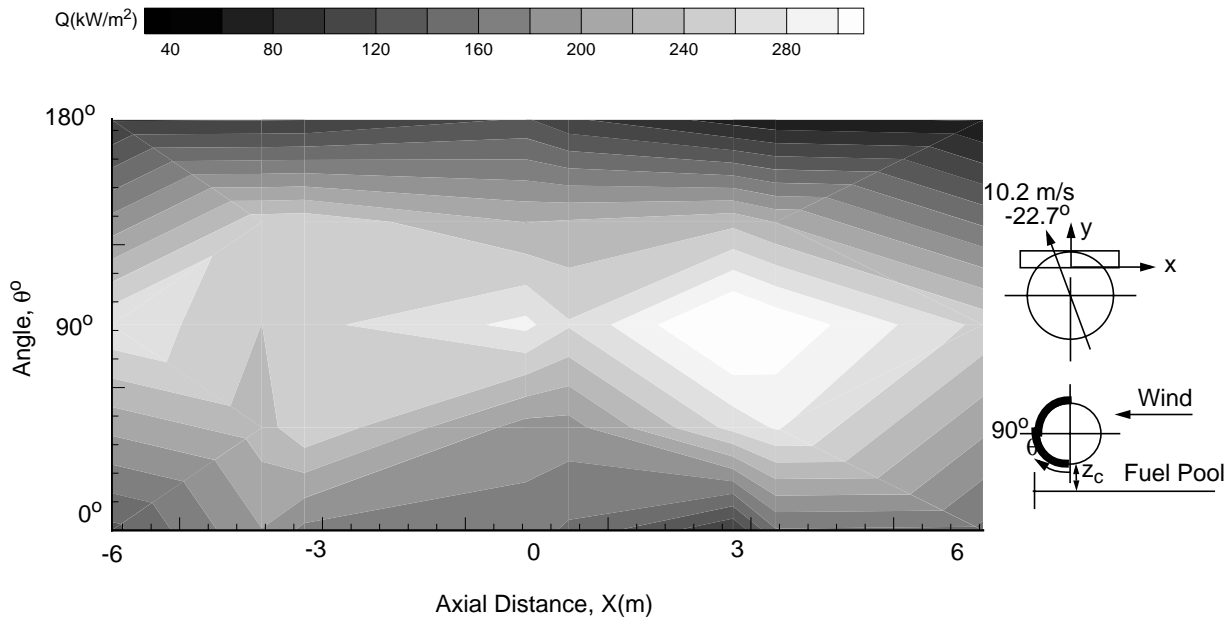
fuselage to over 300 kW/m^2 on the leeward side of the mock fuselage at approximately 270^0. The heat flux distributions described are consistent with the flame contours in Figures 4.8-4.10 where high temperature regions also exist on the leeward side and the lower windward side of the mock fuselage.

The second quasi-steady time period is shown in Figures 6.7 and 6.8. These figures show ultra-high heat fluxes ranging from 300-400 kW/m^2 on the lee side of the cylinder. These high heat fluxes are expected to be due to the increased fuel/air mixing resulting from the high winds and the presence of the object in the fire. In this time period the highest heat fluxes and the lowest gradients (<10 kW/m^2/m) are on the left side of the mock fuselage (x<0 m) due to the wind direction as depicted in the diagrams beside the plots. Ultra-high heat fluxes (300-400 kW/m^2) were observed towards the left side of the mock fuselage as a result of the wind speed and direction during the test. A larger area of these ultra-high heat fluxes was observed in this time period due to additional heating since the time of ignition. High temperatures (~1600 K) in the skin temperature distributions (Figures 4.11-4.13) were observed in the same locations as the high heat fluxes in Figures 6.7 and 6.8.

Figure 6.7 - Test 3 Windward Side Skin Heat Flux Distribution, 680-715 sec.
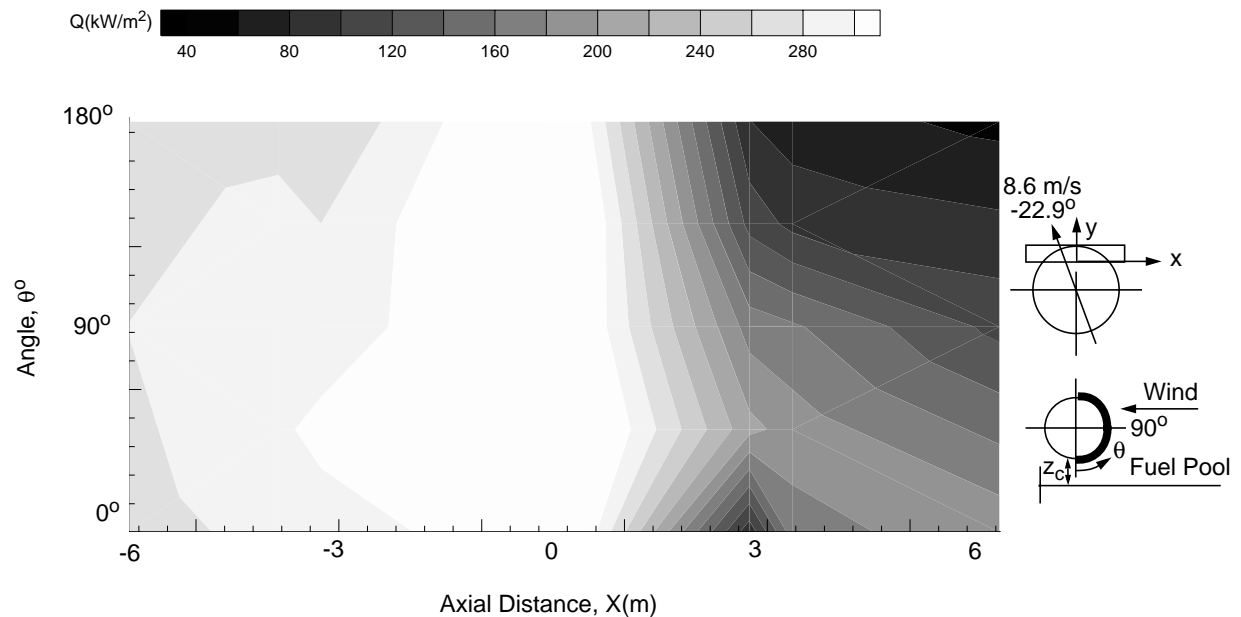
Figure 6.8 - Test 3 Leeward Side Skin Heat Flux Distribution, 680-715 sec.
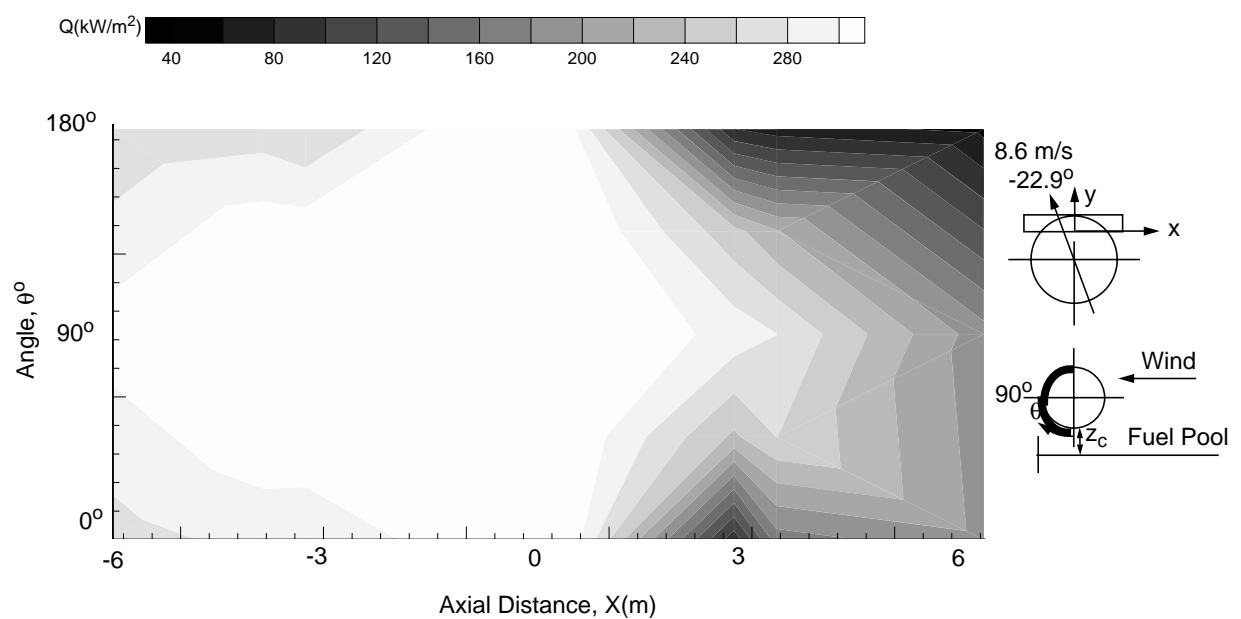
6.2.4 Skin Fluxes for Test 4

Two quasi-steady time periods were identified for Test 4. The periods were 120-240 seconds following ignition with an average wind speed of 5.1 m/s at -52.8^0 and 360-480 seconds following ignition with an average wind speed of 3.6 m/s at -26.7^0. The wind speeds and directions are depicted in a small diagram beside the contour plots in Figures 6.9-6.12.

The range of heat fluxes observed in the first quasi-steady period was 20-250 kW/m^2 with typical gradients of 25 kW/m^2/m. The maximum heat flux was observed on the left side of the calorimeter 6 m from the centerline at an angle of 90-180^0. The magnitude of the flux in this region was 220-250 kW/m^2 and the region extended slightly over the top of the calorimeter to the leeward side. The flame zone is directed towards this area by the wind component parallel to the axis of the mock fuselage. The wind component perpendicular to the axis of the mock fuselage causes the actively combusting region to impinge on the windward side of the mock fuselage surface creating increased heat fluxes in the area. The location and temperature distribution of the flame zone was clearly displayed in Figures 4.14-4.16.

Figure 6.9 - Test 4 Windward Side Skin Heat Flux Distribution, 120-240 sec.
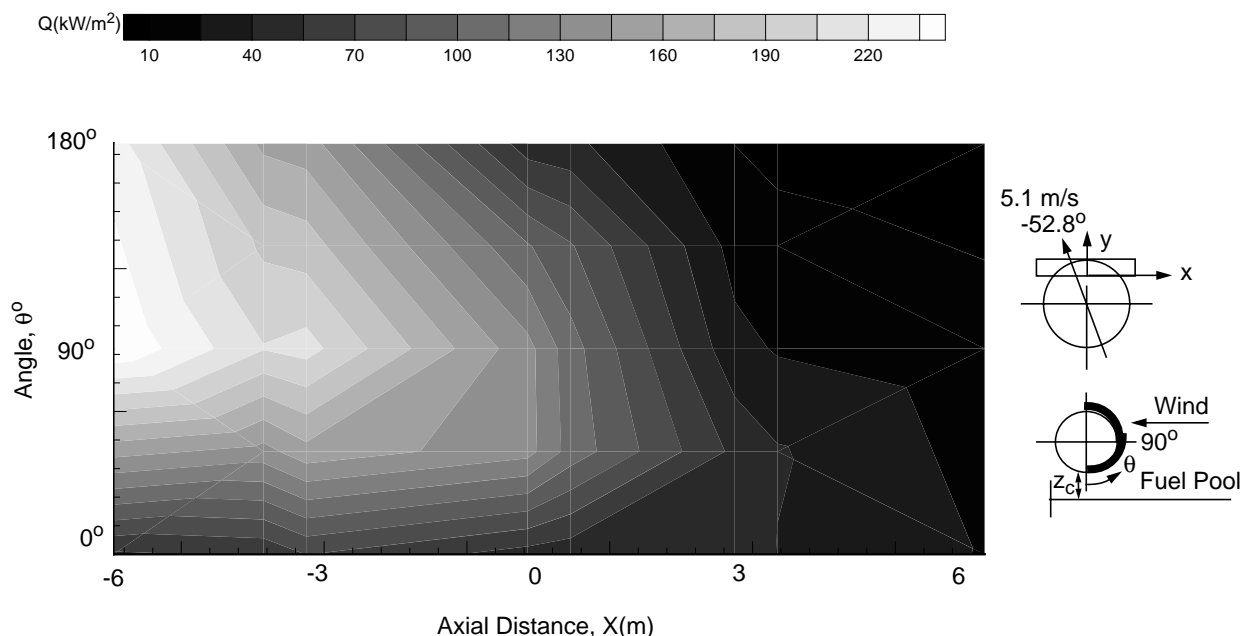
Figure 6.10 - Test 4 Leeward Side Skin Heat Flux Distribution, 120-240 sec.
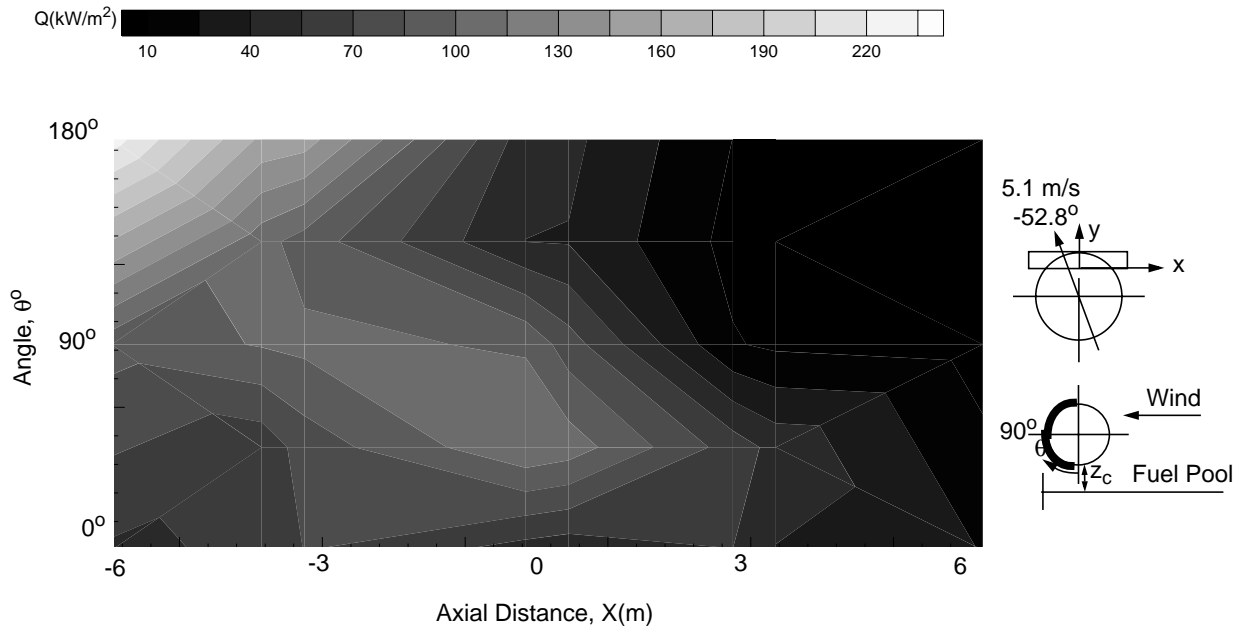
Much higher heat fluxes (40-300 kW/m^2) were experienced in the second quasi-steady time period from 360-480 seconds after ignition. The high heat flux region includes a larger area on the windward and leeward sides of the mock fuselage due to additional heating of the test fixture since the time of ignition. The high heat flux region on the windward side is caused by the impingement of the high temperature, continuous flame zone on the surface of the mock fuselage as shown in Figures 4.17-4.19. As in the previous time period, the high flux region extends to the leeward side of the mock fuselage.

6.2.5 Skin Fluxes for Test 5

As in the previous tests, two quasi-steady time periods were identified for Test 5. The time periods were 400-575 and 250-670 seconds following ignition with wind speeds of 5.4 m/s (11.4^0) and 6.7 m/s (5.6^0), respectively. Figures 6.13-6.16 display the contour plots of the calorimeter during the time periods. Almost identical trends were observed for both quasi-steady time periods. The heat fluxes were 40-300 kW/m^2 with gradients of 25-55 kW/m^2/m. The test was conducted under

Figure 6.11 - Test 4 Windward Side Skin Heat Flux Distribution, 360-480 sec.
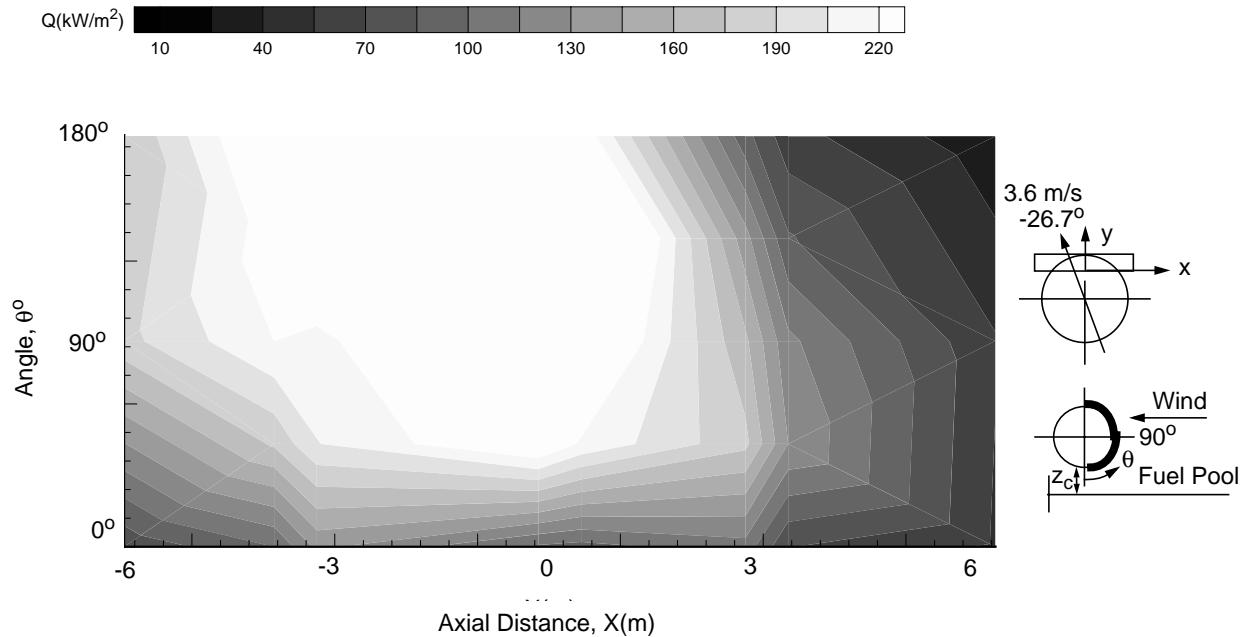
Figure 6.12 - Test 4 Leeward Side Skin Heat Flux Distribution, 360-480 sec.
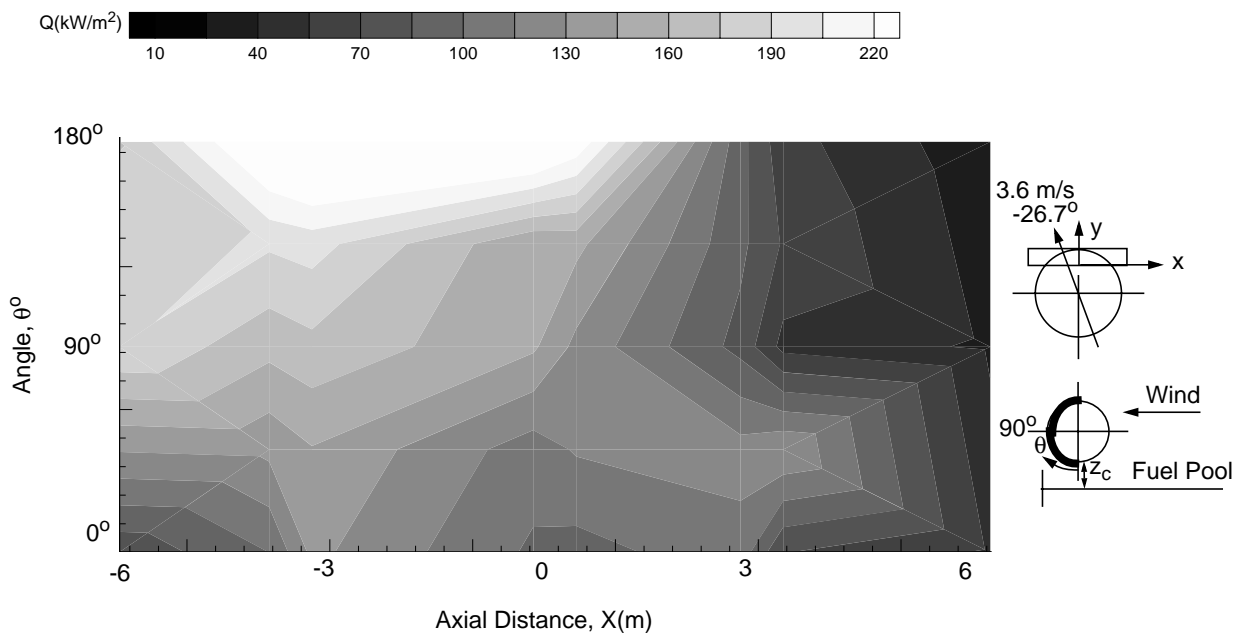
Figure 6.13 - Test 5 Windward Side Skin Heat Flux Distribution, 400-575 sec.
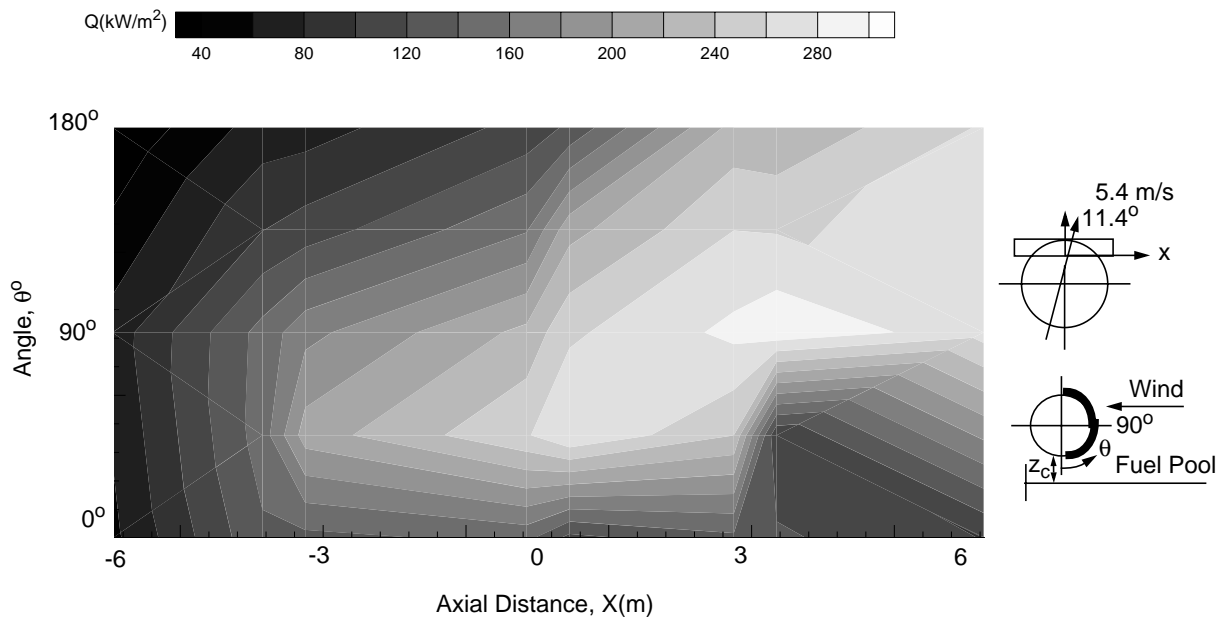
Figure 6.14 - Test 5 Leeward Side Skin Heat Flux Distribution, 400-575 sec.
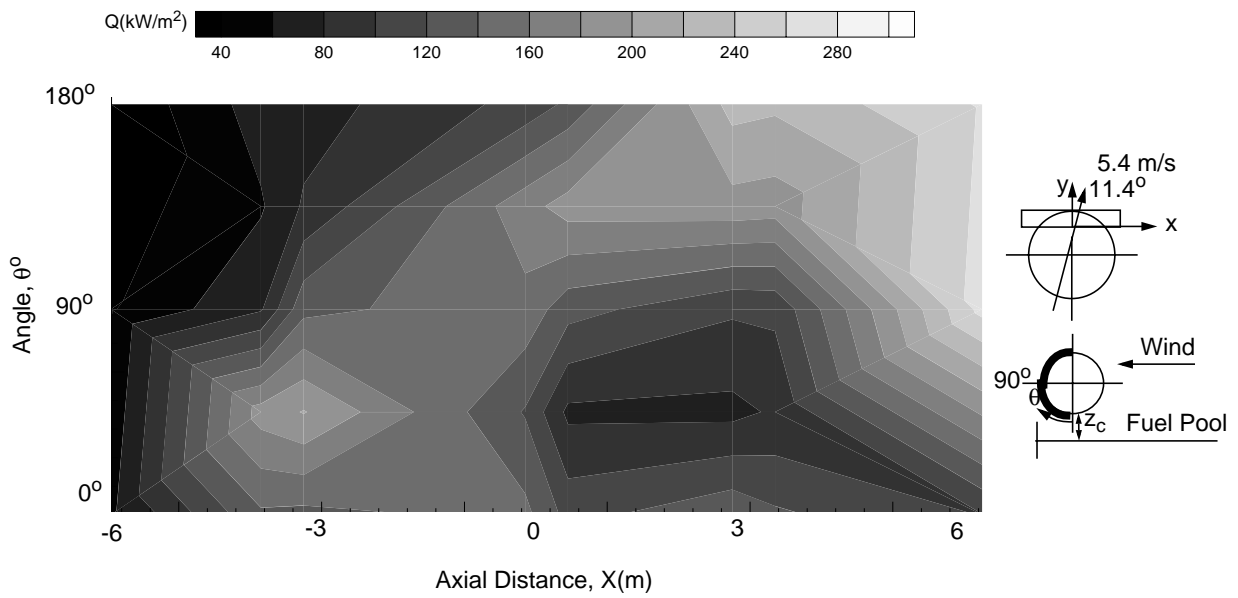
Figure 6.15 - Test 5 Windward Side Skin Heat Flux Distribution, 250-670 sec.
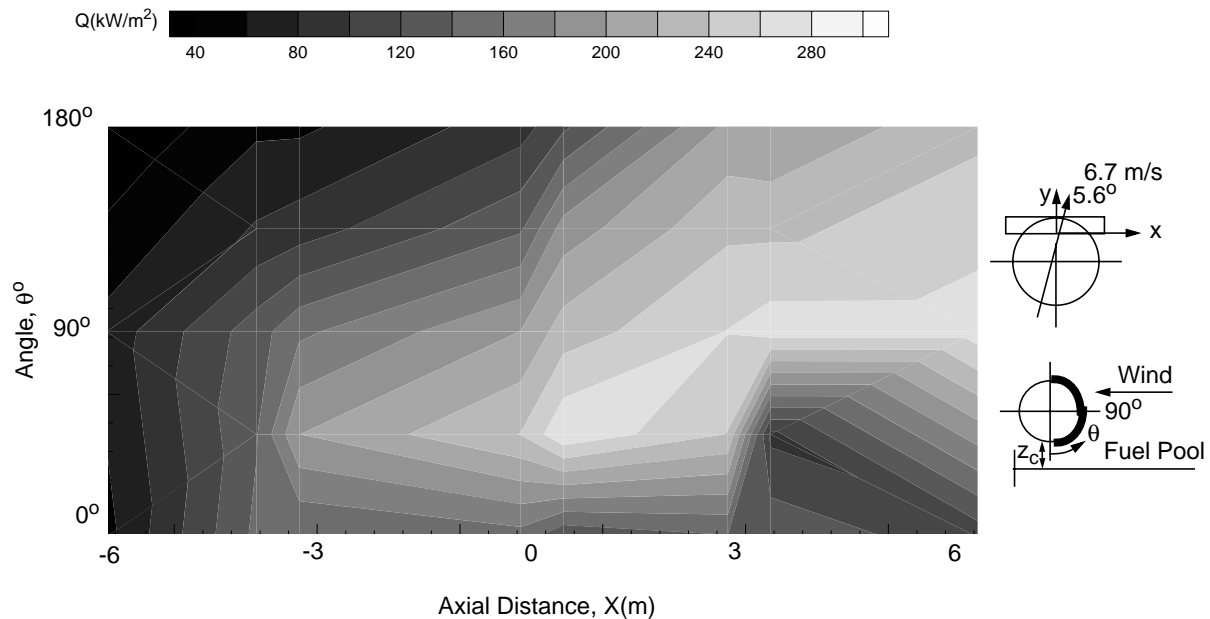
Figure 6.16 - Test 5 Leeward Side Skin Heat Flux Distribution, 250-670 sec.
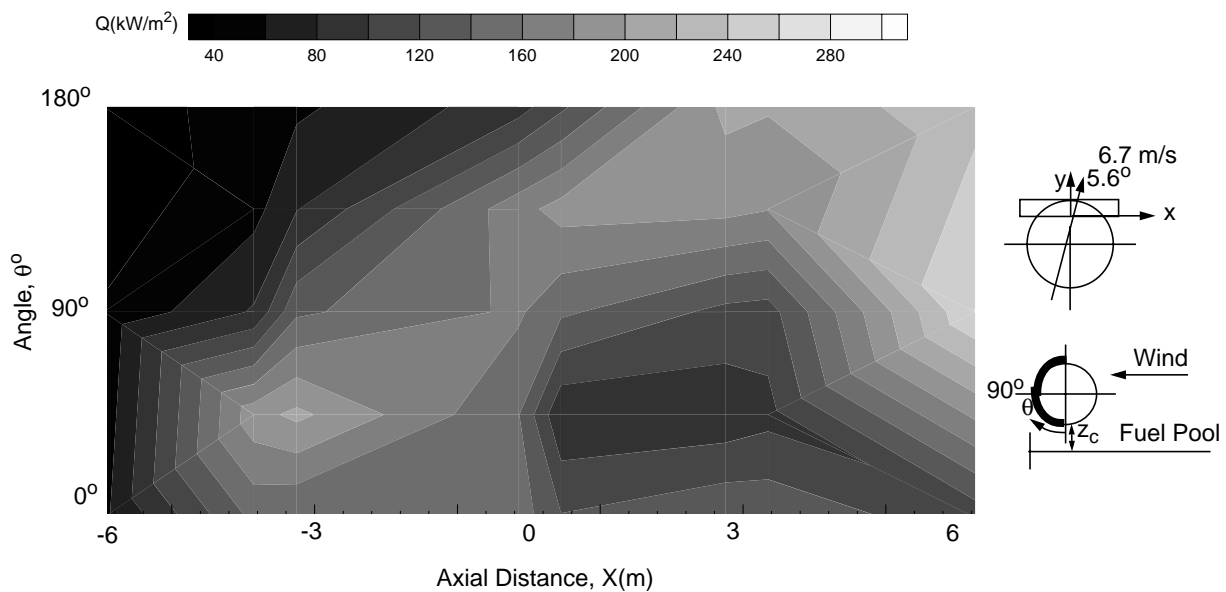
medium speed wind condition and the highest fluxes were observed on the windward side of the calorimeter at x=3.66 m and 90° with a magnitude of 300 kW/m^2 from the impingement of the buoyant plume on the mock fuselage surface. The lowest heat fluxes are seen on the left side of the mock fuselage due to the redirection of the flame zone by the wind component parallel to the axis of the mock fuselage. A high heat flux region exists at x=-3.66 m, shown on the contour plot of the leeward side at 45°. There is an area of low heat flux (50 kW/m^2) on the leeward side of the mock fuselage at 45° between x=0 m and x=3 m. The trends observed in the skin heat flux distributions are directly related to the flame shape contours (Figures 4.20-4.25) and the skin temperature (Figures 5.13-5.16) distribution profiles.

6.2.6 Skin Fluxes for Test 8

Test 8 was performed with the intention of reproducing the extreme fluxes achieved during Test 3 with high speed wind conditions. The heat flux distribution contours are shown in Figures 6.17 and 6.18. The wind during the quasi-steady time period 475-598 seconds after ignition was 9.9 m/s in the same direction (-19.5^o) as in Test 3. The wind conditions for this quasi-steady time period are most similar to the wind conditions of the first quasi-steady time period in Test 3.

Figure 6.17 - Test 8 Windward Side Skin Heat Flux Distribution, 475-598 sec.
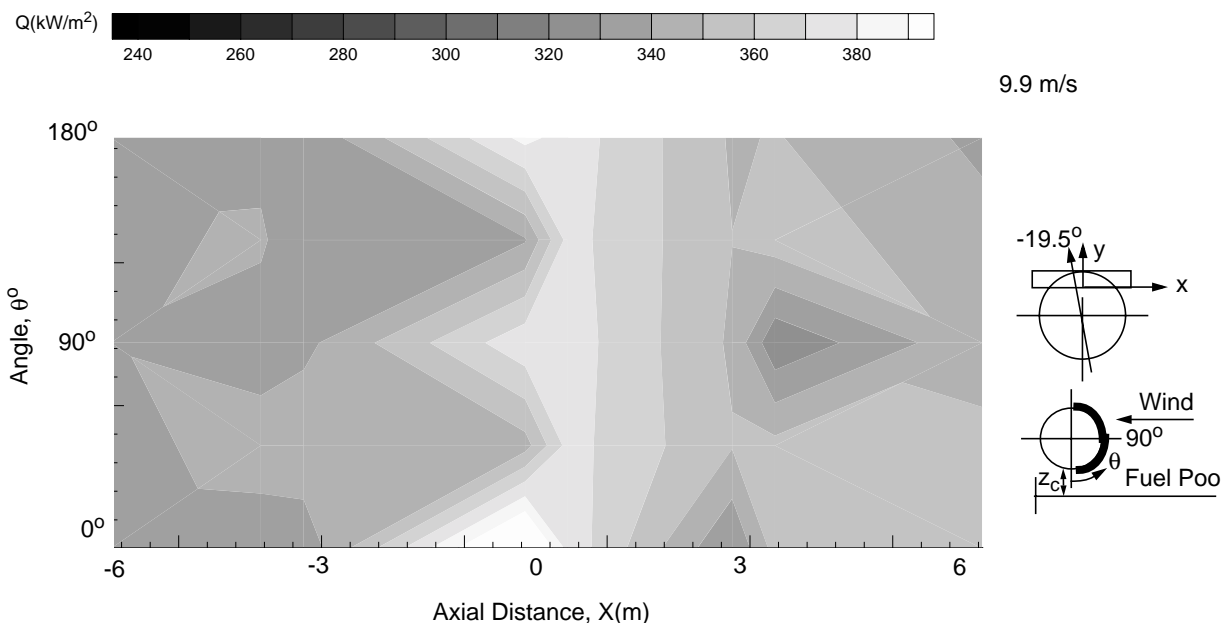
Figure 6.18 - Test 8 Leeward Side Skin Heat Flux Distribution, 475-598 sec.
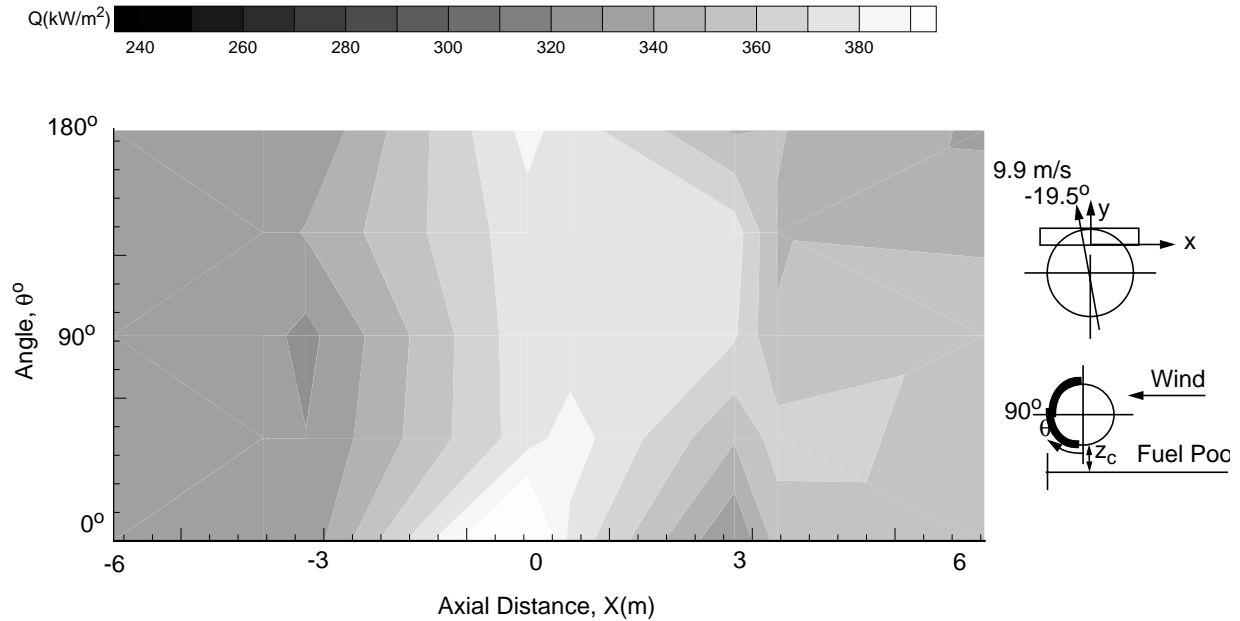
The heat fluxes are generally uniform along the mock fuselage skin around 325-400 kW/m^2 with very low gradients of less than 5 $kW/m^2/m$. These heat fluxes are much higher than is generally expected in a fire, but they are about the same magnitude as the heat fluxes in Test 3 under similar wind conditions. When comparing the results of Test 3 with Test 8, note that the heat flux scales are quite different. Almost all of the heat fluxes observed in Test 8 would have exceeded the maximum flux on the scale for Test 3; therefore a scale of 240-380 kW/m^2 was chosen for Test 8. The data trends from Test 3 were successfully reproduced in Test 8.

6.3 Skin Heat Flux Distributions for Small Pool

Two tests, numbers six and seven, were performed in a 10 m fuel pool which was instrumented according to the plan stated in a previous chapter. The heat fluxes acquired from the instrumentation (Figure 2.4) on the front and back skin of the mock fuselage are displayed in contour plots. The rough transitions that sometimes occur in these plots are the result of the interpolation.

6.3.1 Skin Fluxes for Test 6

Test 6 was conducted in the small pool under high wind conditions of 9.5 m/s during the quasi-steady time period from 270-390 seconds after ignition. The direction of wind was nearly normal (2.0^o) to the longitudinal axis of the mock fuselage. The temperature distribution contours are shown in Figure 6.19 and Figure 6.20. Heat fluxes observed ranged from 40-320 kW/m^2 with typical heat flux gradients from 5-20 kW/m^2/m. Ultra-high heat fluxes (220-320 kW/m^2) were recorded during the quasi-steady time period. The largest region of these ultra-high heat fluxes existed on the leeward side of the mock fuselage caused by the interaction of the high winds with the mock fuselage to enhance mixing in the region. High temperatures were

Figure 6.19 - Test 6 Windward Side Skin Heat Flux Distribution, 270-390 sec.
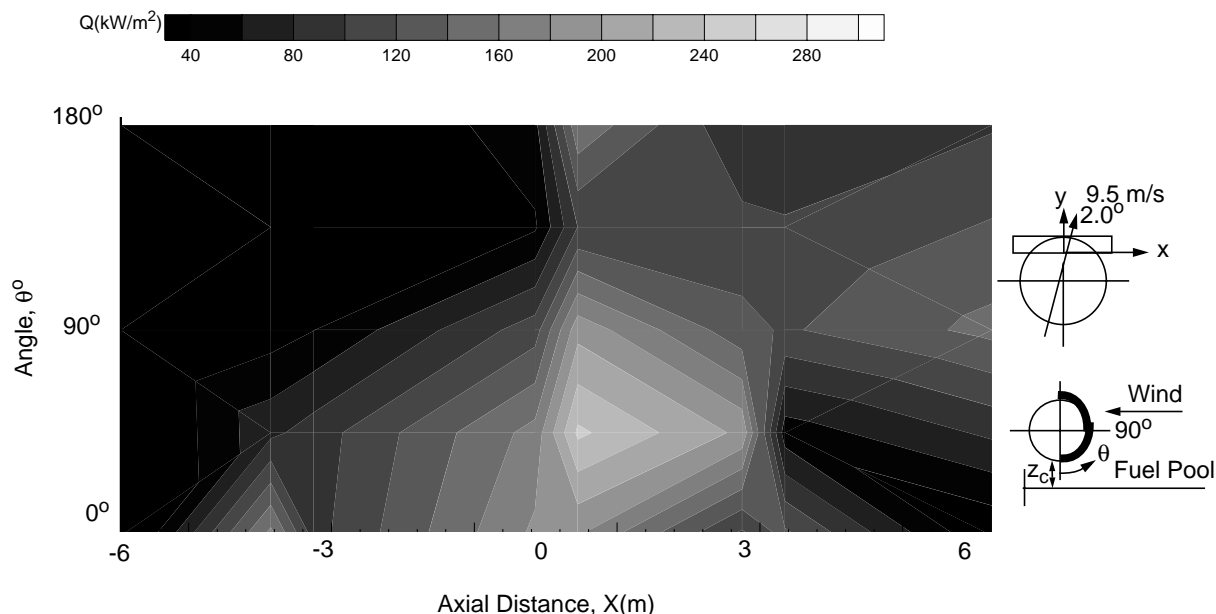
Figure 6.20 - Test 6 Leeward Side Skin Heat Flux Distribution, 270-390 sec.
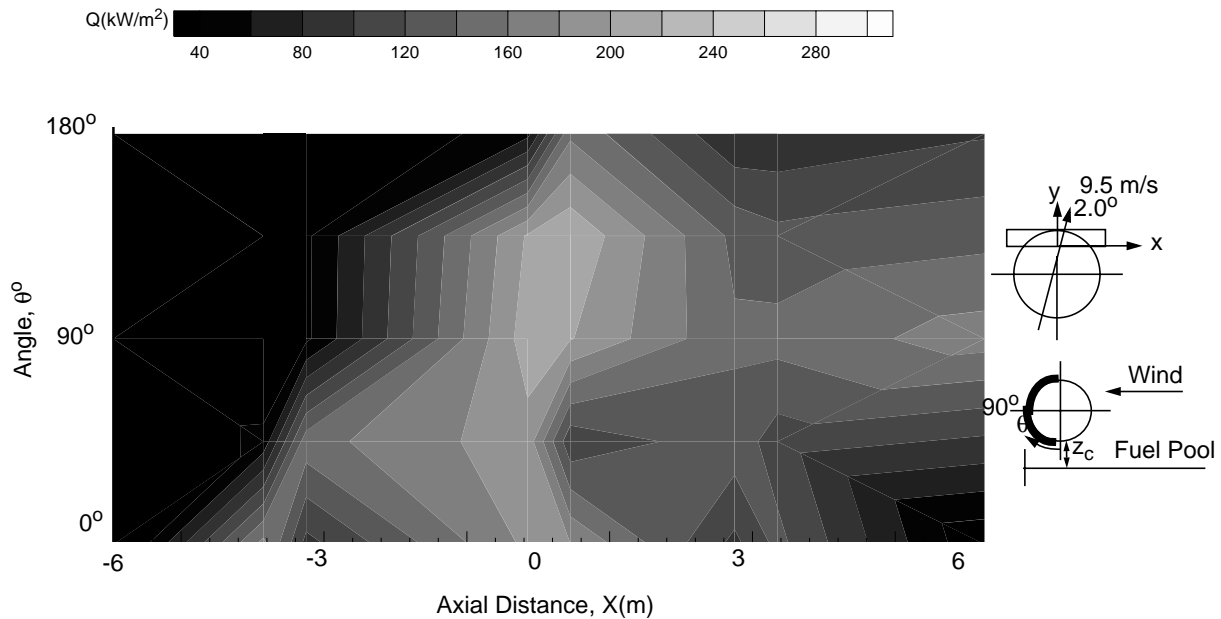
observed and analyzed in the flame shape contours (Figures 4.30-4.32) in the same location as the high heat fluxes.

6.3.2 Skin Fluxes for Test 7

Test 7 was conducted in a small fuel pool with a wind speed of 2 m/s (-36.1°) during the quasi-steady time period from 250-500 seconds following ignition. Temperature distributions are shown in Figures 6.21 and 6.22. The wind conditions for this test were exactly the same as the wind conditions for Test 2. This similarity allows for the analysis of the effect of pool size on heat fluxes. The maximum heat flux in both tests is approximately 220 kW/m^2 but the large pool test has a much larger region at that high flux. The high flux region located from the centerline to 6 m left of centerline with the maximum being centered at 3 m to the left of centerline in both tests. The leeward side of both the small and the large pools show similar trends although Test 2 has a slightly larger area of increased heat flux. As described in the analysis of the skin heat fluxes for Test 2, the high heat flux region on the leeward side is caused by the impingement of the flame zone (see Figure 4.34) on the surface of the mock fuselage.

Figure 6.21 - Test 7 Windward Side Skin Heat Flux Distribution, 250-500 sec.
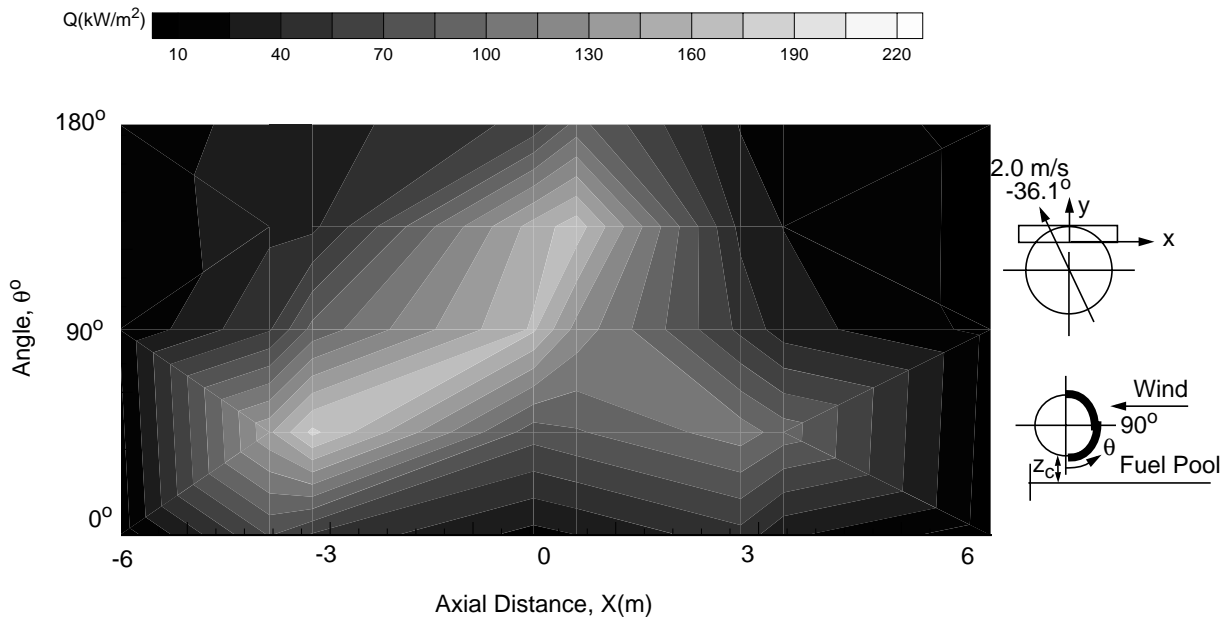
Figure 6.22 - Test 7 Leeward Side Skin Heat Flux Distribution, 250-500 sec.
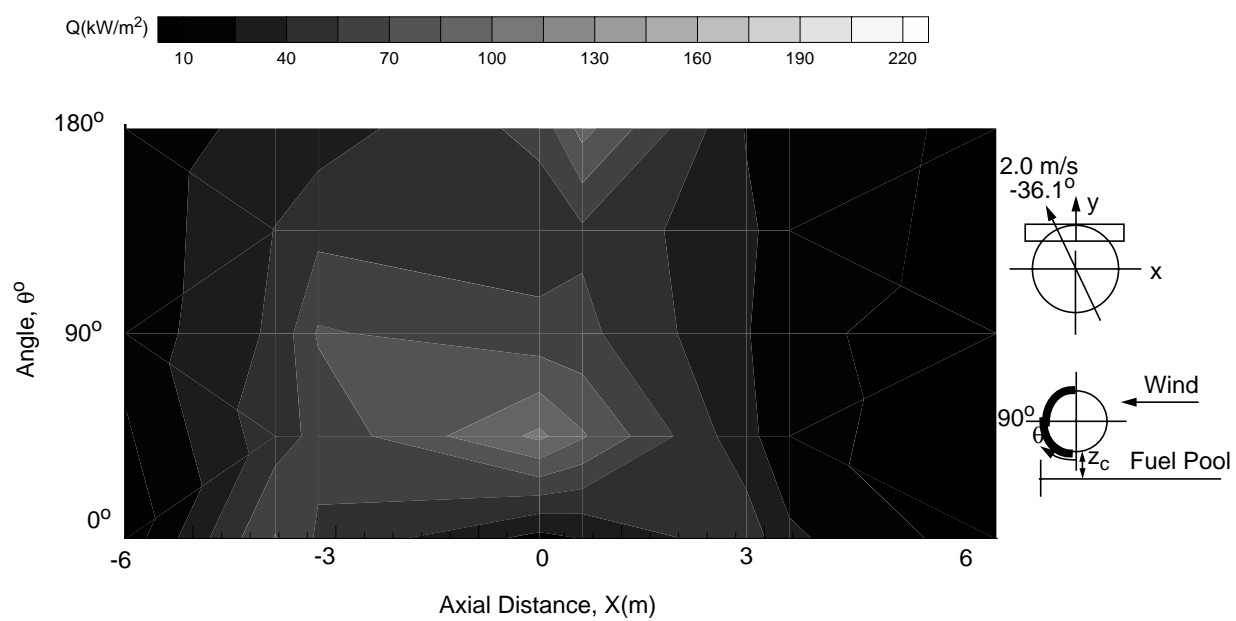
7. Experimental Results - Heat Fluxes to Pool Surface

7.1 Overview of Experiments

The vaporization rate of liquid fuel from the surface of pool fires determines the amount of fuel available for burning. The fuel is vaporized as a consequence of the heat transfer to the pool surface. Knowledge of the spatially-resolved heat transfer to the fuel surface is therefore necessary to understand pool fires and to develop numerical fire models. The HFG data from the fuel surface at locations shown in Chapter 2 were transformed into contour plots to show the time-averaged heat flux distribution to the pool during each quasi-steady time period. These plots present the data in a suitable format for fire model comparisons. There is insufficient measurement resolution at the leading edge to capture the expected decrease in heat flux due to reduced flame cover. Smoothing of the contour plots was not performed; therefore, some coarseness in the plots occurs as a result of the interpolation of values between experimental data points.

7.2 Large Pool Heat Flux Distributions

The first six tests were conducted in a 18.9 m pool of JP-8 jet fuel. The fuel surface of the pool was instrumented with HFGs as specified. Differences in test instrumentation from the specifications in Chapter 2 (Figure 2.7) will be stated as the results are presented in each section. Each contour plot includes a diagram depicting the wind vector during the time period.

7.2.1 Pool Heat Fluxes for Test 1

A quasi-steady time period was identified between 300 and 480 seconds following ignition for Test 1. The time-averaged wind speed and direction during this time period were 3.8 m/s and 26.2⁰, respectively. Figure 7.1 shows the distribution of heat flux incident on the fuel surface. The fluxes range from 50-130 kW/m^2. Measurements show a high heat flux near the leading edge of the fuel pool. Video coverage of the fire confirmed that thin flame coverage existed near the leading edge, therefore low heat fluxes were expected. Gauges located in regions of minimal flame cover generally measure low heat fluxes due to the lack of an optically thick flame and the influence of the relatively cool environment outside the flame zone. In Test 1, gauges near the leading edge were not included, therefore the leading edge heat fluxes used in the contour plots were interpolated from nearby HFGs (located in thick flame cover regions) resulting in higher heat fluxes near the leading edge than expected. There is also an area of low (50 kW/m^2) heat flux on the windward side of the mock fuselage

Figure 7.1 - Test 1 Pool Surface Heat Flux Distribution, 300-480 sec.

3.8 m/s, 26.2^o Wind

Q(kW/m^2)

150
140
130
120
110
100
90
80
70
60
50
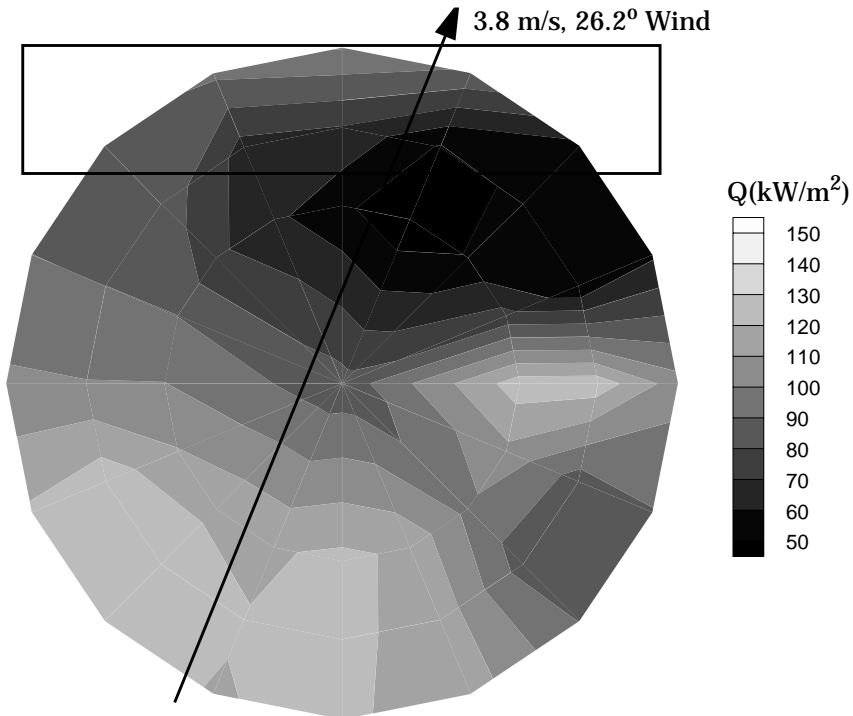
to the right of the centerline. This low heat flux region is consistent with the absence of burning in this region. This oxygen-starved region was also observed in the flame shape contours shown in Figures 4.3 and 4.4. On the windward side of this low flux region, there is a significant increase in heat flux (80-130 kW/m^2) due to the effective entrainment and mixing of air into the fire. The trends in these results are comparable with the data from the thermocouple temperature contours of the fire environment in Chapter 4. This comparison illustrates the high heat flux regions to the pool generally occur underneath regions where the fire temperatures are the greatest. The regions of low heat flux to the fuel surface occur when there is minimum flame cover or low temperatures likely due to insufficient air entrainment.

7.2.2 Pool Heat Fluxes for Test 2

A quasi-steady time period was observed between 225 and 350 seconds following ignition for Test 2. The time-averaged wind speed and direction during this period were 1.9 m/s and -36.9^o, respectively. The heat flux distribution along the leading edge, shown in Figure 7.2, includes uncertainties discussed earlier. The wind vector is redirecting the flame zone to the left of the centerline creating the flame zone shown in Figures 4.5 and 4.6. The deflection of the flame zone due to the wind

Figure 7.2 - Test 2 Pool Surface Heat Flux Distribution, 225-350 sec.
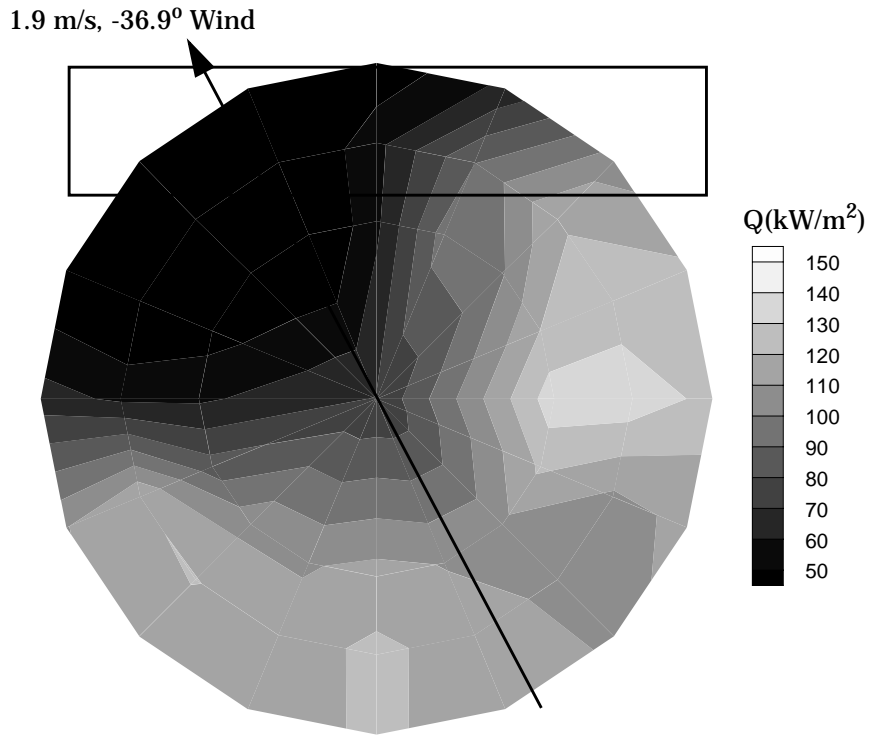
creates an oxygen starved region near the fuel surface shown as a low (50 kW/m^2) heat flux underneath and in front of the mock fuselage. A high (130 kW/m^2) heat flux region is observed on the windward side of the centerline. These trends are consistent with the flame shape temperature contours presented in Chapter 4 (Figures 4.5, 4.6, & 4.7).

7.2.3 Pool Heat Fluxes for Test 3

The two quasi-steady time periods identified for Test 3 were from 300-600 seconds following ignition and 680-715 seconds following ignition. The heat flux distribution contours are shown in Figure 7.3 and Figure 7.4. Lower heat fluxes as expected due to reduced flame cover were measured near the leading edge. The addition of two HFGs near the leading edge improved the resolution of the measurements to reflect the expected decrease in heat flux. The addition of these data points produces some non-physical "sharp" contours due to linear interpolation between data points.

The flux contour plots for the first quasi-steady time period are shown in Figure 7.3. This test showed the effects of high wind speed (10.2 m/s) on the heat flux to the fuel

Figure 7.3 - Test 3 Pool Surface Heat Flux Distribution, 300-600s
10.2 m/s, -22.7⁰ Wind

Q(kW/m^2)

150
140
130
120
110
100
90
80
70
60
50
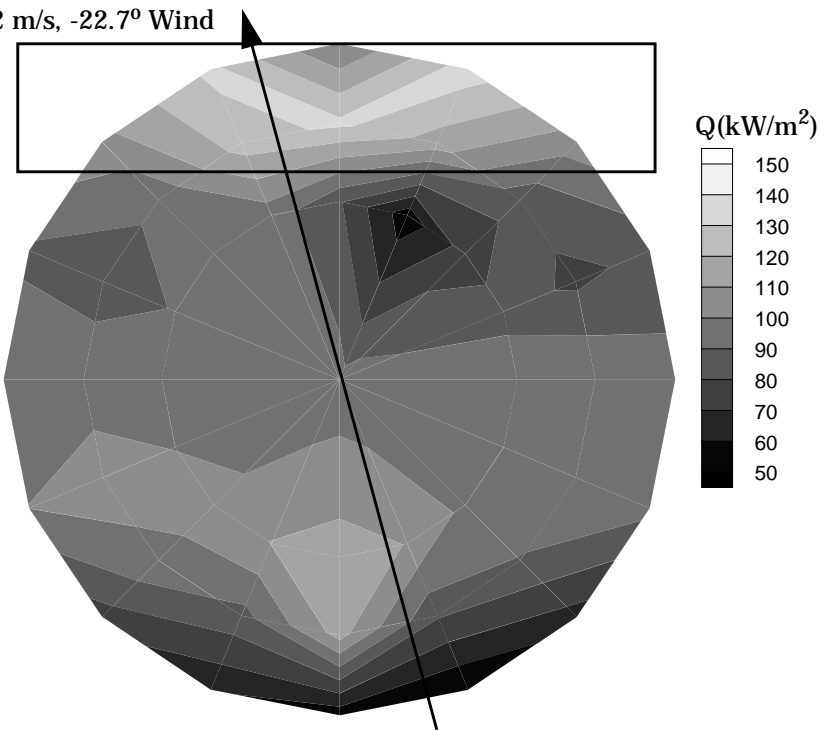
Figure 7.4 - Test 3 Pool Surface Heat Flux Distribution, 680-715s
8.6 m/s, -22.9⁰ Wind

Q(kW/m^2)

150
140
130
120
110
100
90
80
70
60
50
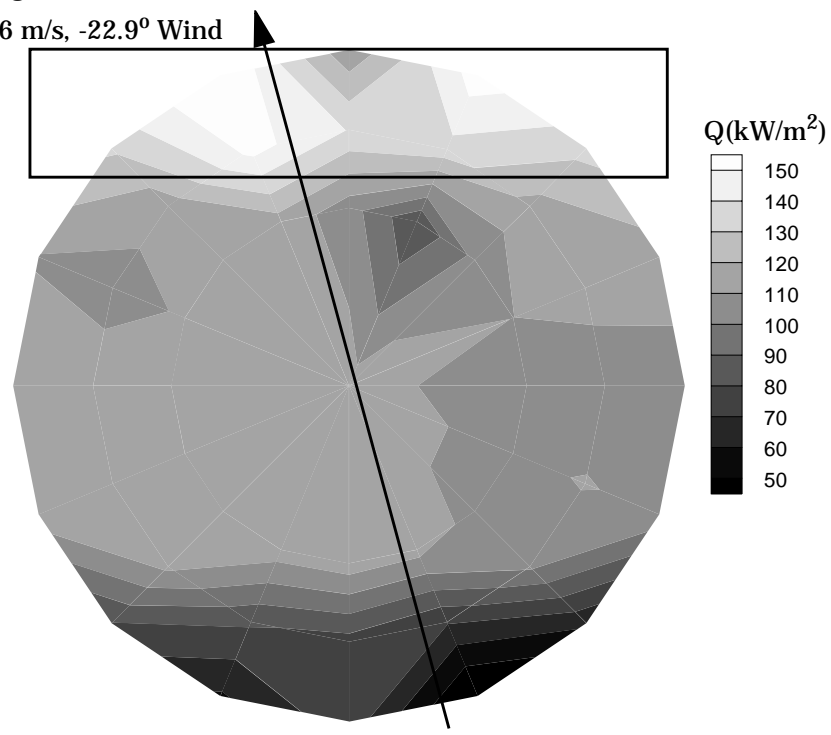
surface. Overall, higher heat fluxes to the pool were recorded during the second time period (Figure 7.4), but the general trends were equivalent to the first quasi-steady time period. There is a significant difference in the flux distribution from the previous two tests in the vicinity of the calorimeter. For higher wind conditions, the highest heat fluxes are observed during both quasi-steady state time periods underneath the mock fuselage (130-150 kW/m^2). The influence of the wind is expected to accelerate the flow underneath the mock fuselage creating a well-mixed region, and therefore also increased heat fluxes to the fuel surface. The oxygen starved regions shown as low temperatures in Figures 4.8, 4.10, 4.11, & 4.13 in front of the mock fuselage are also evident in Figures 7.3 and 7.4 as a lower (80 kW/m^2) heat flux region. All of the trends in the fuel surface heat flux contours are consistent with those observed in the flame shape contours in Chapter 4.

7.2.4 Pool Heat Fluxes for Test 4

Two quasi-steady time periods were identified for Test 4. These periods occurred 120-240 seconds following ignition with an average wind speed of 5.1 m/s and 360-480 seconds following ignition with an average wind speed of 3.6 m/s. Wind vectors are depicted in overlaid diagrams in Figures 7.5 and 7.6 As described in Chapter 2, the leading edge in the remainder of the tests is more heavily instrumented than in the first two tests. Some non-physical sharp contours exist near the leading edge as a result of interpolation between the data points. Similar heat flux distributions were measured during both quasi-steady time periods. Moving downwind from the low heat flux region at the leading edge, the heat fluxes increased to 110 kW/m^2 and then decreased (60 kW/m^2) immediately in front of the mock fuselage. This low flux region in front of the mock fuselage is similar to observations in the previous tests and is expected to be a consequence of the lack of available oxygen in the interior of the flame zone. Similar to Test 3, a region of increased heat flux (100 kW/m^2) is observed underneath the calorimeter. The heat flux contour trends are in agreement with temperature distribution trends shown in Figures 4.14-4.16. .

Figure 7.5 - Test 4 Pool Surface Heat Flux Distribution, 120-240 sec.
5.1 m/s, -52.8° Wind

Q(kW/m²)
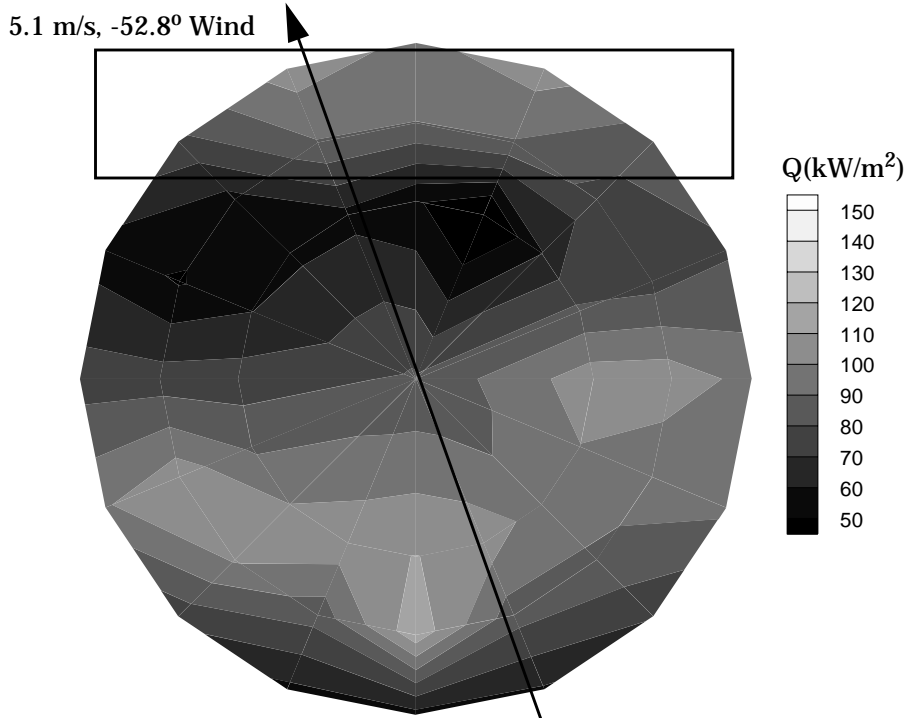
Figure 7.6 - Test 4 Pool Surface Heat Flux Distribution, 360-480 sec.
3.6 m/s, -26.7° Wind

Q(kW/m²)
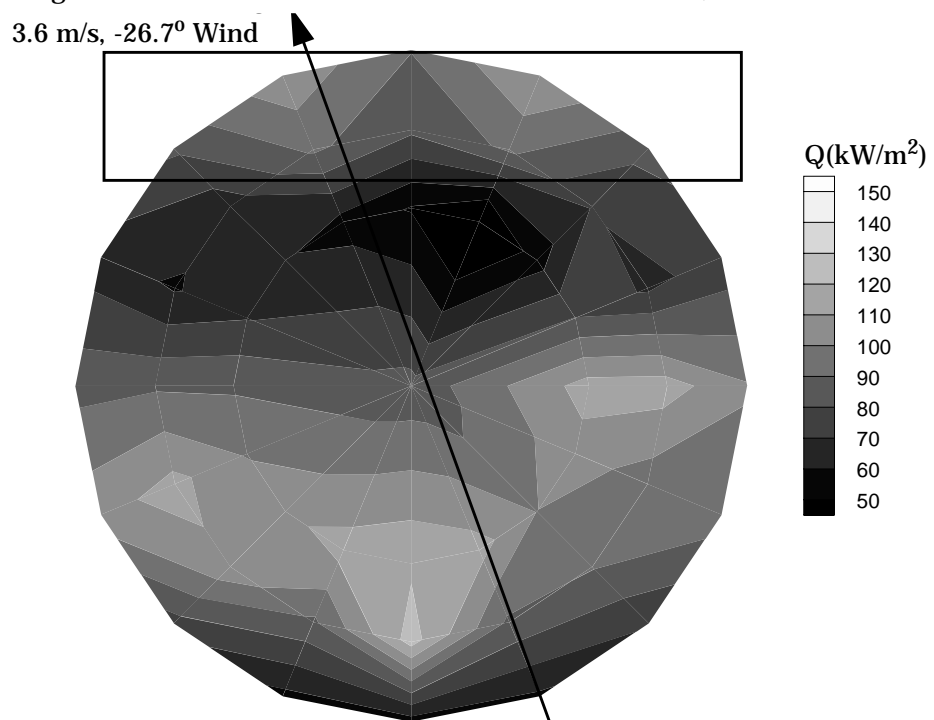
7.2.5 Pool Heat Fluxes for Test 5

As in the previous tests, two quasi-steady time periods were identified for Test 5. The time periods were 400-575 and 250-670 seconds following ignition with wind speeds of 5.4 m/s and 6.7 m/s, respectively. Figure 7.7 and Figure 7.8 show similar heat flux distributions to the fuel pool surface during these periods. A low heat flux (50 kW/m^2) region exists on the right side of the pool due to the wind direction during the test. The results are consistent with the wind directing the flame zone to the right side of the pool, therefore increasing flame cover in the area outside the fuel pool and creating an oxygen-starved region near the fuel pool. Low temperatures in this region, consistent with the lack of oxygen entrainment into the interior of the flame zone, are also clearly shown in the flame shape contours (Figures 4.20 & 4.23). The higher heat flux regions (~120 kW/m^2) exist near the leading edge of the pool, the left side of the pool, and underneath the calorimeter. The trends observed in these contours are consistent with the results in the contours of the flame shapes in Chapter 4 (Figures 4.20-4.25).

Figure 7.7 - Test 5 Pool Surface Heat Flux Distribution, 250-670 sec.
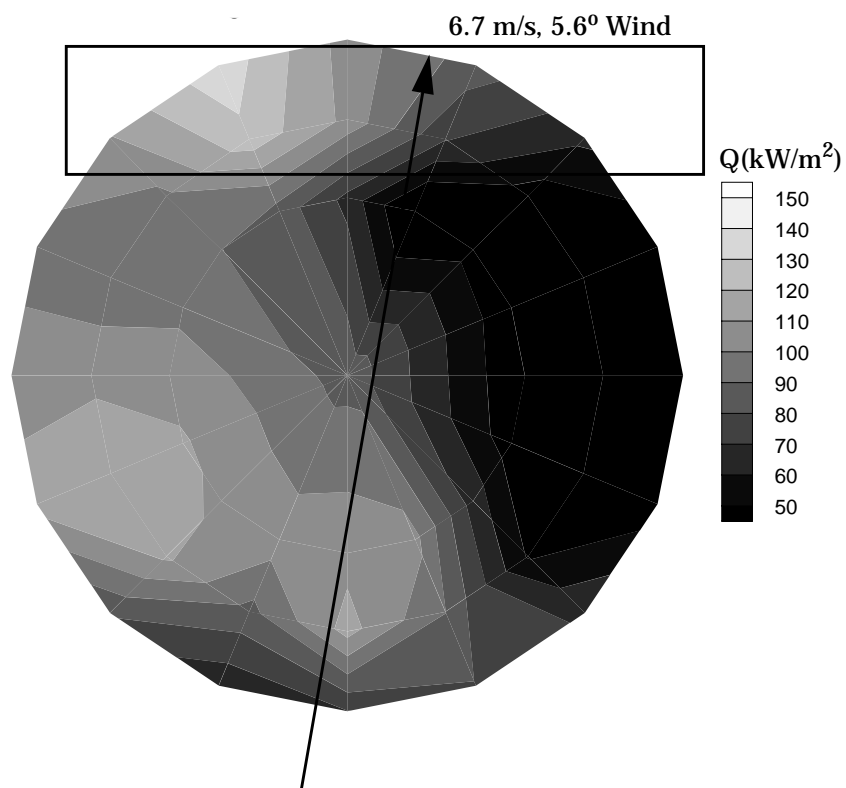
Figure 7.8 - Test 5 Pool Surface Heat Flux Distribution, 400-575 sec.
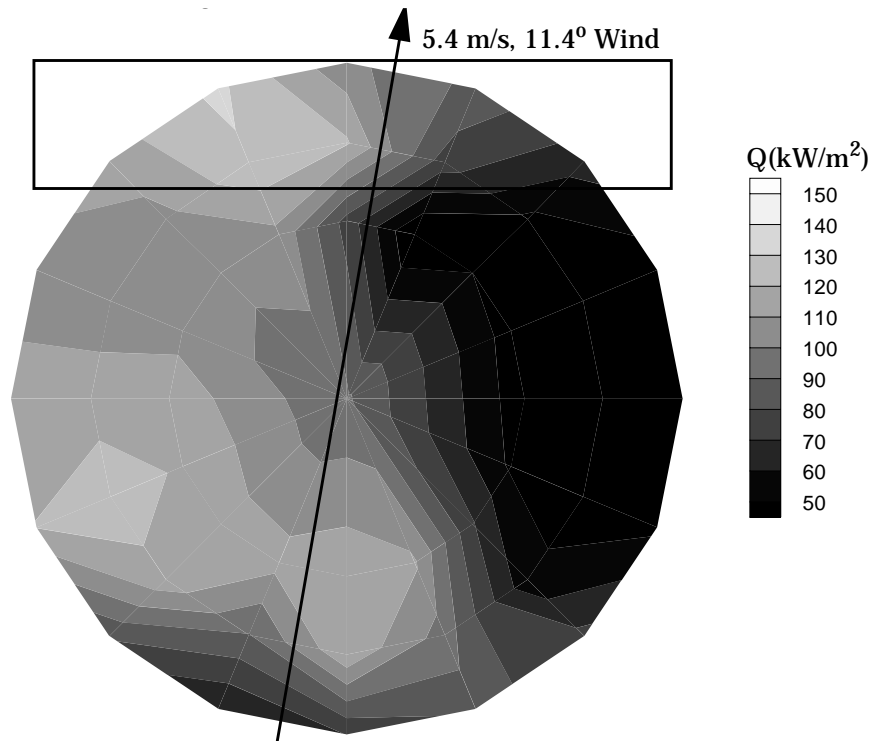
7.2.6 Pool Heat Fluxes for Test 8

Test 8 was performed with the intention of reproducing the very high (>150 kW/m^2) fluxes observed during Test 3 under high speed wind conditions. The wind during the quasi-steady time period 475-598 seconds after ignition was 9.9 m/s in approximately the same direction (-19.5^o) as in Test 3. Figure 7.9 shows the heat flux distribution to the fuel surface. Test 8 did not show the very high heat fluxes (>150 kW/m^2) underneath the calorimeter that occurred during Test 3, but the fluxes were high (100-120 kW/m^2) when compared to other regions of the pool during the same time period. The contours at the leading edge of the fuel pool are sharp: likely resulting from the interpolation between data points. Possible causes for the non-typical contours at the leading edge include a malfunctioning of the centerline gauge or interpolation between the data points. The remaining heat flux distribution trends seem to agree with the results from Test 3 although larger fluxes were measured in Test 3. The difference in the magnitude of the fluxes could be attributed to the difference in the wind speed (0.3 m/s). It has been demonstrated that the flame zone is very sensitive to changes in the wind speed and direction; although it can not

Figure 7.9 - Test 8 Pool Surface Heat Flux Distribution, 475-598 sec.

9.9 m/s, -19.5⁰ Wind

$Q(kW/m^2)$
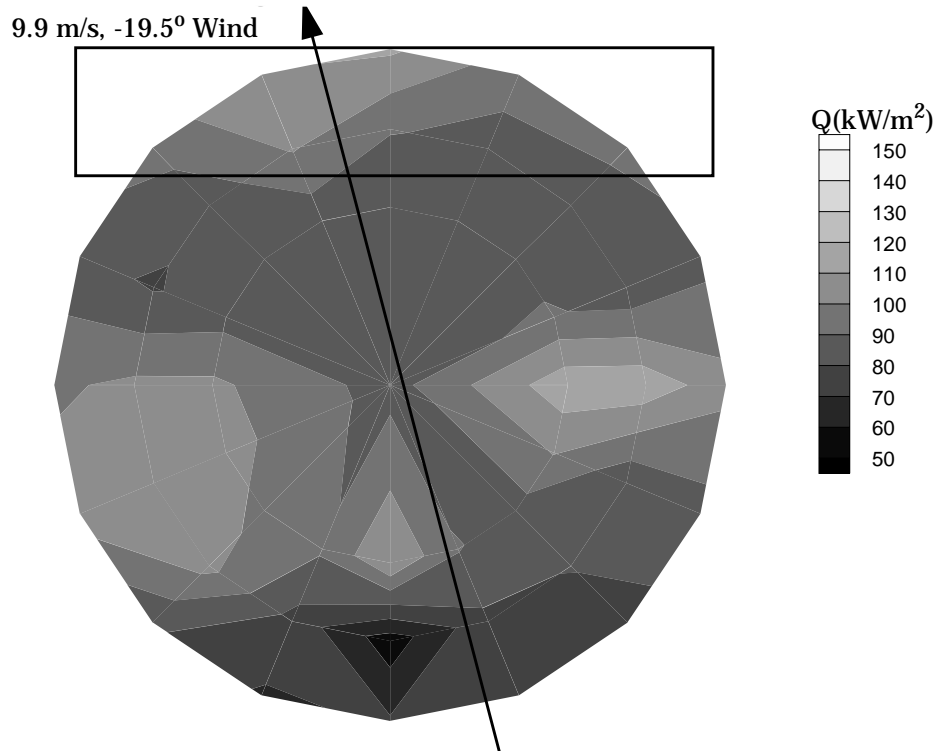
be concluded that a 0.3 m/s change in wind speed would produce such differences in heat fluxes (~40 kW/m^2). Since it is difficult to target wind speed and direction, the repeatability of these pool fire tests is challenging to assess in a limited number of tests. The trends observed, including the increase in heat fluxes underneath the calorimeter, were consistent with the temperature contours in Figures 4.26-4.28.

7.3 Small Pool Heat Flux Distributions

Two tests, numbers six and seven, were performed in a 10 m fuel pool instrumented as stated in Chapter 2 (Figure 2.8). The heat flux contour plots for each test were produced from experimental HFG data at selected locations throughout the pool. The rough transitions that sometimes occur in these plots are the result of the interpolating between data points to create contour plots. Note that the scale used in Tests 6 and 7 is 10-150 kW/m^2 while the scale used for heat fluxes in all other tests is 50-150 kW/m^2.

7.3.1 Pool Heat Fluxes for Test 6

Test 6 was conducted using the small fuel pool under high wind conditions. Average winds of 9.5 m/s were measured during a quasi-steady time period from 270-390 seconds after ignition. The direction of wind was nearly normal (2.0⁰) to the longitudinal axis of the mock fuselage. Figure 7.10 shows the distribution of heat flux to the pool surface during the quasi-steady time period. The highest heat fluxes (120-150 kW/m^2) existed primarily underneath the mock fuselage (due to the accelerated flow between the mock fuselage and the fuel surface) and on the windward side of the centerline. High temperatures in the same region were also observed in Figures 4.30-4.32. The lowest heat fluxes (60 kW/m^2) were observed in the region on the right side of the pool due to the increased flame cover from the redirection of the flame zone by the wind. The heat fluxes to the fuel pool are not symmetrical (40 kW/m^2 difference) indicating that a 2.0⁰ angle significantly affects the flame zone.

Figure 7.10 - Test 6 Pool Surface Heat Flux Distribution, 270-390 sec.
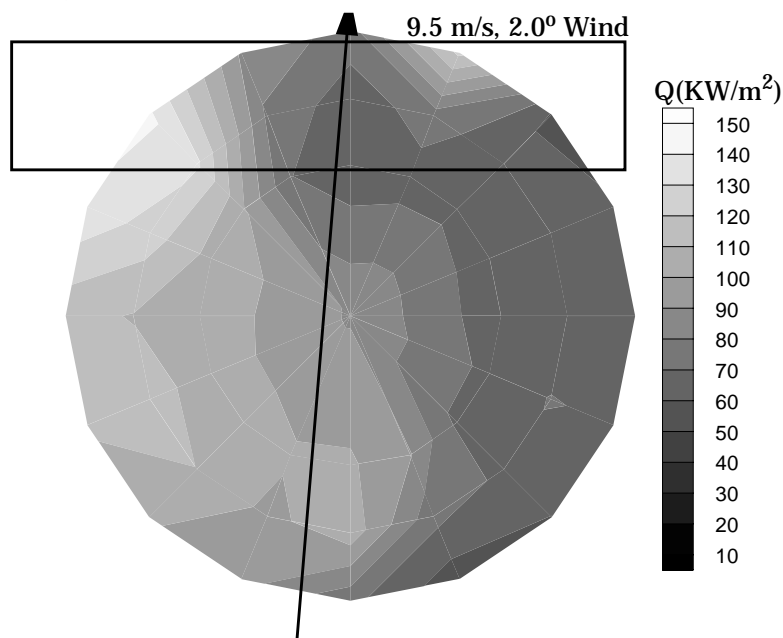
7.3.2 Pool Heat Fluxes for Test 7

Test 7 was conducted in a small fuel pool with a wind speed of 2.0 m/s during the quasi-steady time period from 250-500 seconds following ignition. Figure 7.11 shows the flux distribution for the small pool fuel surface under low speed wind conditions (2.0 m/s, -36.1°). These conditions are identical to the wind conditions during the 20 m pool fire performed as Test 2. Heat fluxes from 70-110 kW/m^2 were observed over a majority of the fuel pool in Test 7. Less necking of the flame zone occurs in smaller fires, therefore the gradients at the edges of the fuel pool are not as steep in the 10 m fires. Along the centerline there is a high flux (130 kW/m^2) region near the leading edge and a low flux region (30 kW/m^2) located underneath the mock fuselage. Figure 4.34 also shows high temperatures near the fuel surface at the leading edge and low temperatures underneath the mock fuselage.

Figure 7.11 - Test 7 Pool Surface Heat Flux Distribution, 250-500 sec.
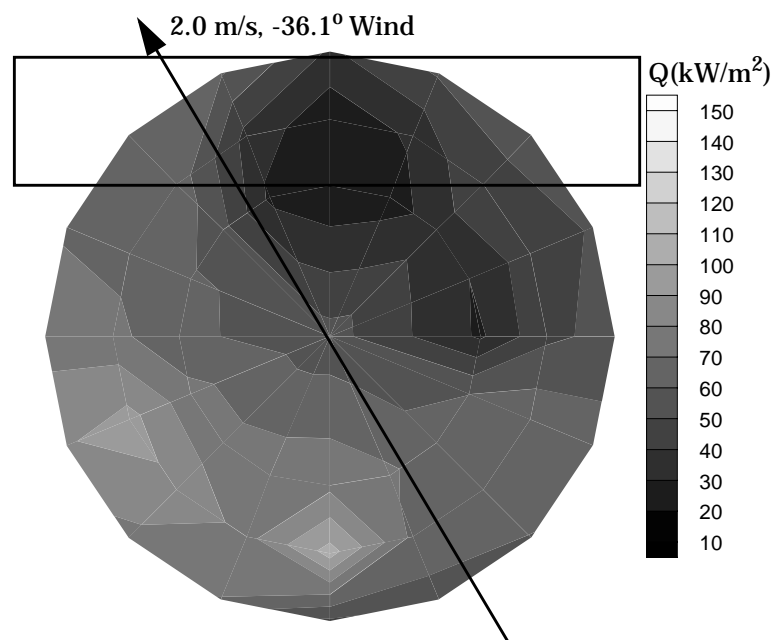
8. Experimental Results - Fuel Temperatures

8.1 Overview of Experiments

For each of these experiments, a prescribed amount of fuel was floated on top of a water layer. Fires were allowed to burn until all fuel was consumed. Thermocouple arrays were placed in the fuel pool for the purpose of identifying liquid fuel thermal response and fuel vaporization (mass loss) mechanisms. Insight gained from these measurements is needed to develop improved submodels for numerical simulations. Furthermore, a knowledge of the liquid fuel thermal response for cases where the fuel is contained in a pool is helpful in evaluating fuel heat transfer (and hence fuel vaporization) for cases where the fuel is flowing on a substrate.

8.2 Large Pool Fuel Temperatures

Six tests were conducted in a 18.9 m pool of JP-8 jet fuel. The fuel and water were instrumented with thermocouple arrays (Figure 2.9) according to the plan stated in Chapter 2. Some tests included two thermocouple arrays. The arrays were intended to be located at a position of high heat flux to the pool surface and at a position of low heat flux to the pool surface. A schematic is included to show the location of the arrays. The legend displays the location of the thermocouples relative to either the fuel/water interface or the bottom of the fuel pan (when the elevation of the fuel/water interface is not known). When the distance from the fuel/water interface is shown, positive distances are located within the fuel and negative distances are in the water.

8.2.1 Fuel Temperatures for Test 1

A single thermocouple array was used in Test 1 to monitor the temperature of the fuel and the water underneath the fuel. The temperatures are shown in Figure 8.1. The level of the fuel/water interface was not measured before the start of the test; therefore, the location of the thermocouple is listed using the bottom of the fuel pan as a reference. From the measured temperatures, it is possible to infer the location of the fuel/water interface. Once the fuel was ignited, temperatures recorded ranged from 600-1100 K. The data indicate that the top two thermocouples were located in the fuel vapor layer and exposed to the burning region. They experience an increase in temperature immediately after ignition as the flame front passes. Once the flame front passed, the thermocouple temperatures decrease. The thermocouple at 0.19 m above the bottom of the fuel pan was located in the fuel and increased in temperature beginning at 5 min. after ignition from 300 K to 1000 K as the fuel was heated by the flame zone. The temperature of the top of the fuel surface can be inferred from these data. A slight leveling in the recorded temperature can be seen at approximately 7.5 min. after ignition which is consistent with a phase change.

The temperature recorded at this time is 490 K which indicates the temperature of the top fuel surface where the phase change is likely occurring. A spike in the temperatures of the top three thermocouples occurs at 14 min after ignition as the fire extinguishes and the flame front passes over the thermocouple. The temperature of the 0.16 m thermocouple remains at 300 K until 10.5 min. after ignition when its temperature rises to a maximum of 450 K. The thermocouple is most likely located within the water and the increase in temperature is a result of absorption of radiation from the flame zone. Since the temperatures of thermocouples at elevations of 0.14 m and 0.11 m never rise more than 20 K, the conclusion can be made that they were located within the water for the duration of the test. Fluctuations are observed in the data for thermocouples in the liquid from absorbed radiation or mixing. For thermocouples above the liquid, fluctuations are caused by flame turbulence.

Figure 8.1 - Fuel and Water Temperatures - Test 1
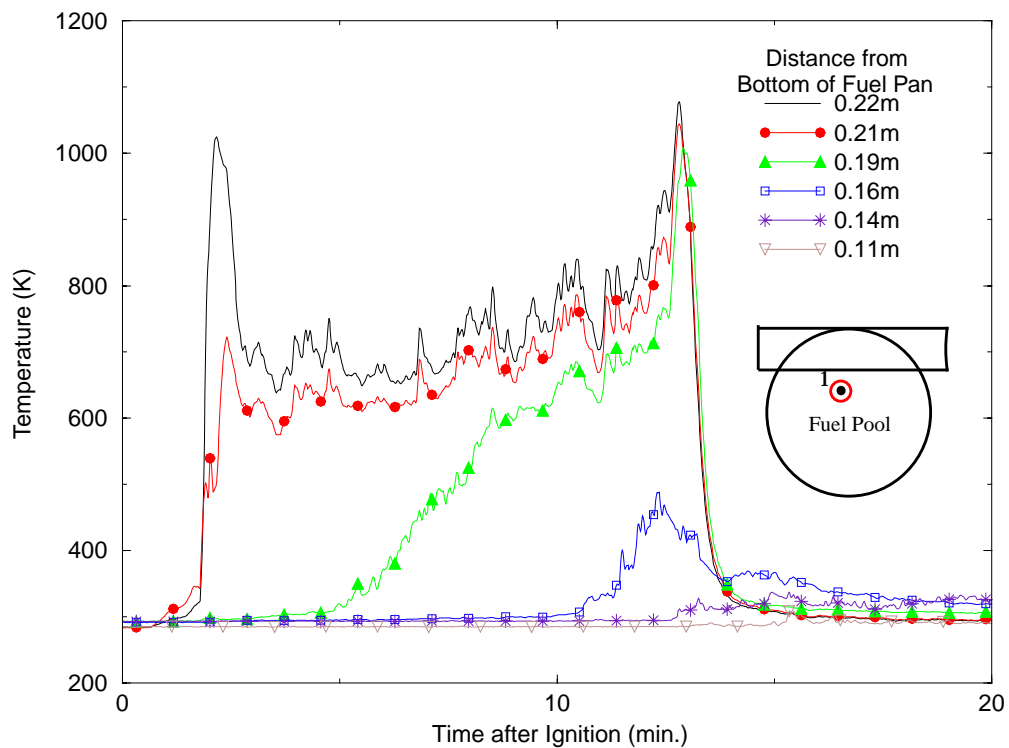
8.2.2 Fuel Temperatures for Test 2

A single thermocouple array was used in Test 2 to monitor the temperature of the fuel and the water underneath the fuel. The temperature data are shown in Figure 8.2. As in Test 1, the level of the fuel/water interface was not measured before the start of the test; therefore, the location of the thermocouple is listed using the bottom of the fuel pan as a reference. The data indicate that the top thermocouple was initially located at or above the fuel surface where burning was occurring since it

briefly recorded a temperature of 1000 K immediately following ignition as the flames spread across the fuel pool. After the flame front passed, the thermocouple temperature dropped and the thermocouple was likely located in the vapor dome since temperatures were not indicative of a burning region. The thermocouples at 0.21 m and 0.19 m were initially located within the liquid fuel. Just after ignition, the temperature of the thermocouple located at 0.21 m increased and the temperature was fairly stable at 600-700 K for the duration of the experiment. As the fuel continued to be heated by the flame zone, the temperatures of the thermocouple at 0.19 m started to increase around 5 min. after ignition. By 13 min. after ignition, the top three thermocouples reached temperatures of 900 K, indicative of an actively combusting region. At approximately 12 min. after ignition, a slight increase (~100 K) in the temperature of the 0.16 m thermocouple was observed due to heating of the water from absorbed radiation. The low temperatures of thermocouples located at elevations of 0.16 m, 0.14 m, and 0.11 m indicates that they were located within the water during the test. There was only minimal heating (<100 K) of these thermocouples as a result of either minimal heat transfer to the water or sufficient mixing within the water to keep the temperatures low. The temperature of the fuel surface can be estimated from the experimental thermocouple data. The phase change for the fuel is indicated by a leveling of the recorded thermocouple temperature. This leveling can be seen for the thermocouple at 0.21 m from 1-2 min. after ignition and for the thermocouple at 0.19 m beginning at 7 min. after ignition. The constant temperature (fuel surface temperature or vaporization temperature) during these times is 490-510 K.

Figure 8.2 - Fuel and Water Temperatures - Test 2

122
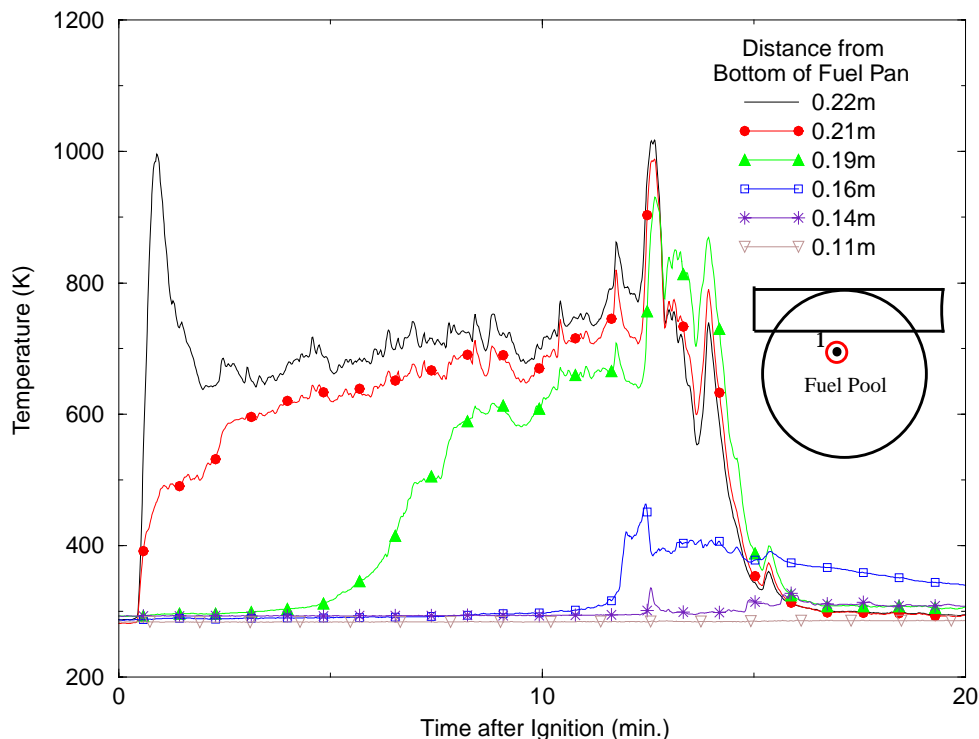
8.2.3 Fuel Temperatures for Test 3

Two thermocouple arrays were used in Test 3 to monitor the temperature of the fuel and the water underneath the fuel. The temperatures are shown in Figure 8.3 and 8.4. Prior to ignition, the location of the fuel/water interface was measured. In this test, the top three thermocouples were located within the fuel and the bottom three were within the water. Immediately following ignition, the temperature of the thermocouple located at 7.0 cm increased to 950 K as the flames spread across the pool. Then the temperature remained steady between 700 K and 850 K for the duration of the test. There was one additional increase (1050 K) in the thermocouple's temperature around 12 min. after ignition as the fire diminished due to lack of fuel and the flame front passed over the thermocouple. The temperatures of the array 1 thermocouples located within the fuel layer at 4.5 cm and 1.9 cm from the fuel/water interface increased slowly as the fuel heated. Eventually (after 10 min.) these two thermocouples were located within the flame zone, as indicated by temperatures near 800K. The temperature of the fuel top surface can be determined by analyzing the temperature trends of the thermocouples located within the fuel (4.5 cm and 1.9 cm). A phase change (fuel vaporization) is indicated when the temperature remains constant for a period of time and then increases rapidly. This fuel surface constant temperature of approximately 500 K can be seen at 2 min. after ignition for the 4.5 cm thermocouple and at 7.5 min after ignition for the 1.9 cm thermocouple. The temperatures of the thermocouples in the water showed minimal increase. The thermocouple located -0.6 cm from the interface increased to about 400 K as a result of absorption of radiative flux by the water. The thermocouples located further away from the flame zone in the water (-2.9 and -5.1 cm) did not increase in temperature due to negligible heat transfer through the water or due to the sufficient mixing within the water to keep them cool.

The maximum temperatures recorded by array 2 were approximately 200 K higher than the temperatures recorded by array 1. Heat fluxes for array 2 were generally 20 kW/m^2 higher than for the array 1 region. The differences in temperatures could also be caused by increased convection in the array 2 region which would cause the temperature of the thermocouple to approach the local temperature. It is also likely that the low array 1 temperatures could be caused by the presence of an oxygen starved region. In array 2, the thermocouple located at 6.4 cm from the interface measured temperatures greater than 800 K almost immediately following ignition. Temperatures greater than 800 K generally occur within the flame zone; therefore, this thermocouple is most likely located above the fuel surface at the start of the test. At some time after ignition the thermocouples at 3.5 cm (2 min. after ignition) and 1.0 cm (8 min. after ignition) begin to increase in temperature gradually until they level off at approximately 490-510 K (inferred as the temperature of the fuel top surface and vaporization) after which they increase significantly in temperature as they are exposed to the flame zone. The remaining three thermocouples (-1.3 cm, -3.2 cm, and -5.1 cm) are located within the water and they do not record any increase in temperature throughout the duration of the test.

Figure 8.3 - Fuel and Water Temperatures - Test 3, Array 1
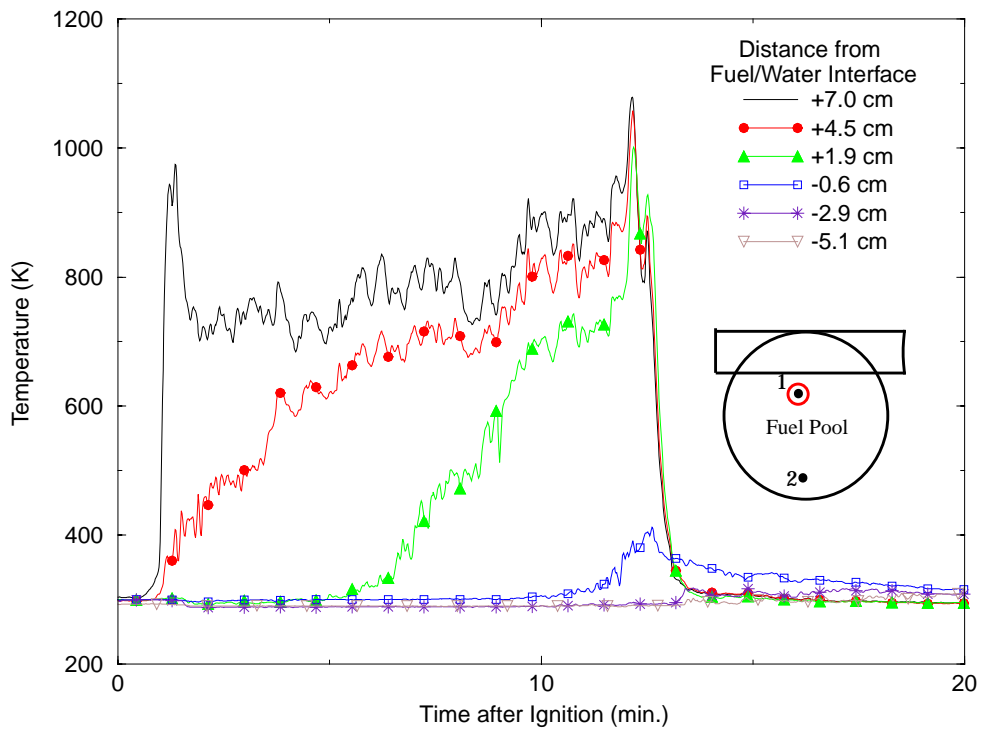
Figure 8.4 - Fuel and Water Temperatures - Test 3, Array 2

124
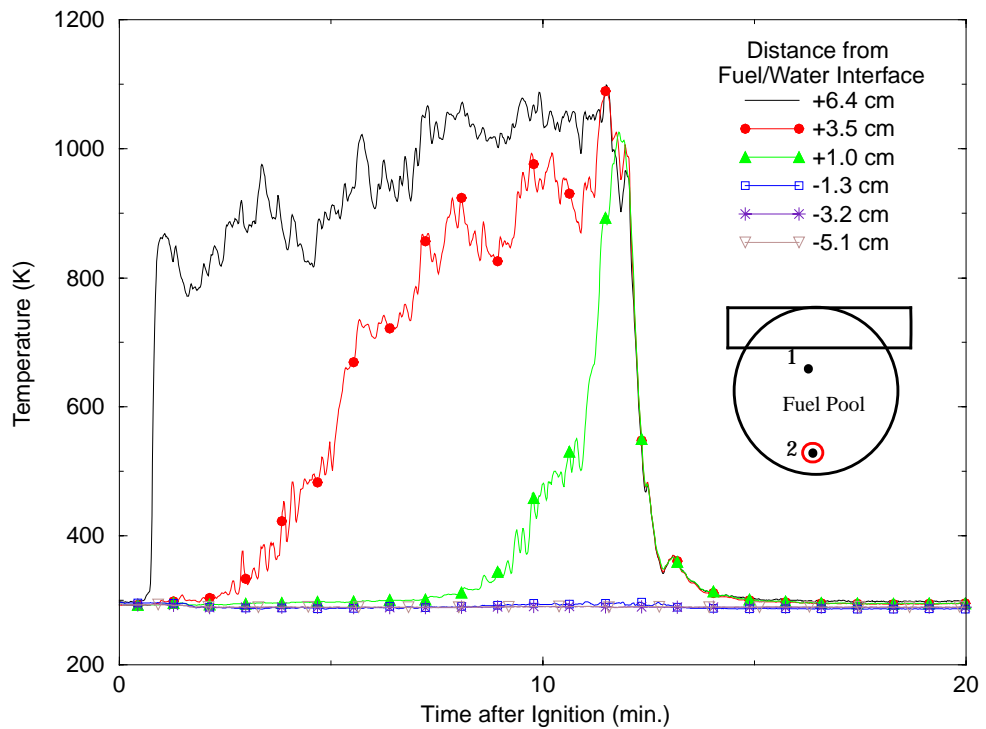
8.2.4 Fuel Temperatures for Test 4

Two thermocouple arrays were used in Test 4 to monitor the temperature of the fuel and the water underneath the fuel. The temperature data are shown in Figure 8.5 and 8.6. In both arrays the top four thermocouples (3.5, 2.9, 1.3, 0.8 cm) were located within the fuel layer. The temperatures of the thermocouples increased beginning with the 3.5 cm thermocouple at 2 min. after ignition. The temperatures of the thermocouples in the fuel layer increased until their temperatures leveled out at approximately 500 K. This constant temperature is most clearly seen in the 2.9 cm thermocouple beginning at 5 min. after ignition. The leveling of temperature generally indicates a phase change (i.e. fuel vaporization). There is a rapid increase in temperature after the fuel was vaporized. A final drastic increase in the thermocouples occurs at 13 min. after ignition when the flame front passes the thermocouples as the fire is diminishing. The thermocouples located in the water remained relatively cool throughout most of the test. The array 1 thermocouple at -1.3 cm shows a slight increase in temperature around 12 min. after ignition due to the heat transfer from the fire. It is evident that the water cooled and/or shielded the thermocouples at -1.3 cm and -2.9 cm from the intense heat of the fire. From these data, the distance of heat absorption by the water is approximately 1-2 cm.

The temperatures measured by the thermocouple array near the leading edge of the fuel pool were approximately 100 K higher than those temperatures recorded near the center of the fuel pool but the trends were similar. The four thermocouples located within the fuel begin increasing slowly in temperature until they leveled off at 490-510 K. The thermocouples remained at this temperature, which appears from these data to be indicative of the fuel surface temperature, for some time before increasing again. The upper thermocouples reached a peak temperature of 1050 K at 12 min. after ignition as the flames passed when the fire was diminishing. The two thermocouples located within the water (-1.3 cm and -3.2 cm) did not rise in temperature indicating that the heat absorption distance was less than ~1 cm.

Figure 8.5 - Fuel and Water Temperatures - Test 4, Array 1
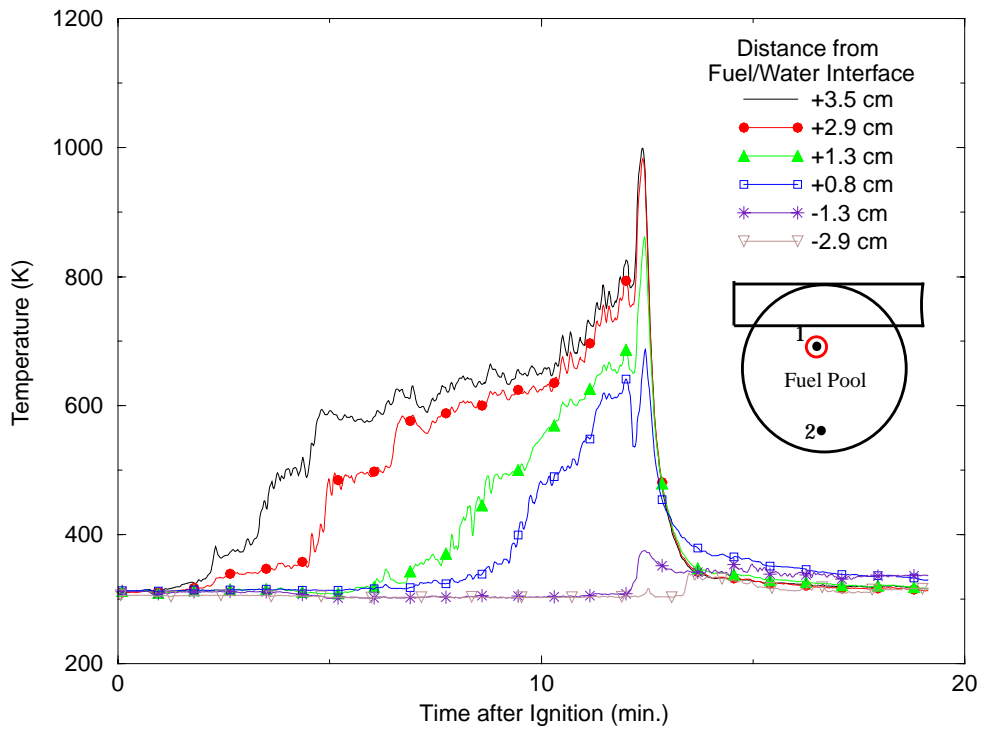
Figure 8.6 - Fuel and Water Temperatures - Test 4, Array 2

126
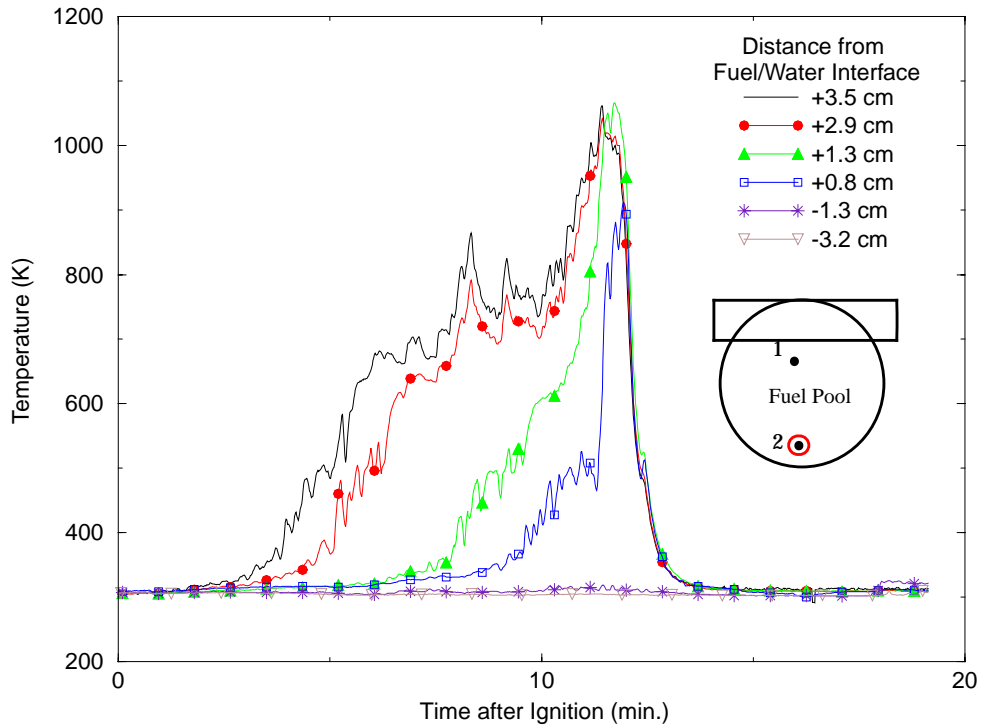
8.2.5 Fuel Temperatures for Test 5

Two thermocouple arrays were used in Test 5 to monitor the temperature of the fuel and the water underneath the fuel. The temperatures are shown in Figure 8.7 and 8.8. The trends observed in the Test 5 fuel temperature data were similar to the previous tests. The top four thermocouples were in the fuel layer and their temperatures increased after ignition beginning with the thermocouple farthest from the fuel water interface (therefore closest to the fuel surface). The temperature trends for the top two thermocouples (4.1 cm and 3.2 cm) are almost identical except that initially the 4.1 cm thermocouple records higher temperatures. After 5 min. their temperature measurements are the same. The thermocouples at 1.6 cm and 1.3 cm begin increasing in temperature around 5.5 min. after ignition. The 1.6 cm thermocouple rises more steeply until it levels off at 7 min. after ignition at 490 K when the phase change occurs. The 1.3 cm thermocouple levels off at the same temperature at approximately 8 min. after ignition. After the phase change, the thermocouples temperature increases by approximately 100 K. At approximately 12 min. after ignition all thermocouples initially located within the fuel increase to a maximum temperature of 1000 K caused by the passing of the flame front as the fire diminishes. The thermocouple located within the water at -1.0 cm experienced only a slight increase in temperature of 50 K, while the -2.9 cm thermocouple remained at 300 K for the duration of the test indicating the maximum distance of heat absorption for the water is between 1.0 cm and 2.9 cm.

Similar to the trends in the previous tests, the temperatures measured by array 2 rise slowly as the fuel is heating, beginning with the thermocouple at 3.5 cm. The temperature where the phase change occurs is difficult to see for any of the thermocouple measurements but it appears to be at approximately 475-500 K. After the temperature rise following the phase change, the measured temperatures for the thermocouples initially located within the fuel are 700-1050 K. The thermocouple located -1.3 cm from the fuel/water interface only experiences a slight increase in temperature (~30 K) about 11 min. after ignition due to the heat transfer from the flame zone through the water. The thermocouple at -2.9 cm was not affected, therefore the distance of heat absorption by the water is between 1.3 and 2.9 cm.

Figure 8.7 - Fuel and Water Temperatures - Test 5, Array 1
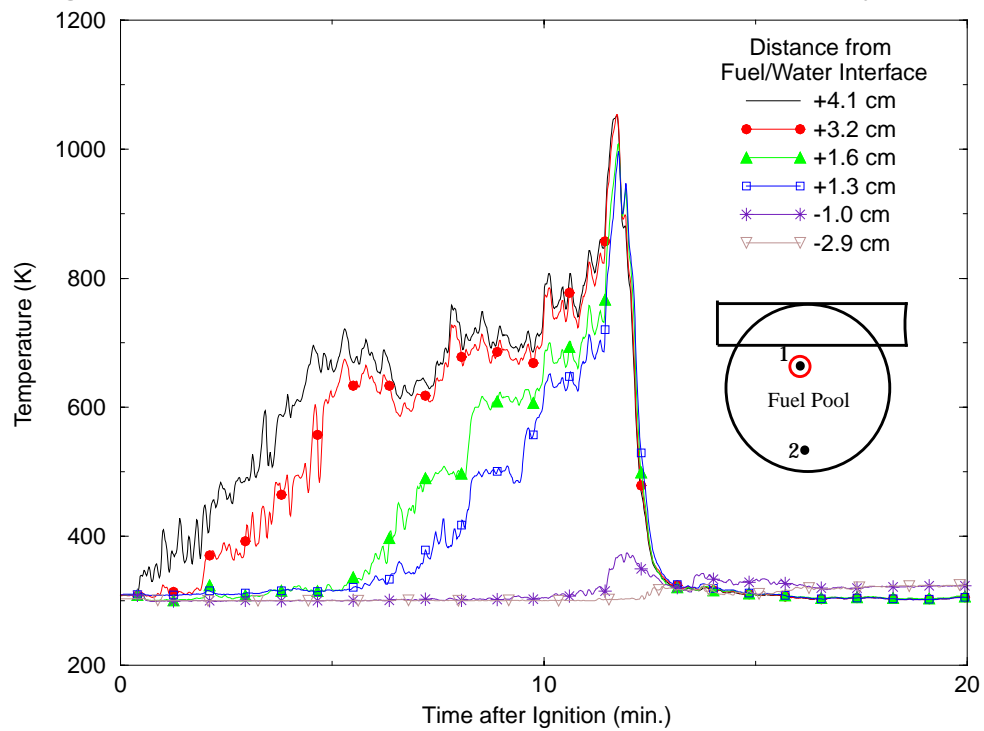
Figure 8.8 - Fuel and Water Temperatures - Test 5, Array 2

128
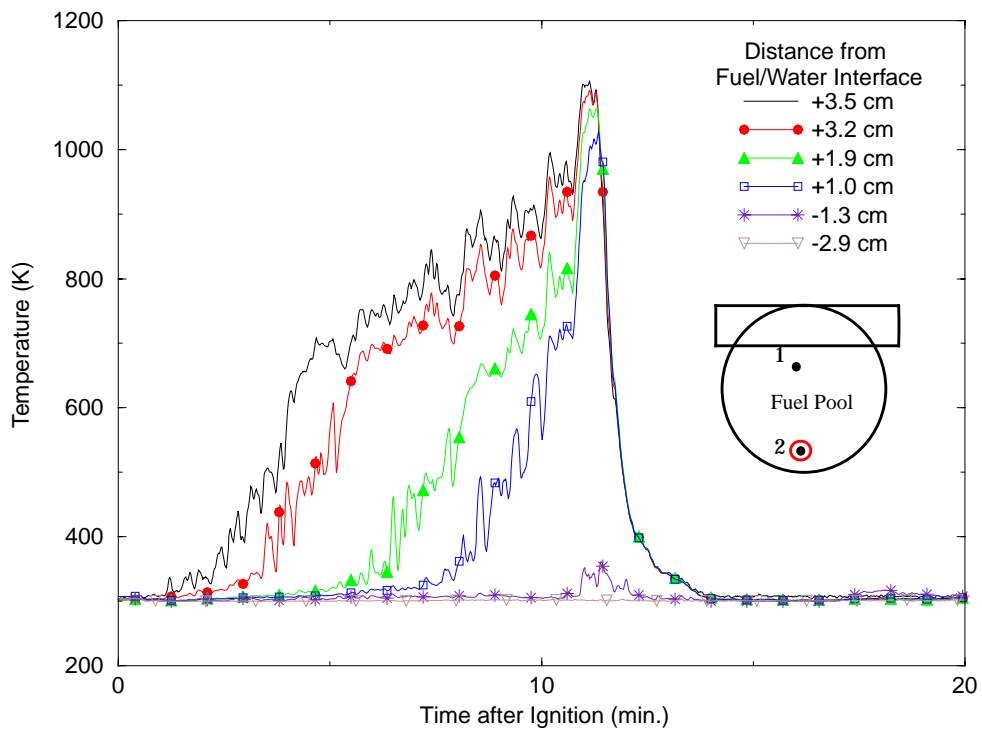
8.2.6 Fuel Temperatures for Test 8

Two thermocouple arrays were used in Test 8 to monitor the temperature of the fuel and the water underneath the fuel. The temperatures are shown in Figure 8.9 and 8.10. The temperature trends observed in the two arrays appear quite different; although the location of the thermocouples with respect to the interface is much different in the two arrays. When comparing the thermocouples both located 2.5 cm from the interface, similar trends are observed. Both arrays display a peak temperature around 13 min. after ignition as the flames pass by at the end of the fire.

The temperatures measured by the array 1 thermocouples located within the liquid fuel (4.5, 3.2, and 2.5 cm) rise slowly as the fuel is heated, beginning with the thermocouple closest to the fuel surface just after ignition. This thermocouple at 4.5 cm rises just after ignition to 475 K at 2 min. after ignition where its temperature remains constant for 1.5 minutes. This temperature plateau represents a phase change and gives an indication of the fuel surface temperature. The other two thermocouples, at 3.2 cm and 2.5 cm, initially located within the fuel layer have similar trends except they begin increasing in temperature at 2 min. and 5 min., respectively. The top three thermocouples experience a peak temperature of 1000 K at 12 min. after ignition. Three thermocouples (-0.6 cm, -2.5 cm, and -3.8 cm) are located within the water below the fuel surface. The thermocouples at -0.6 and -2.5 cm show a slight increase in temperature (<75 K) beginning at 11 and 13 min. after ignition, respectively. Data acquisition noise was responsible for the fluctuations seen in the data which was particularly noticeable in the thermocouples that remained near 300 K.

The array 2 thermocouples located within the liquid fuel take almost 5 min. longer than the array 1 thermocouples to show any increase in temperature due to the increased distance from the fuel surface. At 5 min. after ignition the thermocouple at 2.5 cm begin to increase in temperature. It experiences a steep increase in temperature at 7 min. and again at 11 min. until it reaches a maximum temperature of 1000 K. The thermocouples at 1.3 and 0.6 cm show similar trends. The leveling of temperature, indicating the phase change, occurs at approximately 475-500 K as seen in the 2.5, 1.3, and 0.6 cm thermocouple temperature data. The thermocouples located beneath the fuel/water interface (-1.3 cm, -3.2 cm, and -4.5 cm) remain at ambient throughout the duration of the test indicating that the heat absorption distance for water is less than 1.3 cm for these conditions.

Figure 8.9 - Fuel and Water Temperatures - Test 8, Array 1
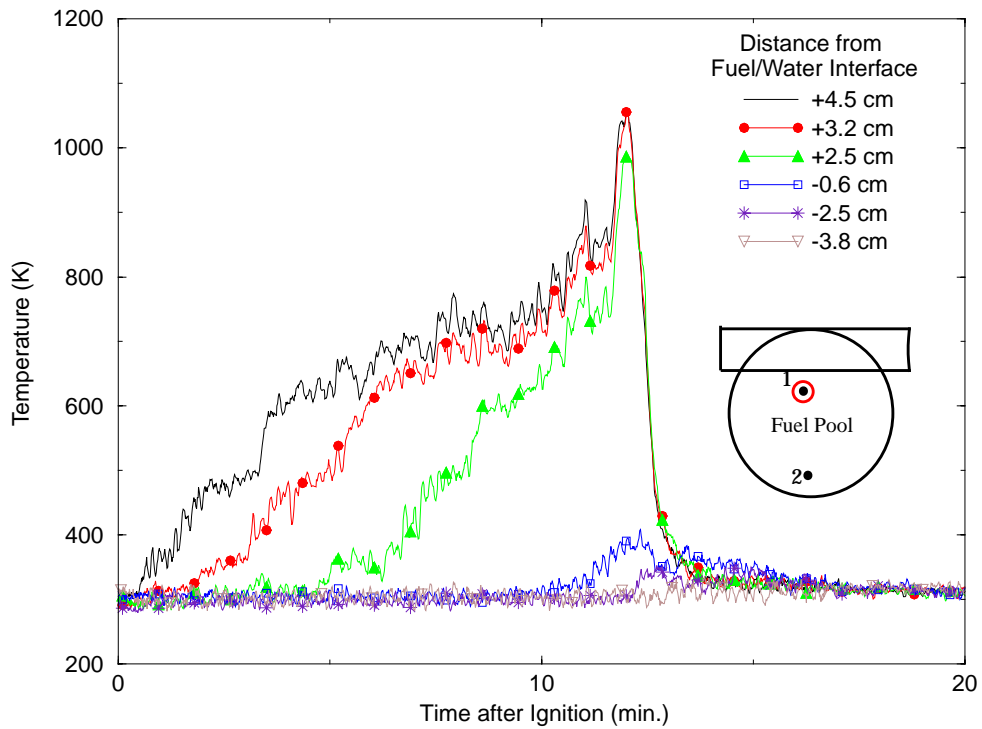
Figure 8.10 - Fuel and Water Temperatures - Test 8, Array 2

130
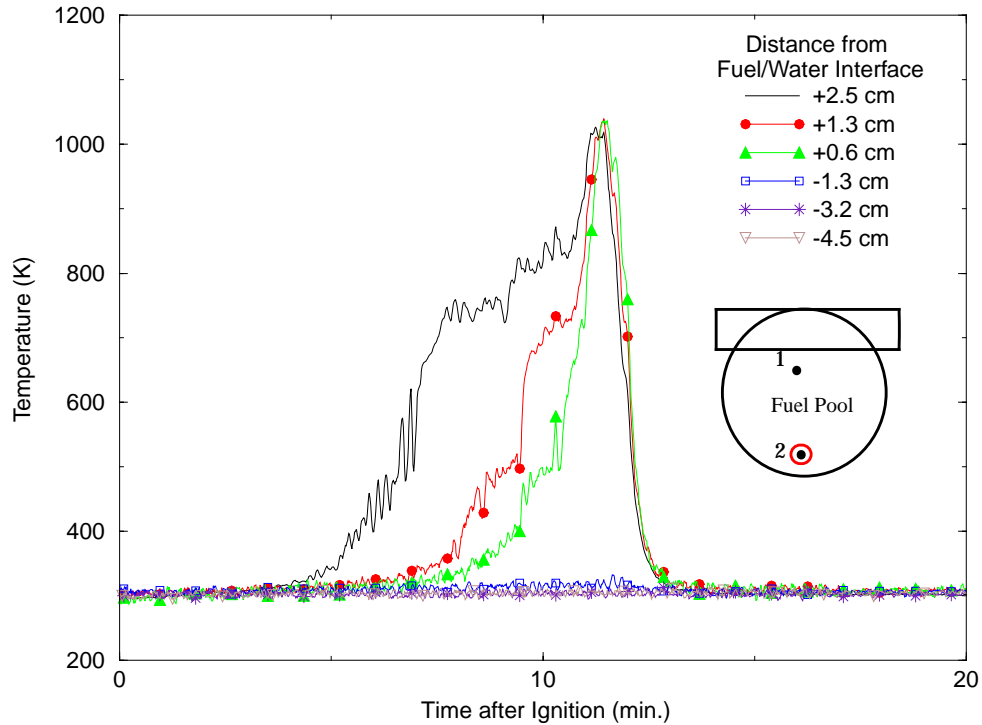
8.3 Small Pool Fuel Temperatures

The next two tests were conducted in a 10 m pool of JP-8 jet fuel. The fuel and water were instrumented with a thermocouple array (Figure 2.9) according to the plan stated in Chapter 2.

8.3.1 Fuel Temperatures for Test 6

A single thermocouple array was used in Test 6 to monitor the temperature of the fuel and the water underneath the fuel. The temperatures are shown in Figure 8.11. The location of the fuel/water interface was not measured prior to beginning the test. Upon visual inspection of the data it appears that only the top thermocouple (0.22m) was within the fuel layer. Its temperature increases slowly until 3 min. after ignition from 300 K to 500 K. When the temperature of the fuel reaches 500 K it remains at 500 K for several minutes indicating a phase change until it sharply increases in temperature to 650 K. At 9 min. after ignition, the temperatures rise to 1000 K as the flames pass by the thermocouple when the fire extinguishes. The other thermocouples remained near 300 K except for a slight increase in the temperature of the thermocouple at 0.21 m (~40 K) caused by the heat transfer to the water from the flame zone.

Figure 8.11 - Fuel and Water Temperatures - Test 6
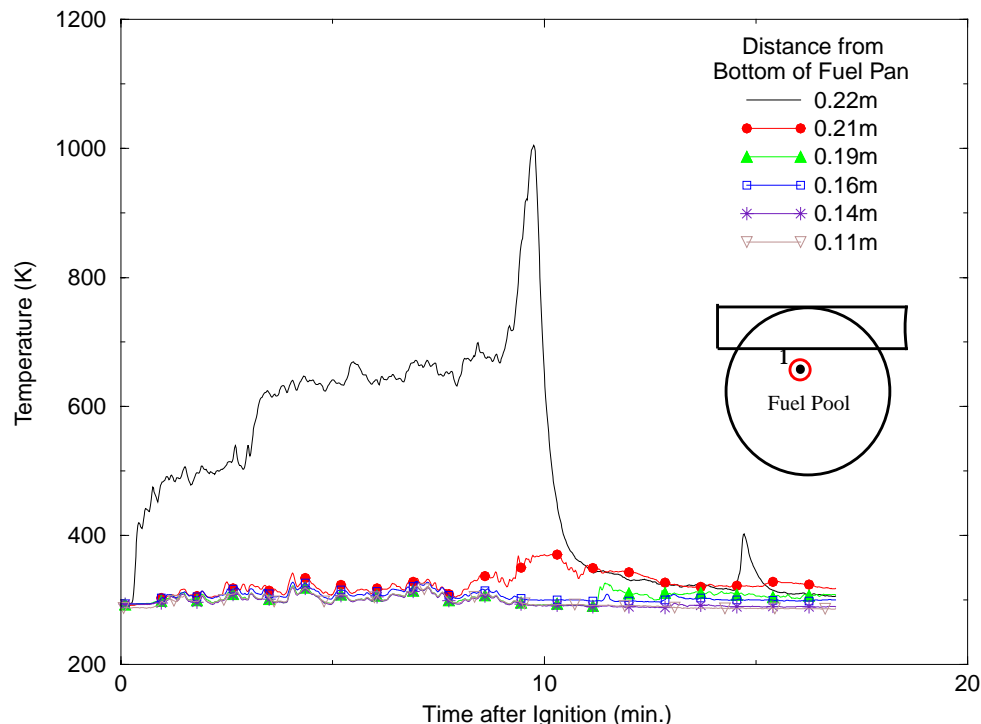
8.3.2 Fuel Temperatures for Test 7

A single thermocouple array was used in Test 7 to monitor the temperature of the fuel and the water underneath the fuel. The temperatures are shown in Figure 8.12. It appears that none of the thermocouples on the array were located within the fuel layer since temperatures only approach 500 K. Data presented earlier indicate the fuel surface temperature is approximately 510 K. Temperatures near 800 K typically represent an actively burning region. It is evident that the thermocouples were located within the water layer, not directly exposed to the fire at any time during the test. The slight increase in the 0.22 m thermocouple was caused by the absorption of radiation by the water from the flame zone although it is somewhat suspicious that the increase in temperature occurs so long after ignition. The fluctuations in the line plot are a result of data acquisition noise.

Figure 8.12 - Fuel and Water Temperatures - Test 7
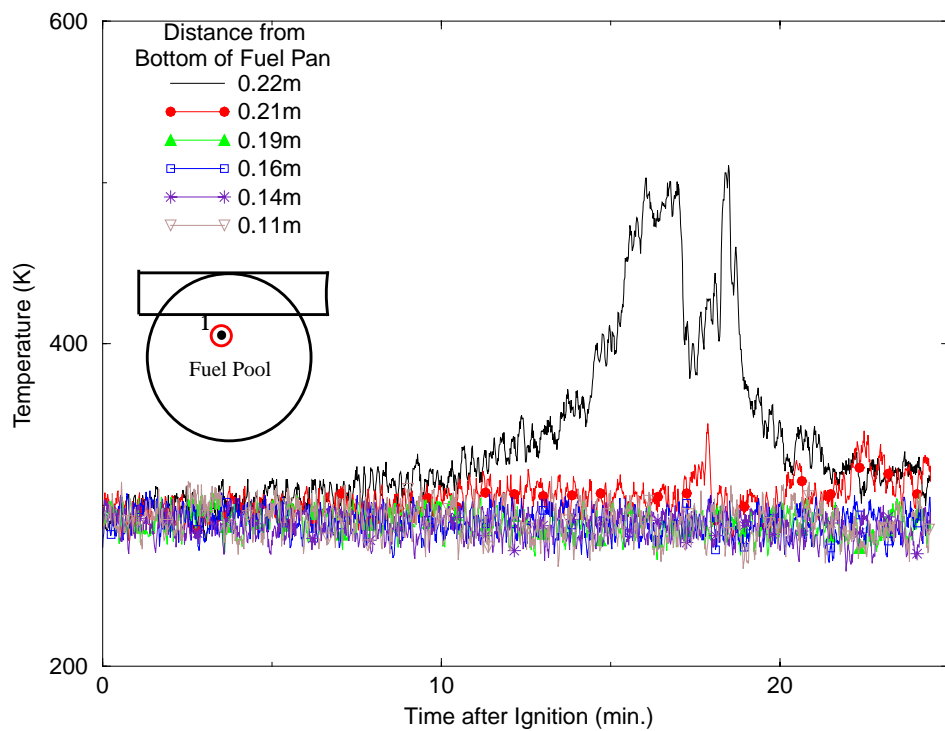
8.4 Fuel Recession Data

The fuel temperature data shown in the previous sections was used to calculate the fuel recession rate for each test. These data are included in Table 8.1. The temperature trends for thermocouples located within the fuel layer (above the fuel/water interface) were analyzed to determine where the phase change occurred. This phase change is visible on the plots as a leveling of the temperature for some period of time during the test followed by a steep increase in temperature. The schematic in Figure 8.13 approximates the constant temperature as a dotted line around 500 K. This temperature is recorded in the first column of the chart as T_{boil}. The average temperature of all tests was 508 K. The second column (t) is the time at which the thermocouple reaches phase change temperature. The third column (tav) is the average time for two adjacent thermocouples to reach the phase change temperature. Then, the fourth column (dt) is the difference between two adjacent thermocouples time to reach the temperature. The final column is the burn rate (dh/dt) in mm/min. The burn rate is determined by dividing the distance between the thermocouples by the time difference (dh and dt are both shown of the schematic). The average heat flux (qav) during the time period (dt) is included in the last column. The average burn rate for all the tests was 4.4 mm/min which is consistent with other pool fire measurements [8]. Note that the chart shows no correlation between average heat flux and fuel recession rate.

Figure 8.13 - Burn Rate Schematic (T4-A1)

133
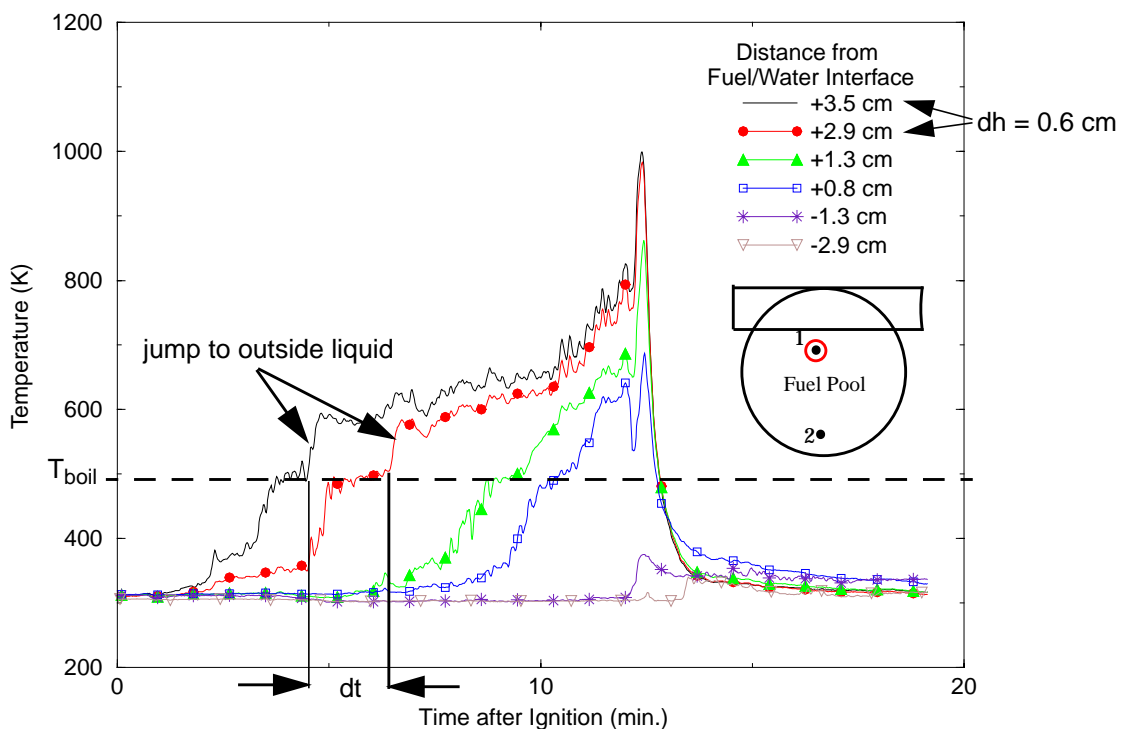
Table 8.1: Fuel Recession Data, Mock Fuselage Test Series

Test and Array number	Tboil (K)	t (s)	tav	dt (s)	dh/dt (mm/min)	qav
Test 3 Array 1	511	210	363	305	5.1	83
	500	515				
Test 3 Array 2	525	307	484	353	4.2	89
	525	660				
Test 4 Array 1	510	270	329	117	3.1	78
	500	387	484	193	5.0	
	500	580	618	75	4.0	
	510	655				
Test 4 Array 2	500	307	344	73	4.9	
	510	380	479	197	4.9	81
	525	577	629	103	2.9	89
	495	680				
Test 5 Array 1	500	197	234	73	7.4	76
	500	270	380	220	4.4	79
	500	490	530	80	2.3	
	500	570				
Test 5 Array 2	525	240	278	75	2.4	
	510	315	398	165	4.7	
	510	480	530	100	5.4	86
	510	580				
Test 8 Array 1	495	180	250	140	5.6	74
	510	320	410	180	2.3	83
	505	500				
Test 8 Array 2	510	420	485	130	5.5	
	510	570	595	60	5.0	89
	510	630				
AVERAGE	**508**				**4.4**	**82**

9. Experimental Results - Pressure

9.1 Overview of Experiments

Four pressure transducers were included in the tests. Each transducer measured differential pressure between two locations. Three of the measurement locations were on the mock fuselage surface and were used to measure the differential pressure between the 90° position (windward) and the 270° position (leeward). The three measurement locations were at the centerline and 3.66 m on either side of the centerline. The last transducer measured differential pressure between the fuel pool and the area outside the fuel pool. A schematic, shown in Figure 9.1, illustrates the location of these transducers.

Figure 9.1 - Location of Pressure Measurements
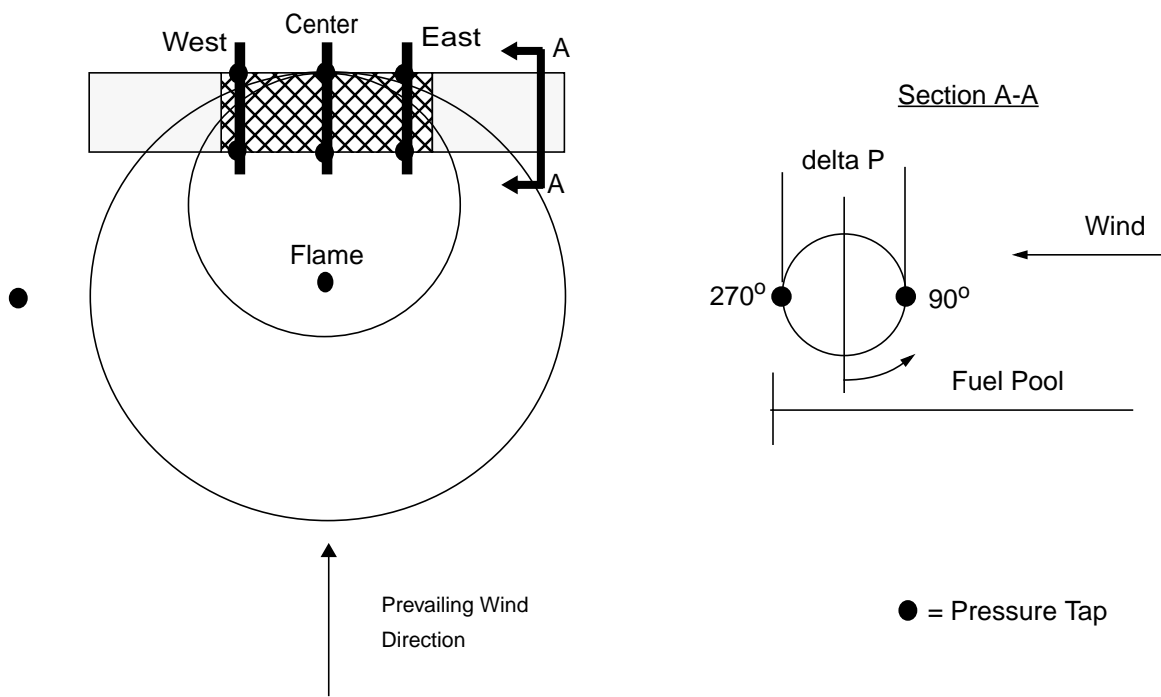
9.2 Large Pool Pressure Transducer Measurements

9.2.1 Pressures for Tests 1 - 3

Pressure transducers were not included in Tests 1-3.

9.2.2 Pressures for Test 4

The pressures recorded during Test 4 are shown in Figure 9.2. Refer to Figure 9.1 for the location of the pressure measurements. The center transducer malfunctioned and was therefore not included in the plot. The pressure on the windward side is the highest. The pressure in the center of the fire is lowest possibly due to air entrainment. The wind speed data shows that the lowest wind speeds (3 m/s) were recorded between 7 and 11 min. after ignition which corresponds to the time when the smallest differences occurred in the pressure plot.

Figure 9.2 -Test 4 Pressures
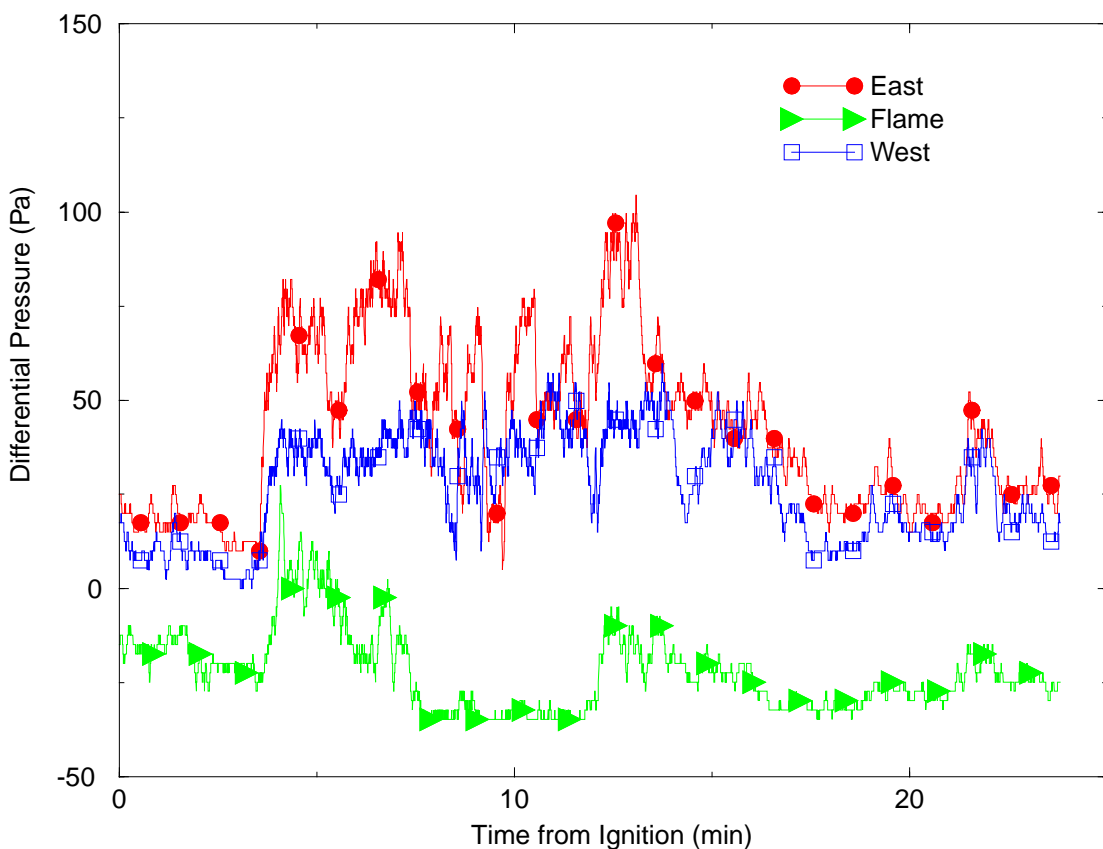
9.2.3 Pressures for Test 5

The pressures recorded during Test 5 are shown in Figure 9.3. Similar to Test 4, the pressures are highest on the windward side and lowest in the center of the fuel pool. The center, east, and west transducers appear to track changes in the wind conditions. The wind speeds begin high at around 10 m/s but drop suddenly about 1 min. after ignition. This drop can also be seen in the pressures at the same time. The pressures drop from a peak of 75 Pa to approximately 25 Pa. At 2.5-3 min. after ignition, an increase in wind is accompanied by a corresponding increase in pressure up to 75 Pa. The wind speed and the pressure remain stable for about 4 min. until they both begin decreasing again.

Figure 9.3 - Test 5 Pressures

138
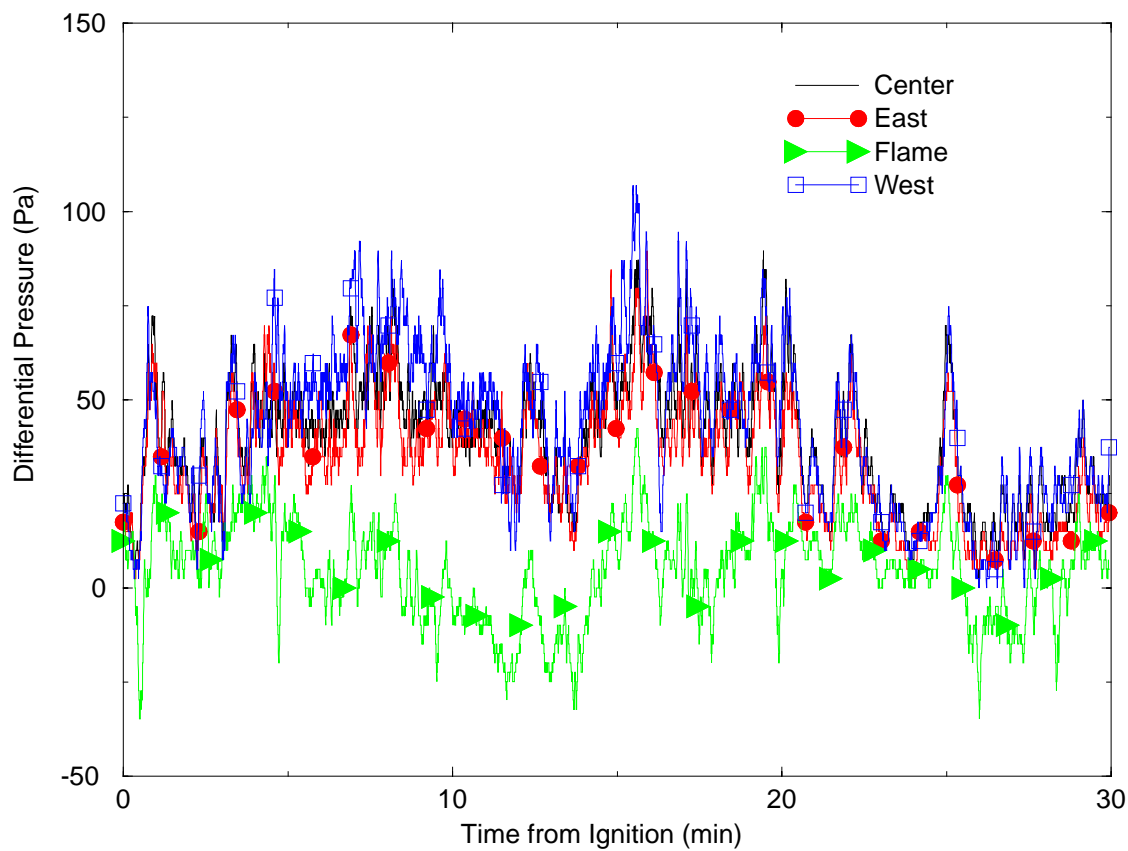
9.2.4 Pressures for Test 8

The pressures recorded during test 8 are shown in Figure 9.4. The pressures recorded by the flame transducer appeared suspect and were therefore omitted from the plot. The pressures are highest on the windward side of the mock fuselage. The wind speeds and directions are stable throughout Test 8; therefore, changes in the pressure plot can perhaps be attributed to natural fluctuations in the fire.

Figure 9.4 - Test 8 Pressures
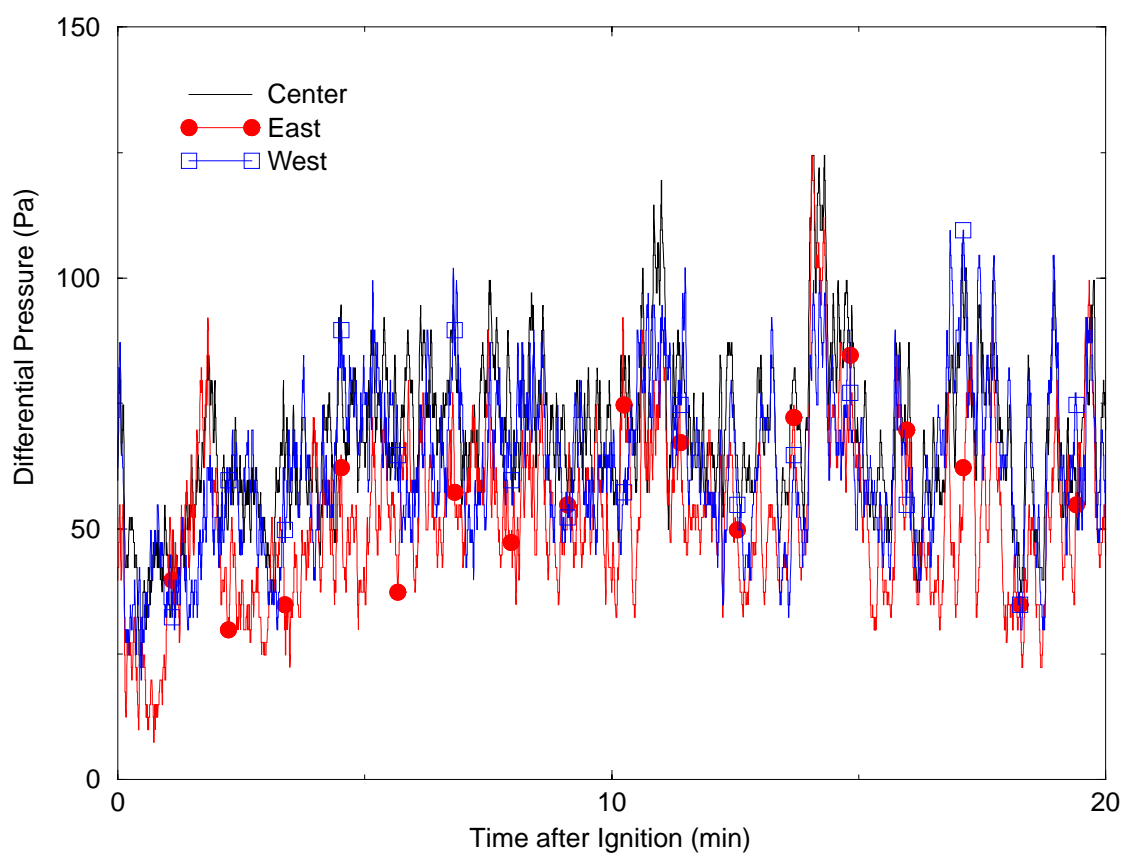
9.3 Small Pool Pressure Transducer Measurements

9.3.1 Pressures for Test 6

The pressures recorded during test 6 are shown in Figure 9.5. An anomaly occurred in the data recorded by the flame and west gauges and therefore those data were omitted from the plot. As indicated by the center and east transducers, the pressures are highest on the windward side. The wind speeds are fairly stable with the exception of one small decrease observed about 1-2 min after ignition. It is possible that this decrease causes the decrease in pressure from 85 Pa to 30 Pa which occurs about the same time for the east transducer. The center transducer also experiences a decrease at this same time.

Figure 9.5 - Test 6 Pressures

140
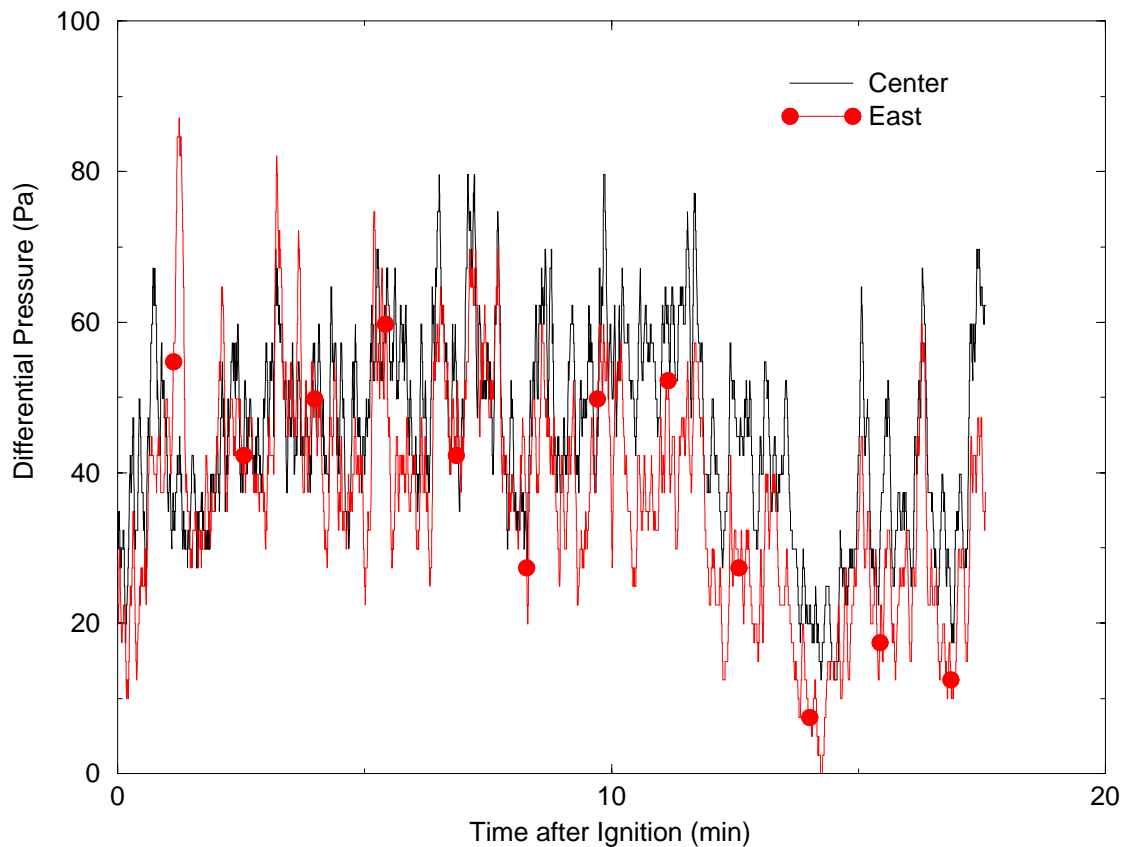
9.3.2 Pressures for Test 7

The pressures recorded during test 7 are shown in Figure 9.6. The flame gauge data appeared suspect and was omitted from the plot. The differential pressures recorded for Test 7 are the lowest of all the tests. This feature is most likely caused by the low wind speed during the test (~2 m/s). The variation in the wind speed during the test was minimal.

Figure 9.6 - Test 7 Pressures
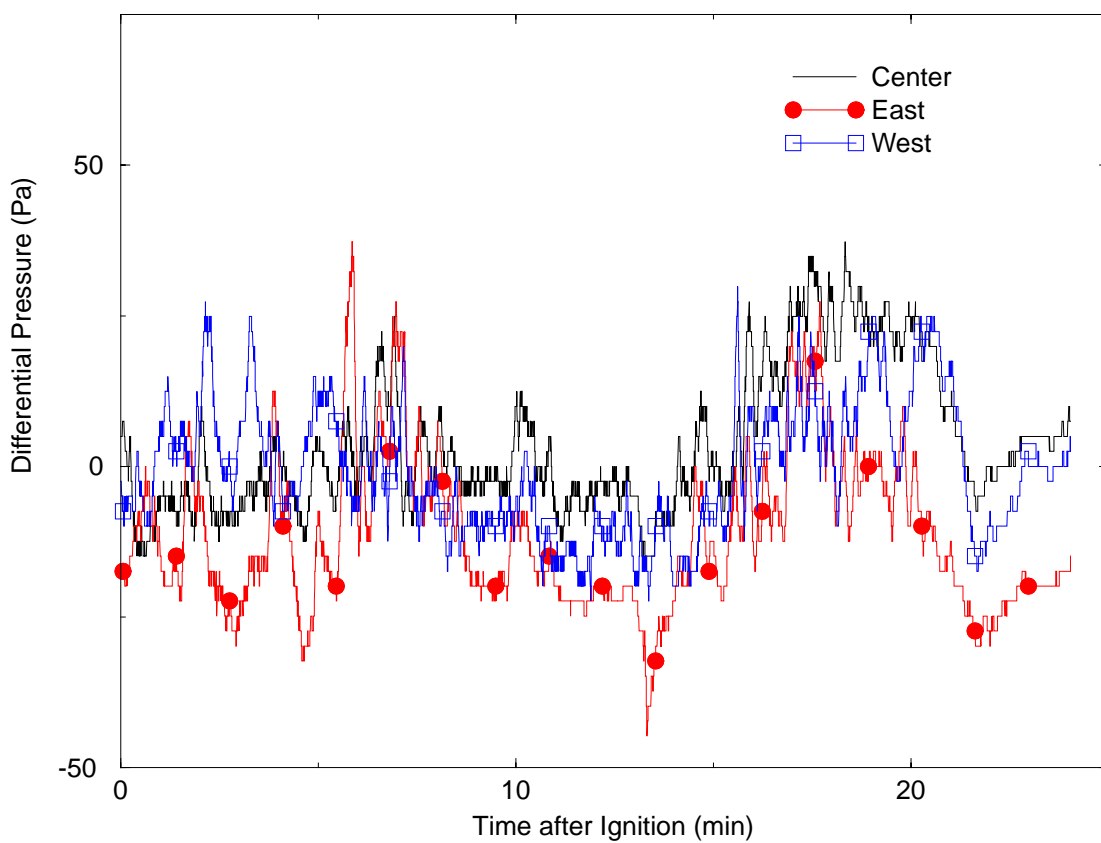
10. Experimental Results - External Heat Flux

10.1 Overview of Experiments

Spatial and temporal heat flux measurements from the exterior of the fire were used for comparison with models that predict the heat flux to an object located a finite distance from the continuous flame zone. To characterize the heat flux to an object near the flame zone, four water-cooled, 2.03 cm foil-type Gardon gauge calorimeters with signal conditioning amplifiers were placed 30 m from pool center; 1 windward, 1 leeward, and 1 on each side. A minimum of 1/8 GPM of cooling water at a temperature above the local dew point was supplied to each gauge. To quantify the heat flux to an object a significant distance from the flame zone (a region where existing correlations are expected to be inaccurate), 1 heat sink gauge was placed on the lee side of the pool at a distance of ~80 m from the pool center. All gauges were mounted in the insulated steel panel, adjustable angle fixture shown in Figure 2.10. A thermocouple mounted to the back side of the fixture provided a second technique for estimating the heat flux. In an attempt to resolve the primary transient changes in plume geometry, (i.e. "the puffing") the Gardon gauge measurements were performed every 0.1 seconds. The thermocouple temperatures were recorded at 1 Hz.

10.2 Large Pool External Heat Flux Measurements

The incident heat flux was calculated from the TC data using the transient temperature change and the material properties.   To reduce noise amplification in the data, eight future times were used in differencing the temperature data. Temperature data was also smoothed using a 10 point running average prior to calculations to reduce noise amplification. The material properties used were for 0.32 cm thick mild steel and the emissivity used in the heat flux calculations was 1.0. The calculated heat flux from the temperature data is presented in the plots along with the heat flux obtained from the Gardon gauge. The heat fluxes are only presented up to 12 min. after ignition. After this time the fire is going out but the wind continues to affect the gauges by convective cooling. The magnitude of the net incident heat fluxes dropped below zero beyond 12 min. after ignition due to convective cooling of the gauges.

10.2.1 Tests 1 - 3

External heat flux gauges were not included in Tests 1-3.

10.2.2 Test 4

The heat fluxes recorded during Test 4 are shown in Figures 10.1-10.5. The heat fluxes recorded by the 60 m north location range from 0-2 kW/m^2.   The heat fluxes

recorded by the Gardon gauge were approximately half of the fluxes computed using the TC temperatures but their trends were the same. Both gauges increased approximately 1 min. after ignition and recorded heat fluxes with minimal fluctuations until the fire began to extinguish around 10 min. after ignition. The TC heat fluxes were lower than the Gardon gauge heat fluxes at all other stations in the test except at the 60 m north station which suggests that the gauges may not have functioned correctly at this location. The heat fluxes (up to 30 kW/m^2) recorded by the 30 m north station were considerably higher than the 60 m north station primarily due to the close proximity of the station to the leeward edge of the flame zone. The heat fluxes measured at this location were higher than all other stations included in the test. These high heat fluxes at the 30 m north station were caused by flame tilt as well as the interaction of the wind with the object to create higher temperatures with smoke clearing, enhanced mixing, and burning in the wake of the mock fuselage section. The data from the Gardon gauge shows large fluctuations. Since the Gardon gauge is recording data at 10 Hz it is able to pick up the high frequency variations in the fire. The trends recorded by the TC and the Gardon gauge at the 30 m north station were very similar in spite of the large fluctuations occurring in the Gardon gauge data.

The overall magnitude of the 30 m south heat fluxes measured by the Gardon gauge and the TC were in good agreement (~2 kW/m^2). The 30 m east stations recorded 1-6 kW/m^2 for the Gardon gauge and the heat flux from the TC was fairly stable at just under 2 kW/m^2. Although the agreement of the trends from both the east and the west stations were very good when comparing the TC to the Gardon gauge readings, the magnitudes were off by approximately a factor of 1.5. The cause of this is not known at this time. It is also interesting that the west heat fluxes are considerably higher than the east heat fluxes, which was caused by the wind direction toward the west during the test.

Overall, the trends for the heat fluxes measured by the Gardon gauge and the TC were similar although the magnitudes were different. It appears that the magnitudes of the heat fluxes were fairly close early in the test and diverged as the test continued. This is believed to be caused by the difference in the sensitivity of the gauges to convection. The TC is easily affected by convection when it becomes very hot therefore the TC heat flux measurement would be less accurate at later times. Figures 10.3-10.5 show the divergence of the two different types of heat flux measurements clearly.

Figure 10.1 -Test 4 Heat Fluxes North 60 m
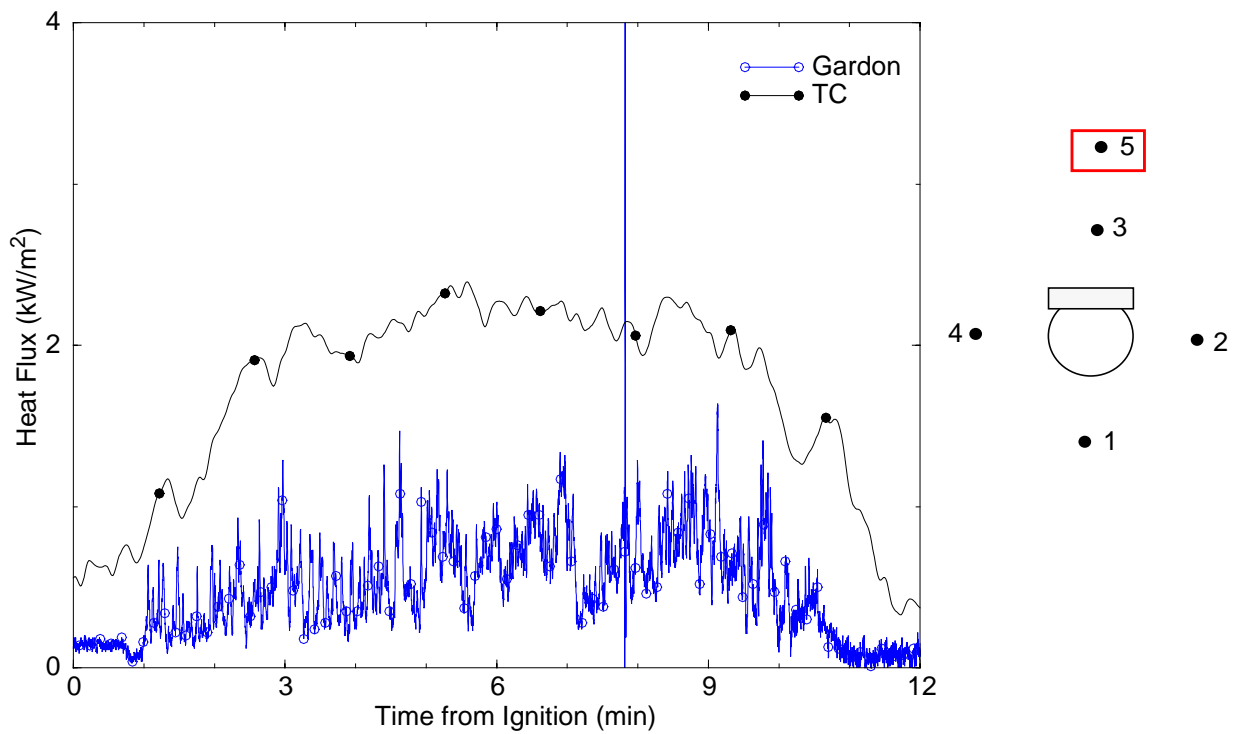
Figure 10.2 -Test 4 Heat Fluxes North 30 m
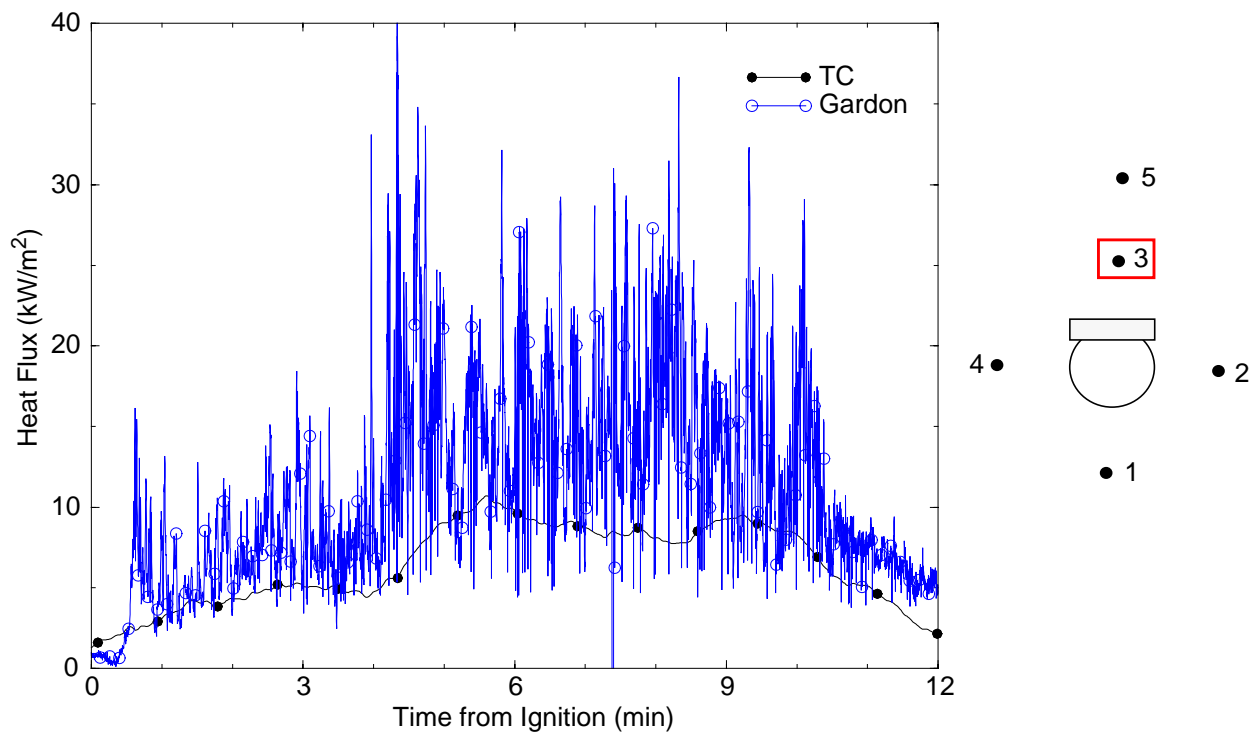
Figure 10.3 -Test 4 Heat Fluxes South 30 m
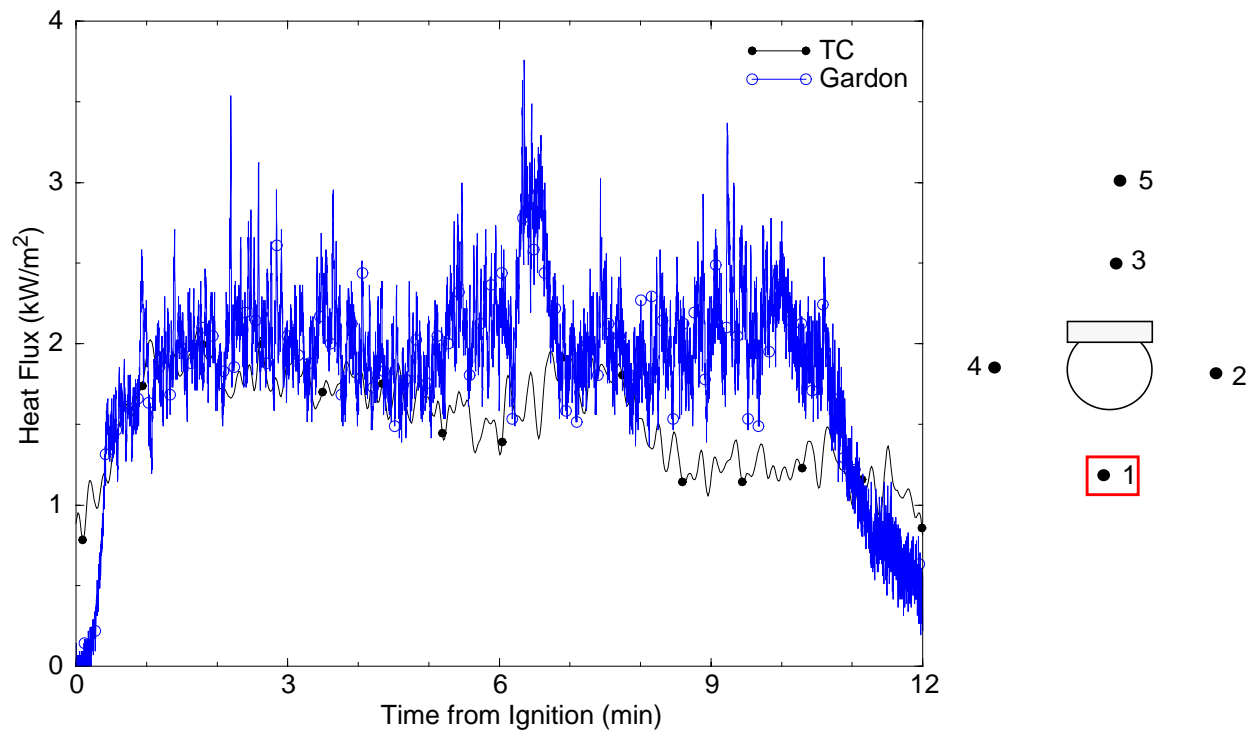
Figure 10.4 -Test 4 Heat Fluxes East 30 m

145
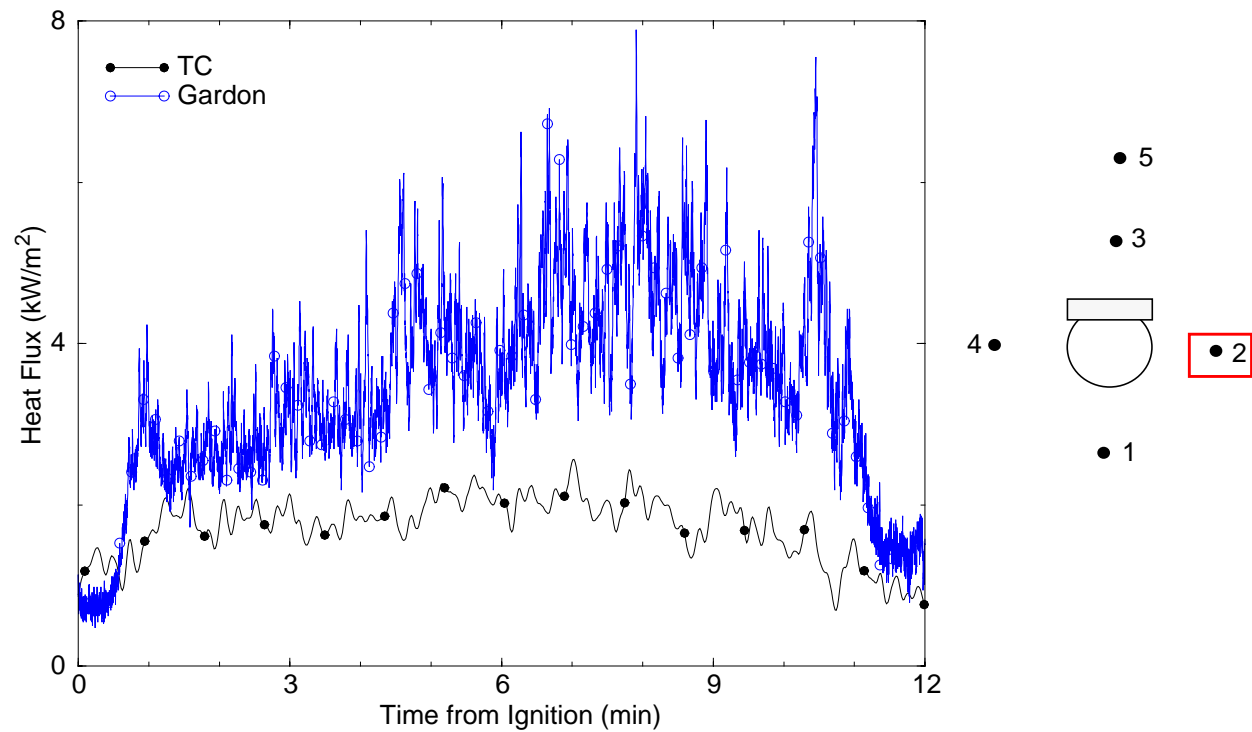
Figure 10.5 -Test 4 Heat Fluxes West 30 m
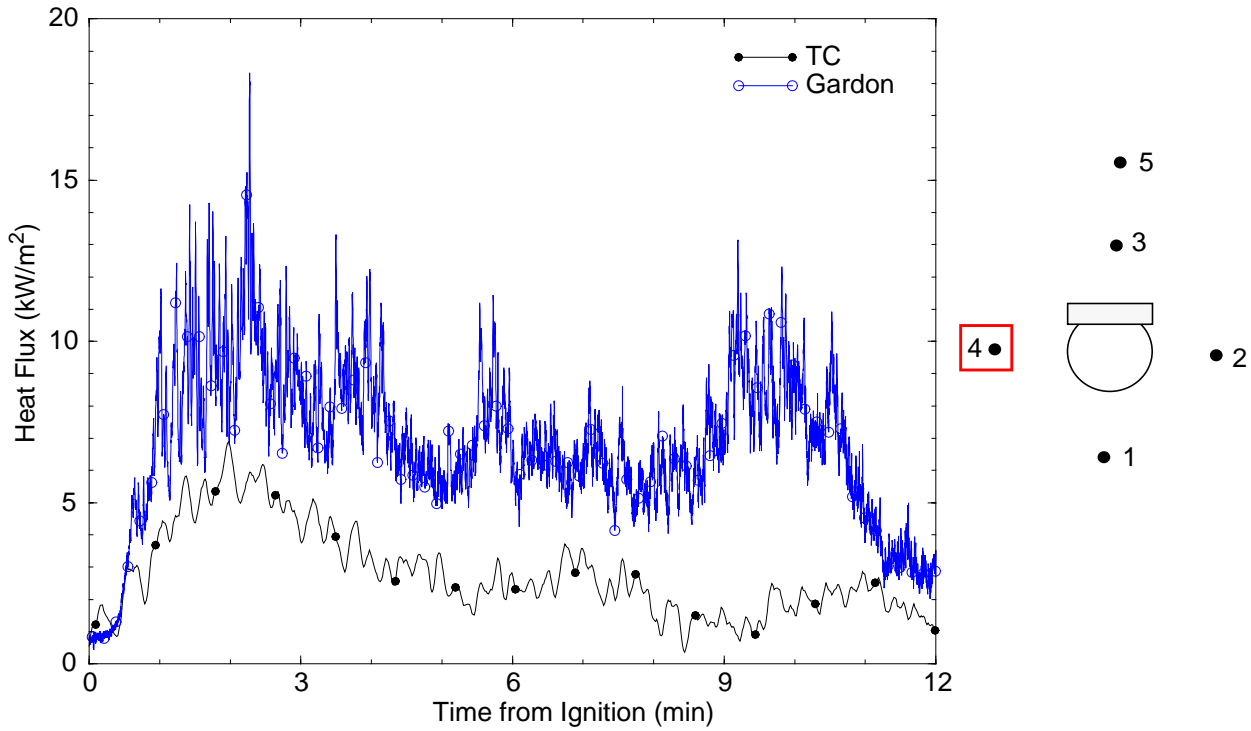
10.2.3 Test 5

The heat fluxes recorded during Test 4 are shown in Figures 10.6-10.10.   The heat fluxes recorded by the 60 m north location range from 0-2.5 kW/m^2. The trends of the heat fluxes measured by both Gardon gauge and the TC data were quite similar, although their magnitudes were slightly different. As stated in the previous section, the TC heat fluxes were higher than the Gardon gauge heat fluxes which was unique to this location. The heat fluxes recorded by the 60 m station appear to track the changes in the wind speed very well. The lowest wind speeds occur between 2 and 4 minutes and the highest wind speeds occur between 5 and 7 minutes after ignition. Significantly higher heat fluxes were recorded by the station at 30 m north (up to 40 kW/m^2). It is evident that the fire was changing rapidly by the fluctuation in the data recorded by the Gardon gauge at 10 Hz. The magnitude of the heat fluxes measured by the Gardon gauge were larger than the TC and the two measurements diverged due to the different sensitivities of the gauges to convection (evident at all other locations as well). The lowest heat fluxes were measured by the south station (~2 kW/m^2). These low heat fluxes are a result of the fire plume being directed away from the leading edge of the pool and therefore the south station. The agreement between the two heat flux measurements at the south station was very good. The east station measured heat fluxes up to 15 kW/m^2 but the TC calculated heat fluxes were lower than the Gardon heat fluxes. The agreement between the 30 m west station heat fluxes was good with an average measured heat flux of 3 kW/m^2.

Figure 10.6 -Test 5 Heat Fluxes North 60 m
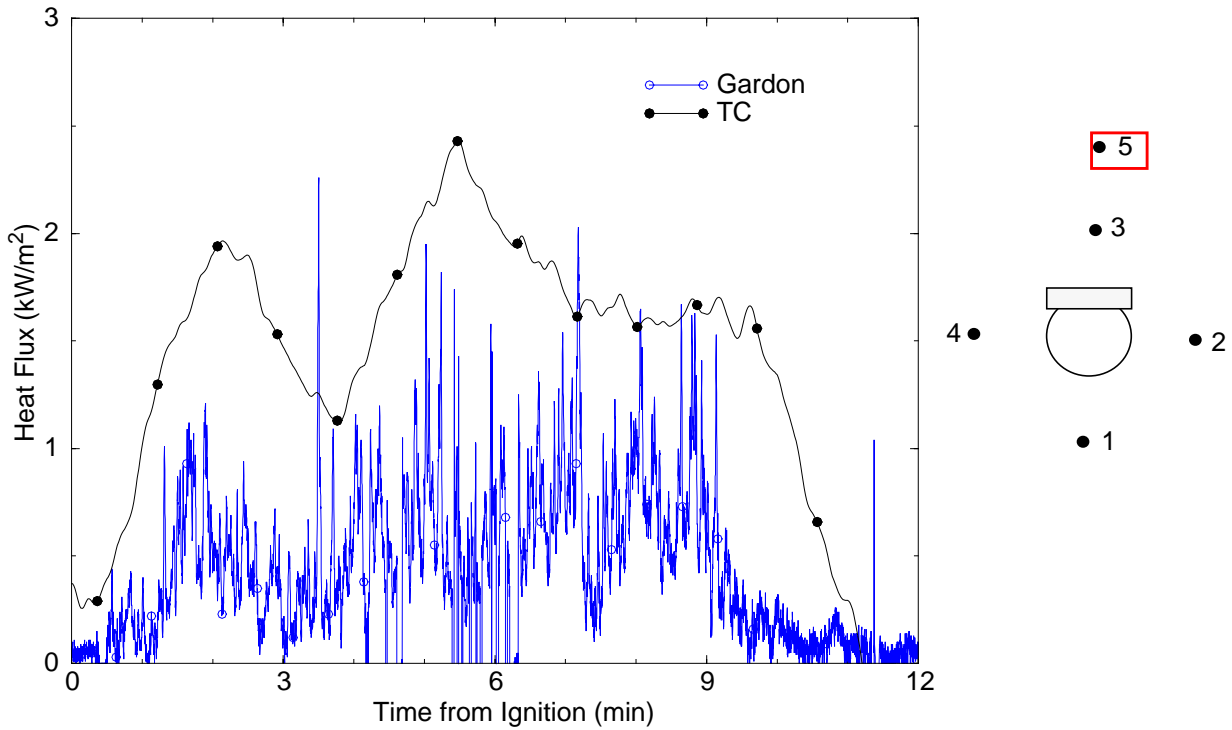
Figure 10.7 -Test 5 Heat Fluxes North 30 m
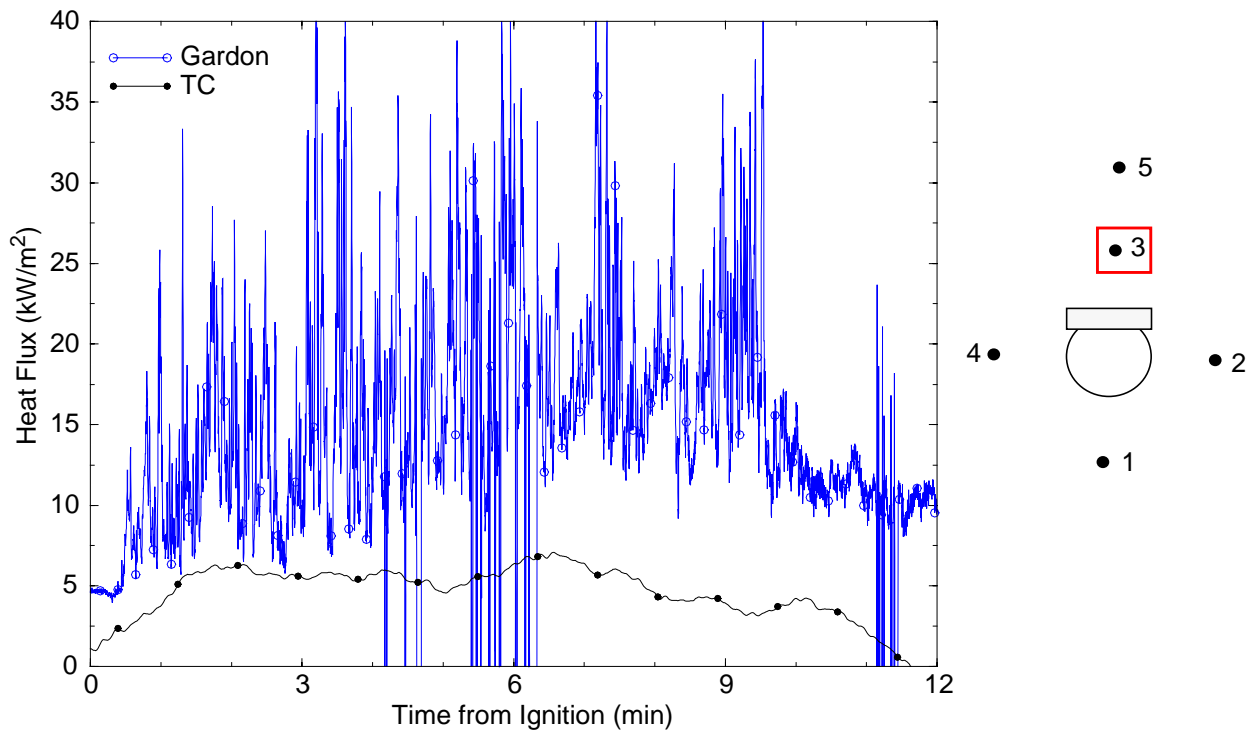
Figure 10.8 -Test 5 Heat Fluxes South 30 m
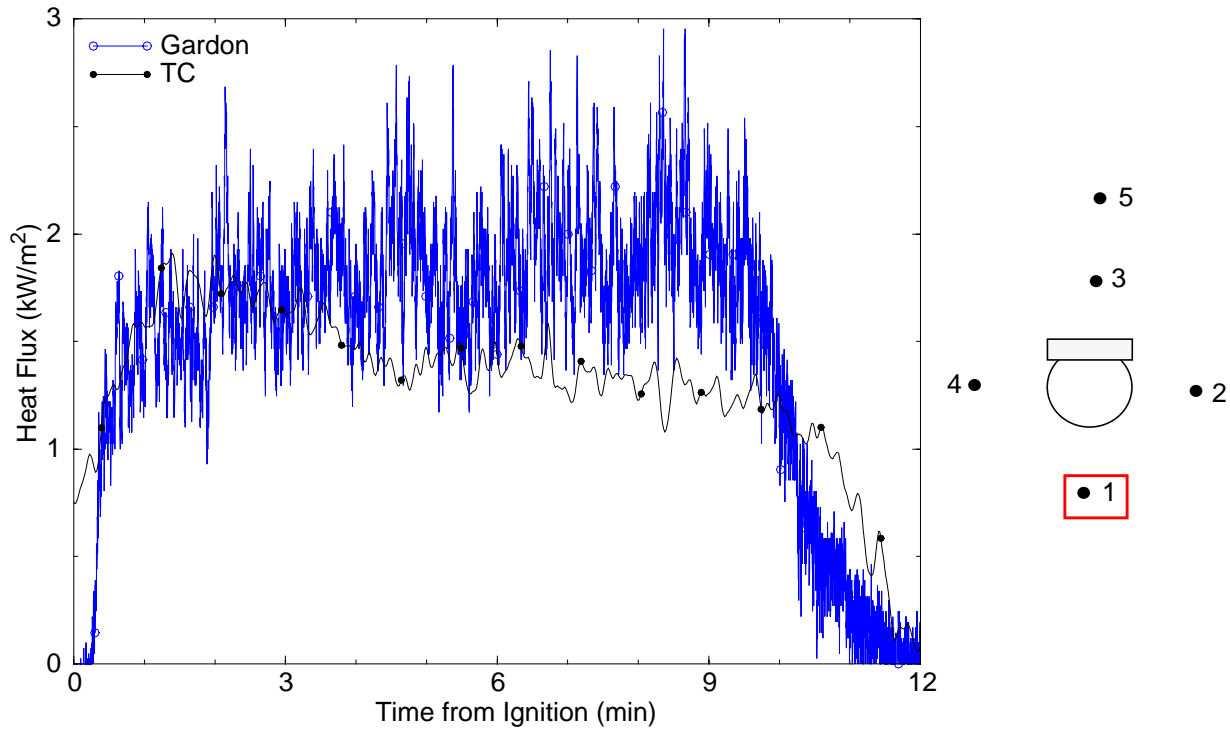
Figure 10.9 -Test 5 Heat Fluxes East 30 m
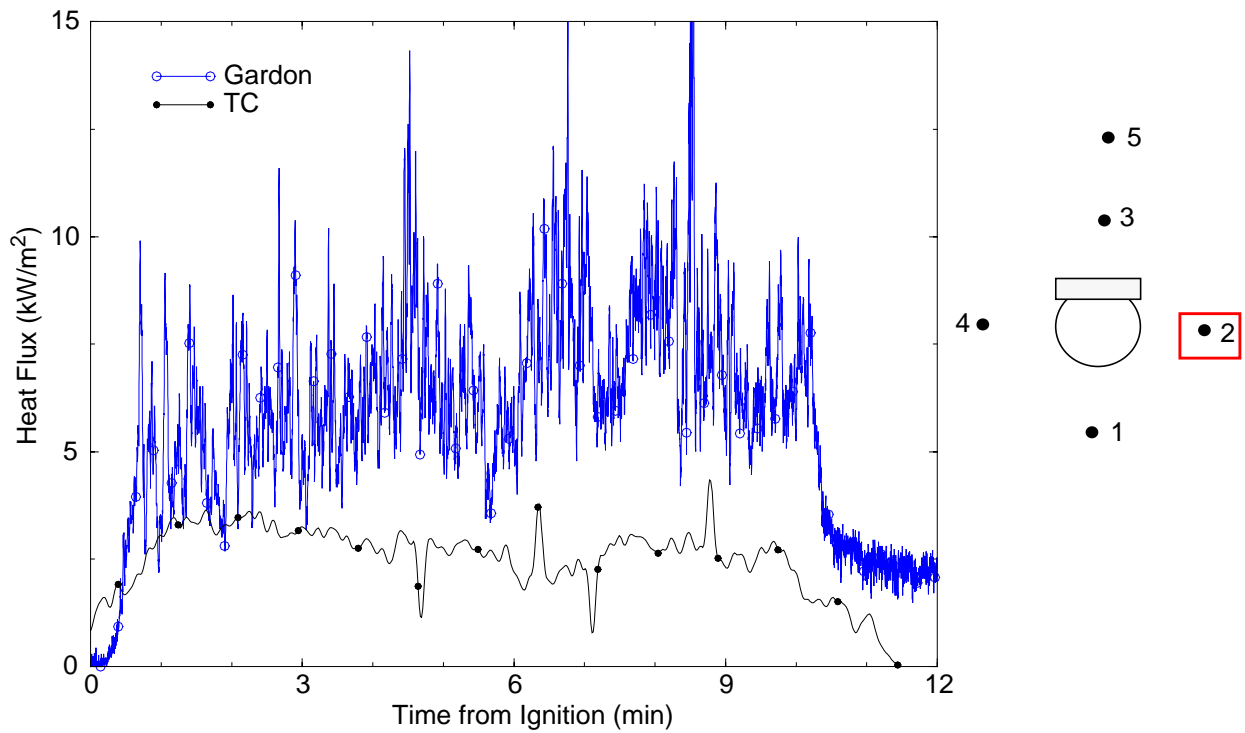
Figure 10.10 -Test 5 Heat Fluxes West 30 m
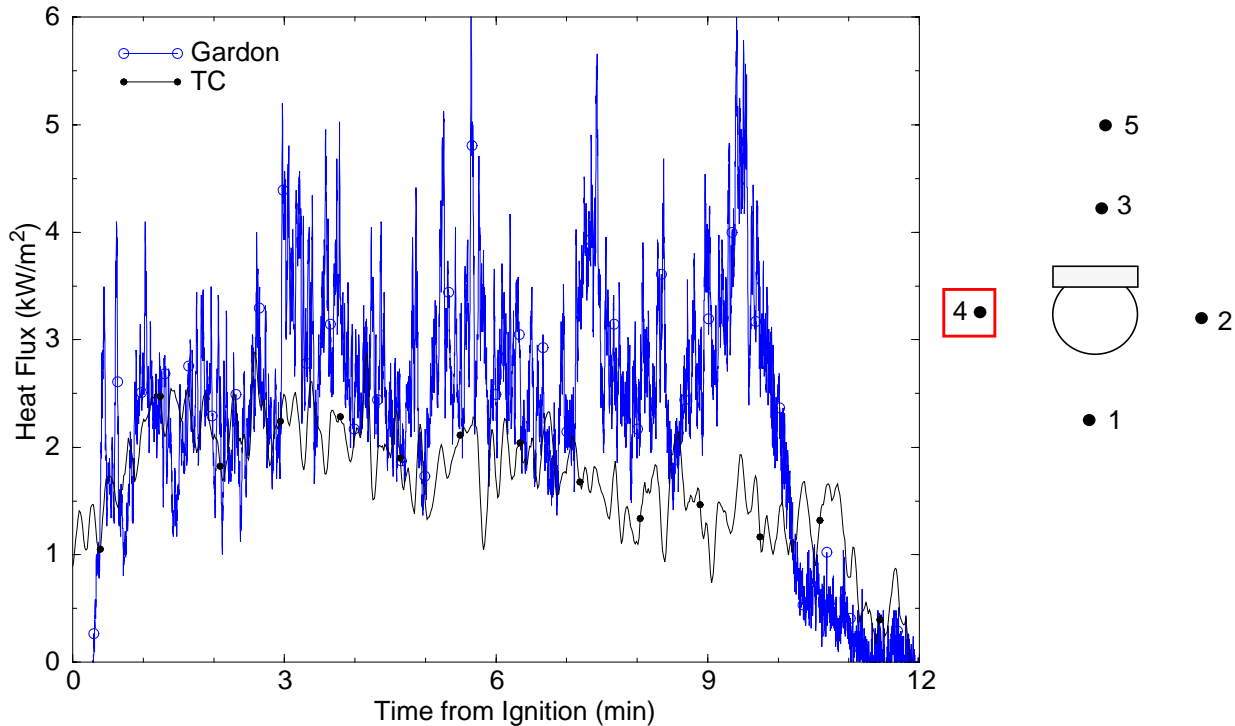
10.2.4 Test 8

The heat fluxes recorded during Test 8 are shown in Figures 10.11-10.15. The wind direction and speed during Test 8 were very stable and variations in the heat fluxes can be attributed to the natural fluctuation of the fire. The heat fluxes recorded by the 60 m north location range from 0-1 kW/m^2. The heat fluxes calculated from the thermocouple and measured by the Gardon gauge had similar trends and magnitudes. Significantly higher heat fluxes were recorded by the station at 30 m north (up to 45 kW/m^2) but the data was very noisy. It is evident the fire was changing rapidly by the fluctuations in the data. The fluctuations were captured by the high sampling rate of the Gardon gauge. The thermocouple heat fluxes measured fall on the low side of the fluctuations of the Gardon gauge measurements (~10 kW/m^2). Heat fluxes measured at the south station range from 1 to 3 kW/m^2. The Gardon gauge heat fluxes at the south station are very stable at 2.5 kW/m2 while the TC heat fluxes are steadily decreasing throughout the test. This decrease in the TC heat fluxes can be attributed to the sensitivity of the gauge to convective cooling. The TC heat fluxes for the east and west stations also display decreasing trends. The Gardon gauge measurements for the south, east, and west stations are all higher than the TC measurements.

Figure 10.11 -Test 8 Heat Fluxes North 60 m
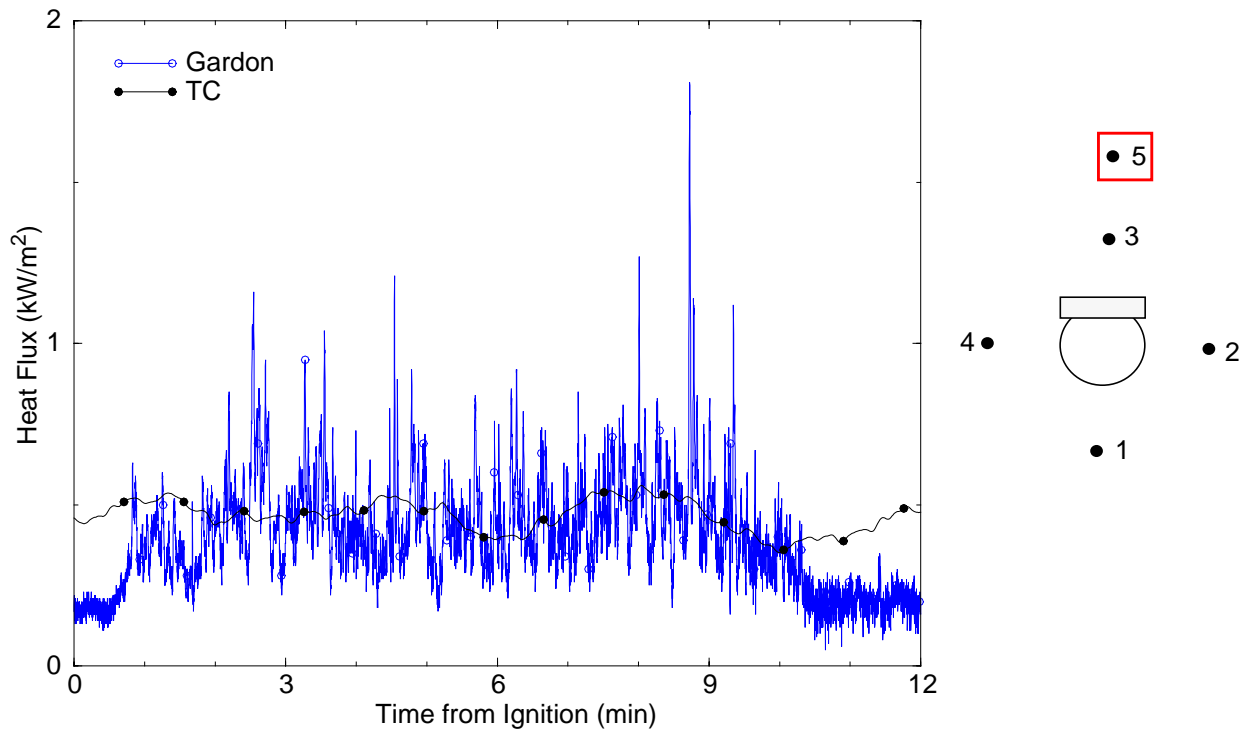
Figure 10.12 -Test 8 Heat Fluxes North 30 m

150
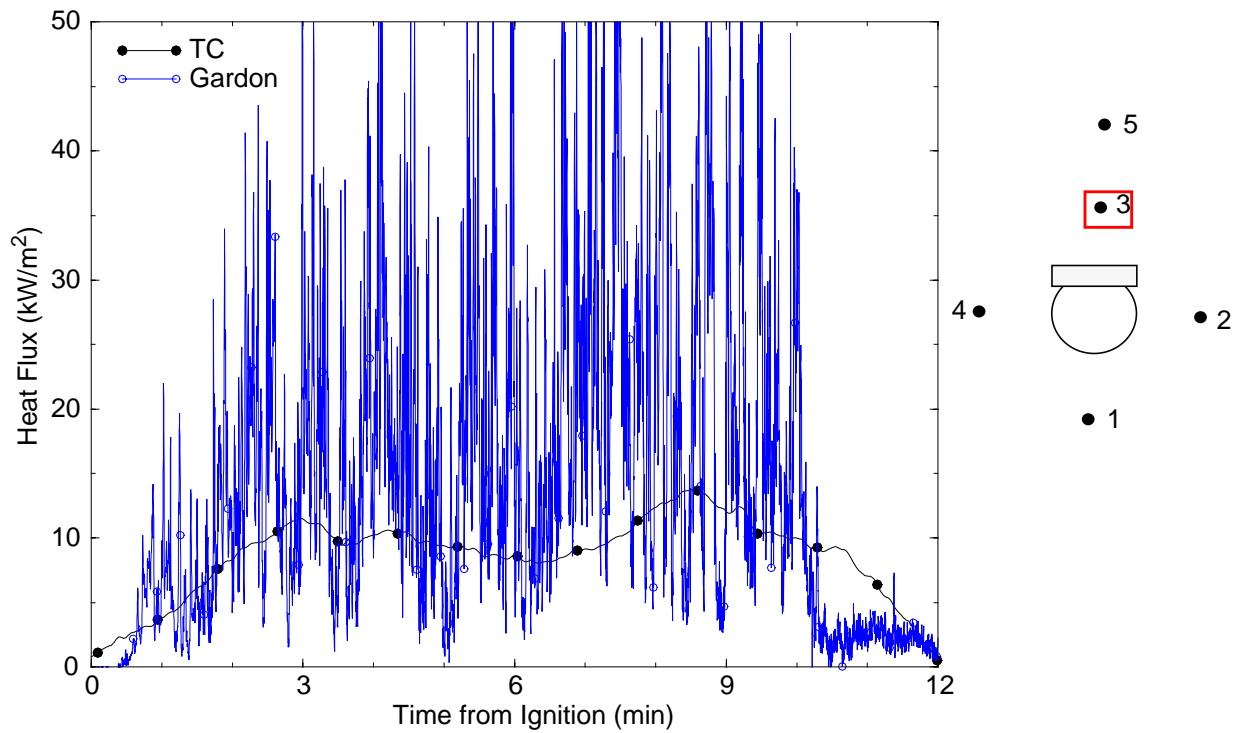
Figure 10.13 -Test 8 Heat Fluxes South 30 m
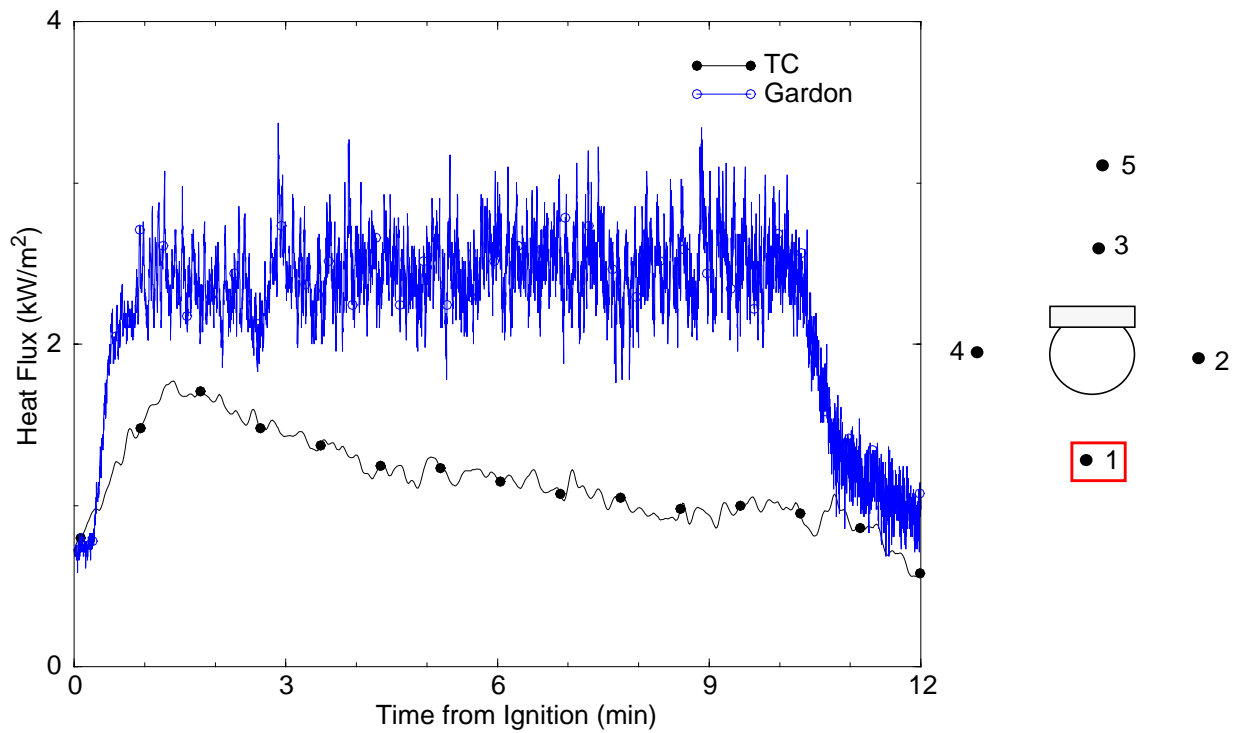
Figure 10.14 -Test 8 Heat Fluxes East 30 m
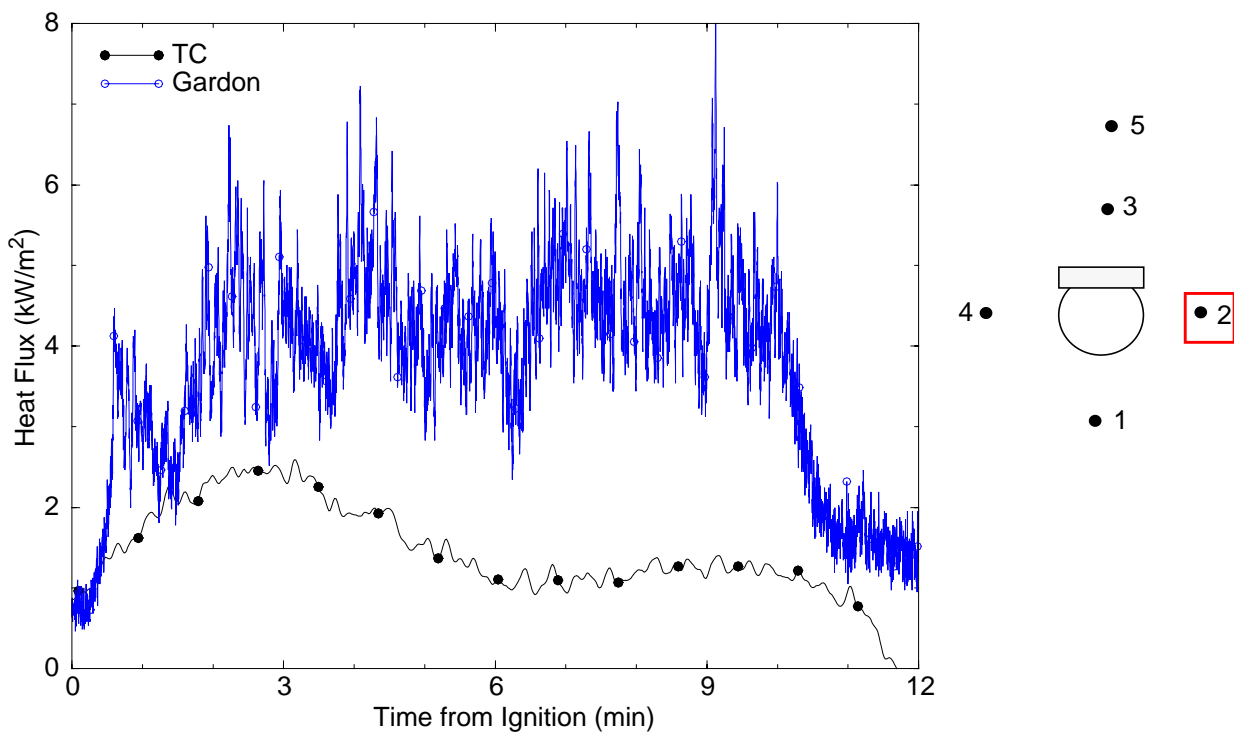
Figure 10.15 -Test 8 Heat Fluxes West 30 m
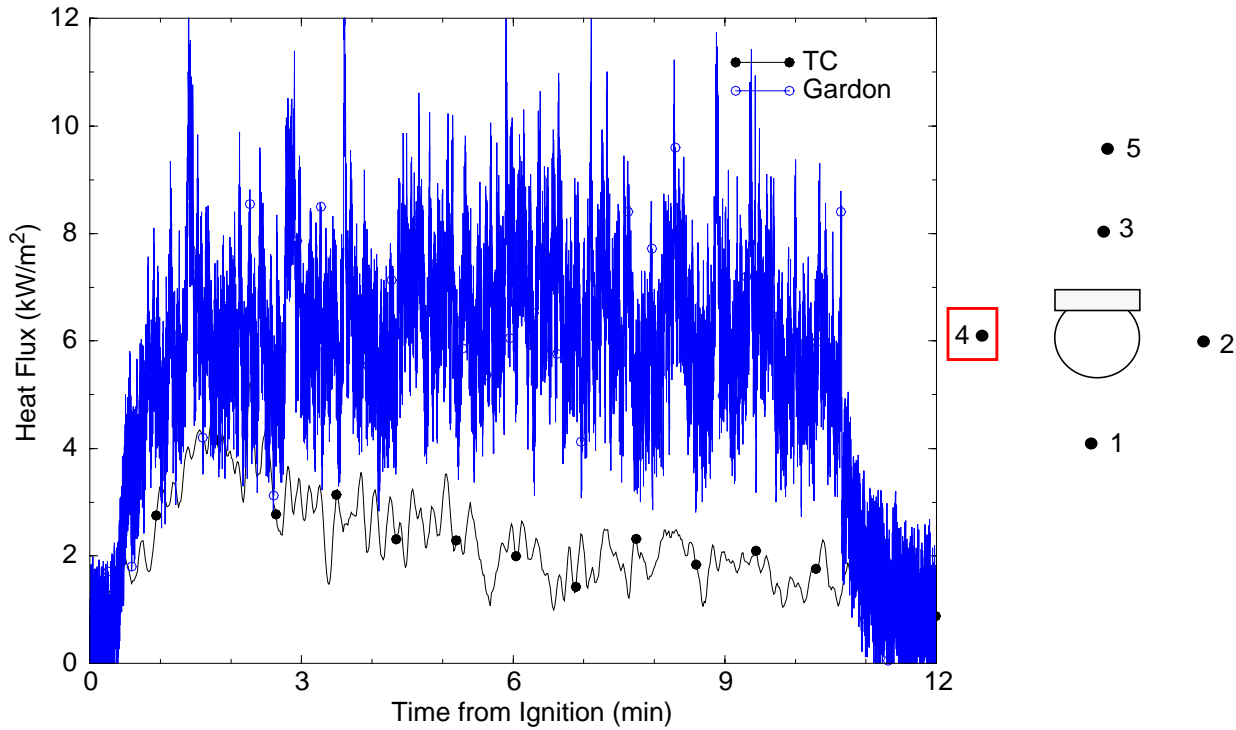
10.3 Small Pool Heat Flux Measurements

The heat flux measurements for the small pool were obtained using the same instrumentation and data reduction procedures as presented in sections 10.1 and 10.2 for the large fuel pool.

10.3.1 Test 6

 The heat fluxes recorded during Test 6 are shown in Figures 10.16-10.20. The winds were stable throughout the test (approximately 9 m/s and 5^0). The heat fluxes recorded by the 60 m north location range from 0-0.5 kW/m^2. These heat fluxes were among the lowest recorded in all of the tests. The heat fluxes calculated from the thermocouple were higher than the Gardon gauge, which was unique to this location, but since the magnitude of the measured heat fluxes was so small the difference was only ~0.3 kW/m^2. Higher heat fluxes were recorded by the station at 30 m north (up to 15 kW/m^2) but strong fluctuations existed due to the sensitivity of the gauge to the flame tilt. The fluctuations were on the order of 12 kW/m^2 in the worst cases. The trends for both measurement techniques at the 30 m north station were similar although the heat fluxes calculated from the TC were on the low end of the heat fluxes measured by the Gardon gauge. The heat fluxes for the remaining three stations were lower than seen in the large pool tests at these locations. There was good agreement in the trends of the Gardon gauge and TC measurements. Heat fluxes at

the south 30 m station were less than 2 kW/m^2. Two peaks in the Gardon gauge heat fluxes are seen at 2.5 and 5.0 min. after ignition. The heat fluxes measured by the east 30 m station do not exceed 6 kW/m^2. Both gauges at the 30 m east station measure the greatest heat fluxes between 3 and 7 min. after ignition although their magnitudes differ by approximately 4 kW/m^2. The agreement between the gauges at the west 30 m location was very good. The average heat flux recorded was approximately 1 kW/m^2 with increases up to 3 kW/m^2.

Figure 10.16 - Test 6 Heat Fluxes North 60 m
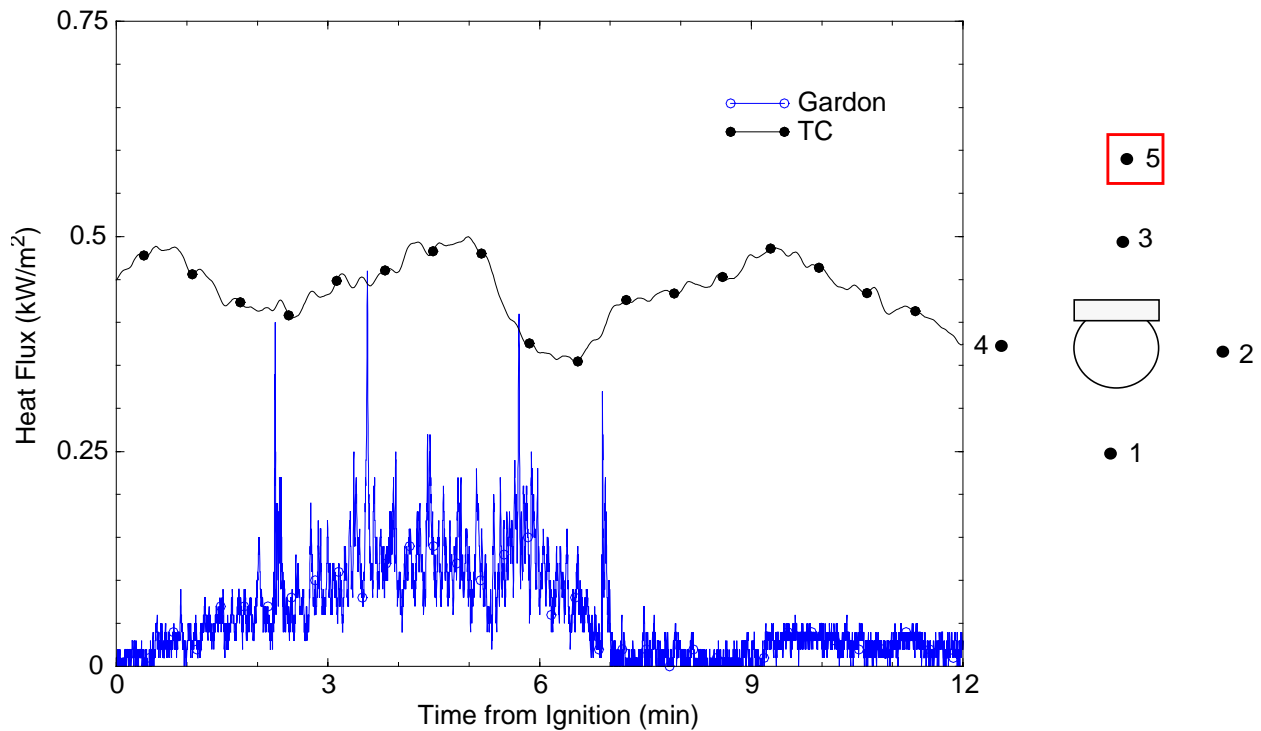
Figure 10.17 -Test 6 Heat Fluxes North 30 m
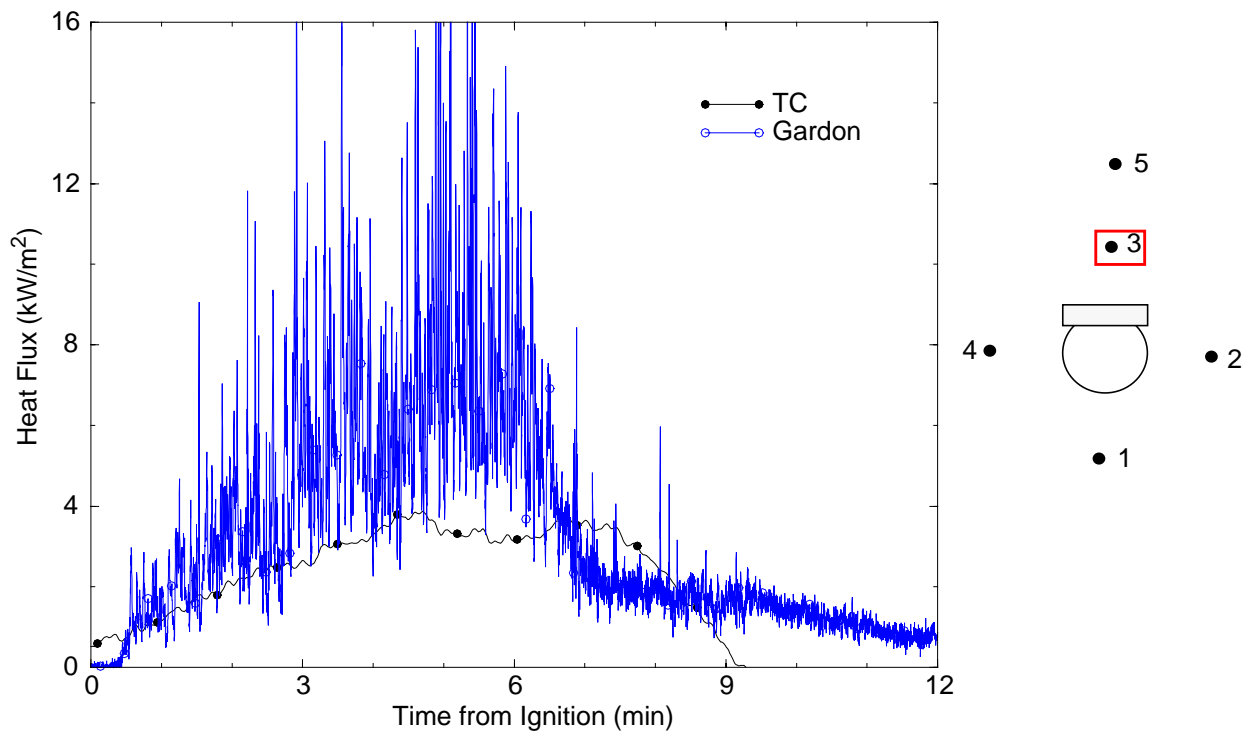
Figure 10.18 -Test 6 Heat Fluxes South 30 m
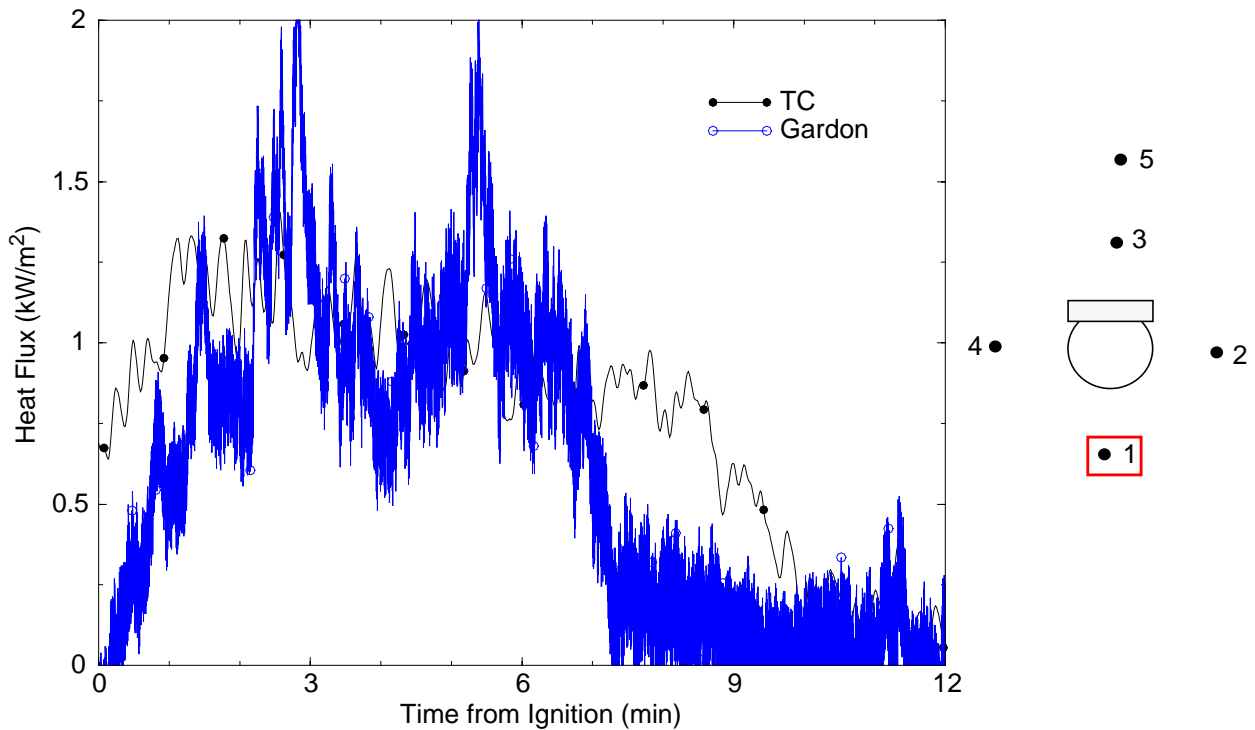
Figure 10.19 -Test 6 Heat Fluxes East 30 m
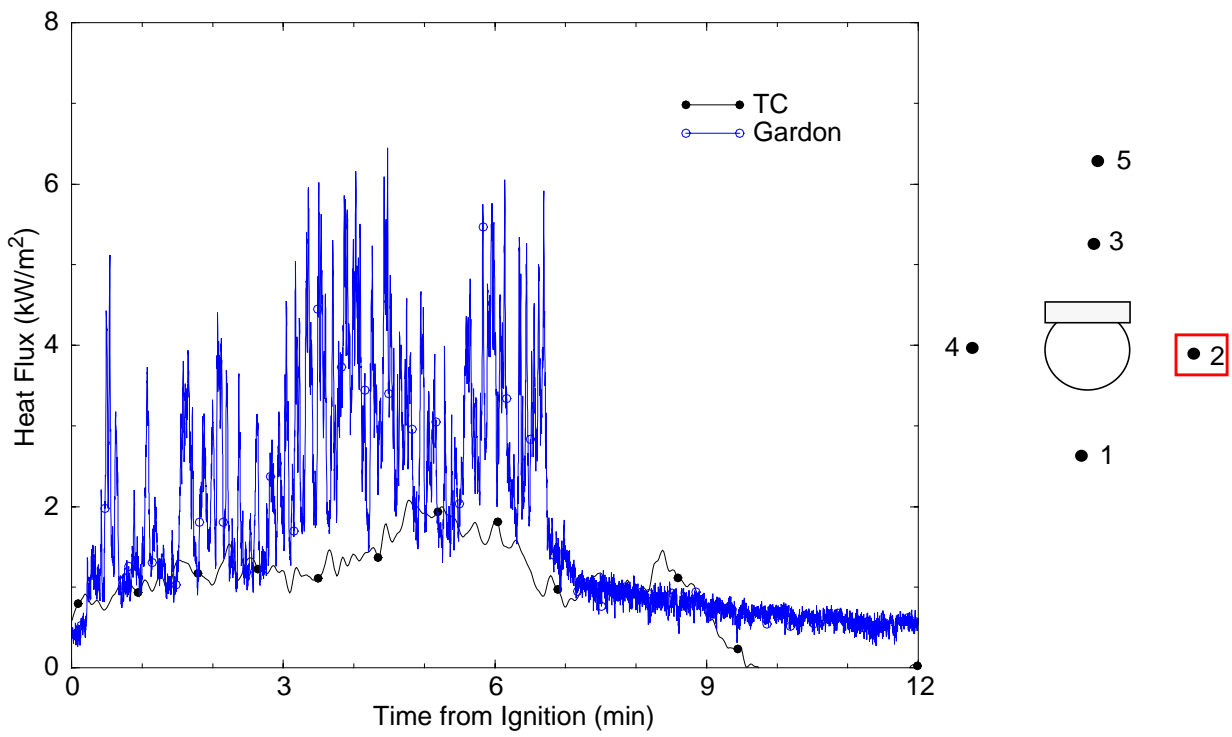
Figure 10.20 -Test 6 Heat Fluxes West 30 m
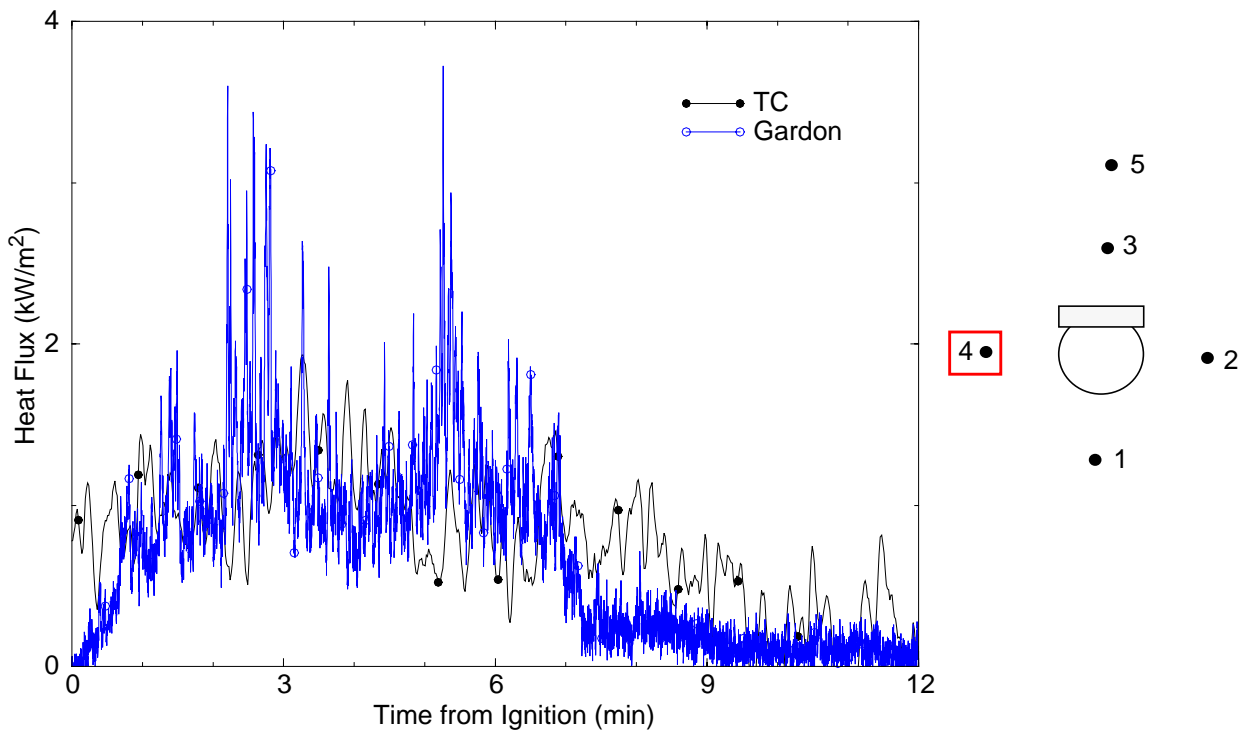
10.3.2 Test 7

The heat fluxes recorded during Test 7 are shown in Figures 10.21-10.25. Similar to Test 6, the heat fluxes recorded by the 60 m north location range from 0-0.5 kW/m^2. The heat fluxes calculated from the thermocouple were higher than the Gardon gauge in magnitude, but since the magnitude of the measured heat fluxes was so low that the difference was not significant (~0.2 kW/m^2). The 60 m north station TC consistently recorded higher heat fluxes than the Gardon gauge in all the tests. The Gardon gauge measured higher heat fluxes at all other stations in the tests.

Higher heat fluxes were recorded by the station at 30 m north (up to 8 kW/m^2). It is evident that the fire was changing rapidly by the fluctuation in the data. The fluctuations were captured by the high sampling rate of the Gardon gauge. The trends for both measurement techniques at the 30 m north station were similar although their magnitudes begin to diverge at 8 min. after ignition. This is caused by the difference in the sensitivity of the gauges to convection.

The Gardon gauge at the 30 m south location recorded heat fluxes slightly larger than the TC calculated heat fluxes. The range of heat fluxes was from approximately 1 to 3.5 kW/m^2. The last two locations showed good agreement between the heat fluxes measured using the Gardon gauge and those calculated using the TC data. At the 30 m east location heat fluxes were 1-3 kW/m^2 and at the 30 m west location they were 1-7 kW/m^2. The difference in the east and west stations, primarily after 8 min., was caused in the decrease in wind direction.

Figure 10.21 -Test 7 Heat Fluxes North 60 m
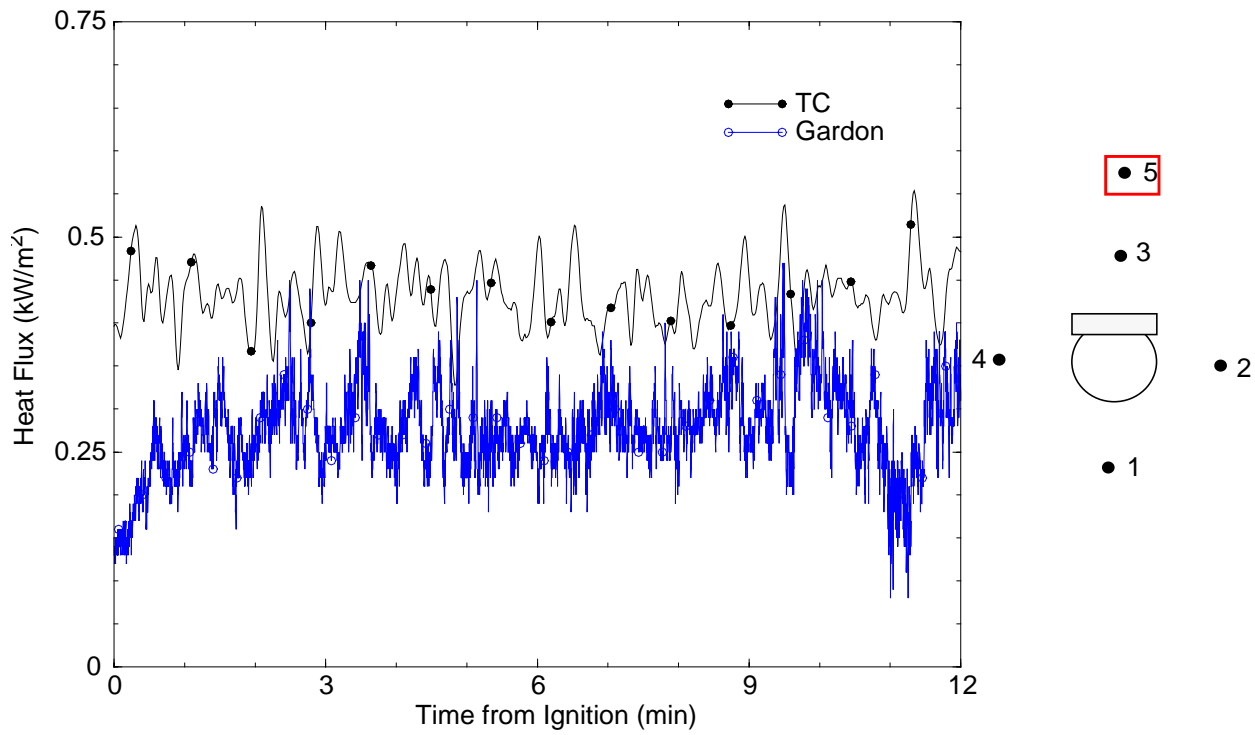
Figure 10.22 -Test 7 Heat Fluxes North 30 m
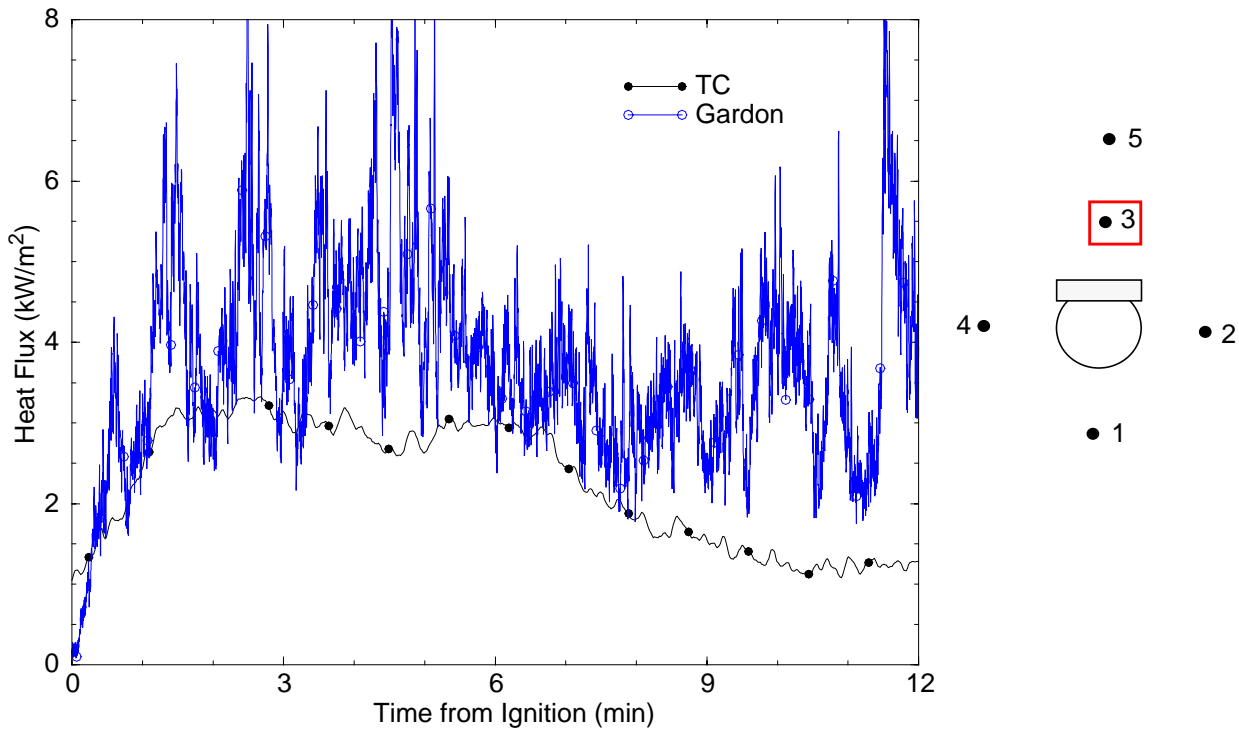
Figure 10.23 -Test 7 Heat Fluxes South 30 m
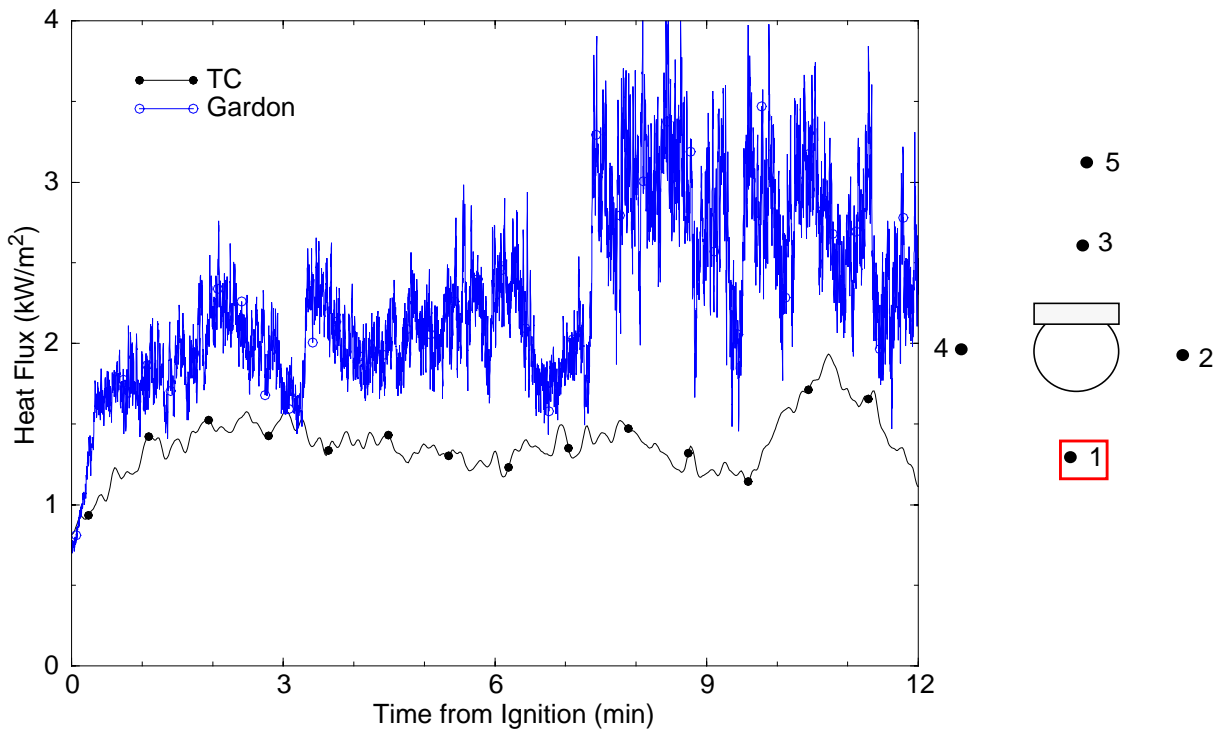
Figure 10.24 -Test 7 Heat Fluxes East 30 m

158
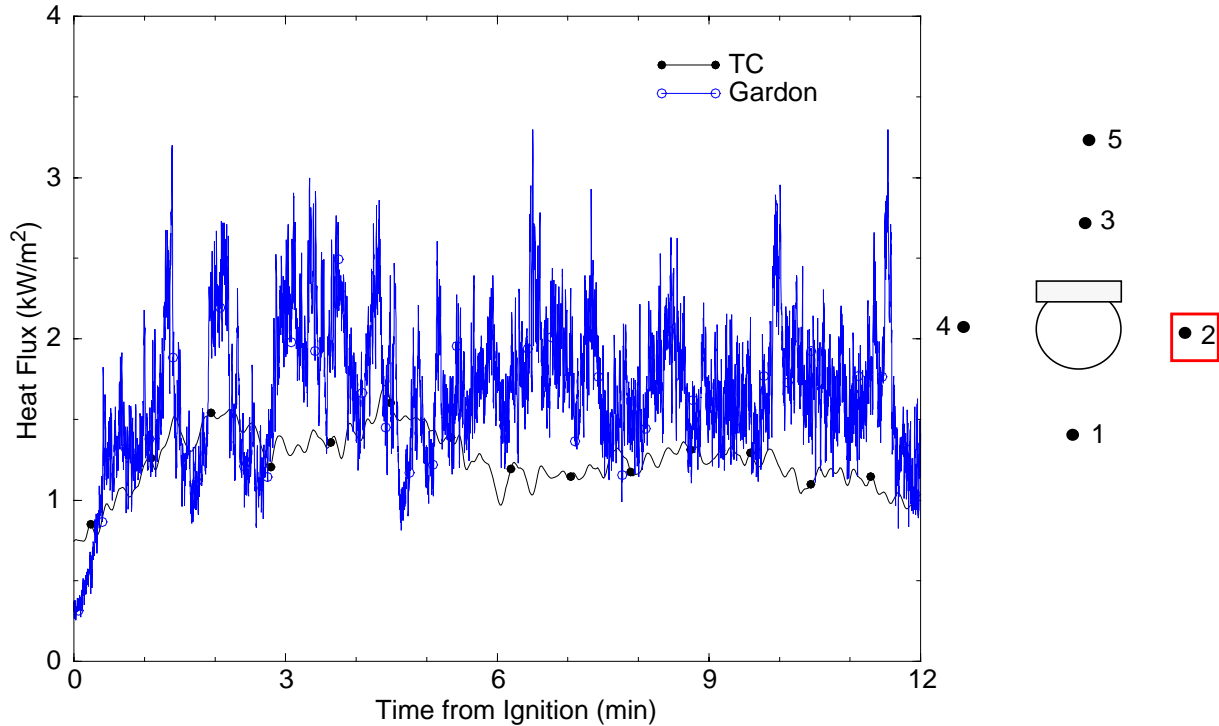
Figure 10.25 -Test 7 Heat Fluxes West 30 m
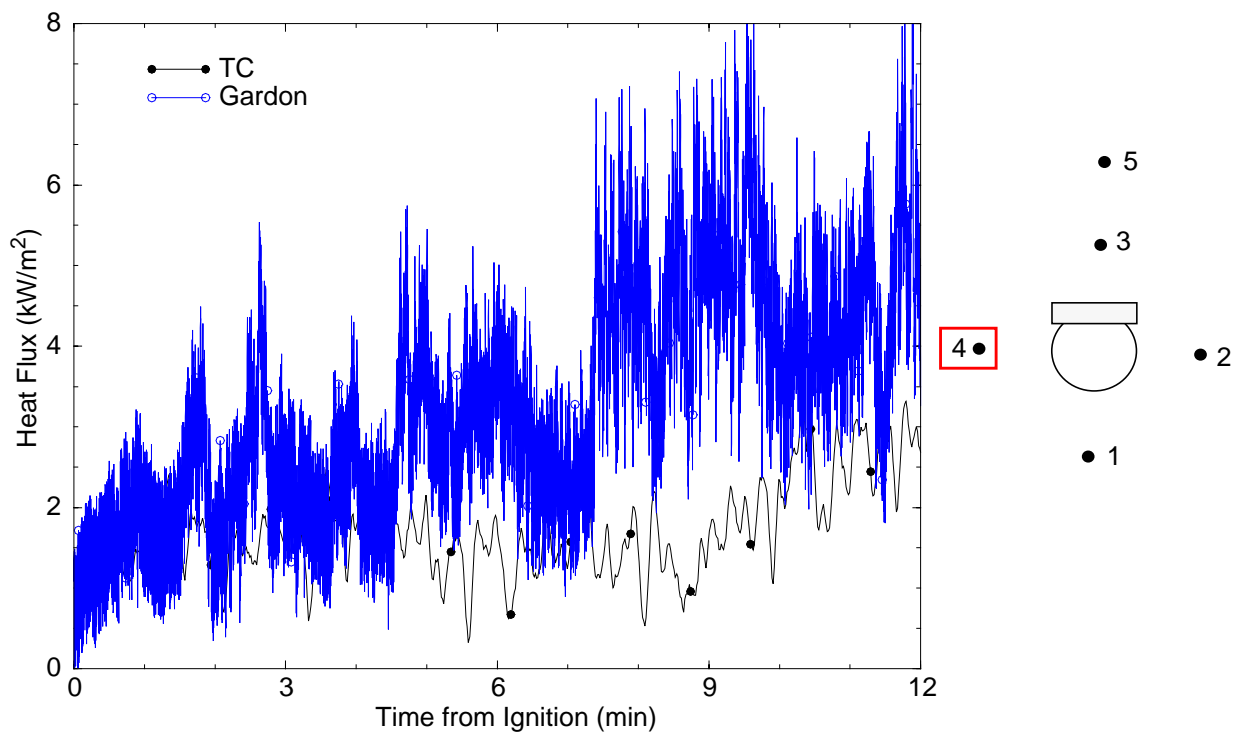
11. Experimental Results - Photographs

11.1 Experimental Setup

The following photographs were taken before the start of the tests to show the instrumentation and experimental setup. Two different sized pools, 10 m and 20 m diameter, were used in this test series. The instrumentation for the different tests was very similar. Figures 11.1 and 11.2 show the experimental setup for the large 20 m pool fire from upper and side views. Figures 11.3 and 11.4 show similar views of the experimental setup for the 10 m pool fire. Thermocouple arrays are visible in the fuel pool and surrounding the mock fuselage. Heat flux gauges can also be seen throughout the pool near at fuel surface. All instrumentation (TC's, Heat Flux Gauges) is shown wrapped with ceramic fiber blanket insulation.

Figure 11.1 -20m Pool Experimental Setup (Upper View)
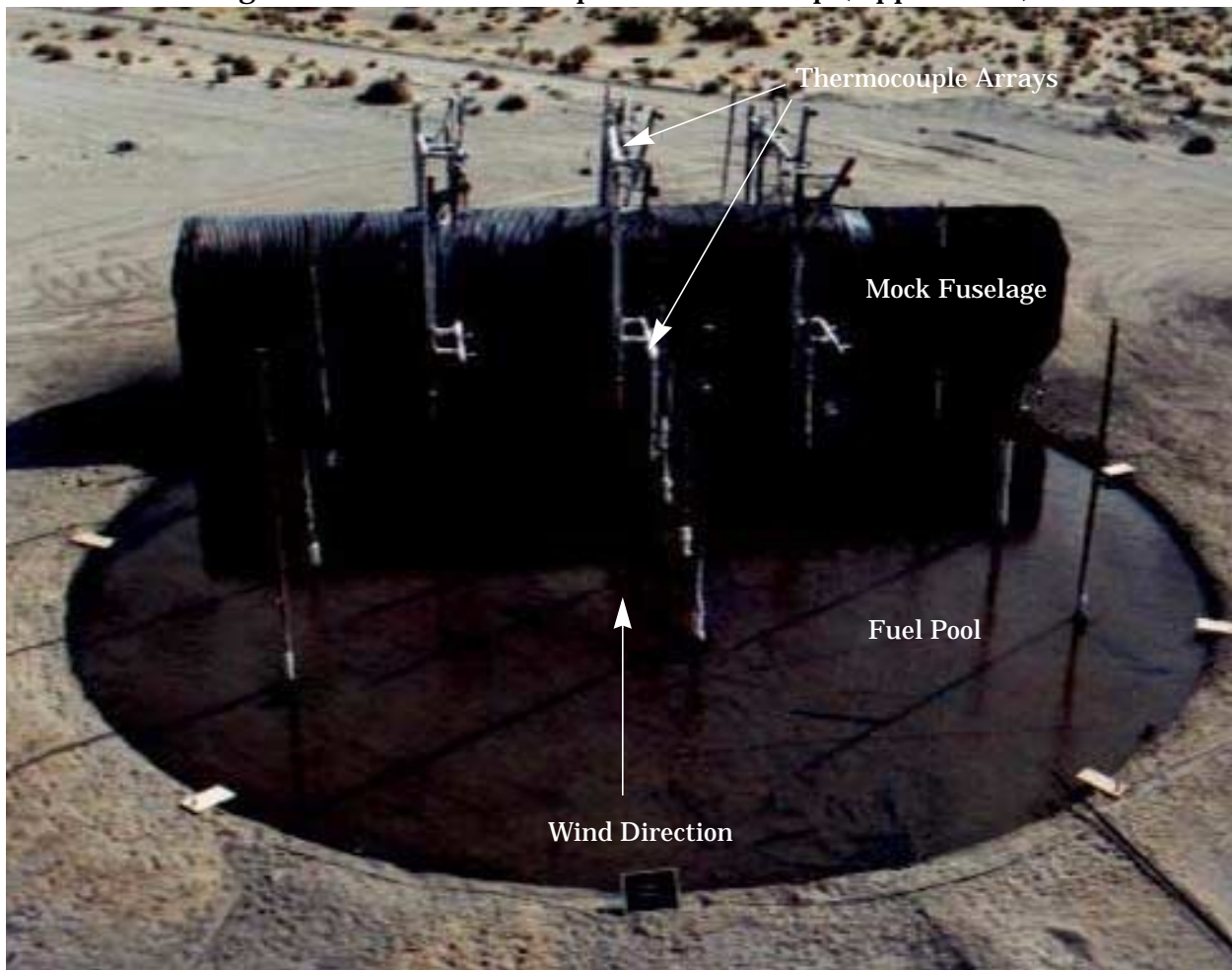
Figure 11.2 - 20 m Pool Experimental Setup (Side View)
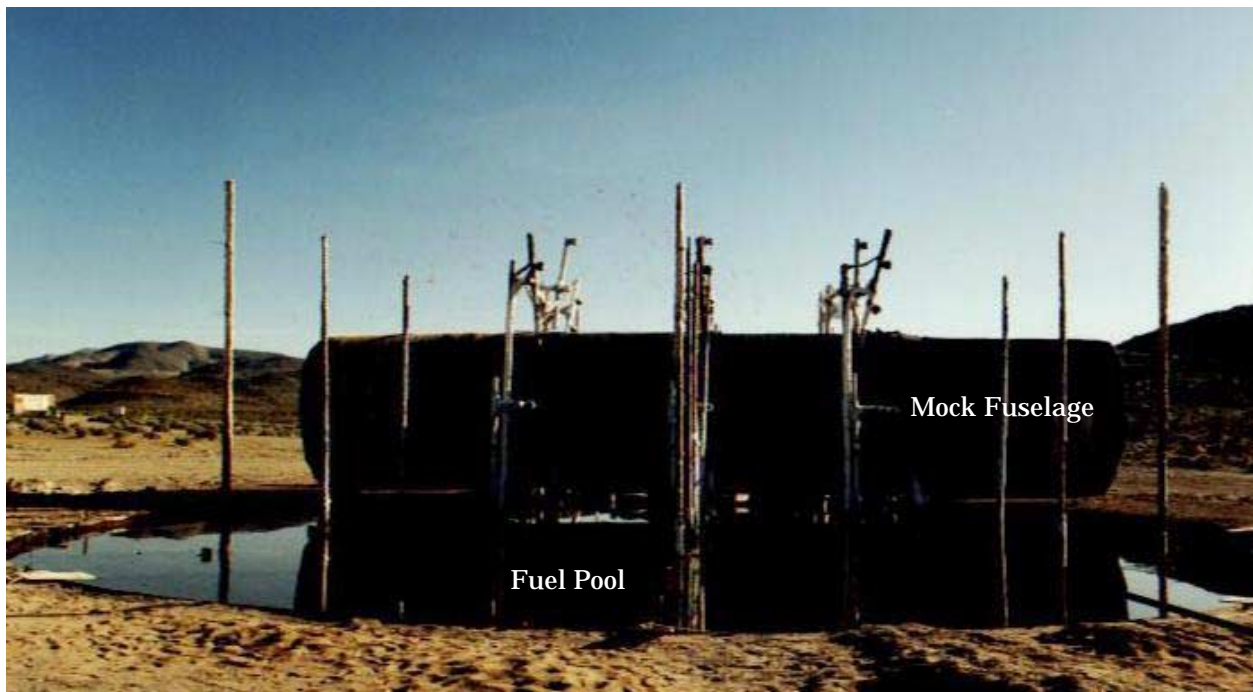
Figure 11.3 -10 m Pool Experimental Setup (Upper View)
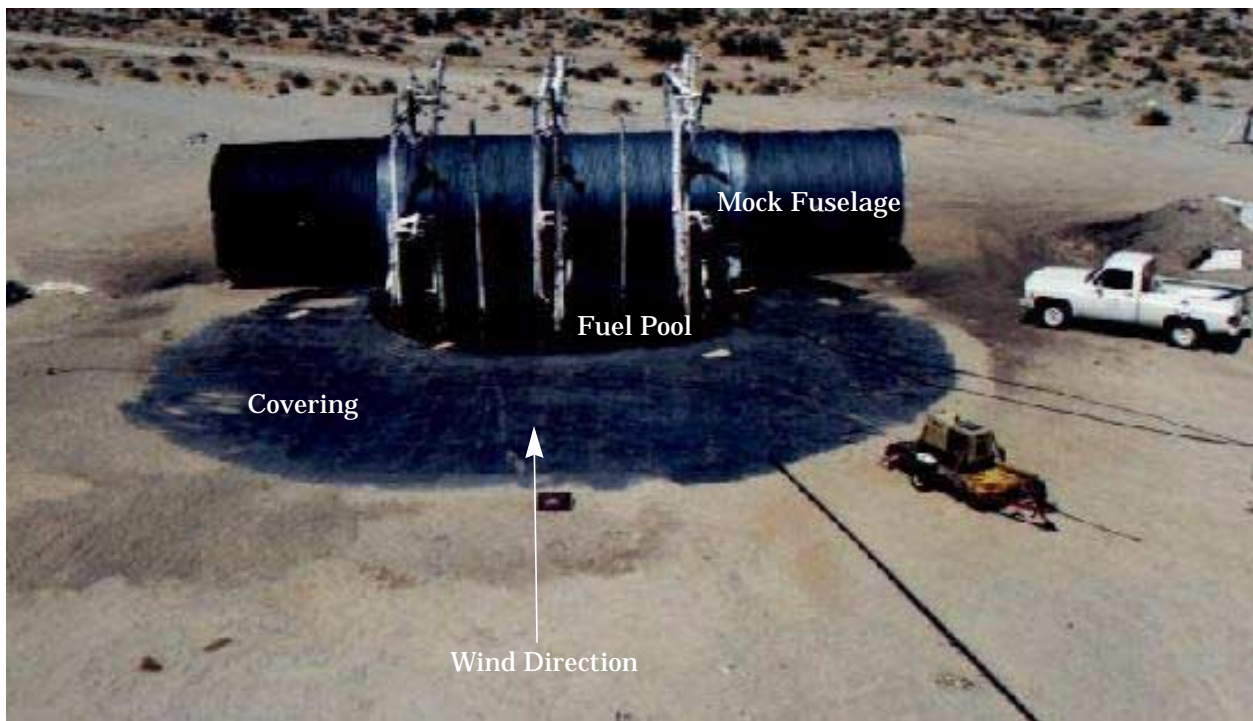
Figure 11.4 - 10 m Pool Experimental Setup (Side View)

11.2 Test Photographs

Photographs were taken during the fires at different locations surrounding the fires. A sampling of those photographs are provided here. It is evident that the flame zone is greatly affected by the wind speed and direction. Photographs were taken with short shutter speeds and with long shutter speeds which provided a time averaged image.

11.2.1 Large Pool Photographs

The large pool photographs shown in Figures 11.5 and 11.6 were taken during Test 5. Figure 11.6 is a time-averaged photograph taken by keeping the shutter open for 8 seconds. The wind conditions for Test 5 were characterized as medium (5-7 m/s). For contrast, a time-averaged photograph for a high wind speed test (~10 m/s, Test 8) is shown in Figure 11.7. It is evident that the wind has sufficient momentum to direct the flame away from the leading edge of the pool and expose the thermocouple towers in both tests. Much larger deflection of the flame zone is observed in the high wind speed test. Figure 11.7 shows the entire leeward side of the mock fuselage is covered by flames and the thick, black smoke. The landscape behind the mock fuselage in not visible as it is in the medium wind speed test.

Figure 11.5 -Test 5 Photograph (medium winds)

Figure 11.6 -Time-averaged Test 5 Photograph (medium winds)

Figure 11.7 -Time-averaged Test 8 Photograph (high winds)

11.2.2 Small Pool Photographs

The small pool photographs shown in Figures 11.8 and 11.9 were taken during Test 7. Figure 11.9 is a time-averaged photograph taken with an exposure time of 8 seconds. The wind conditions for Test 7 were characterized as low (2 m/s). For contrast, a time-averaged photograph for a high wind speed test (~10 m/s, Test 6) in the 10 m pool is shown in Figure 11.10. The deflection of the flame zones are significantly different in the two tests shown. Under low wind speed conditions the flame zone is only slightly affected by the wind, while significant deflection of the flame zone and hence difference in flame cover is observed for the high wind speed tests.

Figure 11.8 -Test 7 Photograph (low winds)
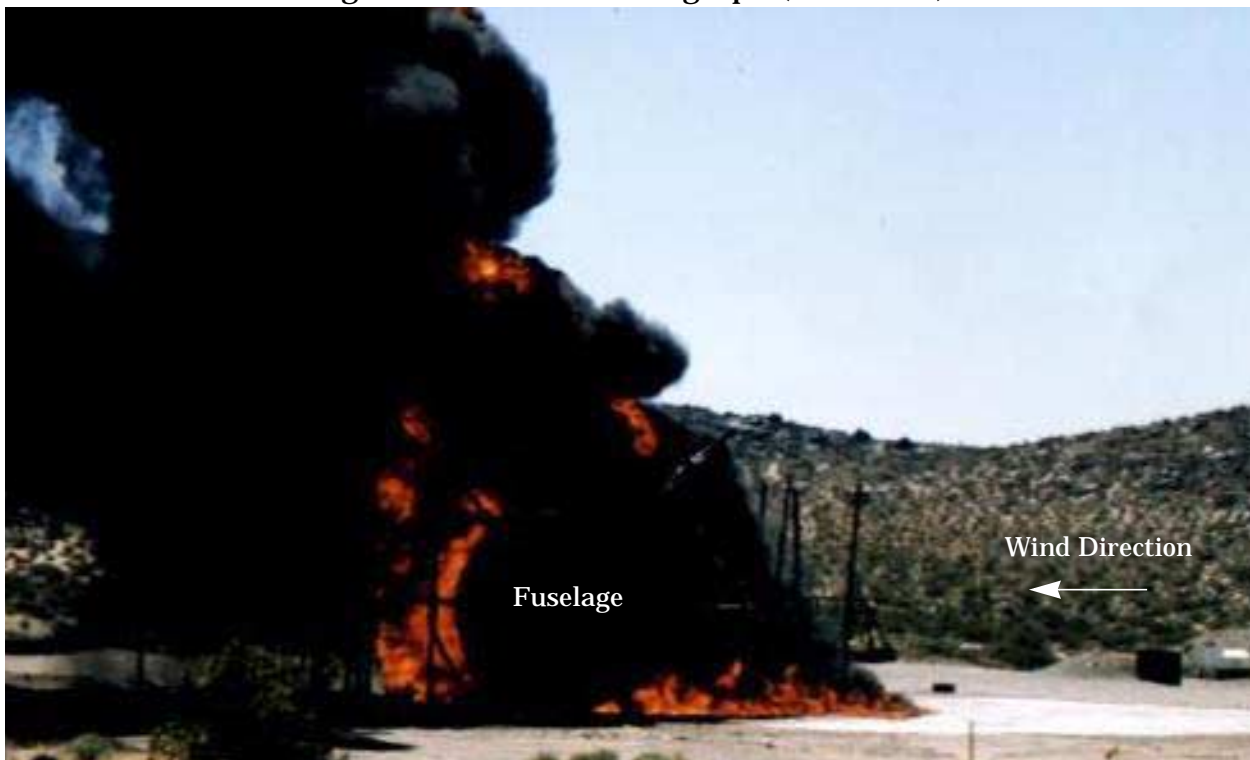
Figure 11.9 -Time-averaged Test 7 Photograph (low winds)
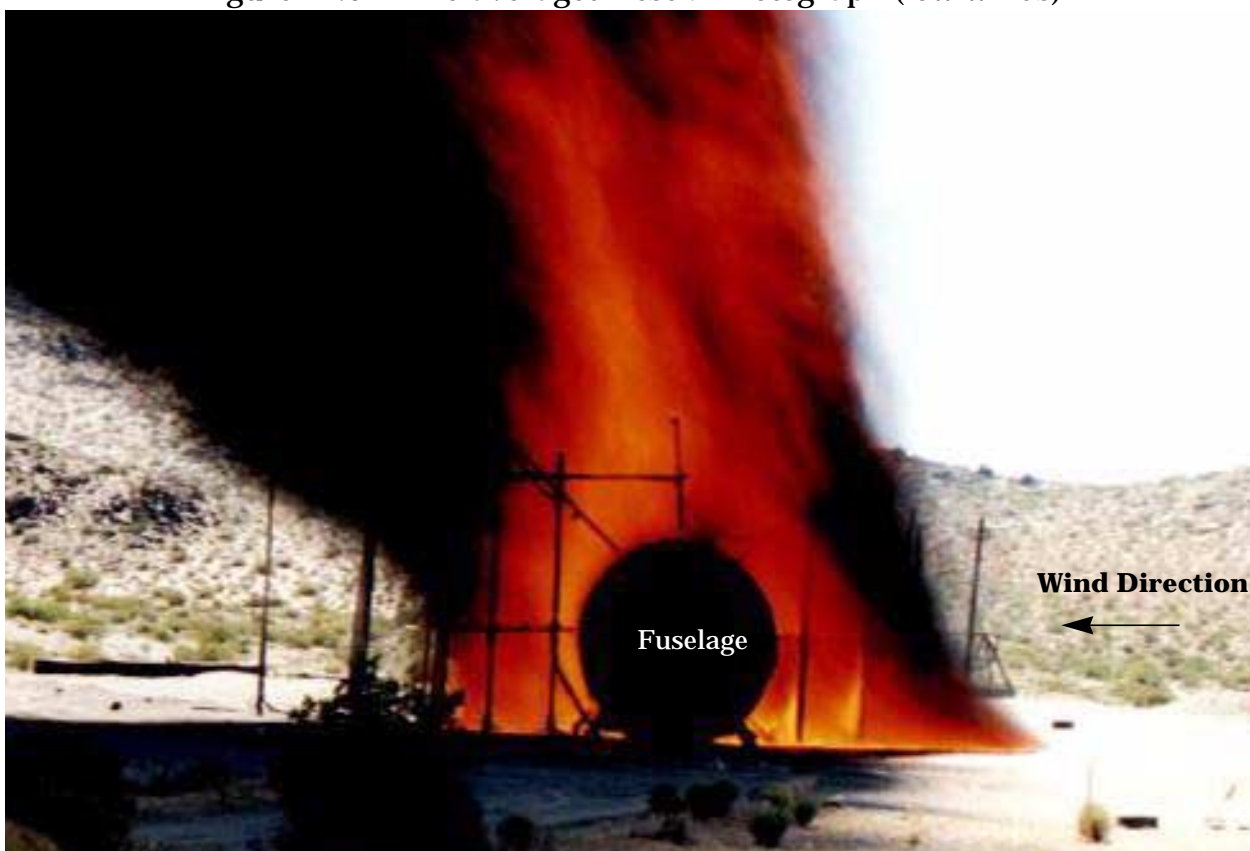
Figure 11.10 -Time-averaged Test 6 Photograph (high winds)
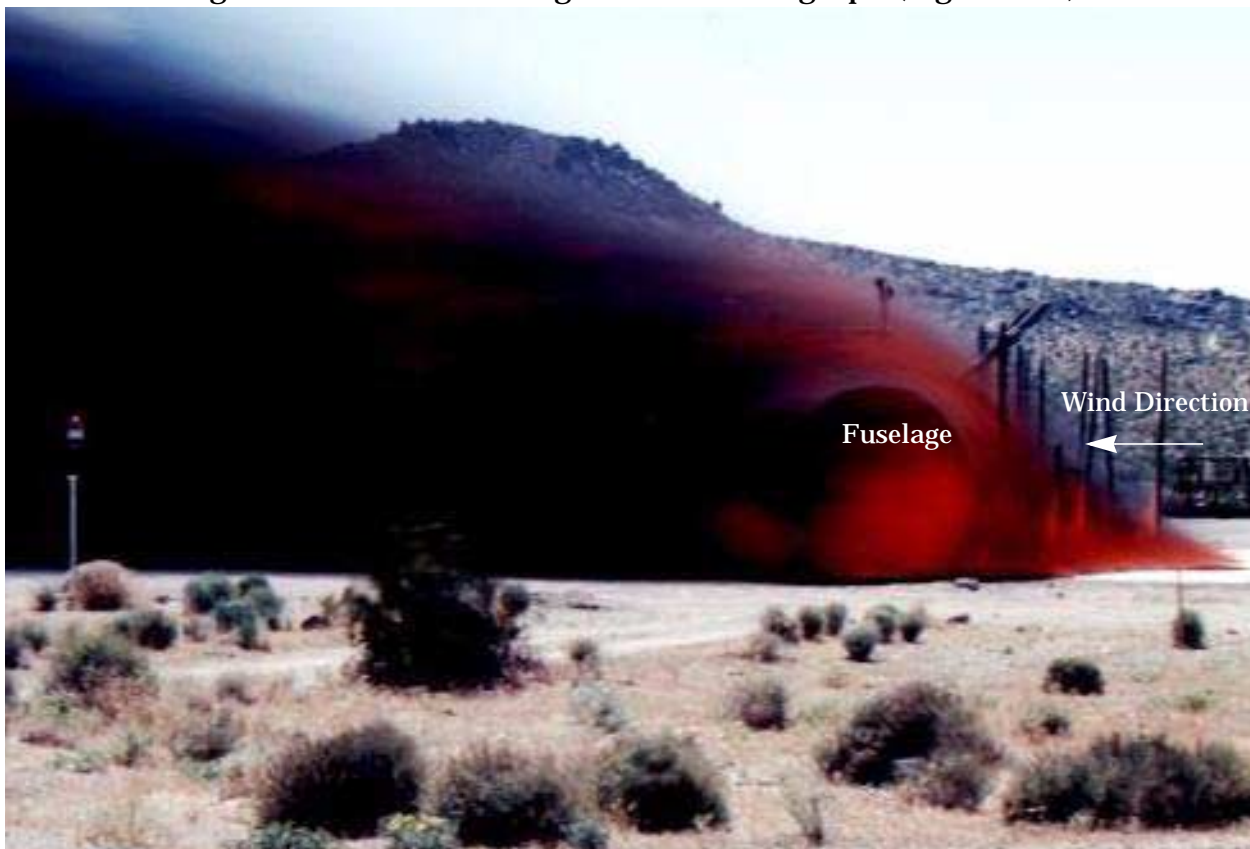
12. Summary and Conclusions

12.1 Wind Conditions

- A 2-4 minute period of wind conditions with only very minor fluctuations in speed and direction existed for all tests.
- This quasi-steady period of wind conditions was identified and used for time-averaging of data to construct contour plots representative of the test.
- Tests targeted different conditions to determine the effect of the wind on the behavior of the pool fire.

12.2 Flame Zone Contours

- Flame zone contour plots present the data in a suitable format for time-averaged fire model comparisons.
- The direction and speed of the wind greatly affected the flame coverage of the pool and the mock fuselage.
- High wind speed tests produced extreme temperatures of approximately 1600 K beyond the leeward edge of the pool in the wake of the mock fuselage.
- Low wind speed tests produced the highest temperatures (1400-1500 K) near the center of the fuel pool.
- The highest temperatures for the medium wind speed tests (1500 K) occurred in the region directly surrounding (on top or just in front) the mock fuselage.

12.3 Skin Temperatures

- Contour plots are provided to show the temperature distribution on the skin of the mock fuselage during each quasi-steady time period.
- Low temperature areas on the skin indicate oxygen starved regions.
- Skin temperature trends varied with the wind speed and direction.
- Low wind speeds produced the highest temperatures on the windward skin (1400-1500 K) as a result of flame impingement.
- Temperatures of 1600K were measured on the leeward side of the mock fuselage in high wind speed tests as a result of fuel/air mixing (near the failure point of the instrument).

12.4 Skin Heat Flux

- Plots are provided to show the heat flux distribution on the skin of the mock fuselage during the quasi-steady time periods for each test in a manner suitable for fire model comparisons.
- Heat fluxes differed from test to test due to the various wind conditions.
- Heat fluxes varied greatly within a test from the windward to the leeward skin.

- Heat fluxes up to 400 kW/m^2 were measured on the leeward side of the mock fuselage in high wind speed tests due to enhanced mixing, and therefore, improved burning in the wake region. Heat fluxes of this magnitude are much higher than what is generally estimated or predicted for large fires.

12.5 Pool Surface Heat Flux

- Contour plots of the heat flux distribution (50-150 kW/m^2) to the pool during the quasi-steady time period are provided for comparison to fire model results.
- Low heat flux areas (< 50 kW/m^2) indicate oxygen starved regions.
- The location of the oxygen starved regions in the interior varied with the wind speed and direction.
- Trends in pool heat fluxes are consistent with the flame shape contour characteristics.

12.6 Fuel Temperatures

- Fuel temperature data are provided to identify liquid fuel thermal response and fuel vaporization (mass loss) mechanisms.
- These data are needed to develop improved submodels for numerical simulations.
- The arrays were intended to target a position of high heat flux to the pool surface and a position of low heat flux to the pool surface.
- Only thermocouples located within the fuel or very close to the fuel/water interface increased in temperature during the test.
- The average burn rate for all the tests was 4.4 mm./min which is consistent with other pool fire measurements.

12.7 Pressure

- The pressure transducers measured differential pressure between selected locations.
- The highest pressures were measured on the windward side.
- Some data show lower pressures in the fire interior than the flame exterior.

12.8 External Heat Flux

- Spatial and temporal heat flux measurements from the exterior of the fire are provided for comparison with models that predict the heat flux to an object located a finite distance from the continuous flame zone.
- Heat fluxes were obtained from a Gardon heat flux gauge and from a thermocouple attached to the plate (data reduced from temperatures to heat fluxes).
- Overall, the trends recorded by the Gardon gauge and the thermocouple were similar.

- The different sensitivities of the gauges to convection caused the measurements to diverge.
- The highest heat fluxes were recorded on the leeward side of the pool since the wind deflected the fire plume towards this gauge (30 m North).
- The lowest heat fluxes were generally measured toward the windward side of the pool (South) since the plume was directed away from the leading edge of the fuel pool
- Large fluctuations observed in the data existed due to the sensitivity of the gauge to the rapidly changing environment.

12.9 Photographs

- Experimental setup photographs were taken for both pool sizes.
- The fire was photographed using time-averaging and instantaneous shutter speeds.
- Photographs show that the flame zone is greatly affected by the wind speed and direction.

13. References

[1] Gritzo, L. A., Moya, J. L., and Nicolette, V. F., "Use of Simplified Deterministic Fire Models to Estimate Object Response for Probabilistic Fire Safety Assessments," Proceedings of the NIST Annual Conference on Fire Research, Rockville, MD., October 18-22, 1993.

[2] Nicolette, V.F, Tieszen, S.R., Gritzo, L.A., Holen, J. and Magnussen, B.F., "Field Model Validation for Pool Fires," Poster Presented at Fourth International Symposium on Fire Safety Science, Ottawa, Canada, June 13-17, 1994.

[3] Lopez, A.R., Gritzo, L.A., and Sherman, M.P., "Risk Assessment Compatible Fire Models (RACFMs)," SAND Report 97-1562, Sandia National Laboratories, Albuquerque, NM. July 1998.

[4] Mudan, K. S., and Croce, P. A., "Fire Hazard Calculations for Large, Open Hydrocarbon Pool Fires," *The SFPE Handbook of Fire Protection Engineering, First Edition*, National Fire Protection Association, Quincy, MA, 1990.

[5] Blanchat, T.K., Humphries, L.L., and Gill W., "Sandia Heat Flux Gauge Thermal Response and Uncertainty Models," SAND Report 2000-1111, Sandia National Laboratories, Albuquerque, NM. May 2000.

[6] Gritzo, L.A., Nicolette, V.F., Tieszen, S.R., and Moya, J.L., "Heat Transfer to the Fuel Surface in Large Pool Fires," *Transport Phenomenon in Combustion*, S.H. Chan, ed., Taylor and Francis, 1996.

[7] Handbook of Aviation Fuel Properties, Coordinating Research Council, Inc., Atlanta, Georgia, CRC Report No. 530, 1983.

[8] Blinov, V.I., and Khudyakov, G. N., "Diffusion Burning of Liquids," English Translation: U.S. Army Engineering Research and Development Labs, Fort Belvoir, VA, Report AERDL-T-1490-A, 1961

[9] Blackwell, B.F., Douglass, R.W., and Wolf, H., "A User's Manual for the Sandia One-Dimensional Direct and Inverse Thermal (SODDIT) Code," SAND85-2478, Sandia National Laboratories, Albuquerque, NM, Reprinted 1990.

[10] Longenbaugh, R.S., Sanchez, L.C., and Mahoney, A.R., "Thermal Response of a Small Scale Cask-Like Test Article to Three Different High Temperature Environments - Appendix B, Thermal Radiative Properties of Pyromark Series 2500 Black Paint," SAND 88-0661, Sandia National Laboratories, Albuquerque, NM, 1989. Alternate Reference DOT/FRA/ORD-90/01, February 1990.

[11] Koski, J.A., Gritzo, L.A., Kent, L.A., and Wix, S.D.,"Actively-Cooled Calorimeter Measurements and Environment Characterization in a Large Pool Fire," *Fire and Materials*, Vol. 20, pp. 69-78, 1996.

[12] Incropera, F. P., Dewitt, D.P., *Fundamentals of Heat and Mass Transfer*, Second Edition, Wiley & Sons, New York, 1985.

[13] Gritzo, L.A., Gill, W., and Keltner, N., "Thermal Measurements to Characterize Large Fires," Proceedings of The 41st International Instrumentation Symposium, Denver, CO, May 7-11, 1995.

[14] Nicolette, V. F. and Larson, D. W., "The Influence of Large Cold Objects on Engulfing Fire Environments," Heat and Mass Transfer in Fires. J. G. Quintiere and L. Y. Cooper (eds), ASME HTD Vol. 141, pp. 63-70, 1992.

[15] Gritzo, L.A., and Nicolette, V.F., "Coupled Thermal Response of Objects and Participating Media in Fires and Large Combustion Systems," *Numerical Heat Transfer, Part A*, 28:531-545, 1995.

[16] Gritzo, L.A., Time-Averaged Photographs of Experiments Performed NAWC. Copies available by request.

[17] Gritzo, L.A., Moya, J.L. and Nicolette, V.F., "Continuous Flame Zone Measurements and Analysis from Large, Open JP-4 Pool Fires including the Effects of Wind," Proceedings of the 1994 NIST Annual Conference on Fire Research, Gaithersburg, MD, October 1994.

[18] Cetegen, B. M., and Ahmed, T.A., "Experiments on the Periodic Instability of Buoyant Plumes and Pool Fires," *Combustion and Flame*, Vol. 93, pp. 157-184, 1993.

[19] Gritzo, L.A., Nicolette, V.F., and Tieszen, S.R, "Preliminary Comparison of KAMELEON Fire Model Results to Data from Large Open Pool Fires Including the Effects of Wind and Objects," Presented at the Open Forum on Fires and Combustion at the 1993 ASME Winter Annual Meeting.

[20] Blanchat, T. and Verner, D., "Sandia Heat Flux Gage Calibration Experiment," Letter report to C. Hickox, Sandia National Laboratories, August 1998.

Distribution

Copies	Mail Stop	Org.	Name
1	0841	9100	T. Bickel
1	1139	6423	T.K. Blanchat
1	0834	9100	T. Y. Chu
1	0835	9141	R. J. Cochran
1	0836	9132	P. E. Desjardin
1	0836	9141	S. P. Domino
2	0836	9116	E. S. Hertel
1	0836	9117	C. E. Hickox
1	0836	9132	W. Gill
1	0836	9117	R. O. Griffith
8	0839	16000	L. A. Gritzo
1	0835	9141	S. N. Kempka
1	0825	9133	A. R. Lopez
1	9042	8728	C. Moen
1	0828	9130	J. L. Moya
1	0555	9132	J. T. Nakos
1	0836	9132	V. F. Nicolette
1	0834	9110	A. C. Ratzel
1	1221	15002	R. D. Skocypec
8	0836	9132	J. M. Suo-Anttila
1	1146	6422	A. J. Suo-Anttila
1	0836	9132	S. R. Tieszen
1	9018	8945-1	Central Technical Files
2	0899	9616	Technical Library
1	0612	9612	Review and Approval desk

4   Defense Threat Reduction Agency (DTRA)
    Attn: Gerald Baird
    6801 Telegraph Road
    Alexandria, VA 22310-3398

1   Miles Greiner
    Professor of Mechanical Engineering
    Mail Stop 312
    University of Nevada, Reno, NV 89557